NORTHWESTERN UNIVERSITY

Discerning the Therapeutic Potential of Peptoid-Based Mimics of Bioactive Proteins

A DISSERTATION

SUBMITTED TO THE GRADUATE SCHOOL

IN PARTIAL FULFILLMENT OF THE REQUIREMENTS

for the degree

DOCTOR OF PHILOSOPHY

Field of Chemical Engineering

By

Ann Marie Czyzewski

EVANSTON, ILLINOIS

December 2008

Abstract

Discerning the therapeutic potential of peptoid-based mimics of bioactive proteins

Ann M. Czyzewski

Nature has been evolving innovative solutions to complex design challenges for billions of years, the success of which is evidenced by the myriad of life-sustaining systems that operate with unparalleled simplicity, efficiency, and durability. Biomimetic researchers derive inspiration from principles underlying natural phenomena to solve design challenges. This work is focused on the development of *N*-substituted glycines (peptoids) as functional mimics of bioactive proteins including antimicrobial peptides (AMPs) and lung surfactant (LS) proteins. Peptoids are synthetic, sequence-specific biopolymers that are well-suited for use in therapeutic applications; they exhibit a stable secondary structure similar to that of α-peptides, and their non-natural backbone renders them impervious to proteases.

The ever-increasing rate at which bacteria evolve to effect multi-drug resistance has spurred research interest in novel antibiotic agents. Natural AMPs are ubiquitous components

of innate immunity that have evolved to defend host organisms against a wide variety of pathogenic species. AMPs thwart the development of bacterial resistance because they employ a generalized mode of action, involving electrostatic and hydrophobic interactions with cellular membranes and intracellular targets. While the susceptibility of AMPs to proteases reduce their bioavailability, peptoid-based AMP mimics ("ampetoids") can circumvent this shortcoming. Here we explore three areas relevant to the therapeutic potential of ampetoids: selectivity, broad-spectrum activity, and *in vivo* efficacy. Structure-activity relationships reveal that selectivity is modulated in predictable ways by changes in physicochemical properties and subtle changes in sequence characteristics. Ampetoids were found to exhibit broad-spectrum activity, and we report the first demonstration of ampetoids reducing bacterial counts *in vivo*.

Lung surfactant, comprised of lipids and surface-active proteins, reduces surface tension at the alveolar air-liquid interface to enable normal breathing. The absence or dysfunction of LS leads to respiratory distress syndrome. While animal-derived surfactants are commonly used to treat neonatal RDS, the development of a wholly-synthetic LS replacement formulation would afford distinct advantages discussed herein. Here we report that peptoid-based mimics of the surfactant proteins SP-B and SP-C interact synergistically to reduce surface activity *in vitro*. Moreover, we present studies using two animal models of RDS, which suggest that peptoid-enhanced LS replacements can mitigate some symptoms of the disease.

Acknowledgements

I gratefully acknowledge my advisor, **Annelise E. Barron**, Ph.D., for providing the inspiration and continued support necessary for making this project a reality.

I am grateful to our collaborating PIs, including **Boris Kramer** M.D., Ph.D. (University of Maastricht, NL), **Jim Lewis**, M.D., Ph.D. (University of Western Ontario, CA), **David Steinhorn**, M.D. (Children's Memorial Hospital, Chicago), **Xiodi Tan**, Ph.D. (Children's Memorial Hospital, Chicago),and **Ruud Veldhuizen** (University of Western Ontario, CA), whose guidance, assistance, and expertise in animal model experimentation were indispensible to the success of this project.

I sincerely thank my advisory committee members, past and present, including **Vassily Hatzimanikatis**, Ph.D., **Lonnie Shea**, Ph.D., **William Miller**, Ph.D., **Wesley Burghardt**, Ph.D., and **David Steinhorn**, M.D. for their input and guidance.

I would also like to sincerely acknowledge my fellow lab members, especially those who have worked in peptoid-based projects, without whom graduate school could not have been such a rewarding experience. I thank those who trained me in basic experimental techniques necessary for this work, including **Matt Honaberger** and **Dr. Shannon Servoss,** and **Dr. Nathan Brown**. I also acknowledge **Lauren Jones** and **Rinki Kapoor**, who assisted in the completion of this work while being trained by me. I am especially grateful to **Nate Chongsiriwatana**, with whom I have had many brain-storming sessions as well as fruitful scientific discussions and debates. I am fortunate to have had him as a colleague, and truly blessed to count him among my friends.

It is with tremendous gratitude that I thank **Christine Moore, Ph.D.** and **Ahmad Sheikh, Ph.D.**, two scientists in whom I hold in highest regard, that were extremely instrumental in sparking my interest in graduate school.

I am truly grateful to my husband, **Chris**, and children, **Mark** and **Teresa,** who have always been there with me to celebrate the successes and share the burden during challenging times.

Lastly, I am forever indebted to my parents, **Maryellen** and **Gordon Shute**, for instilling the confidence in me that enables me to follow my dreams.

Abbreviations

A-a – alveolar-arterial

ACUC – animal care and use committee

AMP – antimicrobial peptide

ARDS – acute respiratory distress syndrome

ATCC – American Type Culture Collection

BAA – bromoacetic acid

BAL – broncheoalveolar lavage fluid

BL – baseline

BLES – bovine lung extract surfactant

BP – blood pressure

BSL2 – biosafety level 2

CAMHB – cation-adjusted Mueller Hinton broth

CD – circular dichroism

CDMEM – complete Dulbecco's modified Eagle's media

CFU – colony forming unit

CH – cholesterol

CLP – cecal ligation and puncture

CLSI – Clinical and Laboratory Standards Institute

CTLR – charge-to-length ratio

DIC – diisopropylcarbodiimide

DPPC – 1,2-dipalmitoyl-sn-glycero-3-phosphocholine

DPX – Dansyl polymyxin B

DSPL – disaturated phospholipids

ESBL – Extended spectrum β-lactamase

Fmoc – Florenyl-methoxy-carbonyl

FIO_2 – fraction of inspired oxygen

HD – hemolytic dose

HR – heart rate

ID – inhibitory dose

LA – large aggregate

LES – Liverpool epidemic strain

LPS – lipopolysaccharide

LS – lung surfactant

MAP – mean airway pressure

MDR – multidrug resistant

MHB – Mueller Hinton broth

MIC – minimum inhibitory concentration

MRSA – methicillin-resistant *Stapholococcus aureus*

MTS – 3-(4,5-dimethylthiazol-2-yl)-5-(3-carboxymethoxyphenyl)-2-(4-sulfophenyl)-2H-tetrazolium, inner salt

NCCLS – National Council of Clinical and Laboratory Standards

nRDS – neonatal respiratory distress syndrome

OI – oxygenation index

PA – palmitic acid

paO_2 – arterial partial pressure of oxygen

pAO_2 – alveolar partial pressure of oxygen

PBS – phosphate buffered saline (**Chapters 2** and **3**); pulsating bubble surfactometer (**Chapter 4**)

pCO_2 – arterial partial pressure of carbon dioxide

PEEP – positive end expiratory pressure

PG – phosphatidylglycerol

PIP – peak inspiratory pressure

PL – phospholipid

POPC – 1-palmitoyl-2-oleoyl-*sn*-glycero-3-phsophocholine

POPE – 1-palmitoyl-2-oleoyl-*sn*-glycero-3-phosphoethanolamine

POPG – 1-palmitoyl-2-oleoyl-*sn*-glycero-3-[phosphor-rac-(1-glycerol)]

Pre-Rx – Pre-treatment

RDS – respiratory distress syndrome

RP-HPLC – reversed phase high performance liquid chromatography

RR – respiratory rate

SA – small aggregate

SD_{pooled} – pooled standard deviation

SEM – standard error of the mean

SP – surfactant protein

SR – selectivity ratio

SRT – surfactant replacement therapy

SUV – small unilamellar vesicle

TFA – trifluoroacetic acid

TL – Tanaka lipids

VEI – ventilation efficiency index

VRE – vancomycin-resistant enterococcus

For my parents, Gordon and Maryellen

For my husband, Chris

For my children, Mark and Teresa

Table of Contents

Abstract 3

Acknowledgements 5

Abbreviations 7

Table of Contents 11

List of Figures 17

List of Tables 22

1. Protein and Peptide Biomimicry: Gold-Mining Inspiration from Nature's Ingenuity 23

1.1 Biomimicry 23

1.2 Mimicry of protein function 24

1.3 β-peptides, α/β-peptides, and peptoids 27

1.4 Enabling technology for foldamer-based biomimicry 28

1.5 Mimics of short elements of peptide secondary structure 31

1.6 Foldamers as mimics of tertiary and quaternary structures 34

1.7 Outlook 37

1.8 The niche of biomimicry addressed in this work 39

2. Ampetoids as selective, broad-spectrum mimics of antimicrobial peptides 43

2.1 Introduction 43

2.2 Results 46

2.2.1 Study design 46

2.2.2 Initial screening of activity and selectivity 47

2.2.3 Structure-activity studies 52
2.2.3.1 Register and sequence variants. 52
2.2.3.2 Charge density variants. 54
2.2.3.3 CTLR variants. 56
2.2.3.4 L-proline substitution variants. 59
2.2.3.5 Achiral monomer variants. 61
2.2.3.6 Opposite chirality substitution variants 64
2.2.3.7 Aliphatic monomer variants 66
2.2.4 Broad spectrum activity 69
2.3 Discussion 71
2.4 Materials and Methods 79
2.4.1 Compound synthesis and purification 79
2.4.2 Circular dichroism spectroscopy 80
2.4.3 Screening antibacterial assays 80
2.4.4 Broad-spectrum antibacterial assays 80
2.4.5 Hemolysis assays 81
2.4.6 MTS assays 82
2.5 Study contributions 82
3. An *in vitro* and *in vivo* study of a peptoid-based antimicrobial peptide mimic 83
3.1 Introduction 83
3.2 Results 86
3.2.1 Broad-spectrum activity 87
3.2.2 LPS binding activity of AMP mimics 88
3.2.3 Sensitivity to bacterial load in the inoculum 90

3.2.3 Biocompatibility of peptoid 1 with intact physiology 91
3.2.4 *In vivo* efficacy of peptoid 1 in the treatment of *S. aureus* intraperitoneal challenge . 91
3.2.5. *In vivo* efficacy of peptoid 1 using the cecal ligation and puncture animal model..... 92
3.3 Discussion 96
3.4 Materials and Methods 99
3.4.1 Peptoid synthesis and purification 99
3.4.2 Broad spectrum minimum inhibitory concentration (MIC) testing 100
3.4.3 Dansyl Polymyxin B (DPX) displacement assay 101
3.4.4 Bacterial load minimum inhibitory concentration (MIC) testing 101
3.4.5 Murine model of *S. aureus* bacterial infection..... 102
3.4.6 Cecal ligation and puncture animal model 102
3.4.7 Statistical Methods 103
3.5 Study contributions 103
4. A study exploring synergy between peptoid-based mimics of lung surfactant proteins SP-B and SP-C. 104
4.1 Introduction 104
4.2 Results 108
4.2.1 Study design 108
4.2.2 Pulsating bubble surfactometry..... 110
4.2.2.1 Static mode pulsating bubble surfactometry..... 111
4.2.2.2 Dynamic mode pulsating bubble surfactometry. 115
4.2.2.3 Comparison to natural surfactant 119
4.3 Discussion 119
4.4 Materials and Methods 122
4.4.1 Peptoid synthesis and purification. 122

4.4.2 PBS sample preparation. 122

4.4.3 Pulsating bubble surfactometry 123

4.5 Study contributions 123

5. Peptoid-enhanced synthetic lung surfactant replacements demonstrate efficacy in an animal model of acute respiratory distress syndrome ……124

5.1 Introduction 124

5.2 Results 127

5.2.1 Proof-of-concept piloting studies 127

5.2.2 *In vivo* efficacy of SP-B and SP-C mimics alone and in a combined formulation 130

5.2.2.1 Study design 130

5.2.2.2 Physiological responses 132

5.2.2.2.1 Baseline and post-lavage equivalency 132

5.2.2.2.2 Gas exchange and pulmonary function 133

5.2.2.2.3 Surfactant pool evaluation 136

5.2.2.2.4 Inflammatory Response 138

5.3 Discussion 138

5.4 Materials and Methods 143

5.4.1 Peptoid synthesis and purification 143

5.4.2 Preparation of synthetic surfactant mixtures 143

5.4.3 Animal experimentation – piloting studies 144

5.4.4 Animal experiments 145

5.4.5 Surfactant pool and total protein analysis 146

5.4.6 Cytokine analysis 147

5.4.7 Statistical Analysis 147

5.5 Study contributions 147

6. An *in vivo* study of peptoid-based surfactants using an ovine model of nRDS 148

6.1 Introduction 148

6.2 Results 153

6.2.1 Study design 153

6.2.2 Preparation of surfactants 155

6.2.3 Physiological response 156

6.2.3.1 Baseline characteristics 156

6.2.3.2 Measures of gas exchange and pulmonary function 157

6.2.3.3 Ventilation indicies 159

6.2.3.4 Lung compliance 160

6.2.3.5 Lung injury 161

6.2.3.5.1 Surfactant pool evaluation 161

6.2.3.5.2 Cell Count 163

6.3 Discussion 164

6.4 Materials and Methods 169

6.4.1 Peptoid synthesis and purification 169

6.4.2 Surfactant preparation 170

6.4.3 Preterm lambs 170

6.4.3.1 Delivery, treatment, and ventilation 170

6.4.3.2 Lung processing 171

6.4.4 Biochemical Analyses 172

6.4.5 Statistical analyses 172

6.5 Study contributions 173

7. Future directions and new frontiers 174

7.1 The development of antimicrobial peptoids as therapeutic agents 175

7.1.2 *In vitro* tests 175

7.1.3 *In vivo* tests 177

7.2 Lung surfactant protein mimics 178

7.2.1 *In vitro* formulation development 178

7.2.2 *In vivo* studies 179

7.3 Development of an antimicrobial lung surfactant replacement 181

7.4 Structural implications of diastereomeric peptoids 182

References 183

A. Quantifying the cytotoxicity of therapeutic peptoids against eukaryotic mammalian cells 202

A.1 Trypan blue staining 202

A.2 Viacount Microcytometry 205

A.3 MTS colorimetric Assay 209

B. Cost analysis of the peptoid made for the study using the ovine model of nRDS. 213

List of Figures

Figure 1.1: Chemical structures of various foldamer scaffolds. 26

Figure 1.2: Schematic summarizing the sub-monomer approach to peptoid synthesis[3]. The reaction between bromoacetic acid (BAA) and the resin-bound amide group is activated by diisopropylcarbodiimide (DIC). The bromoacetylated intermediate is then reacted with a primary amine, and, through S_N2 displacement, the nacent peptoid chain is grown. 30

Figure 1.3: (**A**) Ribbon diagram of the Zwit-1F octamer, with parallel 3_{14} helices in like shades. (**B**) Space-filling rendering of β^3-homoleucine sidechains in green illustrate the well-packed hydrophobic core, while interior (**C**) and exterior (**D**) views of each hand detail the hydrophobic and electrostatic interactions of the assembly. Reproduced with permission from [4]. 34

Figure 1.4: Comparison of secondary and quarternary structures among α/β-peptides 1 (PDB: 2OXJ) and 2 (PDB: 2OXK) and analogous α-peptides GCN4-p1-N_{16}→T (PDB: 1IJ2) and GCN4-pLI (PDB: 1GCL). (**A**) Overlay of individual helix from 2 with an α-helix from GCN4-pLI (**B**) Overlay of the helix bundle quaternary structures of 1 with that of GCN4-p1-N_{16}→T and (**C**) 2 with that of GCN4-pLI. Adapted and used with permission from [5]. 35

Figure 1.5: Structure and self assembly of fragments 1 and 2 α-peptides. (**A**) Amino acid sequence of fragments 1 and 2. The glycine residue preceding the adjacent cysteines in the α2 strand establishes the requisite register for triple-helix formation with the identical α1 and α1' strands. Hyp, (2S,4R)-4-hydroxyproline. (**B**) Representation of the self-assembly process; green, red, and blue are used simply to distinguish individual fragments. Reproduced, with permission, from [7]. 36

Figure 2.1: Schematics of ameptoid variants and side chain structures. Note that the schematics shown here are for visualization purposes only and not intended to imply the actual folding behavior of each molecule. Points on the triangular helicies that have no marker are *N*spe monomers. 49

Figure 2.2: CD spectra of ampetoid register and sequence variants. Ampetoid concentrations were 60 µM. (**A**) CD in 10 mM Tris buffer (pH 7.4) (**B**) CD spectra in 10 mM Tris buffer with 5mM erythrocyte-mimetic POPC:cholesterol (2:1) SUVs. (**C**) CD in 10 mM Tris buffer with 5 mM bacteria-mimetic POPE:POPG (3:7) SUVs. 53

Figure 2.3: CD spectra of net charge variants in (**A**) 10 mM Tris buffer and (**B**) same buffer with 5 mM POPC/cholesterol 2:1 SUVs. Ampetoid concentration is 60 µM. 56

Figure 2.4: CD spectra of length variants in (**A**) 10 mM Tris buffer and (**B**) same buffer with 5 mM POPC/cholesterol 2:1 SUVs and (**C**) same buffer with 5 mM POPE/POPG 3:7 SUVs. Ampetoid concentration is 60 µM. 58

Figure 2.5: CD spectra of proline variants in (**A**) 10 mM Tris buffer and (**B**) same buffer with 5 mM POPC/cholesterol 2:1 SUVs and (**C**) same buffer with 5 mM POPE/POPG 3:7 SUVs. Ampetoid concentration is 60 µM. 59

Figure 2.6: CD spectra of ampetoids containing achiral monomers in (**A**) 10 mM Tris buffer and (**B**) same buffer with 5 mM POPC/cholesterol 2:1 SUVs and (**C**) same buffer with 5 mM POPE/POPG 3:7 SUVs. Ampetoid concentration was 60 µM. 61

Figure 2.7: CD spectra of ampetoids containing opposite chirality monomers in (**A**) 10 mM Tris buffer and (**B**) same buffer with 5 mM POPC/cholesterol 2:1 SUVs and (**C**) same buffer with 5 mM POPE/POPG 3:7 SUVs. Ampetoid concentration was 60 µM. 65

Figure 2.8: CD spectra of ampetoids containing aliphatic monomers in (**A**) 10 mM Tris buffer and (**B**) same buffer with 5 mM POPC/cholesterol 2:1 SUVs and (**C**) same buffer with 5 mM POPE/POPG 3:7 SUVs. Ampetoid concentration was 60 µM. 67

Figure 2.9: Comparison of antimicrobial / hemolytic activity profiles for selected ampetoids. Those with the most favorable profiles appear at the lower right portion of each plot. 77

Figure 3.1: Peptoid schematic and monomer chart. (**A**) Schematic of peptoid 1 with a 3-fold periodic, helical architecture. Positively charged *N*Lys side chains are indicated with + ; *N*spe side chains are at all other positions. (**B**) Chemical structures of peptoid side chains *N*Lys and *N*spe side chains. (**C**) Summary of peptoid 1 and comparator peptide characteristics, with positively charged monomers indicated in bold type. *NC = net charge. 86

Figure 3.2: Minimum inhibitory concentration as a function of bacterial concentration of the inoculum for ampetoid 1 and comparator peptide pexiganan against (**A**) Gram-negative *E. coli* (ATCC 35218) and (**B**) Gram-positive *B. subtilis* (ATCC 6633). 90

Figure 3.3: *In vivo* efficacy of peptoid 1 to treat an infection. Four hours after i.p. challenge with methicillian susceptible *S. aureus*, peptoid 1 was administered locally at a concentration of 4 mg/kg. Colony forming units (CFU) in the peritoneal lavage fluid from individual mice (plated in duplicate) at 24 hours are shown as circles in the vehicle and peptoid 1 treatment groups. Solid lines indicate the geometric mean of each group. Dead animals at 24 hours were assigned the highest colony count observed in the experiment. $p<0.0007$ by Kruskal-Wallis analysis. 92

Figure 3.4: Extent of bacteriemia results for initial round of murine CLP studies. Colony forming units (CFU) per gram tissue for CLP alone and experimental groups 94

Figure 4.1: Schematics of lung surfactant proteins SP-B and SP-C. (**A**) Schematic of SP-B monomer. Charged lysines are shown in red and arginines in purple. Intramolecular disulfide bonds are shown at positions 8, 11, and 35. The intermolecular bond that forms the dimer is at position 48. (**B**) Schematic of SP-B dimer interacting with lipid bilayer headgroups. (**C**) Schematic of SP-C. Palmitoylated cysteine monomers at positions 5 and 6 are shown in blue. **(D**) Schematic of SP-C interacting with a lipid bilayer. Panels (**A**) and (**C**) were adapted from [6] and (**B**) and (**D**) were adapted from [9]. 105

Figure 4.2: Structures of peptoid-based mimics of SP-B and SP-C[1, 8]. The *N*-terminal sequences **B** and **C** are unalkylated mimics, $\mathbf{B}_{mono}$ and $\mathbf{C}_{mono}$ are monoalkylated, and $\mathbf{B}_{di}$ and $\mathbf{C}_{di}$ are dialkylated at the *N*-terminus, as shown. 109

Figure 4.3: Experimental design. The nine combi-nations of SP-B mimic / SP-C mimic combinations are designated by red circles in the coordinate space. Other variables held constant in this study are: (**1**) total

of 2 mol%, (**2**) 50/50 concentration ratio (1 mol% each mimic), and (**3**) Tanaka lipids (1 mg/mL) for all samples. 110

Figure 4.4: Static mode pulsating bubble surfactometer data. Each panel displays a formulation of SP-B/SP-C mimics along with the individual components at an equivalent mol% (2 mol% total). (**A**) **B**/**C** formulation, (**B**) $\mathbf{B}_{mono}/\mathbf{C}_{mono}$ formulation, (**C**) $\mathbf{B}_{di}/\mathbf{C}_{di}$ formulation. Formulations were comprised of 1 mol% of each mimic. 112

Figure 4.5: Static mode PBS runs of six formulations containing one SP-B and one SP-C peptoid-based mimic. Each plot contains a binary formulation (2 mol% total, 1 mol% each mimic) and the individual peptoid components (2 mol%) prepared at 1 mg/mL. Formulations shown include (**A**) $\mathbf{B}/\mathbf{C}_{mono}$; (**B**) $\mathbf{B}/\mathbf{C}_{di}$; (**C**) $\mathbf{C}/\mathbf{B}_{mono}$; (**D**) $\mathbf{B}_{mono}/\mathbf{C}_{di}$; (**E**) $\mathbf{B}_{di}/\mathbf{C}$; (**F**) $\mathbf{B}_{di}/\mathbf{C}_{mono}$. 114

Figure 4.6: Static mode pulsating bubble surfactometer data. Each panel displays a formulation of SP-B/SP-C mimics along with the individual components at an equivalent mol% (2 mol% total). (**A**) **B**/**C** formulation, (**B**) $\mathbf{B}_{mono}/\mathbf{C}_{mono}$ formulation, (**C**) $\mathbf{B}_{di}/\mathbf{C}_{di}$ formulation. Formulations are comprised of 1 mol% each mimic. 115

Figure 4.7: Dynamic mode PBS runs of six formulations containing one SP-B and one SP-C peptoid-based mimic. Each plot contains a binary formulation (2 mol% total, 1 mol% each mimic) and the individual peptoid components (2 mol%) prepared at 1 mg/mL. Formulations shown include (**A**) $\mathbf{B}/\mathbf{C}_{mono}$; (**B**) $\mathbf{B}/\mathbf{C}_{di}$; (**C**) $\mathbf{C}/\mathbf{B}_{mono}$; (**D**) $\mathbf{B}_{mono}/\mathbf{C}_{di}$; (**E**) $\mathbf{B}_{di}/\mathbf{C}$; (**F**) $\mathbf{B}_{di}/\mathbf{C}_{mono}$. 118

Figure 4.8: PBS data comparing the surface activity of the $\mathbf{B}_{mono}/\mathbf{C}_{mono}$ formulation to that of natural surfactant. (**A**) Static adsorption equilibrium curves and (**B**) dynamic cycling hysteresis loops, cycling at 37^{o}C at an oscillatory frequency of 20 cycles/minute. 119

Figure 5.1: Chemical structures of peptoid-based SP-B mimics used in initial piloting studies of the rat washout experimental model of ARDS. 127

Figure 5.2: Physiologic data from piloting rat washout model studies. (**A**) Average blood oxygenation levels in all treatment groups post-lavage and 20 minutes after exogenous surfactant treatment. (**B**) Average pressure-volume (PV) inflation curves and calculated compliance for all treatment groups. Error bars indicate the standard error of the mean. 128

Figure 5.3: Chemical structures of peptoid-based mimics of SP-B and SP-C. 130

Figure 5.4: Vital signs of all animals throughout the timecourse of the experiment. (**A**) Heart rate and (**B**) Blood pressure at baseline measurement (BL), after lavage and before exogenous surfactant treatment (Pre-Rx), and at time points through ventilation period. $p>0.05$ at all time points. 133

Figure 5.5: Physiological indicators of pulmonary gas exchange function over time. (**A**) PaO_2/FIO_2 over time and (**B**) Blood pH over time. Error bars indicate the standard error of the mean. Statistical significance indicators ($p < 0.05$): * indicates BLES vs. TL alone; a indicates $\mathbf{C}_{mono}$ vs. TL alone; c indicates $\mathbf{B}_{mono}$ vs. BLES. 134

Figure 5.6: Physiological indicators of pulmonary function. (**A**) Peak inspiratory pressure (PIP) and (**B**) Shunt fraction over time. Error bars indicate the standard error of the mean. Statistical significance

indicators ($p < 0.05$): * indicates BLES – TL alone; a indicates C_{mono} – TL alone; b indicates B_{mono}/C_{mono} – TL alone. 135

Figure 5.7: Surfactant pool characterization in broncheoalveolar lavage (BAL). (**A**) Average amounts of total surfactant, large aggregates, and small aggregates in BAL. (**B**) Average total protein content in the BAL of each treatment group. Error bars indicate the standard error of the mean. Statistical significance indicators: * indicates $p < 0.05$ for the difference between the designated group and TL alone group... 137

Figure 5.8: Pro-inflammatory cytokine levels in BAL and blood serum. 138

Figure 6.1: Schematic representation of the physiological effects of surfactant deficiency. Adapted from a figure of Boris Kramer, M.D., Ph.D. obtained through direct communication. 148

Figure 6.2: Schematic comparing the pulmonary development of humans to sheep. Adapted from [2].. 152

Figure 6.3: Chemical structures of B_{mono} and C_{mono}, peptoid-based mimics of SP-B and SP-C. 153

Figure 6.4: Arterial partial pressure of oxygen (paO_2) normalized to the fraction of inspired oxygen (FiO2) over time..... 157

Figure 6.5: Physiological parameters related to CO_2 exchange. (**A**) Arterial blood pH, (**B**) Arterial partial pressure of carbon dioxide (pCO_2). Error bars indicate the standard error of the mean. Statistical significance: * indicates statistical significance ($p < 0.05$) between Curosurf and TL alone treatment groups, determined using a one-sided ANOVA and Tukey-Kramer method. 158

Figure 6.6: Pulmonary ventilation indicies. (**A**) Oxygenation index (OI) over time (**B**) Ventilation efficiency index (VEI) over time. Error bars indicate the standard error of the mean (SEM). 159

Figure 6.7: Deflation pressure-volume (PV) curve. Compliance is calculated as $\Delta V/(\Delta P)$, normalized to body weight. Error bars indicate the standard error of the mean..... 161

Figure 6.8: Surfactant pool phospholipid and protein content normalized to body weight. (**A**) Protein content, (**B**) Total phospholipid content, (**C**) Disaturated phospholipid (DSPL) content. Error bars indicate the standard error of the mean (SEM). * denotes a statistically significant ($p < 0.05$) difference between the Curosurf treatment group and the designated group. 162

Figure 6.9: Average cell content of broncheoalveolar lavage (BAL). Error bars indicate the standard error of the mean (SEM). Statistical significance: * indicates a $p < 0.05$ compared to the value for the TL alone treatment group. 164

Figure 7.1: Chemical structures of non-alkylated (top) and mono-alkylated (bottom) mimics of SP-C[1]. 180

Figure A.1: Chemical structure of Trypan blue stain. 202

Figure A.2: Day-old monolayer of NIH 3T3 mouse fibroblast cells treated with 0.2% Trypan blue. (**A**) Control cells treated with media only (no peptoid) retained none of the trypan blue stain. (**B**) Cells treated with 100 μM peptoid 5 were clearly stained with Trypan blue. 204

Figure A.3: Trypan blue assay results with selected antimicrobial peptoids. The average of four independent experiments is shown, with > 400 cells counted at each concentration. Error bars indicate the standard error of the mean (SEM). 205

Figure A.4: Easycyte Mini microcytometer (Guava Technologies, Inc.). Source of image: www.guavatechnologies.com..... 206

Figure A.5: Viacount microcytometry results for selected antimicrobial peptoids against NIH 3T3 mouse fibroblast cells. Error bars are the standard error of the mean (SEM). 207

Figure A.6: Viacount microcytometry results for selected lung surfactant protein mimics against A549 lung epithelial cells. Error bars indicate the standard error of the mean (SEM). 208

Figure A.7: The chemical reaction underlying the principle of the MTS toxicity assay. The MTS reagent is reduced by NADH, which is produced by metabolically active cells, to produce a colored Formazan product. 209

Figure A.8: 96-well plate design of MTS cytotoxicity assays. Peptoid concentrations are serially diluted (2:1) from 100 µM to 0.78 µM (rows A through H). A_{cells} = absorbance of experimental wells. $A_{o\ cells}$ = absorbance of control wells (no treatment), $A_{cell\text{-}free}$ = blank for experimental wells (no cells, but with peptoid at appropriate concentration), and $A_{o\ cell\text{-}free}$ = blank for control wells (no cells, no peptoid). 210

Figure A.9: Cytotoxicity (ID_{50}) of first generation antimicrobial peptoids using the MTS assay. Measurements were made against NIH 3T3 cells and A549 lung epithelial cells. Error bars are shown as the standard error of the mean (SEM). 211

List of Tables

Table 2-1: Sequence and molecular properties of ampetoids and comparator peptide pexiganan. See **Figure 1** for the structures of the peptoid monomers indicated in each sequence. HPLC elution is reported as the average percentage of acetonitrile in the solvent mixture upon compound elution for three injections. A linear acetonitrile/water (0.1% trifluoroacetic acid) gradient of 5% - 95% acetonitrile over 45 minutes was run on a C18 column. [§] CTLR stands for charge-to-length ratio, which is defined as the ratio of the total number of charged monomers to the total number of monomers in each sequence. 50

Table 2-2: Activity of ampetoids and pexiganan against bacteria and mammalian cells. Presented are the minimum inhibitory concentrations (MICs) against *E. coli* (ATCC 35218) and *B. subtilis* (ATCC 6633), 10% and 50% hemolytic doses (HD), and 50% inhibitory doses (ID) against NIH 3T3 mouse fibroblast cells. [*]Selectivity ratio (SR) is defined as the ratio of the 10% hemolytic dose to the MIC for the bacterial strain of interest. 51

Table 2-3: Broad spectrum activity and selectivity of selected ampetoids and pexiganan. (**A**) MICs (in µg/mL) of selected ampetoids against BSL2 microbial strains. (**B**) Selectivity ratios are defined as the 10% hemolytic dose divided by the MIC for the organism of interest. The hemolytic dose (µg/mL) of each compound (**Table 2-2**) was multiplied by its molecular weight (**Table 2-1**) to calculate the selectivity ratio. Notes: [*] indicates NCCLS recommended standard strain; [§] indicates methicillian-resistant *S. aureus* (MRSA) strain; [†] indicates vancomycin-resistant strain; [‡] indicates linezolid-resistant strain. 70

Table 3-1: Minimum inhibitory concentrations (MICs) for peptoid 1 and comparator peptides against 20 clinically-relevant biosafety level 2 (BSL 2) microbial strains. MIC is defined as the lowest concentration at which no bacterial growth was observed. ESBL = Extended-spectrum β-lactamase producing organism; MDR = multi-drug resistant organism; VRE = Vancomycin resistant *Enterococcus;* LES = Liverpool epidemic strain. 88

Table 5-1: Average values of vital signs and selected physiologic indices for all groups. Statistical significance indicator *: a statistically significant ($p < 0.05$) difference between baseline and post-lavage measurements using the Kruskal-Wallis method was detected. 132

Table 6-1: Exogenous surfactant replacement therapies used clinically to treat nRDS[120, 180]. 149

Table 6-2: Average baseline characteristics of all treatment groups ± standard error of the mean (SEM). 156

Table 6-3: Statistical power calculation results using a one-sided ANOVA analysis. Statistical significance was designated as $p < 0.05$. Power assumed was 90%. SD_{pooled} is the calculated pooled standard deviation based on the data set at t=180 (p = 40 mL/(cm H_2O*kg). The expected differential is the expected mean difference between treatment groups. 166

Table A-1: Selected antimicrobial peptoids for toxicity screening using Trypan blue exclusion assay. *E. Coli* (ATTC 35218) and *B. Subtilis* (ATCC 6633). 203

1. Protein and Peptide Biomimicry: Gold-Mining Inspiration from Nature's Ingenuity

1.1 Biomimicry

Biomimicry, a word derived from the Greek words "bios", meaning "life", and "mimesis", meaning "to imitate", has been accurately described by the Biomimicry Institute as a design principle that uses Nature as model, mentor, and measure. Nature's elegant processes, refined over the course of evolution, provide myriad examples of systems that operate with unparalleled simplicity, efficiency, and durability. It is the essence of elegance in engineering. Through careful observation and dedicated study, Nature's secrets begin to unfold and the fundamental principles underlying natural phenomena can become clear. Recognizing the wisdom that Nature has to offer, biomimetic researchers derive inspiration from or attempt to mimic directly the form and/or function of natural designs.

The field of biomimicry has enjoyed a long and rich history spanning many decades, and has influenced a variety of disciplines, ranging from architecture and economics, to materials science and bioengineering. A particularly notable example of bioinspired design is Velcro®, the hook-and-eye fastener invented by George de Mestral and modeled after the microscopic hooks on seed-bearing burrs that enable them to cling to animal fur and become dispersed. What began as natural curiosity in the mind of a Swiss mountaineer has today become a multimillion dollar global industry.

State-of-the-art technology is enabling biomimeticists to examine Nature with an eye capable of resolving structures well below the macro and micro scales; the concerted efforts of microbiologists, chemists, physicists, and engineers have made observation at the nano and even the molecular scale a reality. Technological advances are continually expanding the

frontier of what is possible in this field, which remains in its infancy. In particular, interdisciplinary research in biomimetic polymer engineering is poised to make lasting contributions to both the fundamental science and engineering applications of the basic building blocks of life – proteins. Hence, we focus here on the mimicry of these natural molecules, in particular.

1.2 Mimicry of protein function

In the post-genomic era (so called, even while genomes and their organization still offer us much to learn), we are only beginning to understand the exquisite array of complex functions that proteins facilitate. Proteins not only comprise extraordinarily strong and versatile cellular structures, but also very precisely control nearly all cellular functions, including molecular recognition, catalysis, regulation of growth cycles, and structural stabilization. In short, proteins constitute the basic currency of life. The prospect of being able to control cellular function predictably at the molecular level is in many ways the Holy Grail of drug discovery, and promises tremendous impact on scientific research, the medical industry, and human health worldwide.

In biological systems, form and function are intimately intertwined; properly designed structural mimics of a molecule will often be able to perform analogous functions. While protein engineers are making real strides in designing *de novo* tailor-made proteins to perform specific functions, the complexity of protein folding mechanisms has limited the ability to reliably engineer a specific tertiary structure, even for just average-size proteins[10]. As an alternative approach to circumventing the "protein folding problem", there is growing interest in recapitulating protein function in simplified synthetic scaffolds, or "foldamers". Foldamers are typically oligomeric or polymeric molecules (up to ~ 50mers) based on a non-natural backbone, and are able to mimic a variety of simple secondary structures[11]. Beyond strictly achieving the

same result using non-natural molecules, foldamers are uniquely advantageous for mimicking biological systems. While synthetic analogs are typically simpler structures that can often be produced more efficiently and in a more cost-effective manner, they also can "transcend Nature" by imparting improvements in biostability and bioavailability compared to their natural counterparts. Additionally, a simple foldamer-based biomimetic system in which parameters can be precisely and independently controlled is well-suited for interrogating structure-activity relationships. Furthermore, as conclusions from these studies are often transferable back to the natural system, more broadly applicable knowledge may result. Lastly, many researchers that derive inspiration from Nature conceive of entirely new and useful applications for the technology being developed. For all of these reasons, the use of foldamers to mimic bioactive proteins and protein domains continues to be a very active area of research.

Many types of foldamer backbone scaffolds have been found to mimic simple helical, turn, and sheet-like peptide secondary structures. Examples of well-characterized foldamer scaffolds, shown in **Figure 1.1**, include α/β peptides[12], β-peptides and γ-peptides[13], *N*-substituted glycines (peptoids)[11, 14], phenylene ethynylenes[15], and urea derivatives[16]. All of these classes of non-natural oligomers have been shown to exhibit kinetic and thermodynamic stability and can mimic some functions of bioactive peptides. Interestingly, despite the overall complexity of protein function, several bioactive peptides exhibit surprisingly short and simple architectures that are amenable to biomimicry. The literature provides abundant examples of simple proteins that have been mimicked including antimicrobial peptides, lung surfactant proteins, protein binding domains, cell penetrating mediators, and proteins that target a variety of biologically relevant targets (for a recent review, see[17]).

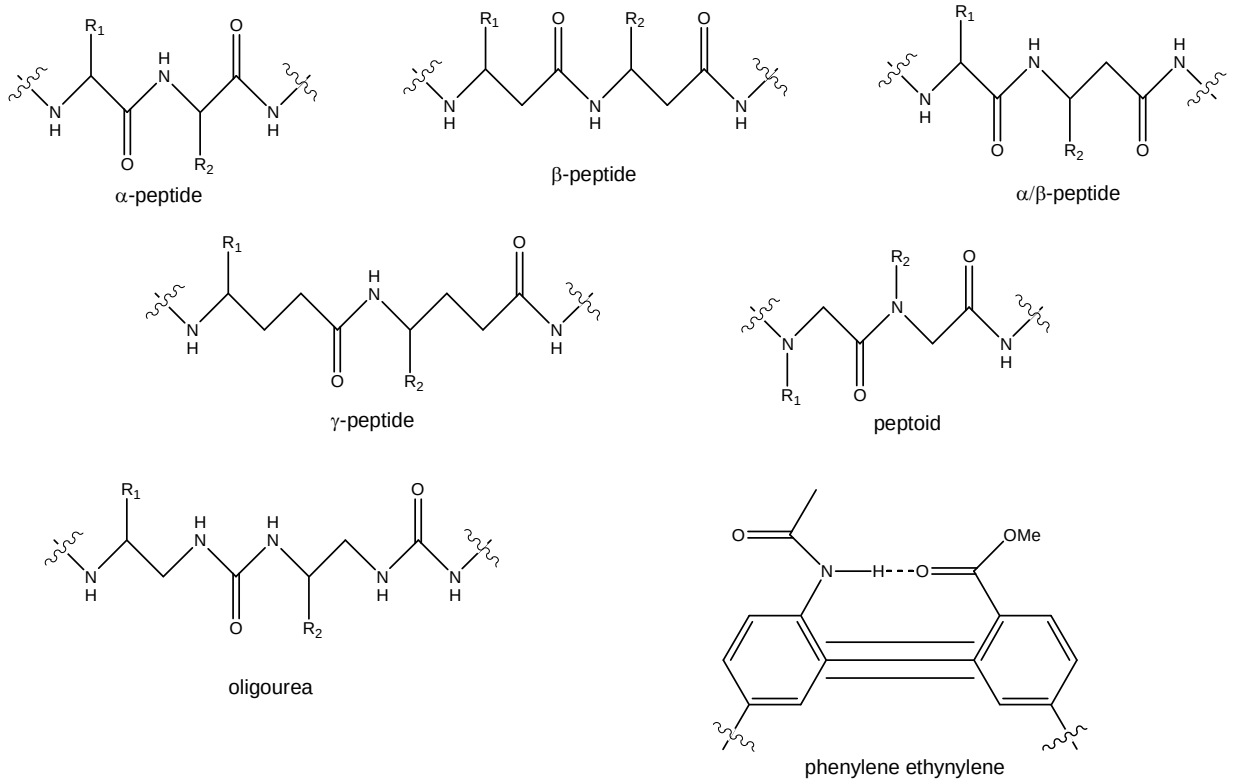

Figure 1.1: Chemical structures of various foldamer scaffolds.

While notable progress has been made in mimicking simple protein/peptide secondary structures, the prospect of creating foldamer-based supramolecular assemblies that adopt discrete tertiary and quaternary structures opens up the possibility of regulating far more complex protein-like functions. Since the average protein length is approximately 250 amino acids, and contains two 15-kilodalton domains[18], engineering of a stably folded supramolecular foldamer structure has proven to be a formidable challenge. As will be discussed, however, significant progress has been realized in the case of β-peptides, α/β-peptides, and peptoids. These three classes of foldamers, which have demonstrated potential for use as pharmaceutical agents, are the primary focus of this discussion. Recent advances in foldamer biomimicry are ushering in a new era in the design of functional protein mimics; as our ability to use synthetic monomers to construct complex structures is improved, so too will be our ability to mimic their function.

1.3 β-peptides, α/β-peptides, and peptoids

As shown in **Figure 1.1**, the extended backbone of β-peptides contains an "extra" methylene group between amide groups, in comparison to natural α-peptides. β-peptides are capable of adopting a variety of structures, including helices, turns, and sheet-like architectures (for reviews see[13, 17]). A hybrid structure with a heterogeneous backbone can also be formed using a combination of α-peptide and β-peptide monomers in the same molecule[12]. Sporadic inclusion of β-peptide residues can induce turns and can cause minor changes to foldamer structure[19]. Molecules with a regularly repeating arrangement of α- and β-peptide monomers have been made and found to form stable structures closely related to those of natural peptides[12].

Peptoid structure is isomerically related to that of peptides, in that the side chains are attached to amide nitrogens rather than to α-carbons, as shown in **Figure 1.1**[14]. The conformational and stereochemical ramifications of the *N*-substituent on the peptoid backbone (which is identical to a peptide backbone in its sequence of atoms) are significant[11]. The lack of amide protons and chiral centers in the peptoid backbone results in the absence of backbone-mediated hydrogen bonding in a fully substituted peptoid chain, and also precludes the formation of intrinsic backbone handedness. It has been shown, however, that incorporation of α-chiral side chains generates steric and, in some cases, electronic repulsions that can induce the formation of a helical backbone conformation reminiscent of the polyproline type-I helices-like those found in collagen (~3 residues per turn, pitch of ~ 6 Å), stabilizing the secondary structure[11].

The structural differences between these classes of foldamers and the natural peptides that inspired them have important implications for biomimicry. The non-natural backbone renders them impervious to protease activity, thereby increasing bioavailability and reducing specific recognition by the immune system[20, 21]. These foldamers, so far, have been shown to induce

only very low-level antibody response and certain peptoids have been found to be bioactive, non-toxic, and non-immunogenic[22, 23].

Here we discuss how foldamer biomimicry has evolved from a curiosity involving a few peptide chemists to a highly interdisciplinary field that has the potential to significantly improve our ability to understand and treat disease. We highlight accomplishments of using β-peptides, α/β-peptides, and peptoids to mimic small bioactive molecules as well as more recent work demonstrating foldamers' ability to adopt more complex supramolecular tertiary and quaternary structures. We conclude with an outlook on the interdisciplinary character of the field and postulate future directions in the pursuit of making non-natural protein-like assemblies.

1.4 Enabling technology for foldamer-based biomimicry

The foundation of foldamer science is deeply rooted in the achievements of peptide chemistry's founding fathers over the past century. Since the first report of α-peptide synthesis in 1901, great strides in technology development have been made that now make routine the synthesis of long biopolymers (for review see[18]). Over the past one hundred years, improvements in protecting group design and coupling agents have greatly increased product yields and coupling efficiencies. A major breakthrough occurred in 1963 with the introduction of solid-phase α-peptide synthesis by R.B. Merrifield[24]. This innovative approach of building molecules on solid support enabled the easy removal of by-products and reagents through washing and filtration between subsequent couplings, and made the process amenable to automation using a single reaction vessel. The development of improved resin solid supports was critical, along with parallel advancements in purification and analysis technology. Together, these have made synthesis of linear, sequence-specific α-peptide polymers up to 50 monomers long easily achievable with the use of careful procedure and best practices[18].

A second milestone was achieved in the development of chemical ligation, a technology that enables the solution-phase coupling of unprotected peptide fragments[25]. The basis for this technique is the use of two components with unique, mutually reactive functionalities resulting in a "chemo-selective" reaction. Since the first demonstration of this technique, this methodology has seen the benefit of several generations of improvements and variations[26].

Synthetic methods to make foldamers have been adapted from solid-phase methods used for conventional peptides. While short sequences of β-peptides can be made using a standard fluorenyl-methoxy-carbonyl (Fmoc) protecting group-based solid-phase synthesis protocol, the yield of longer molecules is significantly reduced due to incomplete deprotection and the need for extended coupling times[18]. Recently, however, Seebach *et al*. developed a thioligation strategy that can be used to construct longer β-peptides and α/β-peptides in improved yields[18]. A method to efficiently synthesize β-peptide combinatorial libraries has been reported, which is an important step for screening the bioactivity of several drug candidates[27].

Peptoid synthesis was revolutionized by the work of Zuckermann *et al.*, who reported the "sub-monomer" approach shown schematically in **Figure 1.2**[3]. Using a solid-phase protocol and an automated peptide synthesizer, this novel synthetic route gives access to a diversity of functionalized peptoids at modest cost and effort[28]; the high sub-monomer coupling efficiencies (comparable to those attained in Fmoc peptide synthesis) coupled with the low cost of production from inexpensive and readily available starting reagents set peptoids apart. Diverse, sequence-specific peptoids up to at least 50 residues in length can be readily synthesized in high yields.

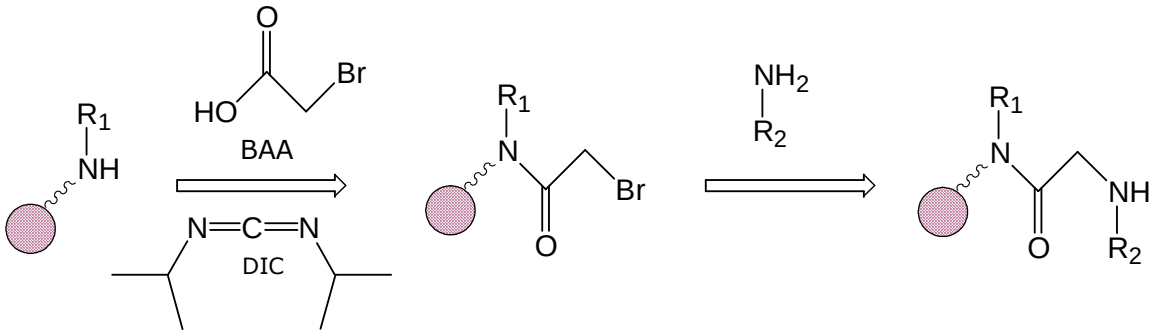

Figure 1.2: Schematic summarizing the sub-monomer approach to peptoid synthesis[3]. The reaction between bromoacetic acid (BAA) and the resin-bound amide group is activated by diisopropylcarbodiimide (DIC). The bromoacetylated intermediate is then reacted with a primary amine, and, through S_N2 displacement, the nacent peptoid chain is grown.

Peptoids are a highly suitable family of foldamers for use in commercializable medical applications for a variety of reasons. A robotic synthesizer can be used to make many peptoid chains in parallel, or to create large combinatorial libraries of peptoids to quickly screen thousands of molecules for bioactivity[29]. One can also alternate between sub-monomer and monomer protocols (whereby peptoids are made by coupling of activated Fmoc-protected monomers[14, 30]) within a single, automated solid-phase synthesis, enabling the facile creation of peptoid-peptide hybrid sequences. Incorporation of natural and non-natural sequences in the same molecule can be used to achieve the optimal balance of good bioactivity and an appropriate rate of biodegradation.

Peptide and peptoid chemists have therefore laid the fundamental groundwork upon which the field of molecular biomimicry is being built. The establishment of these enabling technologies began over one hundred years ago, and innovations are continuing to be made today. This work has paved the way for researchers from many disciplines to ponder ways to design and control foldamer structure and to consider potential applications of these versatile materials.

1.5 Mimics of short elements of peptide secondary structure

The establishment of robust methods to synthesize non-natural peptide and peptoid foldamers has enabled researchers to probe a few practical applications of sequences designed to adopt stable secondary structures. This work has involved the joint efforts of chemists, chemical biologists, microbiologists, clinicians, and chemical engineers. Among the many classes of bioactive peptides that have been mimicked[17], antimicrobial peptides (AMPs) are one of the most active areas of study due, in part, to their relatively simple structural requirements and their potential to meet a pressing clinical need.

Antimicrobial peptides (AMPs) are a ubiquitous class of short (< 40 amino acids), amphipathic, naturally occurring molecules that defend organisms against a broad spectrum of bacterial invaders through a generalized membrane permeabilization mechanism of action. Because AMPs do not operate through specific receptor-mediated events, bacteria have been largely unable to develop resistance to AMPs over the course of evolution, making them attractive candidates as lead compounds in the development of novel antibiotic agents. However, AMPs suffer from proteolytic susceptibility and a resultant poor *in vivo* bioavailability, which has curtailed their clinical use. The non-natural, protease-stable foldamer backbone offers a means for recapitulating these peptides' function while circumventing their shortcomings.

The linear, cationic, mostly helical class of antimicrobial peptides, such as the magainins and cecropins, exhibit an amphipathic structure that is readily recapitulated in a foldamer helix. The work of several laboratories has shown that β-peptides and α/β peptides can exhibit potent and selective antimicrobial activities (reviewed in[17]). Structure-activity relationship studies have demonstrated that several parameters including molecular hydrophobicity, sequence length, and amphipathicity modulate the selectivity. It has also been shown that while the

amphipathicity of a molecule once it is in the membrane environment is important for activity, a rigid structure outside of a membrane is not. Moreover, α-peptides and their non-natural peptide counterparts appear to share a common mechanism of action, as they both appear to be bounded by low-micromolar minimum inhibitory concentrations (MICs).

Our lab has focused on designing peptoids to be potent and selective antimicrobial agents. The helicity induced by incorporating α-chiral side chains results in a regular periodicity of three monomers per turn, which is highly amenable to designing amphipathic structures. We have synthesized, designed, and characterized over 50 sequences with diverse side chain functionalities and have found many of them to be potent and selective antibiotics, killing bacteria with low-micromolar MICs while not harming mammalian cells until their concentrations are well above the respective MICs[31]. In tests of broad-spectrum activity, it is interesting how the activity of a given peptoid against certain strains will often closely parallel that of the natural peptide it mimics. Moreover, structure-activity relationship studies have also determined that peptoid-based AMP mimics appear to utilize a mechanism of action strikingly similar to that of AMPs themselves[32].

Whereas AMP function is related to overall molecular architecture (e.g. amphipathicity, hydrophobicity, overall charge), the proper function of other types of proteins depends on more precise replication of a particular monomer arrangement in space. Non-natural peptides have been used to mimic a variety of structurally specific proteins, including inhibitors of protein-protein interactions, HIV fusion inhibitors, inhibitors of fat and cholesterol uptake, and RNA binding (for reviews see[17, 33, 34]). Similarly, peptoids have also been used to inhibit protein interactions and receptor binders as well as to mimic the “physical catalysis” of lipid film behavior that is naturally accomplished by the hydrophobic lung surfactant proteins, SP-B and SP-C, which enable normal breathing[35-37].

An aspect of foldamer biomimicry that has been championed primarily by engineers is the use of synthetic polymers, often derivatized with small peptides, to create novel biomaterials and “smart” devices. The impetus of this line of research resides in the fact that cell behavior is affected by stimulation from its external environment as well as by specific signaling molecules. Specifically, integrins have been shown to influence cell growth, differentiation, adhesion, and motility. Research in this area is directly applicable to the design of biomaterials for tissue engineering, reactive coatings, and smart surfaces. The ability to control the properties of biomaterials as they morph in time and space adds a new dimension that until now has set natural materials apart. Advances in these areas have been focused in the areas of tissue engineering, the development of diagnostic tools, and surface engineering[38].

Foldamers have also been created to mimic a variety of different structures. β-peptides have been assembled to form a variety of helical conformations, as well as stacks, sheets, and turns[13]. Because the typically bulky nature of peptoid side chains limits the conformational freedom of a peptoid backbone, peptoids are usually contorted to form polyproline type-I-like helices, which are longer in pitch than α-helices, with helix handedness being directed by the side chain enantiomers used. Fully substituted peptoids are also precluded from forming sheet-like or hairpin structures due to the lack of hydrogen bonding. Well-designed peptoid helices are stable in a variety of organic solvents. While peptoids that incorporate α-chiral side chains typically form these collagen-like helices, a novel “threaded loop” structure, adopted by a particular family of nonamers in acetonitrile solution only, has been reported[39]. A very interesting aspect of this structure is that it is stabilized by hydrogen bonds involving the *C*-terminus as well as backbone carbonyl groups, and in essence shows a structure that is folded “inside out”, with a burial of hydrophilic surface area and exposure of side-chain hydrophobes to the non-hydrogen bonding, polar organic solvent acetonitrile; yet these nonamers form regular peptoid

helices in methanol. As in natural proteins, the *N*- and *C*-termini end up very close in space in the threaded loop structure (which, interestingly, was discovered in a study of many different peptoids in solution, not designed). It has also been shown that peptoids can be made to form cyclic structures easily and efficiently[40].

1.6 Foldamers as mimics of tertiary and quaternary structures

As has been discussed, foldamers designed to mimic simple secondary structures have proven to offer some interesting biological functions and to exhibit promise as mimics of small bioactive proteins. The ability to mimic a protein's tertiary and quaternary structure is a further level of sophistication that would unmask the potential to mimic even more complex functions. While this represents a tremendous challenge, exciting progress has already been made in many areas just in the past year. Recent work from the Schepartz lab reports the first high-resolution structure of a stable, discrete, and compact β-peptide assembly, Zwit-1F (**Figure 1.3**)[4]. This β-dodecamer spontaneously self-assembles into an octameric, bundled β-peptide quaternary structure driven by non-covalent inter-residue interactions. Biophysical characterization of the Zwit-1F structure confirmed that the kinetic and thermodynamic properties of the β-peptide analogue are strikingly similar to those of natural peptide bundles[41].

The Gellman lab has reported the first helix bundle architecture created using the

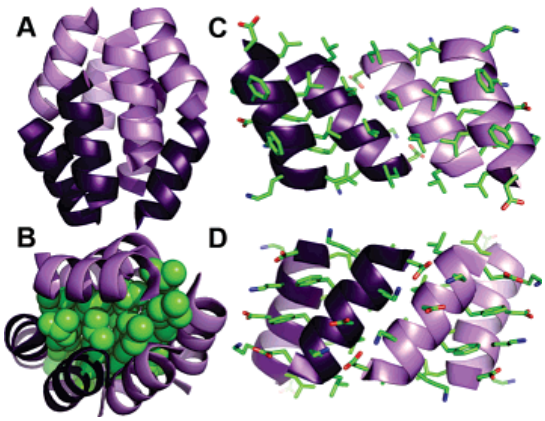

Figure 1.3: (**A**) Ribbon diagram of the Zwit-1F octamer, with parallel 3_{14} helices in like shades. (**B**) Space-filling rendering of β^3-homoleucine sidechains in green illustrate the well-packed hydrophobic core, while interior (**C**) and exterior (**D**) views of each hand detail the hydrophobic and electrostatic interactions of the assembly. Figure adapted from [4].

heterogeneous α/β-peptide scaffold (**Figure 1.4**)[5]. Indeed, direct translation of a protein GCN4 known to self assemble into the α/β-peptide scaffold retained its ability to self-assemble, albeit with somewhat altered stability and helix association geometry[5]. Helix bundles composed of both α/β-peptides and α-peptides have also been demonstrated[42]. This report opens the door to entirely new conformational possibilities; the prospect of being able to fine-tune tertiary structure by using a combination of different foldamer backbones may be the key step in mimicking more complex protein functions, since each scaffold offers its own unique limitations and possibilities.

A recent report also demonstrates the potential for foldamers to adopt a zinc finger-like architecture found in a class of transcription factors that recognize and bind specific DNA[43]. A β-peptide 16mer consisting of a turn and helix structure was designed with strategically placed histidine and cysteine residues that have a strong affinity for binding zinc. It was found that indeed the β-peptide folds in the presence of Zn^{+2}, as was hoped.

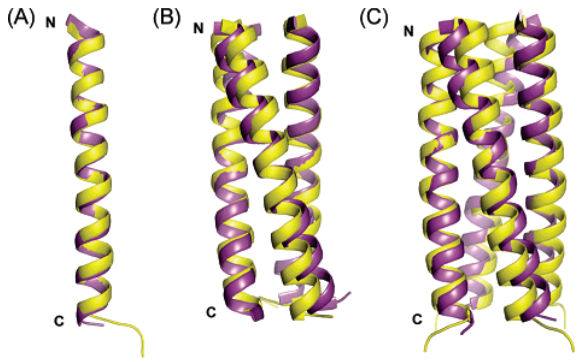

Figure 1.4: Comparison of secondary and quarternary structures among α/β-peptides 1 (PDB: 2OXJ) and 2 (PDB: 2OXK) and analogous α-peptides GCN4-p1-N_{16}→T (PDB: 1IJ2) and GCN4-pLI (PDB: 1GCL). (**A**) Overlay of individual helix from 2 with an α-helix from GCN4-pLI (**B**) Overlay of the helix bundle quaternary structures of 1 with that of GCN4-p1-N_{16}→T and (**C**) 2 with that of GCN4-pLI. Adapted from [5].

Quaternary helix bundle architectures have also been reported for peptoid scaffolds[44, 45]. A library of 3400 amphipathic 15mers was screened for the presence of a hydrophobic core using a 1,8-ANS binding assay. Several sequences were found that appear to self-associate. In a subsequent study, one of the sequences showing a high propensity to self-assemble was selected to determine the effect of coupling four repeats of the 15mer sequence together[45]. Indeed it was found that peptoids can assemble to form a hydrophobic core and to display apparently cooperative folding transitions.

An impressive and beautiful accomplishment was reported by the Raines lab in which synthetic collagen was created by the self-assembly of chemically synthesized α-peptide fragments into a triple-helix (**Figure 1.5**)[7]. Three separate peptide fragments were connected in a precise chemical architecture through disulfide bonds that facilitated self-assembly. This landmark achievement marks the first reporting of mimics with lengths (> 400 nm) that rival and even exceed that of natural collagen assemblies (~ 300 nm).

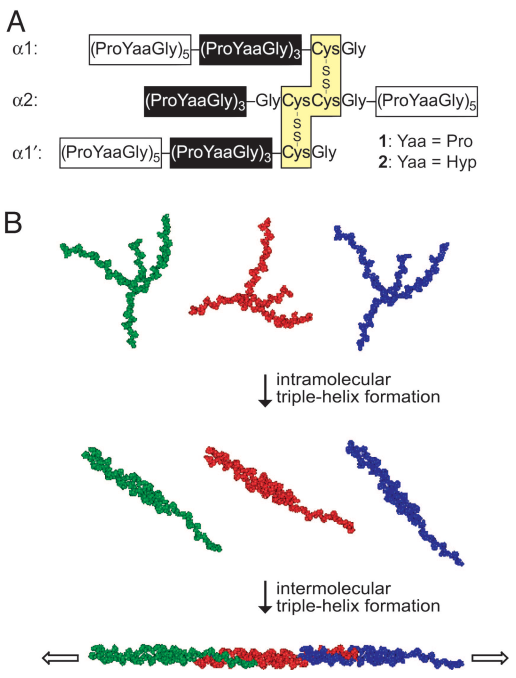

Figure 1.5: Structure and self assembly of fragments 1 and 2 α-peptides. (**A**) Amino acid sequence of fragments 1 and 2. The glycine residue preceding the adjacent cysteines in the α2 strand establishes the requisite register for triple-helix formation with the identical α1 and α1' strands. Hyp, (2S,4R)-4-hydroxyproline. (**B**) Representation of the self-assembly process; green, red, and blue are used simply to distinguish individual fragments. Adapted from [7].

1.7 Outlook

While biomimicry is a design principle that has been utilized successfully for decades, the advancement of technologies to probe Nature on the molecular level has initiated a new era in the field; the potential of biomimicry is now becoming less constrained by technological capability and tempered primarily by the capacity of our imaginations. The use of non-natural foldamers to mimic the function of bioactive proteins is an active area of research that was founded by peptide chemists and has grown into a discipline that also benefits from the work of microbiologists, chemical biologists, clinicians, and chemical engineers. While there have been many significant successes in foldamer biomimicry to date, the potential of this field is only beginning to be realized and the possibilities only beginning to be explored. It is notable, for example, that most of the sequences of peptoids and β-peptides to date have sequences that are dominated by repeating motifs; this is not necessarily always dictated by limitations of the synthesis, but clearly, also by the reluctance of molecular engineers to create a system that cannot be predicted nor understood. If we are taking our inspiration from Nature's ingenuity as we design the first truly functional peptide and protein mimics, it must be admitted that we have only succeeded, so far, in scratching our way down a few feet into the dirt, and gaining our first glimpses of the riches that lie below to be further excavated, by the years of back-breaking work that remain ahead of us.

Combining the precepts of a selection process with a relatively high-throughput, parallel synthesis, as Dill and Zuckermann have done, will allow unfettered imaginations to find the proverbial "needle in a haystack" – the structured foldamer that has not been precisely designed to form a discrete structure from *de novo* principles, but rather, painted in soft focus with water colors (as a family of sequence motifs, with diversity in specific side chains) to offer the chance to collapse into a reasonably well-ordered structure that has some function such as metal binding. Successful *in vivo* testing of bioactivity of foldamers in animals, and eventually

humans, will put some real wind behind the sails of biomimeticists and attract even more researchers and funding to the area.

A highly effective means of accelerating the rate of progress in this area will be through knowledge sharing and collaborations that cross disciplines. For example, it is important for those who perform physical experiments to have an understanding of the work of those who use computer modeling to address similar questions; limited collaborations across these disciplines have benefited the foldamer field to date. Those who work on the engineering design and synthesis of more subtly bioactive foldamer designs can only benefit from knowing about advances in microbiology and structural biology that could inform their work. Engineers that are searching for new biomaterial applications of biomimetic designs need to stay in close contact with clinicians who best understand the needs of patients. Maintaining an awareness of ongoing work across disciplines, and participating in collaborations such as those that have been funded in the past 5-8 years by the NIH's Bioengineering Research Partnership funding program, and the NSF's Collaborative Research in Chemistry program, will facilitate the most efficient and effective advancement of biomimicry and its application to medicine and biotechnology.

Another change that is presently occurring, which facilitates the development of interdisciplinary studies such as these, is the burgeoning extent of cross-training that is now included in scientific and engineering curricula. Today, in addition to core chemistry and engineering classes, many chemical engineering departments require at least an introductory level class in biology and biochemical engineering. Deeper training in the methods of organic synthesis and the purification of particular molecules can put powerful tools in the hands of chemical engineers, who naturally have a keen focus on applications and instinctively wonder what a molecule may "be good for." Many chemical engineering departments have changed

their names to reflect the increasingly biological focus of their research activities; at this point, eight of the top 25 chemical engineering departments in the U.S. have been renamed to reflect a more biological thrust (Chemical & Biological Engineering, and Chemical & Biomolecular Engineering are popular choices), and 16 of these departments now have faculty members actively doing research in the field of biomimicry, broadly defined.

As the frontiers of science expand at an apparently ever-increasing rate, the boundaries between individual scientific disciplines are becoming less and less distinct; and it becomes increasingly challenging for scientists to keep current with each other's work, and with the literature as a whole. Chemical engineers today are beginning to feel that they are part of scientific communities other than the close-knit world of chemical engineers, and that is good. Many chemical engineers are well trained and well poised to catalyze a revolutionary blending of fundamental science and applied engineering that promises to transform the way in which research is done over the next 10-20 years. This is no coincidence. Rather, it is only though the concerted efforts of scientists and engineers that interdisciplinary fields such as foldamer-based biomimicry can emerge. Over time, the contributions that chemical engineers can make, even at the molecular synthesis and discovery stages of protein biomimicry, will increasingly be recognized.

1.8 The niche of biomimicry addressed in this work

The Barron lab's contribution to the field of biomimicry lies primarily in the design and development of peptoid-based mimics of antimicrobial peptides and lung surfactant proteins. As will be discussed, both of these research areas address unmet clinical needs and have the potential to impact healthcare worldwide. Predecessors have shown that peptoid-based mimics of both antimicrobial peptoids[31, 32] and lung surfactant proteins[36, 37, 46, 47] exhibit promising *in vitro* activity. It is upon this foundation that the scope and aims of this work were established. The

next frontier for these research platforms was to go beyond *in vitro* activity and begin to explore areas more directly related to their therapeutic potential. Specifically, the four objectives of this project were: (**1**) Determine the extent to which therapeutic peptoids are cytotoxic to mammalian cells, and develop an understanding of how cytotoxicity can be modulated; (**2**) Evaluate the broad-spectrum antimicrobial activity of antimicrobial peptoids as well as their ability to treat an infection *in vivo*; (**3**) Explore the potential synergy of peptoid-based mimics of lung surfactant proteins SP-B and SP-C *in vitro*; (**4**) Evaluate the *in vivo* efficacy of peptoid-containing lung surfactant replacement therapies in the treatment of respiratory distress syndrome (RDS).

In **Chapter 2**, we present a library of 26 antimicrobial peptoids ("ampetoids") that demonstrates that cell selectivity can be modulated not only by changes in physicochemical properties, but also by more subtle changes in structural properties related to the number, position, arrangement, and chemical structure of substituted hydrophobic moities. Additionally, many of the new, more selective ampetoids retain promising *in vitro* activity against a spectrum of bacterial organisms, including clinically relevant, multi-drug resistant (MDR) strains. The structure-activity relationships derived from this library of compounds reaffirm and extend the analogy between the mechanism of action of AMPs and ampetoids, and design heuristics to aid in the design of selective, future generations of ampetoids are established. **Appendix A** presents a series of studies performed using three different methods for quantifying cytotoxicity. This work was done in the early stages of developing a cytotoxicity method that is suitable for screening large numbers of peptoids.

Chapter 3 comprises a four-part study designed to more fully investigate the therapeutic potential of one particular ampetoid, **1**. We demonstrate that **1** not only exhibits activity antimicrobial against a variety of pathogenic, MDR bacterial strains, comparable to that of pexiganan, (a clinically relevant AMP), but also show that its antimicrobial activity appears less

affected by bacterial load than conventional AMPs. Most importantly, we report a study which demonstrates **1** can reduce colony forming units *in vivo* using both a simple murine model of infection through *S. aureus* intraperitoneal challenge. Preliminary studies using a rodent model of sepsis to test peptoid **1**'s ability to treat a more clinically relevant polyclonal infection are also discussed.

In **Chapters 4**, **5**, and **6**, the focus is shifted from antimicrobial peptoids to peptoid-based mimics of lung surfactant proteins. While peptoid-based mimics of surfactant proteins SP-B and SP-C have been developed and tested for surface activity individually, native lung surfactant contains both proteins. **Chapter 4** comprises an *in vitro* study that evaluates the surface activity of binary formulations containing both SP-B and SP-C mimics. One particular combination of mimics ($\mathbf{B}_{mono}/\mathbf{C}_{mono}$) appeared to exhibit emergent synergistic improvement in surface activity compared to formulations containing the individual components.

In **Chapter 5**, we present the first study designed to evaluate the *in vivo* efficacy of peptoid-based lung surfactant protein mimics. Using a rat model of acute respiratory distress syndrome (ARDS), we demonstrate that treatment with peptoid-enhanced surfactants can improve physiological and biochemical outcomes. **Chapter 6** describes a second *in vivo* study in which a premature sheep model was used to explore the effect of peptoid-enhanced surfactants on surfactant deficiency associated with neonatal RDS (nRDS). While this study was significantly underpowered, the outcomes show trends that suggest treatment with peptoid-containing surfactant could improve physiological outcomes and reduce lung injury compared to treatment with the lipid carrier alone. The challenges encountered with the surfactant preparation and the animal protocol are also discussed, and recommendations for addressing these issues in future studies are made.

The work discussed herein only scratches the surface of what promises to be a very fruitful research area. Possible future directions of this research are discussed in **Chapter 7**.

2. Ampetoids as selective, broad-spectrum mimics of antimicrobial peptides

2.1 Introduction

Bacterial resistance to even the most potent antibiotics has been identified by the World Health Organization as one of the most pressing public health issues[48]. While the development of resistant organisms to antimicrobial agents is an inevitable Darwinian process, the permissive use of antibiotics coupled with the lack of new, unconventional therapies has resulted in a global crisis[49]. New conventional antibacterial agents cannot provide a long-term solution to this problem; the structural and mechanistic similarities among most clinically used antibiotics readily accommodate the development of bacterial resistance and shorten their useful therapeutic lifetime. Among the most promising classes of novel antimicrobial agents to fill this unmet clinical need are antimicrobial peptides (AMPs) and their mimics[50, 51].

AMPs are integral components of innate immunity that are diverse in source, length, and structure[50]. Most AMPs, however, have in common an overall amphipathic architecture and net cationic charge (+2 to +9), which renders them membrane active and enables their antimicrobial activity[50, 52, 53]. Unlike classical antibiotics, for which activity is contingent upon specific receptor-mediated events, more generalized interactions are central to AMPs mechanism of action. While the specific details underlying AMPs' modes of action remain a subject of active debate, some are thought to target and disrupt the membrane directly and others translocate past the membrane to act on intracellular targets, which ultimately leads to cell death[52, 53].

While Daptomycin is a lipopeptide antimicrobial agent that has achieved FDA approval[52, 54], conventional cationic AMPs have underperformed during clinical testing[52, 53]. The unfavorable pharmacokinetic profile and lack of bioavailability exhibited by some AMPs is in part due to their rapid proteolytic degradation *in vivo*[52]. The use of synthetic peptidomimetic

scaffolds, such as *N*-substituted glycines (peptoids), to mimic AMPs is one approach to capturing the desirable attributes of natural AMPs while circumventing their shortcomings.

Peptoids are synthetic, sequence-specific biomimetic polymers that differ from peptides in that the side chains are attached to the amide nitrogens rather than the α-carbons[3]. This subtle structural difference not only renders the peptoid backbone achiral, but the lack of available amide protons also precludes intrachain hydrogen bonding[11, 55]. It has been shown, however, that peptoids adopt a stable, polyproline-type-I-like helical secondary structure when bulky, homochiral side chains are incorporated into their sequences[55-57]. Peptoids exhibit a helical periodicity of approximately three monomers per turn and a pitch of 6.0 – 6.7 Å[11, 55-57], giving them a regular, modular structure amenable to elucidating structure-activity relationships. Furthermore, because the non-natural peptoid backbone is robust to protease activity[21, 58], peptoid-based AMP mimics (ampetoids) could enable the development of clinically useful anti-infectives with extended *in vivo* half-life and enhanced bioavailability compared to what AMPs have historically been able to achieve.

Previous work has shown that peptoids designed to mimic the structural and physicochemical properties of AMPs can exhibit potent antimicrobial activity[31, 32]. These ampetoids have been designed to mimic the class of short, cationic, amphipathic, and helical AMPs (*e.g*. magainins[59]), the simple structure of which is particularly amenable to biomimicy. Interestingly, however, previous studies suggest that while helicity is well-correlated with hemolytic activity, amphipathicity and hydrophobicity of AMPs are more directly related to selectivity for bacteria compared to mammalian cells[32]. The degree of helicity, therefore, has been thought to be an important attribute primarily because it affects how tightly the secondary structure is organized, and the overall resultant molecular amphipathicity.

One obstacle that could stand in the way of advancing both AMPs and their mimics through pharmaceutical development is insufficient target specificity[60]. Cell selectivity is influenced by characteristics of both the cells and the antimicrobial agent. Some measure of target selectivity results from the overall cationic charge of AMPs, which allows them to bind more favorably with the anionic outer membrane of bacterial cells compared with that of more neutral mammalian cells[61,62]. Membrane permeabilization by AMPs, however, is more heavily influenced by other properties including molecular amphipathicity and hydrophobicity[53, 63]. We have previously shown that these same three physicochemical properties (cationic charge, amphipathicity, and hydrophobicity) influence ampetoid activity and selectivity in an analogous manner[32]. Specifically, while potent, but non-selective AMPs and ampetoids tend to be highly hydrophobic[64, 65] and adopt well-defined amphipathic structures[65-67], more selective AMPs and ampetoids are typically highly cationic[68, 69], only moderately hydrophobic[70], and are customarily less amphipathic[70].

The several families of ampetoids reported here were designed not only to deepen our understanding of how these properties affect their antimicrobial activity and cell selectivity, but also to explore the effects of more subtle changes in molecular properties related to the number, position, arrangement, and chemical structure of substituted hydrophobic moities. We report that many of the 26 new ampetoids presented here demonstrate promising *in vitro* activity and selectivity against a variety of bacterial organisms, including clinically relevant, multi-drug resistant (MDR) strains. Moreover, the structure-activity relationships derived from this library of compounds reaffirm and extend the analogy between the mechanism of action of AMPs and ampetoids. Design heuristics to aid in the design of potent, yet selective, future generations of ampetoids are also established.

2.2 Results

2.2.1 Study design

We created several families of ampetoids with the goal of more fully exploring how and to what extent specific structural characteristics influence selectivity. All ampetoids were derived from the previously reported[31, 32] dodecamer, peptoid **1**, which is composed of 1/3 lysine-like charged monomers (*N*Lys) and 2/3 phenylalanine-like hydrophobic monomers (*N*spe) arranged in a repeating sequence H-(*N*Lys-*N*spe-*N*spe)$_4$-NH (**Figure 2.1**, **Table 2.1**). Families of molecules were designed to explore the importance of **(1)** primary sequence, **(2)** sequence register, **(3)** net charge, and **(4)** charge-to-length ratio (CTLR) on antimicrobial activities and cell selectivities. To evaluate the effects of different hydrophobic moieties, in four other families we systematically replaced one or more *N*spe monomers with other hydrophobic moieties: **(1)** *L*-proline monomers **(2)** achiral hydrophobic monomers, **(3)** opposite chirality hydrophobic monomers (*N*rpe), and **(4)** aliphatic hydrophobic monomers. Pexiganan, a widely studied and clinically-relevant AMP analog of magainin-2[71-73], was included in this study as a basis of comparison to AMPs.

Schematic structures showing the three-fold periodic architecture of peptoid **1** (the basis sequence) and ampetoid variants are shown in **Figure 2.1**. This representation is intended to clarify the design strategy and relationships among ampetoid variants discussed herein. The three molecular ampetoid faces discussed throughout this work are depicted as aligned monomers on the left, back, and right sides, as shown. The full sequence of each molecule is displayed in **Table 2-1**, along with other molecular properties including molecular weight, net charge, CTLR, and reversed-phase HPLC (RP-HPLC) solvent composition upon elution, as a measure of molecular hydrophobicity. In general, the naming convention for ameptoids includes the basis compound (**1**, in most cases) followed by a description of how the sequence was modified compared to the basis compound. For example, compound **1**B-*N*Lys$_{4,10}$ describes a

variant based on the sequence of **1**B in which *N*Lys monomers were substituted at positions 4 and 10.

The activities of all compounds against bacterial strains and mammalian cells are summarized in **Table 2-2**. The potencies of all compounds were determined against representative Gram-negative (*E. coli* ATCC 35218) and Gram-positive (*B. subtilis* ATCC 6633) biosafety level 1 (BSL1) organisms. In addition to hemolytic activity, the conventional measure of toxicity to mammalian cells, we also report the effect of each ampetoid on NIH 3T3 mouse fibroblast cells using the MTS tetrazolium salt-based colorimetric assay. While hemolysis measures the degree to which erythrocytes are lysed, the MTS assay indirectly quantifies the extent to which cellular metabolic activity is inhibited.

Because the range of hemolytic activities displayed by these molecules is significantly greater than that of inhibitory activities, hemolysis assays provide a more sensitive gauge of activity against mammalian cells. Therefore, the selectivity of each ampetoid for various bacterial strains compared to erythrocytes is reported as the selectivity ratio (SR), which is defined as the quotient of the 10% hemolytic dose and the minimum inhibitory concentration (MIC) for each bacterial strain.

2.2.2 Initial screening of activity and selectivity

The ampetoids in this library exhibited antibacterial potencies against Gram-negative *E. coli* that ranged from 3.1 μM to > 100 μM. Likewise, hemolytic activity ranged from HD_{10} = 16 μM to HD_{10} > 200 μM and metabolic inhibitory activity from ID_{50} = 4.9 μM to ID_{50} > 100 μM. The breadth of activities and selectivities evidenced by these compounds suggests that this library was well designed to effect a range of responses, which is important for elucidating structure-activity relationships. Compared to **1** ($SR_{E.\ coli}$, = 3.3), 17 of the 26 ampetoid variants demonstrate improved selectivity for *E. coli (*$SR_{E.\ coli}$ = 6.8 – 26). Four ampetoids (**1**-*N*$pm_{2,5,8,11}$,

1$_{11mer}$, **1**$_{ach}$-*N*spe$_2$, **1**$_{ach}$-*N*spe$_{12}$) exhibited equivalent activity (6.3 μM) and superior selectivity ($SR_{E.\ coli}$ = 14 – 26) compared to pexiganan ($SR_{E.\ coli}$ = 11). In comparison to their activities against *E. coli*, all oligomers were more potent against *B. subtilis*, with MICs ranging from 0.78 to 1.6 μM. Corresponding selectivity ratios were as high as > 256.

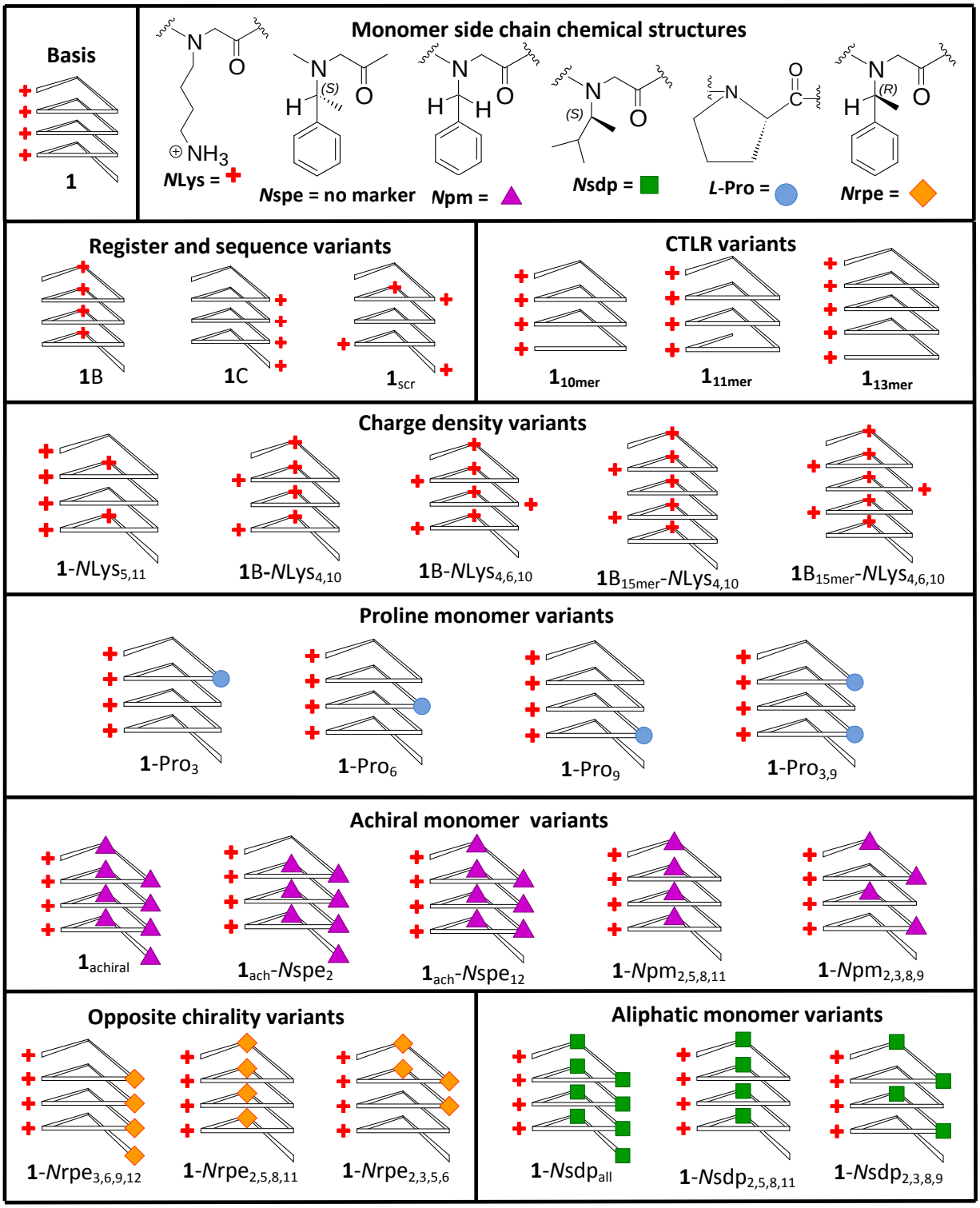

Figure 2.1: Schematics of ameptoid variants and side chain structures. Note that the schematics shown here are for visualization purposes only and not intended to imply the actual folding behavior of each molecule. Points on the triangular helicies that have no marker are *N*spe monomers.

	Compound	MW	Sequence	HPLC elution (% ACN)*	Net Charge	CTLR[§]
Comparators	**1**	1819	H-(*N*Lys-*N*spe-*N*spe)$_4$-NH$_2$	65.1	+4	0.33
	Pexiganan	2477	GIGKFLKKAKKFGKAFVKILKK-NH$_2$	50.2	+9	0.41
Register & sequence variants	**1**B	1819	H-(*N*spe-*N*Lys-*N*spe)$_4$-NH$_2$	63.4	+4	0.33
	1C	1819	H-(*N*spe-*N*spe-*N*Lys)$_4$-NH$_2$	64.8	+4	0.33
	1scr	1819	H-(*N*spe)$_2$-(*N*Lys-*N*spe)$_3$-(*N*spe)$_3$-*N*Lys-NH$_2$	61.1	+4	0.33
Increased charge variants	1-*N*Lys$_{5,11}$	1753	H-(*N*Lys-*N*spe-*N*spe-*N*Lys-*N*Lys-*N*spe)$_2$-NH$_2$	51.2	+6	0.50
	1B-*N*Lys$_{4,10}$	1753	H-(*N*spe-*N*Lys-*N*spe-*N*Lys-*N*Lys-*N*spe)$_2$-NH$_2$	52.7	+6	0.50
	1B-*N*Lys$_{4,6,10}$	1720	H-(*N*spe-*N*Lys)$_2$-*N*Lys$_2$-(*N*spe-*N*Lys)$_2$-*N*Lys-*N*spe)-NH$_2$	45.4	+7	0.58
	1B$_{15mer}$-*N*Lys$_{4,10}$	2204	H-(*N*spe-*N*Lys-*N*spe-*N*Lys-*N*Lys-*N*spe)$_2$-*N*spe-*N*Lys-*N*spe-NH$_2$	55.5	+7	0.47
	1B$_{15mer}$-*N*Lys$_{4,6,10}$	2171	H-(*N*spe-*N*Lys)$_2$-*N*Lys$_2$-(*N*spe-*N*Lys)$_2$-*N*Lys-*N*spe$_2$-*N*Lys-Nspe-NH$_2$	50.8	+8	0.53
Length variants	**1**$_{10mer}$	1497	H-(*N*Lys-*N*spe-*N*spe)$_3$-*N*Lys-NH$_2$	60.9	+4	0.40
	1$_{11mer}$	1658	H-(*N*Lys-*N*spe-*N*spe)$_3$-*N*Lys-*N*spe-NH$_2$	63.5	+4	0.36
	1$_{13mer}$	1948	H-(*N*Lys-*N*spe-*N*spe)$_4$-*N*Lys-NH$_2$	62.8	+5	0.38
Proline containing variants	**1**-Pro$_3$	1755	H-*N*Lys-*N*spe-L-Pro-(*N*Lys-*N*spe-*N*spe)$_3$-NH$_2$	63.0	+4	0.33
	1-Pro$_6$	1755	H-*N*Lys-*N*spe$_2$-*N*Lys-*N*spe-L-Pro-(*N*Lys-*N*spe$_2$)$_2$-NH$_2$	62.4	+4	0.33
	1-Pro$_9$	1755	H-(*N*Lys-*N*spe$_2$)$_2$-*N*Lys-*N*spe-L-Pro-(*N*Lys-*N*spe$_2$)-NH$_2$	62.6	+4	0.33
	1-Pro$_{3,9}$	1691	H-(*N*Lys-*N*spe-L-Pro-*N*Lys-*N*spe-Nspe)$_2$-NH$_2$	58.1	+4	0.33
Chirality variants	**1**-*N*rpe$_{3.6.9.12}$	1819	H-(*N*Lys-*N*spe-*N*rpe)$_4$-NH$_2$	63.5	+4	0.33
	1-*N*rpe$_{2,5,8,11}$	1819	H-(*N*Lys-*N*rpe-*N*spe)$_4$-NH$_2$	66.4	+4	0.33
	1-*N*rpe $_{2,3,5,6}$	1819	H-(*N*Lys-*N*rpe-*N*rpe)$_2$-(*N*Lys-*N*spe-*N*spe)$_2$-NH$_2$	65.0	+4	0.33
Achiral variants	**1**$_{ach}$	1701	H-(*N*Lys-*N*pm-*N*pm)$_4$-NH$_2$	59.8	+4	0.33
	1$_{ach}$-*N*spe$_2$	1721	H-(*N*Lys-*N*spe-*N*pm)-(*N*Lys-*N*pm-*N*pm)$_3$-NH$_2$	60.8	+4	0.33
	1$_{ach}$-*N*spe$_{12}$	1721	H-(*N*Lys-*N*pm-*N*pm)$_3$-(*N*Lys-*N*pm-*N*spe)-NH$_2$	62.0	+4	0.33
	1-*N*pm$_{2,3,8,9}$	1763	H-(*N*Lys-*N*pm-*N*pm-*N*Lys-*N*spe-*N*spe)$_2$-NH$_2$	63.3	+4	0.33
	1-*N*pm$_{2,5,8,11}$	1763	H-(*N*Lys-*N*pm-*N*spe)$_4$-NH$_2$	63.6	+4	0.33
Aliphatic variants	**1**-*N*sdp$_{all}$	1547	H-(*N*Lys-*N*sdp-*N*sdp)$_4$-NH$_2$	63.2	+4	0.33
	1-*N*sdp$_{2,3,8,9}$	1683	H-(*N*Lys-*N*sdp-*N*sdp-*N*Lys-*N*spe-*N*spe)$_2$-NH$_2$	64.7	+4	0.33
	1-*N*sdp$_{2.5.8.11}$	1683	H-(*N*Lys-*N*sdp-*N*spe)$_4$-NH$_2$	63.8	+4	0.33

Table 2-1: Sequence and molecular properties of ampetoids and comparator peptide pexiganan. See **Figure 2.1** for the structures of the peptoid monomers indicated in each sequence. HPLC elution is reported as the average percentage of acetonitrile in the solvent mixture upon compound elution for three injections. A linear acetonitrile/water (0.1% trifluoroacetic acid) gradient of 5% - 95% acetonitrile over 45 minutes was run on a C18 column. [§] CTLR stands for charge-to-length ratio, which is defined as the ratio of the total number of charged monomers to the total number of monomers in each sequence.

		Antimicrobial Activity		Mammalian Cell Activity		Selectivity Ratios*	
	Compound	*E. coli* MIC	*B. subtilis*	HD_{10} / HD_{50}	ID_{50}	$SR_{E.\ coli}$	$SR_{B.\ subtilis}$
Comparative Molecules	**1**	6.3	1.6	21 / 100	5.1	3.3	13
	Pexiganan	6.3	1.6	70 / >200	9	11	44
Register & sequence variants	**1**B	6.3	1.6	55 / > 100	4.9	8.7	34
	1C	6.3	1.6	25 / > 100	5.6	4.0	16
	1scr	6.3	1.6	64 / > 200	8.5	10	40
Increased net charge variants	1-*N*Lys$_{5,11}$	50	1.6	>100 / >100	85	> 2	> 63
	1B-*N*Lys$_{4,10}$	50	0.78	>200 / >200	83	> 4	> 256
	1B-*N*Lys$_{4,6,10}$	> 100	1.6	>200 / >200	> 100	Inactive	> 125
	1B$_{15mer}$-*N*Lys $_{4,10}$	50	0.78	>200 / >200	16	> 4	> 256
	1B$_{15mer}$-*N*Lys $_{4,6,10}$	> 100	0.78	>200 / >200	40	Inactive	256
Length variants	**1$_{10mer}$**	12.5	0.78	>200 / >200	54	> 16	> 256
	1$_{11mer}$	6.3	0.78	103 / > 200	11	16	132
	1$_{13mer}$	3.1	0.78	21 / > 100	5.6	6.8	27
Proline containing variants	**1**-Pro$_3$	12.5	1.6	74 / > 200	12	5.9	46
	1-Pro$_6$	12.5	1.6	83 / > 200	18	6.6	52
	1-Pro$_9$	12.5	1.6	165 / > 200	24	13	103
	1-Pro$_{3,9}$	50	1.6	>200 / >200	71	4.0	125
Chirality variants	**1**-*N*rpe$_{3,6,9,12}$	6.3	1.6	16 / 67	3.8	2.5	10
	1-*N*rpe$_{2,5,8,11}$	6.3	1.6	22 / 95	5.2	3.5	14
	1-*N*rpe $_{2,3,5,6}$	6.3	0.78	25 / 96	4.8	4.0	32
Achiral variants	**1**$_{ach}$	12.5	0.78	183 / > 200	16	15	235
	1$_{ach}$-*N*spe$_2$	6.3	0.78	160 / > 200	11	25	205
	1$_{ach}$-*N*spe$_{12}$	6.3	1.6	164 / > 200	15	26	103
	1-*N*pm$_{2,3,8,9}$	6.3	1.6	39 / > 200	15	6.2	24
	1-*N*pm$_{2,5,8,11}$	6.3	1.6	87 / > 200	6.8	14	54
Aliphatic variants	**1**-*N*sdp$_{all}$	25	0.78	>200 / >200	64	> 8	256
	1-*N*sdp$_{2,3,8,9}$	12.5	0.78	77 / > 200	19	6.2	99
	1-*N*sdp$_{2.5.8.11}$	12.5	0.78	111 / > 200	20	9.7	142

Table 2-2: Activity of ampetoids and pexiganan against bacteria and mammalian cells. Presented are the minimum inhibitory concentrations (MICs) against *E. coli* (ATCC 35218) and *B. subtilis* (ATCC 6633), 10% and 50% hemolytic doses (HD), and 50% inhibitory doses (ID) against NIH 3T3 mouse fibroblast cells. *Selectivity ratio (SR) is defined as the ratio of the 10% hemolytic dose to the MIC for the bacterial strain of interest.

2.2.3 Structure-activity studies

The secondary structure of ampetoids was evaluated using circular dichroism (CD) spectroscopy in 10 mM Tris buffer (pH 7.4) and the same buffer containing small unilamellar vesicles (SUVs) comprised of either POPC/cholesterol (2:1 mole ratio) or POPE/POPG (7:3 mole ratio). Whereas the POPC/cholesterol mixture is a zwitterionic binary model lipid preparation that mimics the membrane of erythrocytes[74], the negatively charged POPE/POPG mixture mimics the composition of the *E. coli* outer membrane[75]. A peptoid composed of aromatic right handed poly-proline-type-I-like helix exhibits spectral features including a maximum at 192 nm and two local minima at ~ 202 nm and ~220 nm, respectively[11].

2.2.3.1 Register and sequence variants.

Peptoid **1**, with a periodic trimer repeat sequence of *N*Lys-*N*spe-*N*spe, is composed of four facially-aligned *N*Lys monomers (positions 1, 4, 7, and 10) along the left molecular face and has a charged *N*-terminal monomer, as shown in **Figure 2.1**. We made two isomeric variants in which the sequence register was modified, a change that most overtly affects the relative position of monomers with respect to the terminal positions. Peptoid **1**B has a trimer repeat of *N*spe-*N*Lys-*N*spe, exhibits charged monomers along the back face (positions 2, 5, 8, and 11) and has hydrophobic moieties at both termini. Ampetoid **1**C exhibits a sequence register of *N*spe-*N*spe-*N*Lys, has charged monomers along the right face (positions 3, 6, 9, and 12), and has a charged monomer at the *C*-terminal position (see **Figure 2.1**). The last variant in this family is a "scrambled" isomer, $\mathbf{1}_{scr}$, which was made with a non-periodic sequence in which the four charged monomers are distributed across all three molecular faces (**Figure 2.1**).

The antimicrobial potencies against *E. coli* (MIC = 6.3 µM) and *B. subtilis* (MIC = 1.6 µM) of all three variants were the same as for **1**, and their toxicities to NIH 3T3 cells were also similar, with ID_{50} values ranging from 4.9 – 5.6 µM. The hemolytic activity, however, was reduced for $\mathbf{1}_{scr}$ (HD_{10} = 64 µM) and **1**B (HD_{10} = 55 µM) compared to **1** (HD_{10} = 21 µM) and **1**C (HD_{10} = 25 µM). As a result, the selectivities for $\mathbf{1}_{scr}$ ($SR_{E.\ coli}$ = 10) and **1**B ($SR_{E.\ coli}$ = 8.7) were

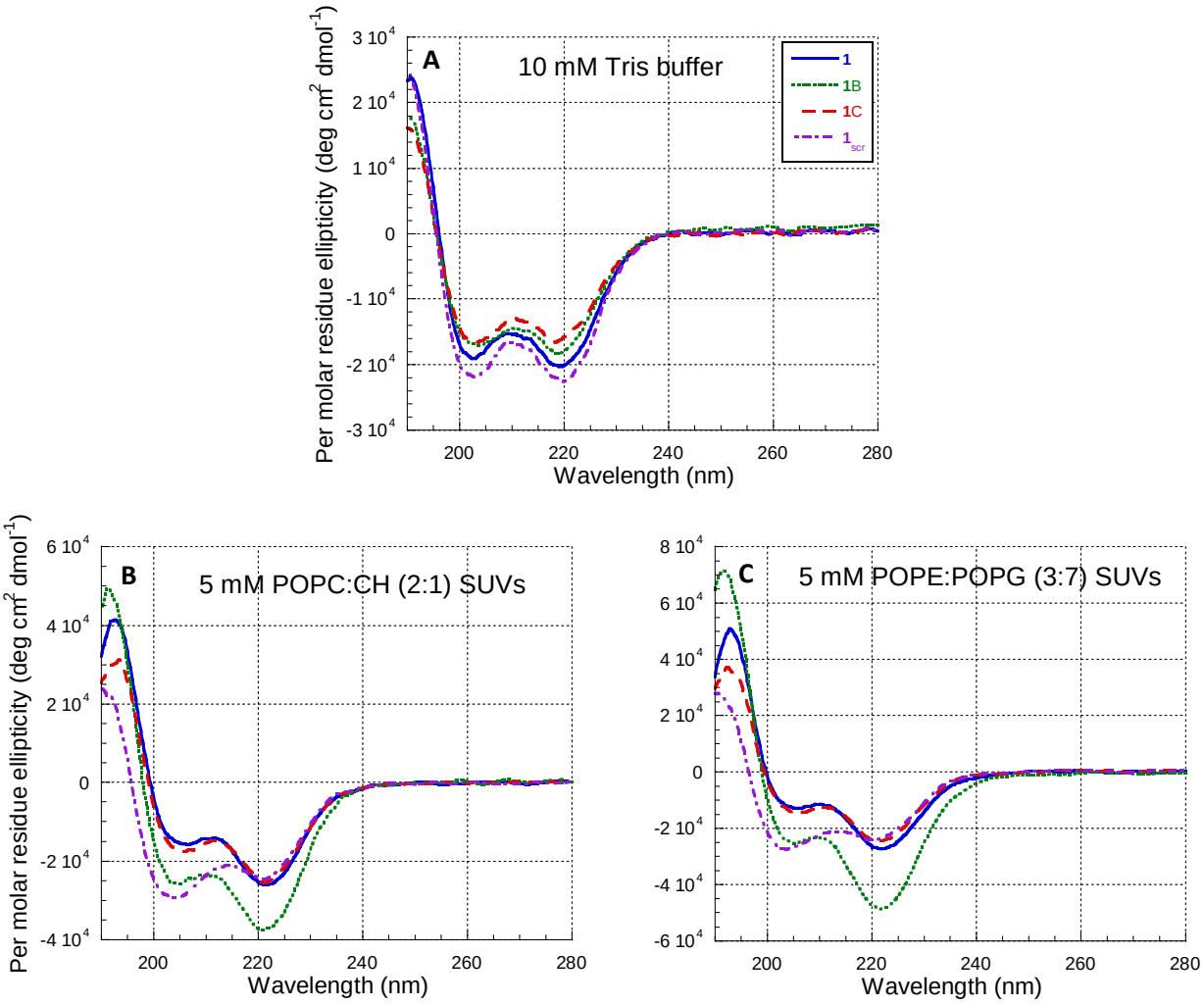

Figure 2.2: CD spectra of ampetoid register and sequence variants. Ampetoid concentrations were 60 µM. (**A**) CD in 10 mM Tris buffer (pH 7.4) (**B**) CD spectra in 10 mM Tris buffer with 5mM erythrocyte-mimetic POPC:cholesterol (2:1) SUVs. (**C**) CD in 10 mM Tris buffer with 5 mM bacteria-mimetic POPE:POPG (3:7) SUVs.

more favorable in comparison to **1** ($SR_{E.\ coli}$ = 3.3) and **1**C ($SR_{E.\ coli}$ = 4.0).

CD spectroscopy showed that all these variants exhibited helicity in 10 mM Tris buffer similar to that of **1**, with $\mathbf{1}_{scr}$ being slightly more helical and **1**C, slightly less (**Figure 2.2A**). In both POPC/cholesterol and POPE/POPG lipids, however, **1**B exhibited significantly increased helical intensity at 220 nm compared to the other variants (**Figure 2.2 B**, **C)**. By nature of its scrambled sequence design, the extent of helicity for $\mathbf{1}_{scr}$ is decoupled from its degree of amphipathicity; the distribution of charges on all three molecular faces reduces its amphipathicity regardless of a three-fold periodic helical architecture. It is possible that the reduced intramolecular electrostatic repulsion of side chain moieties along a given molecular face in $\mathbf{1}_{scr}$ readily accommodates a more helical secondary structure, despite its overall reduced amphipathicity. Based on previous studies, reduction in amphipathicity can improve selectivity without compromising antimicrobial activity[32]. Indeed, $\mathbf{1}_{scr}$ exhibits improved selectivity ($SR_{E.\ coli}$ = 10) compared to **1** ($SR_{E.\ coli}$ = 3.3) with no reduction in antimicrobial activity ($MIC_{E.\ coli}$ = 6.3 µM for both molecules).

2.2.3.2 Charge density variants.

A second family of ampetoids was designed to evaluate the effect of increased charge density on potency and selectivity (**Figure 2.1**). Structure-activity relationships derived from ampetoid variants with decreased net charge were found to significantly reduce their selectivity for bacteria[32], likely due to the less favorable electrostatic interaction with negatively charged bacterial membranes. The variants in this family of ampetoids were designed to explore the effect of increasing net charge and charge-to-length-ratio (CTLR) on cell selectivity. Ampetoid **1**, and most other variants in this library, have a net charge of +4 and CTLR of 0.33. These compounds exhibit net charges ranging from +6 to +8, and CTLRs ranging from 0.47 – 0.58. Additionally, the hydrophobicities of these compounds (ranging from 45.4% to 55.5% acetonitrile

upon HPLC elution) were all significantly reduced compared to **1** (65.1%) (**Table 2-1**). **1**-*N*Lys$_{5,11}$ has a total of six positive charges with two additional *N*Lys monomers (compared to **1**) substituted at positions 5 and 11, which are aligned along a back face of the helix (**Figure 2.1**). **1**B-*N*Lys$_{4,10}$ is an isomeric variant of **1**-*N*Lys$_{5,11}$ with the sequence register of **1**B, and **1**B-*N*Lys$_{4,6,10}$ similarly has a net charge of +7 with cationic charge on all three molecular faces. Longer 15mer variants, **1**B$_{15mer}$-*N*Lys$_{4,10}$ and **1**B$_{15mer}$-*N*Lys$_{4,6,10}$, were also made with an additional (*N*spe-*N*Lys-*N*spe) turn on the *C*-terminus, giving them net charges of +7 and +8, respectively (**Figure 2.1**).

All variants in this family were significantly less active against *E. coli* (MIC = 50 - >100 μM) and were non-hemolytic (HD_{10} > 100 μM), a result largely effected by the reduced hydrophobicity of these variants compared to **1**. Because this family of variants does not exhibit a broad range of selectivities ($SR_{E.\ coli}$ > 2 to > 4), elucidating a meaningful relationship between physicochemical properties and selectivity is difficult. A general trend observed, however, is that variants with a CTLR of less than ~ 0.50, hydrophobicity greater than ~50% acetonitrile, and one completely hydrophobic face (**1**-*N*Lys$_{5,11}$, **1**B-*N*Lys$_{4,10}$, and **1**B$_{15mer}$-*N*Lys$_{4,10}$) exhibited weak activity ($MIC_{E\ coli}$ = 50 μM). Variants with CTLRs greater than ~ 0.50, hydrophobicity less than ~ 50% acetonitrile, and had charges distributed on all three molecular faces (**1**B-*N*Lys$_{4,6,10}$ and **1**B$_{15mer}$-*N*Lys$_{4,6,10}$) were completely inactive ($MIC_{E\ coli}$ > 100 μM). These results are commensurate with structure activity relationships previously established for both AMPs, and ampetoids[32]: (**1**) antimicrobial oligomers must be sufficiently hydrophobic to be potent against Gram-negative bacteria, and (**2**) highly charged and poorly amphipathic structures are generally selective.

It is most notable that the reduction in activity against *E. coli* exhibited by this family of molecules did not carry over to their activities against *B. subtilis*. Despite the marked change in

physicochemical properties (NC as high as +8, hydrophobicity as low as 45.4% acetonitrile, and CTLR as high as 0.58) exhibited by this family of molecules compared to **1** (NC = +4, hydrophobicity = 65.1%, and CTLR = 0.33), the MICs of these variants against *B. subtilis* were very similar to that of **1**, ranging from 0.78 – 1.6 µM. The resultant selectivity ratios of molecules in this library for *B. subtilis* were among the highest of all compounds tested ($SR_{B.\ subtilis}$ > 256).

The CD spectra in **Figure 2.3** show that, with the exception of **1**B-*N*Lys$_{4,6,10}$, all compounds exhibited helicity similar to that of **1** in 10 mM Tris buffer. In POPC/cholesterol lipids, however, helicity was inversely related to CTLR, and concomitantly, achiral monomer content. The effect of increased achiral monomer content on peptoid CD spectra is demonstrated plainly in the hydrophobic environment of lipid vesicles; as shown in **Figure 2.3B**, increased achiral monomer content reduced overall CD signal intensity, particularly at 220 nm.

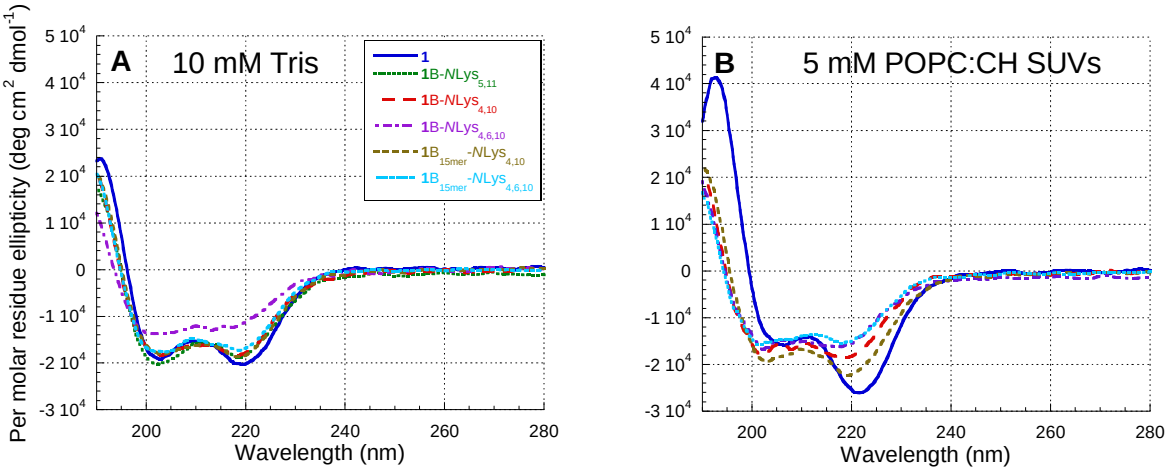

Figure 2.3: CD spectra of net charge variants in (**A**) 10 mM Tris buffer and (**B**) same buffer with 5 mM POPC/cholesterol 2:1 SUVs. Ampetoid concentration is 60 µM.

2.2.3.3 CTLR variants.

We explored variants of the dodecameric peptoid **1** that ranged in length from 10-13 monomers as shown in **Figure 2.1** and **Table 2-1**. Previous studies that explored ampetoid length variants with a constant CTLR (**1**$_{6mer}$, **1**$_{9mer}$, and **1**$_{15mer}$) showed that increased length beyond 12 monomers (ampetoid **1**) only increased hemolytic activity without improving

antimicrobial potency[32]. The variants in this study, **1**$_{10mer}$, **1**$_{11mer}$, **1**, and **1**$_{13mer}$ exhibit small differences in sequence length, but most notably effect a range of CTLRs (0.33 – 0.40). This range of CTLR is significantly lower compared to the range exhibited by charge density variants (0.47 – 0.58). The CD spectra shown in **Figure 2.4** suggest that in both aqueous buffer and lipid environments, all variants are similarly helical, and therefore exhibit similar amphipathicities.

Considering first only those variants with a net charge of +4 (**1**$_{10mer}$, **1**$_{11mer}$, **1**), both hydrophobicity, and CTLR scale monotonically with length. Ampetoid **1** (12mer) is the most hydrophobic (65.1% acetonitrile) and exhibits the lowest CTLR (0.33), while **1**$_{10mer}$ is the least hydrophobic (60.9% acetonitrile) and is characterized by the highest CTLR (0.40). The data in **Table 2-1** show that cell selectivity is directly related to CTLR and inversely related to hydrophobicity. The slight reduction in activity of **1**$_{10mer}$ against *E. coli* (12.5 μM), (a result of its lowered hydrophobicity), was accompanied by a much larger improvement in its hemolytic activity (HD_{10} > 200 μM); **1**$_{10mer}$ is therefore the most selective of this group ($SR_{E.\ coli}$ > 16). **1**$_{11mer}$ retained antimicrobial activity equivalent to that of **1** ($MIC_{E.\ coli}$ 6.3 μM), but was less selective than **1**$_{10mer}$ ($SR_{E.\ coli}$ = 16). Ampetoid **1** was found to be the least selective ($SR_{E.\ coli}$ = 3.3). The same trend was observed for selectivity against *B. subtilis* (**Table 2-2**).

It is notable that based on the above correlation, **1**$_{13mer}$ (CTLR of 0.38) would be expected to have an improved selectivity compared to **1**$_{11mer}$ (CTLR = 0.36), however this is not the case. On the contrary, ampetoid **1**$_{11mer}$ ($SR_{E.\ coli}$ = 16) is more selective than **1**$_{13mer}$ ($SR_{E.\ coli}$ = 6.8). This is likely attributable to the fact that while **1**$_{10mer}$, **1**$_{11mer}$, and **1** all have a net charge of +4, that of **1**$_{13mer}$ is increased to +5. As discussed previously, net charge can affect cell selectivity, particularly against Gram-negative strains. **1**$_{11mer}$, with a CTLR of 0.36 and net charge of +4 represents the optimum balance of potent antimicrobial activity and cell selectivity

from this group of molecules. However, the selectivity ratios of **1**$_{10mer}$ ($SR_{E.\ coli}$ > 16), **1**$_{11mer}$ ($SR_{E.\ coli}$ = 16), and **1**$_{13mer}$ ($SR_{E.\ coli}$ = 6.8) are all superior to that of **1** ($SR_{E.\ coli}$ = 3.3).

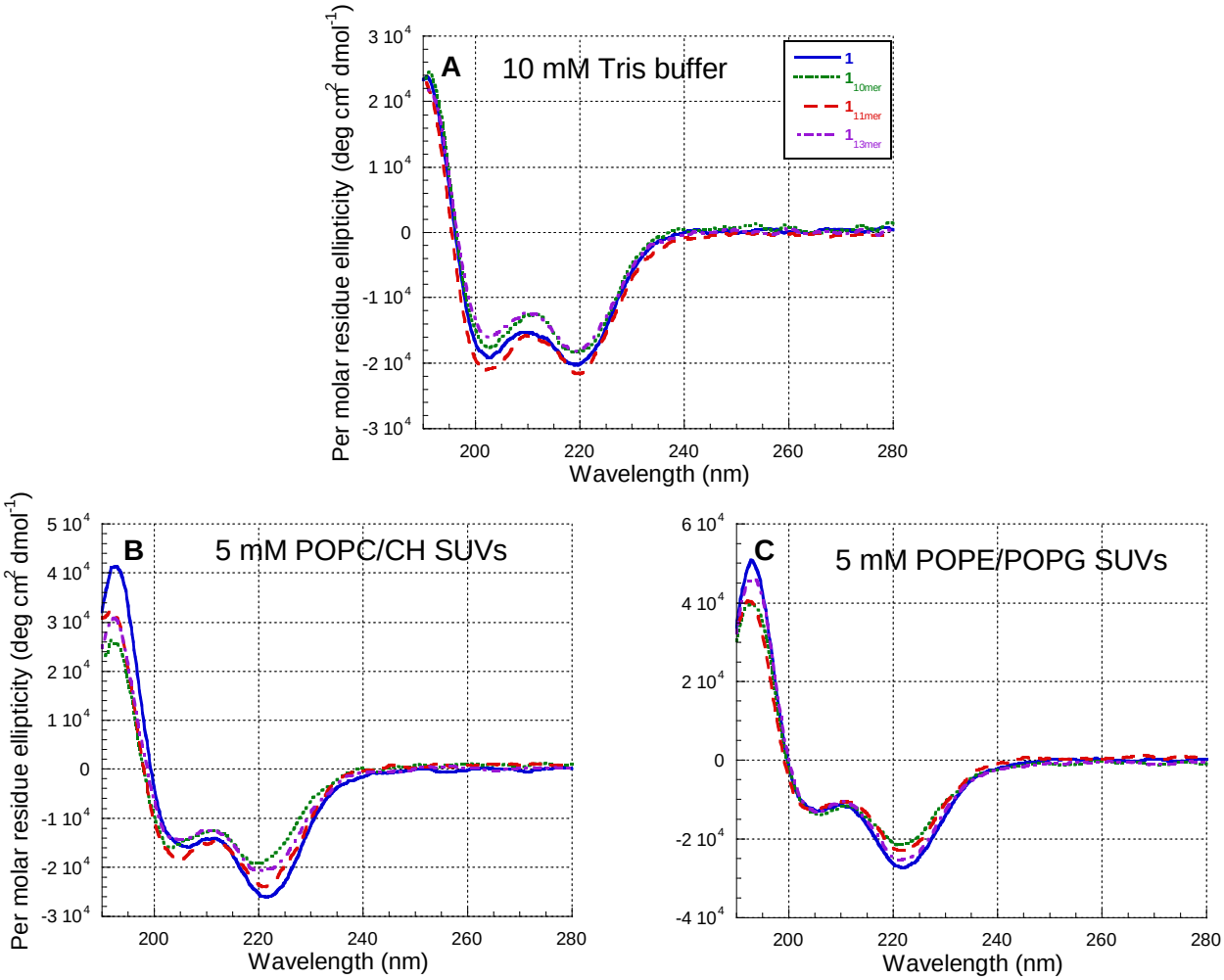

Figure 2.4: CD spectra of length variants in (**A**) 10 mM Tris buffer and (**B**) same buffer with 5 mM POPC/cholesterol 2:1 SUVs and (**C**) same buffer with 5 mM POPE/POPG 3:7 SUVs. Ampetoid concentration is 60 µM.

2.2.3.4 L-proline substitution variants.

While proline monomers in naturally-occurring AMPs are known to destabilize α-helical secondary structure and induce the formation of helix-bend-helix motifs[76], we have shown that proline is well accommodated in the polyproline type-I-like peptoid helical architecture[32]. Because of proline's reduced hydrophobicity compared to *N*spe, substituting *L*-proline for a centrally-located hydrophobic residue in ampetoid **1**'s sequence (variant called **1**-Pro$_6$) was

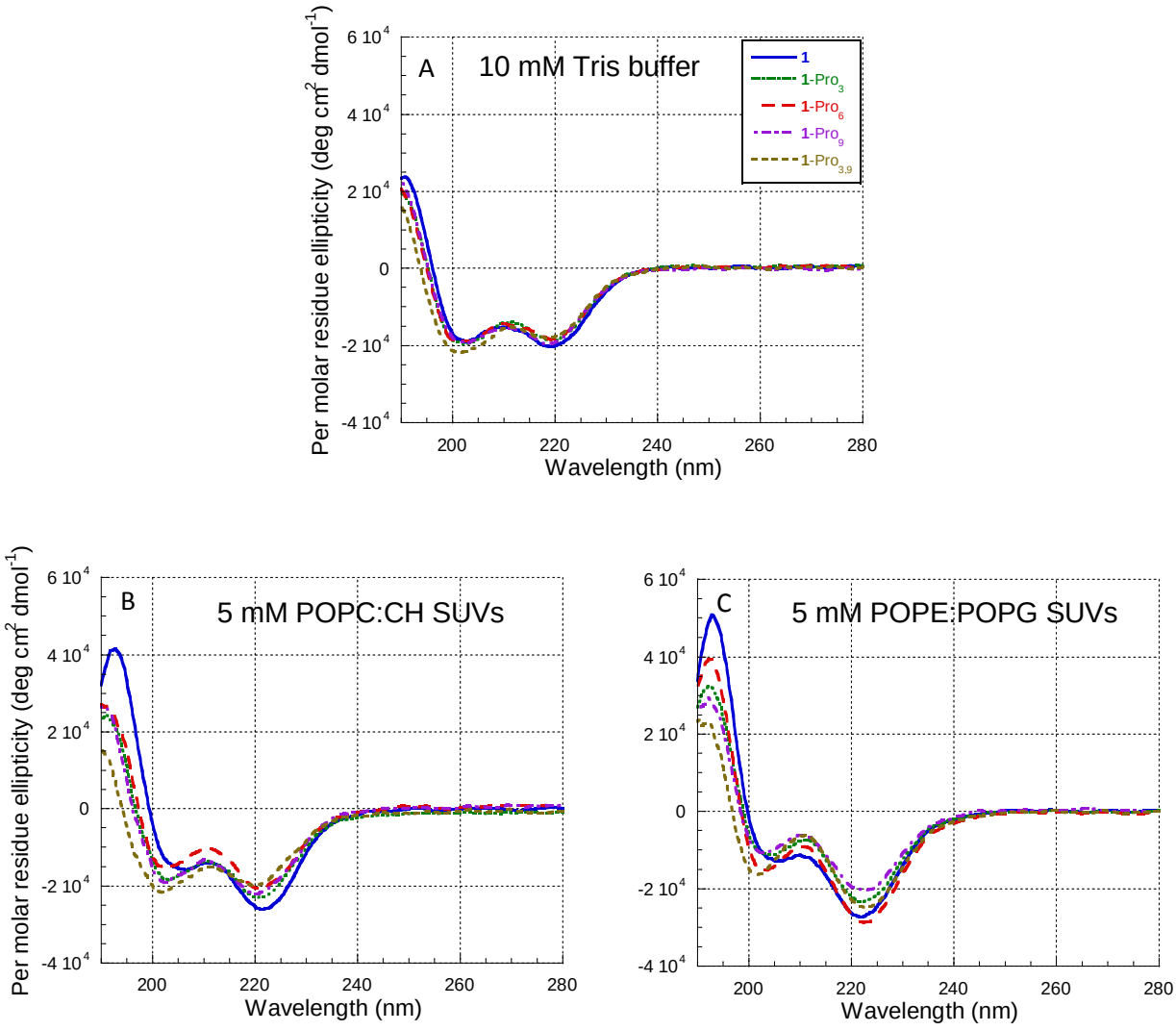

Figure 2.5: CD spectra of proline variants in (**A**) 10 mM Tris buffer and (**B**) same buffer with 5 mM POPC/cholesterol 2:1 SUVs and (**C**) same buffer with 5 mM POPE/POPG 3:7 SUVs. Ampetoid concentration is 60 µM.

found to lower molecular hydrophobicity and improve selectivity[32]. We designed a family of molecules to evaluate how the relative position and number of proline monomers affects potency and selectivity, while maintaining constant CTLR and helicity. Similar to **1**-Pro_6, **1**-Pro_3 and **1**-Pro_9 have a single proline monomer substituted into the third and ninth positions of the ampetoid **1** sequence, respectively. A fourth variant, **1**-$Pro_{3,9}$ incorporates two substituted proline monomers (**Figure 2.1** and **Table 2-1**). The relative hydrophobicities of **1**-Pro_3, **1**-Pro_6, and **1**-Pro_9 are all similar (62.4% - 63%), and reduced compared to **1** (65.1%); **1**-$Pro_{3,9}$ was found to be even less hydrophobic (58.1%). CD spectroscopy in Tris buffer and both zwitterionic and anionic lipids show that proline-containing ampetoids exhibit a similar degree of helicity as does **1** (**Figure 2.5**).

The activity of these variants against *E. coli* scales with hydrophobicity; **1**-Pro_3, **1**-Pro_6, and **1**-Pro_9 exhibited uniformly reduced potencies against *E. coli* (12.5 μM) compared to peptoid **1** (6.3 μM). The potency of **1**-$Pro_{3,9}$ was lessened further against *E. coli* (50 μM). Because these variants also exhibited reduced activity against mammalian cells, selectivity was improved for all the mono-substituted variants ($SR_{E.\ coli}$ = 5.9 – 13) compared to **1** ($SR_{E.\ coli}$ = 3.3).

The most intriguing observation regarding the mono-substituted proline-containing variants is that the relative position of the proline monomer in the sequence affected cell selectivity. **1**-Pro_3, **1**-Pro_6 , **1**-Pro_9 comprise a family of molecules in which CTLR, net charge, and hydrophobicity are held constant. Moreover, the degree of amphipathicity among these variants is similar, based on the similarity of their CD spectra in both aqueous buffer and lipid environments (**Figure 2.5**). Notably, however, shifting the proline from the *N*- to the *C*-terminal region resulted in a progressive increase in selectivity against both erythrocytes and NIH 3T3 cells (**Table 2-2**); whereas **1**-Pro_3 had an HD_{10} = 74 μM and ID_{50} = 12 μM, those of **1**-Pro_9 were 165 μM and 24 μM, respectively. The resultant selectivities monotonically increased from **1**-

Pro_3 ($SR_{E.\ coli}$ = 5.9), to **1**-Pro_6 ($SR_{E.coli}$ = 6.6) to **1**-Pro_9 ($SR_{E.\ coli}$ = 13). A similar trend was observed for selectivity ratios against *B. subtilis*. This suggests that ampetoids may have a preferred orientation upon interacting with mammalian cells. If, for example ampetoids interact with mammalian cells preferentially in the *C*-terminal region, reducing hydrophobicity specifically in that portion of the molecule could impair its activity against mammalian cells and increase selectivity.

2.2.3.5 Achiral monomer variants.

As another strategy for improving selectivity, we created a family of ampetoids with less

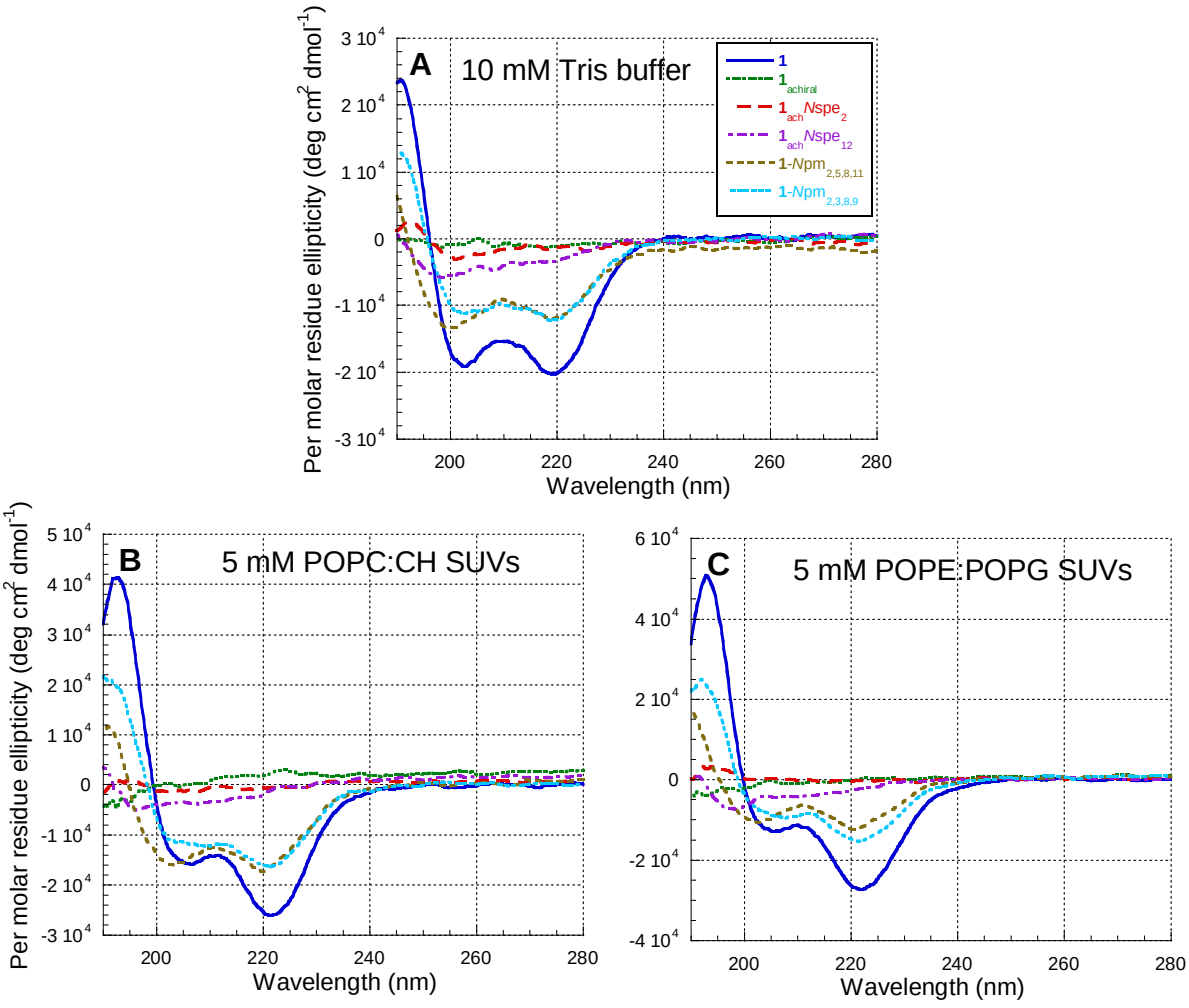

Figure 2.6: CD spectra of ampetoids containing achiral monomers in (**A**) 10 mM Tris buffer and (**B**) same buffer with 5 mM POPC/cholesterol 2:1 SUVs and (**C**) same buffer with 5 mM POPE/POPG 3:7 SUVs. Ampetoid concentration was 60 µM.

hydrophobic, achiral *N*pm side chains in place of selected *N*spe monomers in ampetoid **1** (**Figure 2.1** and **Table 2-1**). Because molecular chirality of peptoids is derived from the chirality of the side chains rather than that of the backbone, a change in the number of chiral monomers is expected to affect the stability of the secondary structure. This family of molecules, therefore, was designed to effect a range of decreased hydrophobicities and helicities compared to **1**, independent of any change in CTLR and net charge constant. $\mathbf{1}_{achiral}$ has all eight *N*spe monomers replaced with *N*pm. Two variants, $\mathbf{1}_{ach}$-*N*spe$_2$ and $\mathbf{1}_{ach}$-*N*spe$_{12}$ each have only one chiral *N*spe monomer at the second and twelfth positions, respectively. Two other ampetoids each contain four achiral *N*pm's, either aligned along the back molecular face (**1**-*N*pm$_{2,5,8,11}$), or distributed across both hydrophobic molecular faces (**1**-*N*pm$_{2,3,8,9}$) (**Figure 2.1**).

The hydrophobicities of these compounds ranged from 59.8% for $\mathbf{1}_{achiral}$ to 65.1% for peptoid **1** and generally increased with *N*spe content. Moreover, as shown in **Figure 2.6**, the intensity of the helical signal, which is correlated with amphipathicity, decreased with *N*spe content. The CD spectrum of $\mathbf{1}_{achiral}$ is flat, which suggests a lack of stable secondary structure and reduced molecular amphipathicity, while that of **1** exhibits the most intense spectral extrema, and correspondingly, the most amphipathic structure. Interestingly, $\mathbf{1}_{ach}$-*N*spe$_{12}$ showed slightly more intense CD spectra than isomerically related $\mathbf{1}_{ach}$-*N*spe$_2$, an observation that further supports a previous finding that the *C*-terminal position plays a particularly important role in stabilizing peptoid helical structure[57].

All variants with achiral side chains exhibit activities similar to peptoid **1** against *E. coli* (MIC = 6.3 – 12.5 μM) and *B. subtilis* (MIC = 0.78 – 1.6 μM), yet have substantially higher selectivities for bacteria over mammalian cells ($SR_{E.\ coli}$ = 6.2 – 26; $SR_{B.\ subtilis}$ = 24 – 235) (**Table 2-2**). In general, selectivity increased with *N*pm content, a monomer substitution for *N*spe that simultaneously decreases amphipathicity and hydrophobicity.

This family of variants provides further insight into how hydrophobicity and helicity impact potency and selectivity. Previous studies have shown that variants designed to be less hydrophobic, (via incorporation of more polar histidine-like side chains (*e.g.* **1**-*N*$His_{6,12}$) or less hydrophobic L-proline monomers (*e.g.* **1**-Pro_6) improved selectivity, but only at the expense of reduced antimicrobial activity. Indeed, this observation also held true for the proline-containing variants reported herein. The activity and selectivity profiles of four molecules in this family, however, demonstrate clearly that hydrophobicity can be reduced to improve selectivity without compromising antimicrobial activity. Variants $\mathbf{1}_{ach}$-*N*spe_2, $\mathbf{1}_{ach}$-*N*spe_{12}, **1**-*N*$pm_{2,5,8,11}$, and **1**-*N*$pm_{2,3,8,9}$) demonstrate antimicrobial activity equivalent to that of **1** ($MIC_{E.\ coli}$ = 6.3 µM), yet significantly improved selectivities ($SR_{E.\ coli}$ = 6.2 – 26) compared to **1** ($SR_{E.\ coli}$ = 3.3). The most overt difference between using achiral *N*pm compared to *N*His or *L*-Pro monomers to lower hydrophobicity is their effect on helicity. While both **1**-*N*$His_{6,12}$ and **1**-Pro_6 exhibited helicity equivalent to that of **1** [32], the substitution of *N*pm monomers resulted in a progressive decrease in helical stability, as shown in **Figure 2.6**. This suggests that the reducing amphipathicity (correlated with helicity) concomitantly with hydrophobicity provides a means of improving selectivity without compromising antimicrobial activity.

Comparison of the isomeric pairs within this group suggest that the relative position of achiral monomers does not have a significant effect on selectivity. For example, comparison of $\mathbf{1}_{ach}$-*N*spe_2 ($SR_{E.\ coli}$ = 25, ID_{50} = 11 µM) and $\mathbf{1}_{ach}$-*N*spe_{12} ($SR_{E.\ coli}$ = 26, ID_{50} = 15 µM) suggests that selectivity against both erythrocytes and NIH 3T3 cells was unaffected by the position of the one chiral *N*spe monomer in the sequence. Comparison of isomeric variants containing equal numbers of *N*pm and *N*spe monomers in different positions (**1**-*N*$pm_{2,5,8,11}$ and **1**-*N*$pm_{2,3,8,9}$) suggest that while **1**-*N*$pm_{2,5,8,11}$ ($SR_{E.\ coli}$ = 14) was more selective against erythrocytes than **1**-*N*$pm_{2,3,8,9}$ ($SR_{E.\ coli}$ = 6.2), the opposite trend was evident in selectivity against NIH 3T3 cells (ID_{50}

= 6.8 μM and 15 μM, respectively). Taken together, these results suggest that there is no clear relationship between the degree of selectivity and relative position of achiral monomers within the ampetoid sequence.

2.2.3.6 Opposite chirality substitution variants

1$_{enantiomer}$, a variant of peptoid **1** in which all *N*spe side chains were replaced with enantiomeric *N*rpe monomers, has previously been shown to exhibit left-handed helicity, but antibacterial activities and cell selectivities congruent to those of peptoid **1** [32]. Because peptoid secondary structure is dictated by the chirality of its side chains, it is unclear what the resultant secondary structure (and associated activity/selectivity profiles) would be in a peptoid that included both enantiomeric side chains. Moreover, diasteriomeric peptides that contain both *D*- and *L*- amino acids were found to exhibit potent, broad-spectrum antimicrobial activity and improved selectivity[77]. Here we report variants of **1** that contain equal numbers of *N*spe and *N*rpe side chains in different arrangements as shown in **Figure 2.1** and **Table 2-1**. **1**-*N*rpe$_{3,6,9,12}$ and **1**-*N*rpe$_{2,5,8,11}$ are enantiomers that have four facially-aligned *N*spe monomers replaced with enantiomeric *N*rpe monomers. **1**-*N*rpe$_{2,3,5,6}$ has terminally segregated enantiomeric monomers with *N*rpe substitutions at positions 2, 3, 5, and 6 in the *N*-terminal portion of the molecule (**Figure 2.1**).

The antibacterial potencies and cell selectivity profiles of these variants are very similar to that of peptoid **1**, despite their disparate secondary structures. **Figure 2.7** shows that in aqueous buffer as well as both lipid environments, the enantiomeric molecules, **1**-*N*rpe$_{3,6,9,12}$ and **1**-*N*rpe$_{2,5,8,11}$, yield mirror image CD spectra**. Figure 2.7A** shows that in buffer, **1**-*N*rpe$_{3,6,9,12}$ and **1**-*N*rpe$_{2,5,8,11}$ appear to adopt helical secondary structures, with the overall handedness commensurate with that of the *C*-terminal monomer. **1**-*N*rpe$_{2,3,5,6,}$ also appears to adopt an overall right-handed spectra, but does not appear to be strongly helical. In both zwitterionic and

anionic lipids, however, the CD of the facially-aligned **1**-*N*rpe$_{3,6,9,12}$ and **1**-*N*rpe$_{2,5,8,11}$ were

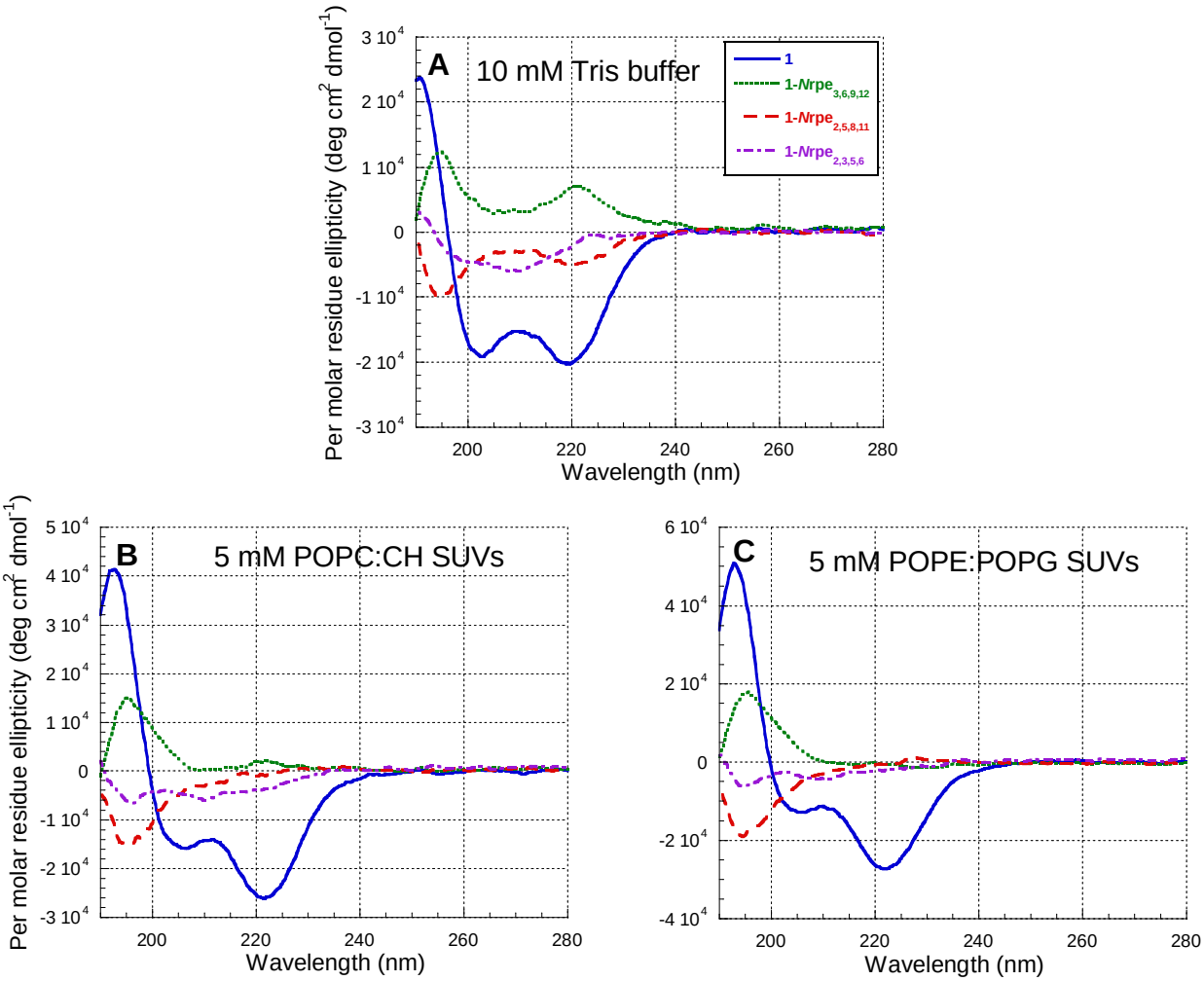

Figure 2.7: CD spectra of ampetoids containing opposite chirality monomers in (**A**) 10 mM Tris buffer and (**B**) same buffer with 5 mM POPC/cholesterol 2:1 SUVs and (**C**) same buffer with 5 mM POPE/POPG 3:7 SUVs. Ampetoid concentration was 60 µM.

markedly altered, suggesting a strong interaction with lipids and a significant change in secondary structure (**Figure 2.7B** and **2.7C**).

The CD spectal intensity for all *N*rpe containing peptoids are significantly reduced compared to that of **1**, an observation that we have previously correlated with decreased amphipathicity. However, because the CD spectra corresponding to variants in cell membrane-

mimetic lipid environments are not typical of a peptoid helical secondary structure, it is not clear how amphipathicity is affected in these molecules.

2.2.3.7 Aliphatic monomer variants

In order to evaluate the effect of side chain chemistry on cell selectivity, we created a family of ampetoids that have bulky, hydrophobic, aliphatic *N*sdp side chains in place of some or all of the aromatic *N*spe monomers in ampetoid **1** (**Figure 2.1** and **Table 2-1**). The previously reported ampetoids containing aliphatic isoleucine-like *N*ssb side chains were selective, but exhibited reduced activity, particularly against Gram-negative bacterial strains[31, 32]. Incorporating the larger and bulkier aliphatic side chains, 1-methylbutyl glycine (*N*smb), led to increased antibacterial potency, but also reduced selectivity[32]. The dipropyl glycine (*N*sdp) (**Figure 2.1**) monomer used in this family of molecules is an isomer of *N*smb and was selected to evaluate if an aliphatic monomer with branched geometry could improve potency while maintaining favorable selectivity. All variants in this group had a CTLR (0.33) and net charge (+4) equivalent to that of **1**.

1-*N*sdp$_{all}$ has *N*sdp substituted at all eight hydrophobic monomers in the peptoid **1** sequence. **1**-*N*sdp$_{2,5,8,11}$ and **1**-*N*sdp$_{2,3,8,9}$ are isomers in which half of peptoid **1**'s *N*spe monomers were replaced with aliphatic *N*sdp's. As shown in **Figure 2.1**, **1**-*N*sdp$_{2,5,8,11}$ exhibits four *N*sdp monomers aligned along the back molecular face, while the four *N*sdp's included in **1**-*N*sdp$_{2,3,8,9}$ are distributed across both hydrophobic faces. Whereas **1**-*N*sdp$_{2,5,8,11}$ contains segregated aromatic and aliphatic faces, **1**-*N*sdp$_{2,3,8,9}$ has a mixture of aromatic and aliphatic monomers in both hydrophobic faces.

The CD spectra of right-handed helical peptoids with chiral, aliphatic side chains have been shown to be distinctly different from those with aromatic side chains in that the most pronounced spectral feature is a maximum at 210 nm [31]. Indeed, the spectrum of **1**-*N*sdp$_{all}$

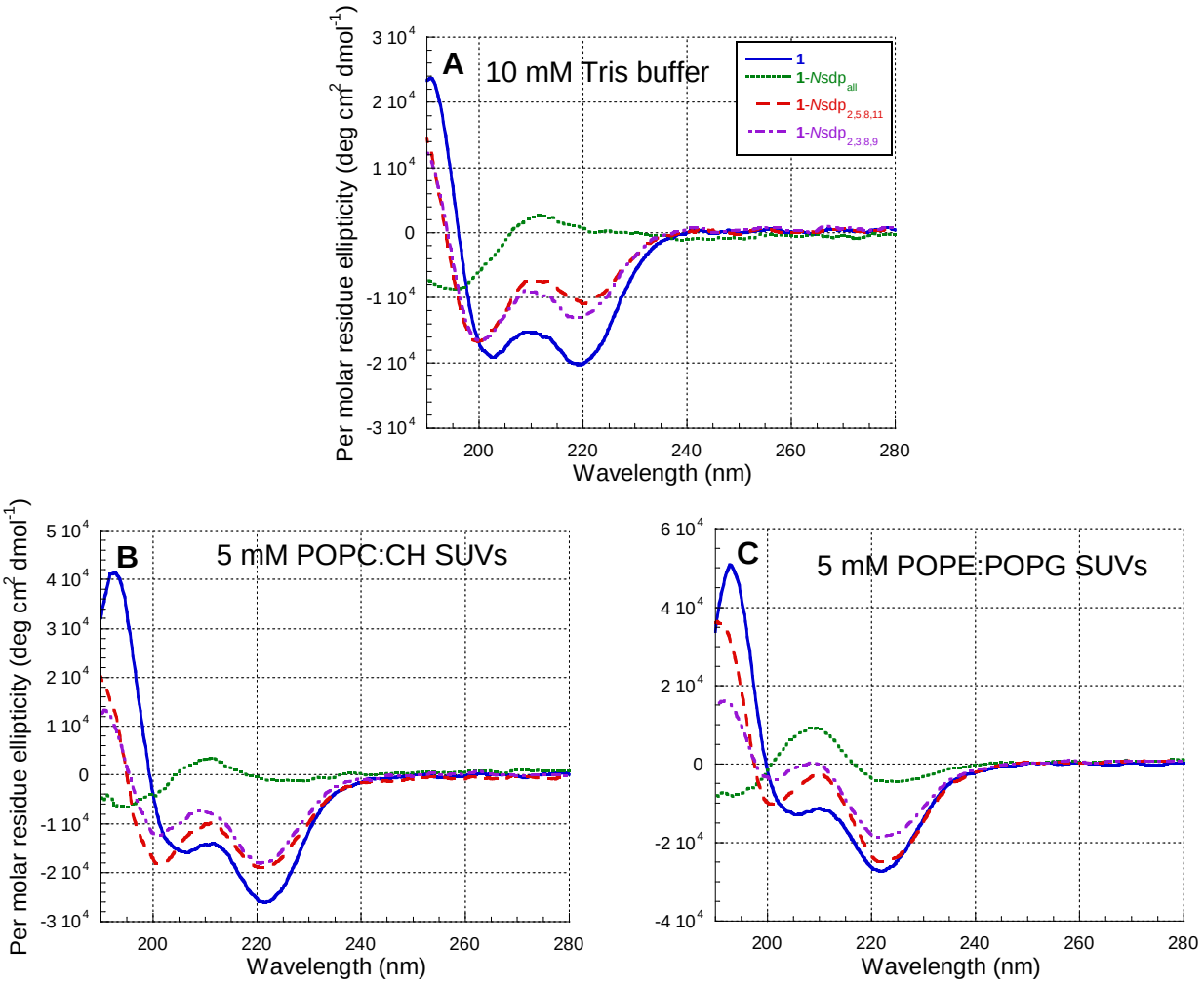

Figure 2.8: CD spectra of ampetoids containing aliphatic monomers in (**A**) 10 mM Tris buffer and (**B**) same buffer with 5 mM POPC/cholesterol 2:1 SUVs and (**C**) same buffer with 5 mM POPE/POPG 3:7 SUVs. Ampetoid concentration was 60 µM.

exhibits this feature in both aqueous and lipid environments (**Figure 2.8**). **1**-*N*sdp$_{2,5,8,11}$ and **1**-*N*sdp$_{2,3,8,9}$ both have spectral characteristics that appear to be a combination of both the aliphatic and aromatic peptoid helical signals. While the resultant "combined" CD spectra appear to be less intensely helical compared to that of **1**, it is unclear how the inclusion of aliphatic and aromatic monomers affected molecular amphipathicity; both **1**-*N*sdp$_{all}$ and **1** exhibit disparate, yet helical CD spectra.

The increase in selectivity of **1**-*N*sdp$_{all}$ ($SR_{E.\ coli}$ > 8) was realized at the cost of significantly reduced activity against *E. coli* of (25 μM) in comparison to **1** ($SR_{E.\ coli}$ = 3.3; $MIC_{E.coli}$ = 6.3 μM). **1**-*N*sdp$_{all}$ was highly potent against *B. subtilis* (0.78 μM), resulting in a selectivity ratio of 256 (**Table 2.2**).

The sequences containing equal numbers of aromatic and aliphatic monomers, **1**-*N*spd$_{2,5,8,11}$ and **1**-*N*sdp$_{2,3,8,9}$, exhibited slightly reduced antimicrobial activity ($MIC_{E.\ coli}$ = 12.5 μM) and improved selectivity ($SR_{E.\ coli}$ = 9.7 and 6.2, respectively) compared to **1** ($MIC_{E.\ coli}$ = 6.25 μM, $SR_{E.\ coli}$ = 3.3). While the slightly reduced hydrophobicity could be in part responsible for the improved selectivity, comparison with other variants suggests that the aliphatic side chain chemistry also plays an important role in its activity profile. Unlike what has been observed in some sequences that contain all aromatic hydrophobic monomers, the incorporation of aliphatic side chains appears to improve selectivity, but only at the expense of antimicrobial activity. For example variants **1**-*N*pm$_{2,3,8,9}$ (63.3% acetonitrile) , **1**-*N*pm$_{2,5,8,11}$ (63.6% acetonitrile) and **1**$_{11mer}$ (63.5% acetonitrile) all exhibit hydrophobicities comparable to that of **1**-*N*sdp$_{2,5,8,11}$ (63.8% acetonitrile). The balance of the antimicrobial activity and selectivity profiles of **1**-*N*sdp$_{2,5,8,11}$, however, is less optimal than for sequences containing only these aromatic side chains; compared with these three molecules ($MIC_{E.\ coli}$ = 6.3 μM, $SR_{E.\ coli}$ = 6.2 – 16) the antimicrobial activity of **1**-*N*sdp$_{2,5,8,11}$ is reduced ($MIC_{E.\ coli}$ = 12.5 μM) and selectivity ($SR_{E.\ coli}$ = 9.7) comparable. The overall hydrophobicities of these three molecules (63.2% – 64.7%) were slightly reduced compared to **1** (65.1%). The reduced hydrophobicity of **1**-*N*sdp$_{all}$ (63.2%) could in part be responsible for its reduced activity, however the lack of aromatic side chains may also play a role. Variants containing both aliphatic and aromatic side chains appear to provide a balance of low antimicrobial activity ($MIC_{E.\ coli}$ = 12.5 μM) and improved selectivity compared to **1** ($SR_{E.\ coli}$ = 6.2 – 12): **1**-*N*sdp$_{2,3,8,9}$ ($SR_{E.\ coli}$ = 6.2 - 12), and **1**-*N*sdp$_{2,5,8,11}$ ($SR_{E.\ coli}$ > 9.7).

2.2.4 Broad spectrum activity

We tested the antimicrobial activity of selected ampetoids and comparator peptide pexiganan against 16 clinically-relevant BSL2 bacterial strains. The panel of bacterial strains included seven Gram-negative species (*Proteus vulgaris*, *Pseudomonas aeruginosa*, *Proteus mirabilis*, *Klebsiella pneumonia*, *Enterobacter aerogenes*, *Escherichia coli*, and *Serratia marcescens*) and nine strains from three Gram-positive species (*Staphylococcus aureus*, *Enterococcus faecalis*, and *Enterococcus faecium*). Ampetoids **1**, **1**-Pro_6, **1**-Pro_9, $\mathbf{1}_{achiral}$, **1**-*N*$pm_{2,5,8,11}$, and **1**-*N*$sdp_{2,5,8,11}$ were tested against these organisms. The MICs (expressed in µg/mL) are shown in **Table 2-3A** and corresponding selectivity ratios (quotient of 10% hemolytic dose and MIC) are presented in **Table 2-3B**.

The activities of the six peptoids tested were all similar to that those of pexiganan against *P. vulgaris* (MIC = 32 – 64 µg/mL), *K. pneumoniae* (MIC = 8 – 16 µg/mL), and *E. coli* (4-16 µg/mL). Against *P. mirabilis* and *S. marcescens*, pexiganan and all peptoids tested were inactive (MIC ≥ 128). The activities of ampetoids tested against BSL2 Gram-positive strains, however, compared very favorably to those of pexiganan. The MIC of pexiganan against the six strains of *S. aureus* tested ranged from 8 – 64 µg/mL, whereas those of all the peptoids tested ranged from 4-16 µg/mL. Interestingly, **1** was uniquely active against both strains of *E. faecalis* (MIC = 4 – 8 µg/mL), compared to other ampetoids (MIC = 8 – 64 µg/mL) and pexiganan (MIC = 32 – 128 µg/mL). All compounds were equally potent against *E. faecium* (MIC = 4 µg/mL).

A	**Minimum inhibitory concentration (MIC) (μg/mL)**						
Bacterial organism	**Pex.**	**1**	**1**-Pro_6	**1**-Pro_9	$\mathbf{1}_{achiral}$	**1**-*N*$pm_{2,5,8,11}$	**1**-*N*$sdp_{2,5,8,11}$
P. vulgaris ATCC 49132	32	32	32	64	32	64	32
P. aeruginosa ATCC 27853*	4	8	32	32	16	64	16
P. mirabilis ATCC 35659	> 128	> 128	> 128	> 128	> 128	> 128	> 128
K. pneumoniae ATCC 33495	8	16	16	16	8	16	8
E. aerogenes ATCC 35029	32	16	128	64	128	64	32
E. coli ATCC 25922*	8	4	16	8	16	8	8
S. marcescens ATCC 13880	> 128	128	> 128	> 128	> 128	> 128	> 128
S. aureus							
ATCC 29213*	32	4	8	16	8	8	8
VAN1§†	16	4	8	8	8	8	8
VAN2§†	8	4	8	8	8	8	8
NRS100 (COL)§	16	4	8	8	8	8	8
NRS119‡	64	4	16	16	16	16	16
NRS120‡	64	8	16	16	16	16	16
E. faecalis							
ATCC 29212	32	4	8	8	16	8	8
99	128	8	64	64	64	64	64
E. faecium 106*	4	4	4	4	4	4	4

B	**Selectivity ratio (SR)**						
Bacterial organism	**Pex.**	**1**	**1**-Pro_6	**1**-Pro_9	$\mathbf{1}_{achiral}$	**1**-*N*$pm_{2,5,8,11}$	**1**-*N*$sdp_{2,5,8,11}$
P. vulgaris ATCC 49132	5.7	1.2	4.6	5.4	**9.8**	2.4	5.8
P. aeruginosa ATCC 27853*	**46**	4.8	4.6	9.0	19	2.4	12
P. mirabilis ATCC 35659	< 1.4	< 0.3	< 1.1	< 2.3	< 2.4	< 1.2	< 1.5
K. pneumoniae ATCC 33495	23	2.4	9.1	18	**39**	9.6	23
E. aerogenes ATCC 35029	5.7	2.4	1.1	5.4	2.4	2.4	**5.8**
E. coli ATCC 25922*	23	9.5	9.1	**36**	19	19	23
S. marcescens ATCC 13880	< 1.4	0.3	< 1.1	< 2.3	**2.4**	< 1.2	< 1.5
S. aureus							
ATCC 29213*	5.7	9.5	18	18	39	19	23
VAN1§†	11	9.5	18	36	39	19	23
VAN2§†	23	9.5	18	36	39	19	23
NRS100 (COL)§	11	9.5	18	36	39	19	23
NRS119‡	2.8	9.5	9.1	18	19	9.6	12
NRS120‡	2.8	4.8	9.1	18	19	9.6	23
E. faecalis							
ATCC 29212	5.7	9.5	18	36	19	19	23
99	1.4	4.8	2.3	5.4	4.9	2.4	2.9
E. faecium 106*	46	9.5	36	72	79	38	46

Table 2-3: Broad spectrum activity and selectivity of selected ampetoids and pexiganan. (**A**) MICs (in μg/mL) of selected ampetoids against BSL2 microbial strains. (**B**) Selectivity ratios are defined as the 10% hemolytic dose divided by the MIC for the organism of interest. The hemolytic dose (μg/mL) of each compound (**Table 2-2**) was multiplied by its molecular weight (**Table 2-1**) to calculate the selectivity ratio. Notes: * indicates NCCLS recommended standard strain; § indicates methicillian-resistant *S. aureus* (MRSA) strain; † indicates vancomycin-resistant strain; ‡ indicates linezolid-resistant strain.

The selectivity ratios presented in **Table 2-3B** show that against most Gram-negative bacterial species, at least one ampetoid had greater selectivity compared to pexiganan; the most favorable selectivity ratio against each Gram-negative species is shown in boldface type in **Table 2.3B**. $\mathbf{1}_{achiral}$, **1**-Pro_9, and **1**-*N*$sdp_{2,5,8,11}$ were the most selective against selected MDR bacterial strains. Against Gram-positive strains, ampetoids more consistently demonstrated improved selectivity compared to pexiganan or ampetoid **1**. Against all *S. aureus* strains, for example, the selectivity ratios of pexiganan ranged from 2.8 - 23, ampetoid **1** ranged from 4.8 – 9.5, and those of the panel of more selective ampetoids ranged from 9.1 – 39.

2.3 Discussion

Ampetoids are a new class of AMP mimics that have been shown to exhibit potent, broad-spectrum antimicrobial activity and appear to use mechanisms of action similar to their natural counterparts[31, 32]. Establishing an improved understanding of factors that influence cell selectivity is paramount to developing them as pharmaceutical agents. In this study, we designed a library of ampetoids to explore how and to what extent various physicochemical properties and structural motifs influenced their cell selectivity.

To broaden our understanding of how ampetoids may be affecting different types of mammalian cells, we determined the hemolytic dose as well as the metabolic inhibitory dose against NIH 3T3 mouse fibroblast cells. While the hemolytic and inhibitory activities exhibited similar trends for many ampetoids, the hemolytic dose was consistently higher than the inhibitory dose for the same compound. This is a trend that has also been reported for pexiganan[32] as well as other AMP mimics[78]. It is possible that the disparity between the hemolytic and inhibitory doses is due in part to differences in membrane composition between the two cell types. The cholesterol content of erythrocyte membranes, for example is approximately 230 µg/mg protein[79], whereas NIH 3T3 cholesterol content has been reported as

only 30.5 µg/mg protein[80]. The increased cholesterol content of erythrocytes may affect the rigidity of the membrane and offer increased resistance to membrane-active antimicrobial agents compared to NIH 3T3 cells.

Another disparity between hemolysis and MTS assays is that they differ in terms of the measure used to quantify cytotoxicity; while hemolysis measures the ampetoid dose needed to lyse erythrocytes, the MTS assay quantifies the dose needed to inhibit cellular metabolism, measured indirectly by the amount of NADH produced by the cell population. It is reasonable to expect, therefore that a dose needed to lyse a cell membrane would not necessarily be equivalent to the dose required to inhibit cellular metabolism. Whereas lysis implies membrane disruption activity, interference with cellular metabolism implies intracellular targets. While animal testing would be required to determine a true therapeutic index for these molecules, hemolysis and MTS assay results together suggest that the relative effect of many ampetoids against both cell types may be similar.

This library of ampetoids was designed to include members that exhibit a variety of structural motifs and possess physicochemical properties that span a wide range of values. Different ampetoids demonstrated promising activities against the various Gram-negative strains, but were most potent against *K. pneumonia* (ATCC 33495) and *E. coli* (ATCC 25922). It is particularly notable that all 26 ampetoid variants were consistently very potent against the Gram-positive screening organism, *B. subtilis*. The broad-spectrum testing results of selected ampetoids against MDR strains of *S. aureus*, *E. faecalis*, and *E. faecium* show that ampetoids are also potent against MRSA (4 – 8 µM) as well as vancomycin- and linezolid-resistant organisms (4 – 8 µM and 4-16 µM, respectively). The corresponding selectivity ratios of **1**$_{\text{achiral}}$ (19 – 39) and **1**-Pro$_9$ (18 – 36) against MDR *S. aureus* strains are particularly favorable compared to those of pexiganan (2.8 – 23) or ampetoid **1** (4.8 – 9.5). The burden of MDR

Gram-positive infections on the healthcare system is significant and only increasing[81]; these results suggest that ampetoids could be a viable alternative to conventional therapies to address this unmet clinical need.

Structure-activity studies have shown that the antibacterial activity and selectivity profiles of ampetoids are governed by the physicochemical properties that, in a similar manner, dictate the activity and selectivity of AMPs[32]. The structure-activity relationships gleaned from these studies not only provide further evidence to re-affirm these findings in ampetoids, but also provide additional insight into principles that influence how more subtle changes related to the number, sequence position, arrangement and chemical structure of specific structural moieties influence activity and selectivity.

Potent, but non-selective AMPs and ampetoids tend to be hydrophobic[64, 65] and adopt well-defined amphipathic structures[65-67], while more selective AMPs and ampetoids are typically highly cationic[68, 69], exhibit only moderate hydrophobicity[70], and are often less amphipathic[70]. As discussed previously, the activity and selectivity results of this study, which included several new ampetoid sequences, re-affirm these general relationships in several ways: (**1**) Comparison of the less amphipathic, more selctive $\mathbf{1}_{scr}$ to **1**; (**2**) Comparison of the highly charged, less amphipathic variants (**1**-*N*$Lys_{5,11}$, **1**B-*N*$Lys_{4,10}$, and $\mathbf{1}B_{15mer}$-*N*$Lys_{4,10,}$ **1**B-*N*$Lys_{4,6,10}$ and $\mathbf{1}B_{15mer}$-*N*$Lys_{4,6,10}$) compared to **1**, (**3**) Comparison of less hydrophobic proline-containing variants (**1**-Pro_3, **1**-Pro_6, **1**-Pro_9, **1**-$Pro_{3,9}$) to **1** (**4**) Comparison among achiral variants ($\mathbf{1}_{achiral}$, $\mathbf{1}_{ach}$-*N*spe_2, $\mathbf{1}_{ach}$-*N*spe_{12}, **1**-*N*$pm_{2,3,8,9}$, **1**-*N*$pm_{2,5,8,11}$), which exhibit a range of hydrophobicities and amphipathicities that scale with selectivity. Taking a closer look at more specific structural characteristics of the ampetoids included in this study, the influence of subtle molecular changes on activity and selectivity can be elucidated.

Comparison among the mono-substituted proline monomers suggests that the position of monomers along the length of the molecule and can impact selectivity. The mono-substituted proline monomers exhibited progressively increased selectivity as the less hydrophobic proline monomer was moved from the *N*-terminal toward the *C*-terminal region.

Trends observed in the selectivity profiles of sequence register variants (**1**, **1**B and **1**C) as well as length variants, $\mathbf{1}_{13mer}$, suggest that monomer position with respect to the termini also influences selectivity. All variants are similarly potent against E. coli: the $MIC_{E.coli}$ of **1**, **1**B, and **1**C was 6.3 µM, while that of $\mathbf{1}_{13mer}$ was improved by one dilution (3.1 µM). While **1** and **1**C each have one charged *N*Lys monomer at the *N* and *C*-termini, respectively, **1**B has hydrophobic *N*spe monomers at both termini. Conversely, $\mathbf{1}_{13mer}$ has charged *N*Lys monomers at both terminal positions. Consider these molecules in two groups: (**1**) those with both termini charged or hydrophobic (**1**B and $\mathbf{1}_{13mer}$), and (**2**) those with one charged and one hydrophobic terminus (**1** and **1**C). Interestingly, the hydrophobicity of those with dissimilar termini, **1** (65.1% acetonitrile) and **1**C (64.8% acetonitrile) is greater than that of variants with like monomers at terminal positions, **1**B (63.4% acetonitrile) and $\mathbf{1}_{13mer}$ (62.8% acetonitrile). Correspondingly, the selectivity of the less hydrophobic variants **1**B and $\mathbf{1}_{13mer}$ ($SR_{E.\ coli}$ = 6.8 – 8.7, $SR_{B.\ subtilis}$ = 27 – 34) is improved compared to that of **1** and **1**C ($SR_{E.\ coli}$ = 3.3 – 4.0, $SR_{B.\ subtilis}$ = 13 – 16). This suggests that having similarly charged termini (either both hydrophobic or both positively charged) reduces molecular hydrophobicity and results in an improvement in selectivity. This could be related to a similar phenomenon reported for antimicrobial peptide analogs of magainins, which found that the relative position of hydrophobic monomers in the sequence can impact resultant hydrophobicity and cell selectivity[82]. These results indicate that a strategy for improving selectivity, while maintaining antimicrobial activity, is to design the sequence with similarly charged or similarly hydrophobic terminal monomers.

As discussed previously, the achiral family of variants provide evidence that suggests the incorporation of achiral *N*pm hydrophobic monomers in place of chiral *N*spe monomers is another means of improving selectivity without compromising antimicrobial activity. Variants in which as many as seven of the eight *N*spe's in ampetoid **1**'s structure exhibited equivalent activity and significantly improved selectivity. It appears that the decrease amphipathicity that occurs concomitantly with increased *N*pm content results in a favorable selectivity profile. It is possible that the less rigid structure of ampetoids with increased achiral monomer content is less able to penetrate the rigid cell membranes of mammalian cells.

A third way in which this library of compounds was designed to affect selectivity is through increased CTLR. The increased charge density variants, with CTLRs in the range of 0.47 – 0.58 (compared to 0.33 for ampetoid **1**), were at best mildly active against *E. coli* (MIC = 50 to > 100 μM). Length variants, however, which were designed to effect a change in CTLR over a lower range (0.33 – 0.40). Of these variants, $\mathbf{1}_{11mer}$ was found to exhibit the most optimum balance of CTLR (0.36) and sufficient hydrophobicity to permeabilize bacterial membranes (63.5%) at a low minimum inhibitory concentrations ($MIC_{E.\ coli}$ = 6.3 μM).

Two other means of reducing hydrophobicity, substituting in *L*-proline content or aliphantic *N*sdp monomers, are less favorable because they improve selectivity at the expense of antimicrobial activity against Gram-negative bacteria. The addition of one proline monomer (**1**-Pro_3, **1**-Pro_6, and **1**-Pro_9, $MIC_{E.\ coli}$ = 12.5 μM) and two proline monomers (**1**-$Pro_{3,9}$, $MIC_{E.\ coli}$ = 50 μM) progressively decreased activity compared to that of ampetoid **1** ($MIC_{E.\ coli}$ = 6.3 μM). Molecules with four (**1**-*N*$sdp_{2,3,8,9}$ and **1**-*N*$sdp_{2,5,8,11}$, $MIC_{E.\ coli}$ = 12.5 μM) and eight (**1**-*N*sdp_{all}, $MIC_{E.\ coli}$ = 25 μM) aliphatic monomers exhibited a similar trend in reduced antimicrobial activity.

Another observation is evident from the characterization of **1**$_{achiral}$, **1**-*N*rpe$_{3,6,9,12}$, and **1**-*N*rpe$_{2,5,8,11}$, which suggests that ampetoids can exhibit potent antimicrobial activity without necessarily adopting a stable helical secondary structure. As the name suggests, **1**$_{achiral}$ is devoid of any chiral monomers and is thus not optically active; the resultant CD spectra in aqueous buffer and lipid environments is flat (**Figure 2.5**). While it is conceivable that **1**$_{achiral}$ could transiently adopt a helical structure of either handedness, there does not appear to be external or intrinsic force to stabilize its structure. **1**-*N*rpe$_{3,6,9,12}$, and **1**-*N*rpe$_{2,5,8,11}$, on the other hand, are enantiomeric molecules that contain equal numbers of *N*spe and *N*rpe hydrophobic aromatic side chains. Interestingly, the overall chirality of these monomers appears to be dictated by the chirality of the monomer in the 12th position, a finding commensurate with the observation that **1**$_{ach}$-*N*spe$_{12}$ exhibits a larger degree of right-handed chirality than does **1**$_{ach}$-*N*spe$_{2}$. This provides further evidence that the *C*-terminal monomer heavily influences structural stability. In buffer, both of these variants produce CD spectra that resemble that of a peptoid polyproline-type-I-like structure with the extrema normally at 202 nm blue-shifted to approximately 195 nm **(Figure 2.7)**. In neutral POPC/cholesterol lipids, however, the extrema at 220 nm is greatly diminished, and in POPE/POPG SUVs, this feature is completely eliminated. This marked change in CD spectra suggests that **1**-*N*rpe$_{3,6,9,12}$, and **1**-*N*rpe$_{2,5,8,11}$ interact strongly with both of these lipid mixtures such that their overall structure is significantly altered. Taken together, it is interesting that **1**$_{achiral}$, which appears to lack a stable secondary structure, as well as **1**-*N*rpe$_{3,6,9,12}$, and **1**-*N*rpe$_{2,5,8,11}$, which have a CD spectra in lipids that are distinct from that of a canonical peptoid polyproline-type-I-like, are all equally potent as ampetoid **1** against *E. coli* (MIC = 6.3 μM). A stable helical secondary structure does not appear to be necessary for ampetoid antimicrobial activity. This finding that a stable helical secondary structure does not appear to be necessary for ampetoid antimicrobial activity goes

beyond previous findings, which suggested that helicity is important only as a means of organizing an amphipathic structure[32].

Lastly, we designed a pair of molecules to evaluate if the facial segregation aliphatic and aromatic hydrophobic monomers impacts selectivity. While **1**-*N*sdp$_{2,5,8,11}$ has four substituted aliphatic monomers aligned along molecular faces, **1**-*N*sdp$_{2,3,8,9}$ has a mixture of aliphatic and aromatic hydrophobic monomers on both faces (**Figure 2.1**). The facially-aligned isomer **1**-*N*sdp$_{2,5,8,11}$ ($SR_{E.\ coli}$ = 9.7; $SR_{B.\ subtilis}$ = 142) was more selective than its facially-distributed counterparts (**1**-*N*sdp$_{2,3,8,9}$ – $SR_{E.\ coli}$ = 6.2, $SR_{B.\ subtilis}$ = 99). While these isomers exhibit similar net charges (both +4), CTLRs (both 0.33), and hydrophobicities (63.8% - 64.7% acetonitrile), a notable difference between them is that while the arrangement of hydrophobic monomers on **1**-*N*sdp$_{2,5,8,11}$, preserved one wholly aromatic face, that of **1**-*N*sdp$_{2,3,8,9}$ exhibits no completely aromatic face. It has been shown previously that the inclusion of at least one aromatic face increases helical stability[57]; the more intense helicity of **1**-*N*sdp$_{2,5,8,11}$ compared to **1**-*N*sdp$_{2,3,8,9}$ in both zwitterionic and anionic lipid mixtures supports this observation (**Figure 2.8**). This

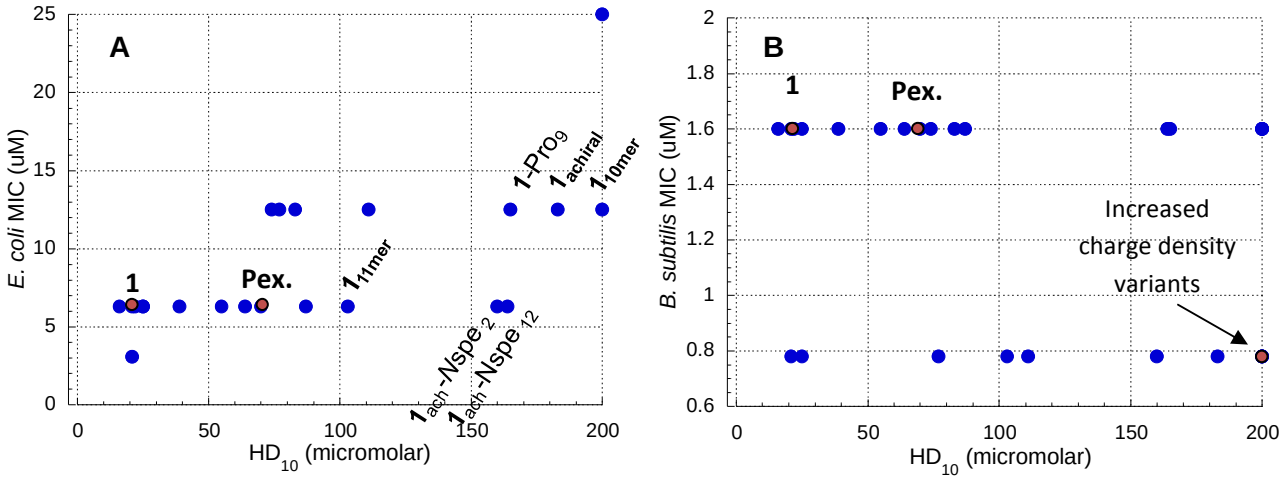

Figure 2.9: Comparison of antimicrobial / hemolytic activity profiles for selected ampetoids. Those with the most favorable profiles appear at the lower right portion of each plot.

suggests that preservation of at least one ampetoid aromatic face may increase its selectivity independent of changes in other physiocochemical parameters.

The most promising therapeutic agents exhibit are highly potent against bacteria and are nontoxic to mammalian cells. This relationship is depicted graphically in **Figure 2.9**, in which the hemolytic dose is plotted versus the *E. coli* (**Figure 2.9A**) and *B. subtilis* (**Figure 2.9B**) minimum inhibitory concentrations for selected peptoids. Peptoid **1** and pexiganan are depicted by red markers for reference. Those peptoids located in the lower right coordinate space have the most promising therapeutic potential. Many compounds reported herein exhibit more favorable activity profiles than peptoid **1** and pexiganan. It is most notable that the increased charge density variants, which were completely non-hemolytic, demonstrated a marked improvement in activity profile against Gram-positive *B. subtilis*.

In summary, ampetoids are a promising class of AMP mimics that exhibit potent, broad-spectrum activity, particularly against many multi-drug resistant Gram-positive organisms. Of the 26 sequences presented here, 17 demonstrate improved selectivity for *E. coli* compared to the basis sequence, **1**. The structure-activity relationships derived from this library of compounds reaffirm and extend the analogy between the mechanism of action of AMPs and ampetoids. Selective ampetoids tended to be only moderately hydrophobic and amphipathic, while non-selective ampetoids were highly hydrophobic and exhibit more highly amphipathic structures. The relationships among ampetoid variants in this library also point to the effects of how more subtle changes in sequence, side chain chemistry, and monomer position effect selectivity. Three strategies to improve ampetoid selectivity without compromising selectivity include (**1**) Positioning of similarly cationic or hydrophobic monomers at the sequence terminal positions, (**2**) Inclusion of hydrophobic achiral *N*pm monomers in place of *N*spe monomers (**3**) Optimizing the CTLR while retaining sufficient hydrophobicity to permeabilize bacterial cell

membranes. Two approaches, specifically designed to reduce hydrophobicity effected the desired outcome of improving selectivity, but only at the cost of reduced antimicrobial activity. This less optimal activity profile resulted from (**1**) Substitution of less hydrophobic *L*-proline monomers as well as (**2**) Substitution of aliphatic *N*sdp monomers. Interestingly, while the relative position along the helix of some monomers played a role in selectivity (*e.g.* mono-proline substituted variants), this was not always the case (*e.g*. achiral variants). The preservation of at least one aromatic face may also play a role in increasing selectivity. Lastly, thus study provides evidence that antimicrobial activity can be maintained in ampetoids which lack a stable secondary structure (**1**$_{achiral}$) or appear to adopt a secondary structure different from that of the canonical peptoid helix (**1**-*N*rpe$_{2,5,8,11}$ and **1**-*N*rpe$_{3,6,9,12}$). Because peptoids are sequence-specific biopolymers that can be made from a diversity of primary amines, it is conceivable that ampetoid potency and selectivity could be finely tuned to fight specific, clinically-relevant organisms. The design heuristics established herein may aid in the design of potent, yet selective, future generations of ampetoids.

2.4 Materials and Methods

2.4.1 Compound synthesis and purification

Peptoids were synthesized using an ABI 433A peptide synthesizer (Applied Biosystems, Inc.) on Rink amide MBHA resin (Novabiochem, Inc.) using the submonomer approach[3]. Briefly, bromoacetic acid, activated by diisopropylcarbodiimide was used to form a bromocetylated intermediate on the terminal amide group. Bromide was then substituted with the desired primary amine through S_N2 displacement to build the peptoid chain. The amines used in peptoid synthesis include benzylamine, octadecylamine, (*s*)-(+)-2-amino-3-methylbutane, (*s*)-α-methylbenzylamine, (*r*)-(α-methylbenzylamine (all purchased from Sigma-Aldrich), and *N*-tert-butoxycarbonyl-1,4 diaminobutane (*N*Lys) that was made using a published procedure[83]. Resin-bound peptoids were then exposed to a mixture of trifluoroacetic acid

(TFA): triisopropylsilane:water (95:2.5:2.5, v:v:v) for ten minutes to cleave peptoids from the solid phase. Peptoids were purified by reversed-phase HPLC (RP-HPLC) (Waters Corporation) using a C18 column and a linear acetonitrile/water gradient. A final purity greater than 97% as measured by analytical RP-HPLC (Waters Corporation) was achieved, and the identity of each molecule was checked using electrospray ionization mass spectrometry. All reagents were purchased from Sigma Aldrich.

2.4.2 Circular dichroism spectroscopy

A Jasco 715 spectropolarimeter was used to perform all CD measurements in a cylindrical quartz cell with a path length of 0.02 cm. Measurements were taken over the range of 190 nm to 280 nm at a scanning rate of 100 nm/min. Other parameters include data pitch of 0.2 nm, bandwidth of 1 nm, response time of 2 seconds, and sensitivity of 100 mdeg. Compound concentration was 60 µM in 10 mM Tris buffer (pH 7.4). For samples in the presence of SUVs, the lipid concentration was 5 mM. 40 accumulations were collected for each sample.

2.4.3 Screening antibacterial assays

MICs were determined in 96-well microtiter plates in accordance with CLSI M7-A6 protocols. Peptoid solutions with 50 µL total volume were prepared using 2:1 serial dilutions. 50 µL of bacteria inoculum (1×10^6 CFU/mL) prepared in cation-adjusted Mueller-Hinton broth (CAMHB) was added to test wells. Control wells contained 100 µL MHB (no growth) or 50 µL inoculums with 50 µL MHB with no peptoid. The MIC was taken as the lowest concentration of peptoid that completely inhibited bacterial growth after 16 hours of incubation at 35^oC. Reported values were reproducible over three experiments, each containing two parallel trials.

2.4.4 Broad-spectrum antibacterial assays

MICs of compounds were determined by microdilution procedure in Mueller-Hinton broth (MHB) in accordance with CLSI M7-A6 protocols in a manner similar to that described for the

screen antibacterial assays. Inoculated microtiter plates were incubated at 35º C for 24 hours prior to the result being recorded. Four ATCC strains that were used as standards are recommended by CLSI: *Pseudomonas aeruginosa* ATCC 27853, *Escherichia coli* ATCC 25922, *Staphylococcus aureus* ATCC 29213 and *Enterococcus faecalis* ATCC 29212. Other strains from the ATCC collection include *Proteus vulgaris* ATCC 49132, *Proteus mirabilis* ATCC 35659, *Klebsiella pneumoniae* ATCC 33495, *Enterobacter aerogenes* ATCC 35029 and *Serratia marcescens* ATCC 13880. *S. aureus* NRS100 (COL) is a well characterized methicillian-resistant *S. aureus* (MRSA) strain. The strains *S. aureus* VAN1 and *S. aureus* VAN2, vancomycin-resistant MRSA strains that were isolated in Michigan and Pennsylvania, were the first vancomycin-resistant strains clinically isolated. *S. aureus* NRS 119 and *S. aureus* NRS 120 are linezolid-resistant isolates from the Network on Antimicrobial Resistance in *S. aureus* (NARSA) collection. *E. faecalis* 99 and *E. faecium* 106 are vancomycin-resistant enterococcal strains.

2.4.5 Hemolysis assays

Erythrocytes were isolated from freshly drawn, heparanized human blood and resuspended in PBS (pH 7.4) to make a 20% volume suspension. Peptoid solutions were prepared by serial dilution (2:1) in a 96-well microtiter plate. For test wells, 100 µL of erythrocyte suspension was added to 100 µL of peptoid solution in PBS; PBS without peptoid was used as the negative control and 0.2 vol% Triton X-100 as the positive control that indicates 100% hemolysis. After 1 hour incubation at 37^{o}C, each well was diluted with 150 µL PBS. Plates were then centrifuged at 1,200 x g for 15 minutes to pellet the cells. 30 µL of the supernatant from each well were transferred to the corresponding well of a second 96-well plate that contains 70 µL PBS. Using a plate reader, the absorbance at 350 nm was measured, and percent hemolysis was defined as $(A - A_0)/(A_{total} - A_0) \times 100$, where A is the absorbance of the

test well, A_0 the average absorbance of negative controls, and A_{total} the average absorbance of 100% hemolysis wells.

2.4.6 MTS assays

NIH/3T3 cells (ATCC Corporation) cultured at 37ºC and 5% CO_2 in complete Dulbecco's modified eagle's media (CDMEM) supplemented with 1% sodium pyruvate, 1% penicillin–streptomycin, 1.5 g/L $NaHCO_3$, and 10% fetal bovine serum. Cells were seeded at a density of 5,000 cells per well for NIH/3T3 cells in 96-well plates (100 µl total volume). A peptoid solution plate (100 µL total volume per well) was prepared by serial dilution of aqueous peptoid stock solution in Hank's balanced salt solution (HBSS) media. The day-old cell monolayers were washed with HBSS and media was replaced with 100 µL HBSS. The contents of the peptoid solution plate were transferred onto corresponding wells of the cell monolayer plate, and 40 µL MTS reagent (Promega, Inc.) was added to each well. After incubating for 3 hours at 37^{o}C, absorbance at 490 nm was determined. The percentage inhibition was determined as $[1-(A - A_{testblank})/(A_{control} - A_{blank})] \times 100$, where A is the absorbance of the test well and $A_{control}$ the average absorbance of the wells with cells exposed to media and MTS (no peptoid). $A_{testblank}$ (media, MTS, and peptoid) and A_{blank} (media and MTS) were measured as background absorbances in the absence of cells. The average of six replicates is reported.

2.5 Study contributions

Ann Czyzewski designed experiments, performed experiments, analyzed results, wrote the paper; Nathaniel Chongsiriwatana designed experiments, performed selected experiments, contributed to paper; Sergei Vakulenko performed selected experiments; Tyler Miller synthesized selected compounds; James Patch designed selected compounds; Rinki Kapoor assisted with experimental work; Shahriar Mobashery (collaborating PI) contributed to experimental design; Annelise Barron contributed to experimental design, contributed to paper.

3. An *in vitro* and *in vivo* study of a peptoid-based antimicrobial peptide mimic

3.1 Introduction

Drug development during the golden age of antibiotics (1960s and 1970s) resulted in an unprecedented reduction in infection worldwide; however, this success bred the false sense of security that modern medicine could completely eradicate bacterial infections[84]. The emergence and re-emergence of multi-drug resistant (MDR) bacteria has since been recognized as an alarming threat to public health and an unmet clinical need. Only three new classes of antibacterial agents have been approved for clinical use over the last 45 years[49, 85]; most of the new antibiotics are closely related in structure to existing ones, making the route to bacterial resistance short and inevitable[49]. The pharmaceutical industry's waning interest in antibiotic development coupled with the permissive use of existing drugs and the threat of bioterrorism and emerging infectious diseases are additional factors contributing to the urgency of this global crisis[86]. Current efforts to ameliorate the development of microbial resistance have largely come from the biotechnology and academic sectors, which are environments that can foster the novel approaches needed to address this complex problem[87]. Among the most notable new classes of antibiotic agents are antimicrobial peptides (AMPs) and their mimics.

AMPs, also known as host defense peptides, are key components of innate immunity that have recently generated significant interest as innovative lead compounds for clinical use[88-90]. While AMPs comprise a family of molecules diverse in source, length, and structure, characteristics common to most AMPs include **(1)** overall amphipathic architecture and **(2)** net cationic charge (+2 to +9)[50]. These physicochemical properties render AMPs membrane-active, thus enabling their typically broad-spectrum antimicrobial activity either by disrupting the membrane directly or permeabilizing the membrane and acting on intracellular targets in such a way as to ultimately cause cell death[52, 53]. While a detailed understanding of the mechanisms

employed by AMPs has not yet been elucidated, it has been shown that some cationic AMPs initially interact with the polyanionic surface of lipopolysaccharide (LPS) in the outer membrane of Gram-negative bacteria, thus destabilizing the membrane structure[91]. It is unlikely that any class of antibacterial agent could entirely thwart the development of resistant bacterial strains[92-94], but it is clear that the different, non-receptor mediated, generalized modes of action employed by AMPs can limit bacterial resistance development[52].

While the use of antimicrobial peptides has met with some successes[52, 54], most recent clinical trials have failed to show efficacy for the newest AMPs[52]. The susceptibility of the peptide backbone to protease activity is thought to be responsible in part for the unfavorable pharmacokinetic profile and lack of sufficient bioavailability of the AMPs[52]. One approach to preserving the desirable features of AMPs (selectivity, broad-spectrum activity and a mode of action that reduces bacterial resistance), while circumventing their shortcomings, is the use of peptidomimetic, non-natural scaffolds. Biomimetic oligomers can be used to create sequences capable of emulating the form and function of helical, cationic AMPs while eluding the vulnerability to protease activity.

N-substituted glycines (peptoids) are a class of sequence-specific biomimetic polymers that can be designed to mimic the helical, cationic, and amphipathic structure of some AMPs; antimicrobial peptoids ("ampetoids") have been shown to exhibit potent and selective antimicrobial activity and to employ mechanisms of action similar to those of their natural counterparts[31, 32]. Peptoids are based on a backbone structure that is identical to peptides, however side chains are appended to the amide nitrogen rather than the α-carbon[3]. This apparently simple modification has important structural implications. The peptoids' achiral backbone structure, which precludes intrachain hydrogen bonding, can be induced to form stable helices by incorporation of bulky, α-chiral side chains[55-57]. Peptoids composed of

homochiral side chains form polyproline type I-like helices with cis-amide bonds exhibit three-fold periodicity[11, 55]. Moreover, a conventional peptide synthesizer can be used to make peptoids on solid phase with high coupling efficiencies in a cost-effective manner.[3]

Small libraries of ampetoids with varying monomer sequences and side chains have been reported[31, 32], from which peptoid **1** (**Figures 3.1 A, B**) was selected as the focus of this work because of its favorable antibacterial potency and cell selectivity profiles. Peptoid **1** is a dodecamer composed of 1/3 lysine-like side chains (*N*Lys) and 2/3 phenylalanine-like side chains (*N*spe) with the repeating sequence H-(*N*Lys-*N*spe-*N*spe)$_4$-NH_2. A schematic representation of peptoid **1**'s three-fold periodic helical architecture and resultant facially amphipathic structure are illustrated in **Figure 3.1 A**. **Figure 3.1 B** shows the chemical structures of the monomer side chains of peptoid **1**.

Here we used a multifaceted approach to more fully investigate the breadth of the therapeutic potential of peptoid **1** as well as its compatibility with *in vivo* use. We first evaluated the *in vitro* antibacterial activity of peptoid **1** against 20 pathogenic and highly antibiotic resistant microorganisms in comparison to that of two clinically relevant antimicrobial peptides. We then determined peptoid **1**'s relative LPS binding affinity in order to learn about its interaction with the outer membrane of Gram-negative bacteria and screen for potential anti-endotoxin activity. We also report a preliminary study that suggests the minimum inhibitory concentration (MIC) of peptoid **1** is less affected by bacterial load than that of the comparator peptide pexiganan. Using a murine model of invasive bacterial infection, specifically an *S. aureus* intraperitoneal challenge, we were able to demonstrate peptoid **1**'s ability to treat an infection *in vivo*. Additionally, we used a more clinically relevant model of sepsis to evaluate the ability of peptoid **1** to treat a clinically relevant polymicrobial infection. Taken together, these results underscore

the significant therapeutic potential of peptoid **1** and of cationic, amphipathic peptoids in general as an important new class of antimicrobial agents.

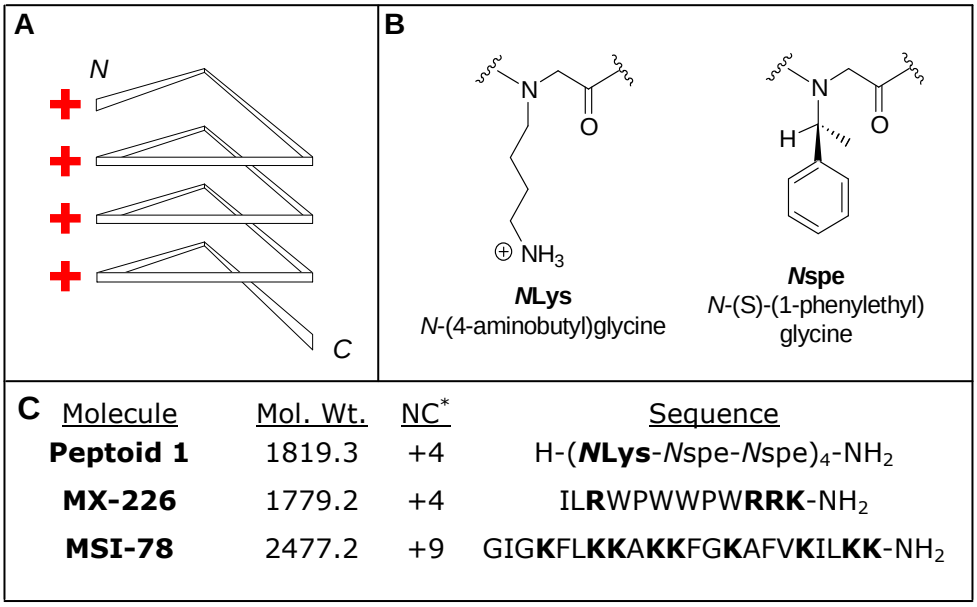

C

Molecule	Mol. Wt.	NC*	Sequence
Peptoid 1	1819.3	+4	H-(***N*Lys**-*N*spe-*N*spe)$_4$-NH_2
MX-226	1779.2	+4	IL**R**WPWWPW**RRK**-NH_2
MSI-78	2477.2	+9	GIG**K**FL**KK**A**KK**FG**K**AFV**K**IL**KK**-NH_2

Figure 3.1: Peptoid schematic and monomer chart. (**A**) Schematic of peptoid 1 with a 3-fold periodic, helical architecture. Positively charged *N*Lys side chains are indicated with + ; *N*spe side chains are at all other positions. (**B**) Chemical structures of peptoid side chains *N*Lys and *N*spe side chains. (**C**) Summary of peptoid 1 and comparator peptide characteristics, with positively charged monomers indicated in bold type. *NC = net charge.

3.2 Results

The sequence, molecular weight, and net charge of peptoid **1** and comparator AMPs, MX-226 and MSI-78, are summarized in **Figure 3.1C**. MX-226, also known as Omiganan®, (Migenix, Inc., Vancouver, British Columbia, Canada) is an indolicidin derivative that is currently being developed to reduce the incidence of device-related infections. Phase III clinical trials have demonstrated that MX-226 reduced local catheter site infection by 50% as well as catheter colonization by 40%, but the peptide failed to show a statistically significant effect on the primary outcome – reduction in the overall rate of infection[53]. Enrollment for a second, re-designed Phase III trial of MX-226 has just been completed, and results are expected later in 2008.

While peptoid **1** and MX-226 differ greatly in primary sequence, they are both dodecamers with similar overall net charge and molecular weights. MSI-78 (pexiganan) is a 22-amino acid analogue of the peptide magainin-2, which was first developed by Magainin Pharmaceuticals Inc. (since renamed Genaera), and was clinically tested for efficacy in the treatment of diabetic foot ulcers. Phase III clinical trials showed that MSI-78 eliminated or significantly reduced infection in over 90% of patients while exhibiting a favorable toxicity profile, yet FDA approval was denied in 1999 because improved efficacy compared to a conventional antibiotic treatment could not be demonstrated[53]. Compared to peptoid **1**, MSI-78 is almost twice as long (22 vs. 12 monomers), is significantly larger (2477 g/mol vs. 1819 g/mol), and has a higher net charge (+9 vs. +4).

3.2.1 Broad-spectrum activity

We tested the antimicrobial activities of peptoid **1**, MX-226, and MSI-78, against 20 different multi-drug resistant, clinically relevant pathogens, including strains of *P. aeruginosa*, methicillin-resistant *S. aureus* (MRSA), *E. cloacae* with depressed chromosomal β-lactamase, extended spectrum β-lactamase (ESBL)-producing *E. coli*, *K. pneumonia*, and vancomycin-resistant *E. faecalis* and *E. faecium* (VRE) (**Table 3-1**). Peptoid **1** was found to be highly potent against 19 of the 20 bacterial strains tested, and its activity compared very favorably to the activity of MX-226; whereas the MICs of peptoid **1** ranged from 2.7 – 21.8 μg/mL, the MICs of MX-226 ranged from 17.2 to > 272 μg/mL.

The potency of MSI-78 was approximately equal to that of peptoid **1** against *P. aeruginosa*, *P. maltophilia*, and *E. cloacae*, however peptoid **1** demonstrated superior potency against Gram-positive strains of *S. aureus*, *E. faecalis*, and *E. faecium*. More specifically, against all Gram-positive strains tested, the MIC of peptoid **1** ranged from 2.7 μg/mL to 11.3 μg/mL, while that of MSI-78 ranged from 4.2 μg/mL to 272.2 μg/mL. These results suggest that

peptoid **1,** if safe for *in vivo* use, is a promising candidate to treat some of the most recalcitrant and dangerous human infections.

	MIC (μg/mL)		
	Peptoid 1	**MX-226**	**MSI-78**
P. aeruginosa			
Strain H103 (wildtype strain)	2.7	33.8	1.0
Strain 9 (MDR from Brazil)	21.8	135.2	17.1
Strain 198 (MDR from Brazil)	5.6	272.2	4.2
Strain 213 (MDR from Brazil)	5.6	67.6	8.4
Strain LES400 (MDR LES)	2.7	135.2	4.2
Strain H1030 (MDR LES)	5.6	135.2	8.4
Strain H1027 (MDR LES)	2.7	67.6	2.0
P. maltophilia			
ATCC 13637	2.7	33.8	2.0
E. cloacae			
218R	2.7	17.1	2.0
E. coli (ESBL)			
63013	2.7	67.6	17.1
63575	2.7	67.6	2.0
K. pneumonia (ESBL)			
61962	5.6	272.2	34.2
63575	5.6	135.2	8.4
S. aureus			
ATCC 25923	2.7	17.1	69.4
MRSA strain C623	2.7	33.8	17.1
E. faecalis			
ATCC 29212	2.7	135.2	17.1
W61950 (Van A)	11.3	272.2	272.5
f43559 (Van B)	5.6	272.2	17.1
E. faecium			
mic80 (Van A)	2.7	67.6	4.2
t62764 (Van B)	2.7	135.2	8.4

Table 3-1: Minimum inhibitory concentrations (MICs) for peptoid 1 and comparator peptides against 20 clinically-relevant biosafety level 2 (BSL 2) microbial strains. MIC is defined as the lowest concentration at which no bacterial growth was observed. ESBL = Extended-spectrum β-lactamase producing organism; MDR = multi-drug resistant organism; VRE = Vancomycin resistant *Enterococcus;* LES = Liverpool epidemic strain.

3.2.2 LPS binding activity of AMP mimics

Because lipopolysaccharide (LPS) is critical to the viability of Gram-negative bacteria, understanding how antimicrobials interact with it can provide insight into their mechanisms of action and their potential as anti-endotoxin agents[95]. The outer membrane of Gram-negative

bacteria not only serves as a physical barrier to external stresses, but also provides structural integrity and plays a major role in the host's immune response[91]. LPS is an integral component of this membrane and consists of a hydrophobic region (Lipid A) covalently linked to a core oligosaccharide and distal repeating unit polysaccharide regions (O-antigen)[96]. The polyanionic surface of LPS also contains divalent cation binding sites that are stabilized and partially neutralized by divalent cations, such as Mg^{2+}. Through a process of self-promoted uptake, cationic peptides capable of displacing divalent cations can disrupt the LPS cross-bridging, thus destabilizing the membrane, and subsequently permitting enhanced influx of polycationic antibiotics[97, 98].

The fluorescently-labeled lipo-peptide dansyl polymyxin B (DPX) binds strongly to LPS, resulting in enhanced fluorescence of the dansyl group[99]. The ability of cationic molecules to displace DPX molecules bound to LPS (monitored by reduction in fluorescence) can thus be quantified as an indirect measure of their relative affinity for LPS[99, 100]. The maximum displacement achieved by each compound normalized to that of polymyxin B (PMB) is a measure of the compound's ability to compete with DPX for LPS binding sites. While the highly cationic MSI-78 (+9 charge) displaced 100% of bound DPX (equivalent to that of PMB), peptoid **1** and MX-226 displaced 71% and 73%, respectively. These results correlate well with previous work, which demonstrated that a variety of polycations were able to displace between 63% and 100% of bound DPX[99]. A second parameter characterizing the LPS/polycation interaction is the I_{50}, which is defined as the concentration of peptoid or peptide that displaces half of the maximal displacement of DPX. The I_{50} is inversely related to the relative affinity of each molecule for binding sites on LPS. For these compounds, I_{50} results indicated the order of decreasing LPS affinity as follows: MSI-78 (I_{50} = 1.4 μM) > Peptoid **1** (I_{50} = 2.6 μM) > PMB (I_{50} = 3.2 μM) > MX-226 (I_{50} = 5.0 μM).

3.2.3 Sensitivity to bacterial load in the inoculum

An issue commonly associated with the clinical development of AMPs is their reduced bioavailability *in vivo*, which is in part attributed to their high susceptibility to protease activity[52]. The large number of proteases released from dying bacteria (which can ultimately lead to sepsis) exacerbates this issue[90, 101]. We hypothesized that the non-natural, protease-resistant backbone of peptoids could afford an advantage in circumventing this phenomenon. We designed a simple test to answer a question that is intimately related to this issue: What is the sensitivity of the *in vitro* antimicrobial activity of both ampetoid **1** and pexiganan to bacterial concentration of the inoculum? We measured the minimum inhibitory concentrations of both molecules as a function of inoculum bacterial load (1 x 10^4 CFU/mL to 1 x 10^8 CFU/mL) for both *E. coli* (ATCC 35218) and *B. subtilis* (ATCC 6633) as shown in **Figure 3.2**. The data show that for ampetoid **1**, the MICs against *E. coli* and *B. subtilis* remain constant within one dilution

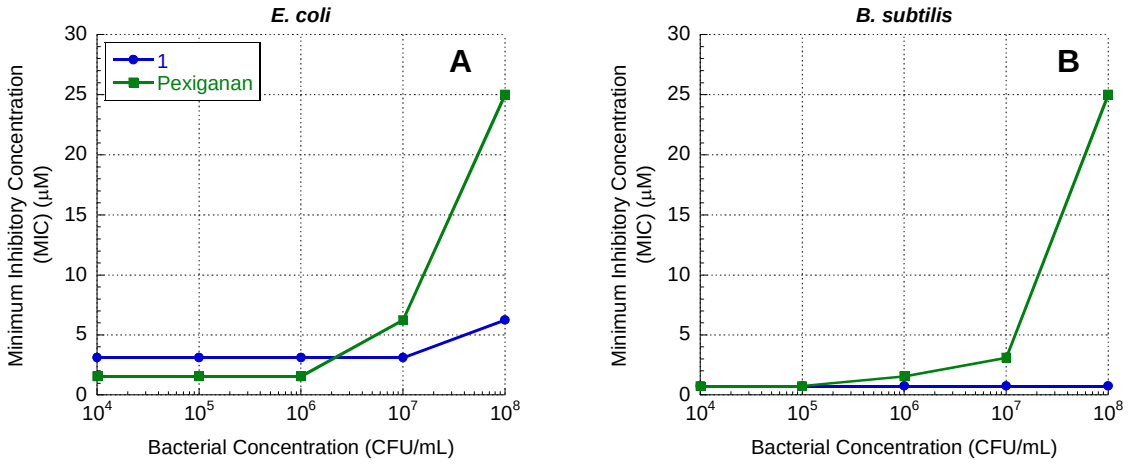

Figure 3.2: Minimum inhibitory concentration as a function of bacterial concentration of the inoculum for ampetoid 1 and comparator peptide pexiganan against (**A**) Gram-negative *E. coli* (ATCC 35218) and (**B**) Gram-positive *B. subtilis* (ATCC 6633).

across five orders of magnitude of inoculum bacterial concentration. For pexiganan, however, at bacterial concentrations of 1 x 10^7 CFU/mL inoculum and above, the MIC began to increase

significantly; the MIC of pexiganan was 3 – 5 dilutions higher after 1 x 10^8 CFU/mL inoculum compared with its value at 1 x 10^4 CFU/mL inoculum.

While this experiment was not designed to directly address the effect of backbone proteolytic susceptibility on bioavailibility, these results reveal a marked difference in in vitro activity that could be related to this phenomenon. It is possible that peptoid 1 can Proteases that are released from dead bacteria and ultimately can lead to septic shock are thought to significantly reduce the bioavailability of clinically-investigated natural antimicrobial peptides. It is possible that peptoids can kill larger numbers of bacteria because they are less susceptible to protease deactivation. A larger number of peptoids that exhibit a range of selectivity profiles need to be investigated to determine if this is a characteristic of all peptoids, or alternatively, related to the mechanism of action employed for a more selective compared to less selective antimicrobial agent.

3.2.3 Biocompatibility of peptoid 1 with intact physiology

Prior to studying *in vivo* efficacy, peptoid **1** was administered to mice at a dosage of 4 mg/kg in order to determine its compatibility with intact physiology. This dosage was selected to be on the conservative end of the dosage range typically evaluated for AMPs (1 mg/kg to 24 mg/kg) in other animal studies[73, 78, 102]. Three healthy mice were injected intraperitoneally (i.p.) with 4 mg/kg peptoid **1**, and a second control group with an equivalent volume of saline. Initially, those mice injected with peptoid **1** appeared sick, with hunch abdomens and slowed movements, but these symptoms appeared to resolve themselves after one hour. At the conclusion of the 24 hour post-injection observation period, all mice appeared to be healthy and exhibited normal activity.

3.2.4 *In vivo* efficacy of peptoid 1 in the treatment of *S. aureus* intraperitoneal challenge

We used an established murine model of bacterial infection[102] to investigate the *in vivo* efficacy of peptoid **1** to treat an infection caused by *S. aureus*, a leading cause of nosocomial infections. Four hours after *S. aureus* i.p. challenge, peptoid **1** was administered i.p. at a concentration of 4 mg/kg. After 24 hours, the animals were euthanized, and the peritoneal cavity was lavaged. The lavage was plated over 5 log dilutions in duplicate for each animal, and colonies were grown overnight and then counted. Animals that died during the experiment were assigned the highest bacterial count. As shown in **Figure 3.3**, bacterial counts in the peritoneal lavage fluid were significantly reduced ($p < 0.0007$) in mice treated with peptoid **1** compared to saline-treated controls. Additionally, mortality at 24 hours was reduced by 75% in the peptoid **1** treated group compared to the saline-treated control group.

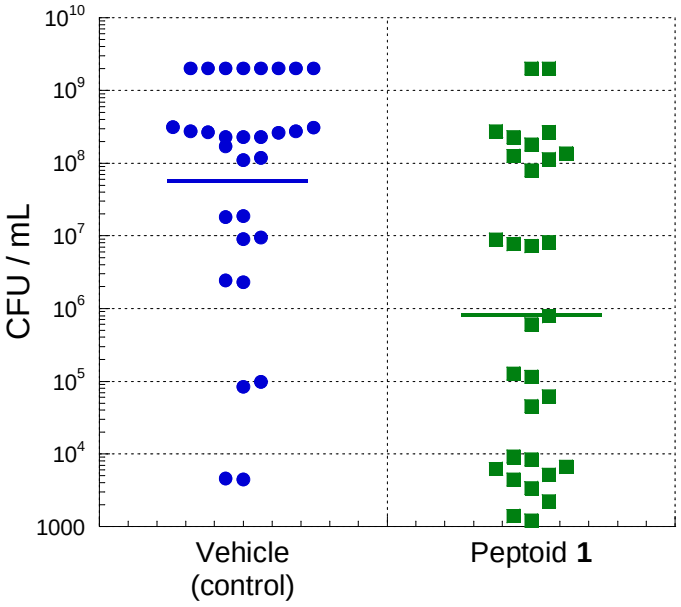

Figure 3.3: *In vivo* efficacy of peptoid 1 to treat an infection. Four hours after i.p. challenge with methicillian susceptible *S. aureus*, peptoid 1 was administered locally at a concentration of 4 mg/kg. Colony forming units (CFU) in the peritoneal lavage fluid from individual mice (plated in duplicate) at 24 hours are shown as circles in the vehicle and peptoid 1 treatment groups. Solid lines indicate the geometric mean of each group. Dead animals at 24 hours were assigned the highest colony count observed in the experiment. $p<0.0007$ by Kruskal-Wallis analysis.

3.2.5. *In vivo* efficacy of peptoid 1 using the cecal ligation and puncture animal model

We used a murine cecal ligation and puncture model of septic peritonitis to assess peptoid **1**'s ability to treat a clinically relevant polymicrobial Gram-negative infection. Briefly, mice were anesthetized, and the cecum was accessed from the peritoneum through a midline incision. The distal portion of the cecum was ligated and then punctured twice using a 25 gauge

needle. (For sham-operated mice, cecum was manipulated and replaced into the peritoneal cavity.) The cecum was compressed to express a small amount of stool. The incision was closed and peptoid **1**, dissolved in sterile PBS, was injected into the peritoneum (4 mg/kg or 8 mg/kg). Mice were monitored for 24 hours, after which the animal was euthanized and the liver, lung, and blood sample (through direct cardiac puncture) were removed. Tissues were homogenized and plated over 5 log dilutions. Colonies were grown overnight at 37^{o}C and counted the following day. The primary outcome was the CFU per gram tissue, and mortality was the secondary outcome.

Of the 36 mice used for the initial round of testing, six were sham operated (and treated with 4 mg/kg peptoid **1** as a biocompatibility screening), 15 were saline-treated controls (CLP only) and 15 were treated with peptoid **1**. Of those treated with peptoid **1**, eight were dosed with 4 mg/kg and four with 8 mg/kg. The sham operated mice exhibited no signs of distress throughout the 24 hour experiment, and plate counts on the harvested tissues indicated no sign of infection (data not shown). Mortality rates were equivalent for the treated and untreated groups (3 out of 15 for each group). The colony forming units (CFU) per gram of tissue for the surviving animals in the CLP only (n = 12) and peptoid treated groups (n = 12) are shown in **Figure 3.4**. The horizontal line in each group indicates the geometric mean.

Figure 3.4 shows that there is a considerable spread in extent of bacteremia among both the CLP alone and peptoid-treated groups. Tissues from some animals were found to be essentially non-bacteremic in both the CLP alone and peptoid-treated groups (shown as CFU/g tissue = 10). While the geometric mean is slightly lower for the treated group, the differences between treatment groups are not statistically significant. Moreover, there was no clear dose response to treatment with peptoid **1**; administering 8 mg/kg peptoid **1** demonstrated no improved efficacy over treatment with 4 mg/kg.

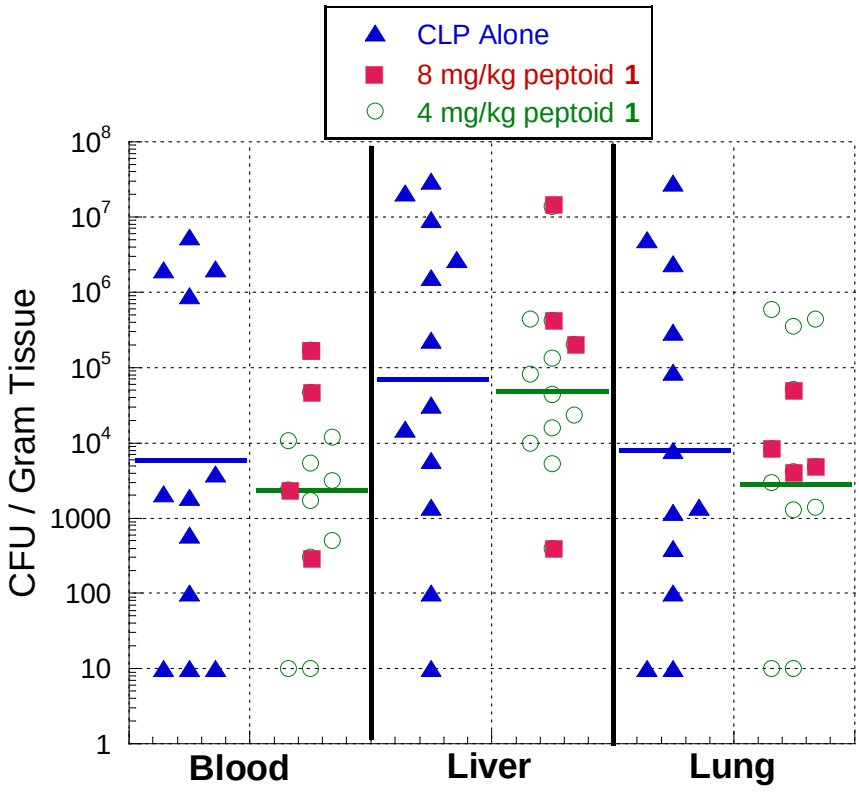

Figure 3.4: Extent of bacteriemia results for initial round of murine CLP studies. Colony forming units (CFU) per gram tissue for CLP alone and experimental groups.

The lack of infection detected in the CLP-alone treatment group is indicative of a problem with the way the model was working in our hands. Potential causes for insufficient bacterial colonization include (**1**) inadequate time for the infection to spread to remote tissues in

which bacterial counts were being made (**2**) the cecal perforation and leakage of cecal contents was insufficient to cause the infection. The protocol was iteratively revised to address these possibilities.

The first protocol revision employed in a subsequent set of studies included changes aimed at minimizing the spread of data within both the control group and treatment group. The post-surgical observation time was extended to 48 hours to ensure that the infection had adequate time to develop (minimize non-bacteremic animals), and treatment (8 mg/kg peptoid **1** or an equivalent volume of saline for controls) was administered every eight hours to maximize the potential to fight infection and mimic a clinical dosing regimen. A small group of 12 animals (six CLP alone controls and six peptoid **1** treated) were used for this study. The mortality rates were increased (50%), but equivalent in both groups. Similar to the data shown in **Figure 3.4**, the bacterial counts of tissues from these animals showed considerable spread and showed no statistically significant difference (data not shown).

The protocol was revised a second time to include two additional modifications aimed at ensuring CLP-alone animals were consistently bacteremic: (**1**) a larger bore needle (21 gauge instead of 25 gauge) was used to puncture the cecum in order to increase the degree of infection , (**2**) the CFU/mL were plated for both the blood and peritoneal lavage fluid instead of remote tissues to increase the potential for measuring a significant reduction in bacterial counts locally in the peritoneum. Animals were observed for 24 hours after treatment. All 12 animals (6 treated, 6 saline controls) survived the 24 hour post-surgical observation time. However, because the lavage fluids were not sufficiently diluted, plates were overgrown and quantitative bacterial counts could not be determined. Based on qualitative visual inspection, however, bacterial counts appeared to be lower on average in the treated group compared to the

untreated group. Bacterial counts of the blood for the control and experimental groups did not demonstrate a statistically significant difference (data not shown).

3.3 Discussion

Our *in vitro* analysis was performed on peptoid **1** and two comparator antimicrobial peptides, the latter chosen based on their clinical relevance and their disparate sizes and structures. The library of organisms we chose for broad-spectrum testing of these molecules was designed to include 20 of the most pathogenic, multi-drug resistant strains, and to include both Gram-negative (13 strains) and Gram-positive (7 strains) species. The MICs we observed for antimicrobial peptides MX-226 and MSI-78 are consistent with previously reported values for these compounds against a similar (but less multi-drug resistant) panel of species[71, 72, 103, 104].

The broad-spectrum activity profile of peptoid **1** was found to be superior to those of both MSI-78 and MX-226. The MIC of peptoid **1** was lower than ~6 μg/mL for 18 out of the 20 pathogens tested; this was the case for only 8 of 20 for MSI-78 and none of 20 for MX-226. Interestingly, MSI-78 and peptoid **1** showed similar activities against most Gram-negative strains, but MSI-78 was found to have lower activity against most of the Gram-positive strains (MRSA and VRE). The MICs of peptoid **1** (2.7 – 21.8 μg/mL) were generally about 10-fold lower than those of MX-226 (17.2 – > 272 μg/mL), demonstrating the superior *in vitro* antimicrobial activity of peptoid **1**. While it has been shown that *in vitro* activity and *in vivo* efficacy are not always directly correlated[102, 105], the potent, broad-spectrum activity of peptoid **1** against bacterial cultures is a very encouraging result.

LPS binding affinity was studied to understand in greater detail the probable initial interactions of peptoid **1** with the surface of Gram-negative bacteria. The reduced competitiveness of peptoid **1** and MX-226 for sites on LPS (71% and 73% displacement, respectively) compared to that of MSI-78 and PMB (100% displacement) suggests that all sites

are not equally accessible for all cationic molecules[99]. Several properties of the cationic molecules that may influence their competitiveness include molecular size, net charge, hydrophobicity, and steric bulk. The relative competitiveness of these molecules, however, does not translate directly to their relative affinity for LPS, a property that is inversely related to the I_{50}. While both MSI-78 (I_{50} = 1.4 μM) and peptoid **1** (I_{50} = 2.6 μM) had stronger affinity for LPS than PMB (I_{50} = 3.2 μM), MX-226 (I_{50} = 5.0 μM) demonstrated a weaker affinity. All of the cationic molecules tested had greater affinity for LPS than the most common cell envelope divalent cation, Mg^{2+} (620 μM)[106], suggesting that they can all initially bind to the outer membrane. Interestingly, however, peptoid **1** and MSI-78 had the best activity against Gram-negative bacteria (**Table 2.1**) and also the highest LPS binding affinity. This correlation is reasonable, since the LPS binding affinity of other polycations correlates well with their ability to permeabilize outer membranes[99].

While LPS binding affinity is not necessarily synonymous with endotoxin neutralizing activity[107, 108], the strong LPS binding of peptoid **1** is also a promising result that encourages further studies. LPS, also known as endotoxin, is one of the primary causes of sepsis, a serious condition that affects many hospital patients[73]. Gram-negative bacteria in septic patients release LPS, which initiates a cascade of proinflammatory events. Many endotoxemia treatments have been investigated, including polymyxin B and a variety of cationic peptides[109]. In a clinical study, polymyxin B immobilized on a surface was shown to improve the survival rates of moderately septic patients, but was ineffective in patients with severe sepsis[110]. MSI-78 was found to not only reduce endotoxin plasma levels in a rat model of sepsis, but also to reduce bacterial counts by four orders of magnitude using the cecal ligation and puncture model of bowel perforation and sepsis[73]. The strong LPS binding affinity of peptoid **1** as well as our promising *in vivo* results suggest that it may also be able to neutralize endotoxin activity in a

clinical setting; however, a series of more comprehensive tests is needed to investigate this more thoroughly.

The data presented in **Figure 3.2** suggest that peptoid **1** retains antimicrobial activity over concentrations of bacteria as high as 1 x 10^8 CFU/mL, while the activity of pexiganan began to decrease significantly at 1 x 10^7 CFU/mL. While it is uncertain if the ability of peptoid **1** to thwart high bacterial loads translates into increased bioavailability, it is an encouraging result that warrants further study. This phenomenon could be related to the invulnerability of the peptoid backbone or related to peptoid **1**'s mechanism of action.

Lastly, we studied the ability of peptoid **1** to treat an infection *in vivo* using both a murine model of i.p. *S. aureus* bacterial challenge and a more clinically relevant murine CLP model of septic peritonitis. The CLP model is recognized as the gold standard animal model for sepsis research because of its similarity to human disease progression[111-113]. The studies reported herein were instructive in developing a protocol in which animals became consistently bacteremic. We demonstrated that peptoid **1** administered at doses as high as 8 mg/kg are well tolerated. While on average animals treated with peptoid **1** exhibited slightly reduced CFU/g tissue, the differences between treatment groups were not significant, and mortality rates were equivalent.

The *S. aureus* challenge model demonstrated that a concentration of 4 mg/kg, peptoid **1** was compatible with intact physiology, and treatment at this concentration resulted in an average two-log order reduction in bacterial counts in the peritoneal lavage fluid. Moreover, mortality was reduced by 75% in the peptoid **1**-treated group compared to saline-treated controls. In contrast, MX-226 in the same model at a two-fold higher input dose failed to provide any protection (Waldbrook, M., unpublished data). While other groups have published *in vivo*

results with several types of non-natural AMP mimics[78, 101, 114, 115], this is the first report of bacterial count reduction after treatment with a peptoid-based AMP mimic *in vivo*. This encouraging proof-of-concept result with peptoid **1** could holds promise for the development of peptoids as a class of clinically useful antimicrobial agents. Several lines of study that warrant further investigation include (**1**) optimal peptoid design for *in vivo* efficacy and safety; (**2**) optimal dosage and full toxicity profile; (**3**) the efficacy of peptoid treatment compared to treatment with other AMPs; (**4**) the ability to treat a polymicrobic infection using an animal sepsis model[73], and (**5**) the metabolic fate of peptoid-based antimicrobial agents.

In summary, this study was designed to use both *in vitro* and *in vivo* techniques to probe the therapeutic potential of peptoid **1**. Broad-spectrum results suggest peptoid **1** has potent antimicrobial activities against a range of Gram-positive and Gram-negative strains, which are superior to those of comparator AMPs. Additionally, the MIC of peptoid 1 against both Gram-negative and Gram-positive bacterial strains is less influenced by bacterial load than pexiganan. Peptoid **1**'s relatively strong affinity for anionic binding sites on LPS suggest that it can displace stabilizing divalent cations and potentially permeabilize the outer membrane of Gram negative bacteria through self-promoted uptake. Most importantly, we present evidence that peptoid **1** can reduce colony forming units and mortality as opposed to a saline-treated control group using a murine model of *S. aureus* i.p. bacterial challenge. Taken together, these results underscore the promising therapeutic potential of peptoids as a new class of clinically useful antimicrobial agents.

3.4 Materials and Methods

3.4.1 Peptoid synthesis and purification

Peptoid **1** was synthesized on an ABI 433 peptide synthesizer (Applied Biosystems, Inc.) using the submonomer method[3] on Rink amide MBHA resin (Novabiochem, Inc.). Briefly,

bromoacetic acid activated by diisopropylcarbodiimide is used to form a bromoacetylated intermediate on the terminal amide group. Bromide is then substituted with the desired primary amine through S_N2 displacement to build the peptoid chain. Primary amines used to make peptoid 1 include (*s*)-α-methylbenzylamine and *N*-tert-butoxycarbonyl-1,4 diaminobutane (*N*Lys) that was made using a published procedure[83]. Synthesized peptoid was cleaved from the resin using trifluoroacetic acid (TFA):triisopropylsilane:water (95:2.5:2.5, v:v:v) for 10 minutes. Peptoid **1** was purified by reversed-phase HPLC (Waters Corporation) using a C18 column and an acetonitrile/water linear gradient. Final purity was greater than 98% measured by analytical RP-HPLC (Waters Corporation) and identity was checked using electrospray ion mass spectrometry. All reagents were purchased from Sigma-Aldrich.

3.4.2 Broad spectrum minimum inhibitory concentration (MIC) testing

MICs of test agents were measured using a modified broth microdilution method in Difco Mueller Hinton (MH) medium[116]. Briefly, serial dilutions were performed in 0.01% acetic acid containing 0.2% bovine serum albumin at 10-fold the desired final concentration. Ten microliters of the 10-fold concentrated test reagents were added to each well of a 96-well polypropylene microtitre plate containing 90 μL of MH media per well. Bacteria were added to the plate from an overnight culture at a final concentration of 2 – 7 x 10^5 CFU/mL and incubated overnight at 37°C. The MIC was defined as the concentration at which no growth was observed.

P. aeruginosa PAO1 strain H103[116], *P. maltophilia* ATCC 13637, *S. aureus* ATCC 25923[116], *E. faecalis* ATCC 29212[117], and *E. cloacae* 218R, constitutively expressing Class C chromosomal β-lactamase[118], were from the Hancock lab strains collection. An MRSA clinical isolate was kindly provided by Anthony Chow (Vancouver General Hospital, Vancouver, Canada). Two *Klebsiella pneumoniae* and two *E. coli* clinical isolates expressing extended

spectrum β-lactamases (ESBL) were kindly provided by George Zhanel (Health Sciences Centre, Winnipeg, Canada). Vancomycin-resistant clinical isolates of *Enterococcus faecalis* and *E. faecium* were obtained from Ana M. Paccagnella (BC Centre for Disease Control, Vancouver, Canada). Three clinical isolates (#9, #198 and #213) of multi-drug resistant *P. aeruginosa*, were kindly provided by Carlos Kiffer (University of São Paulo, Brazil). These isolates all have resistance to piperacillin/tazobactam, meropenem, ceftazidime, ciprofloxacin and cefepime, and while #9 is also polymyxin B resistant. Three *P. aeruginosa* clinical isolates of the Liverpool epidemic strain (LES) (H1027, H1030 and LES400)[119] were all kindly provided by Craig Winstanley (University of Liverpool, UK). LES400 was resistant to gentamicin and tobramicin, while H1030 showed resistance to colistin, amikacin, gentamicin and tobramicin. All tested bacterial strains were categorized as biosafety level 2 (BSL2) pathogens.

3.4.3 Dansyl Polymyxin B (DPX) displacement assay

The DPX displacement assay was carried out as described earlier[99, 100]. In brief, the fluorescence of dansyl Polymyxin B (Invitrogen) bound to LPS (*P. aeruginosa*) was measured by using a luminescence spectrometer LS 50B (Perkin Elmer) with excitation and emission-wavelengths of 340 nm and 485 nm, respectively. A predetermined amount of DPX, resulting in 90% saturation of LPS, was added to 1 mL of 3 µg/mL of purified LPS. Small aliquots (5 µL of 1 µg/mL) of test compounds were added under constant stirring in the cuvette, and the displacement of DPX was measured for 30-60 seconds as a decrease in fluorescence. The process was repeated until maximum displacement was reached.

3.4.4 Bacterial load minimum inhibitory concentration (MIC) testing

MICs were determined in 96-well microtiter plates in accordance with CLSI M7-A6 protocols. Peptoid solutions with 50 µL total volume were prepared using 2:1 serial dilutions. 50 µL of bacteria inoculum (1×10^4, 1×10^5, 1×10^6, 1×10^7, or 1×10^8 CFU/mL) prepared in cation-adjusted Mueller-Hinton broth (CAMHB) was added to test wells. Control wells contained

100 µL MHB (no growth) or 50 µL inoculums with 50 µL MHB with no peptoid. The MIC was taken as the lowest concentration of peptoid that completely inhibited bacterial growth after 16 hours of incubation at 35^{o}C.

3.4.5 Murine model of *S. aureus* bacterial infection

Animal experiments were performed in accordance with UBC animal care ethics approval and guidelines. Female CD-1 mice (6 – 8 weeks old) were weighed, marked, and injected with 200 µL of *S. aureus* (ATCC 25923) in 5% mucin solution i.p. Four hours after infection, animals were treated with 4 mg/kg peptoid **1** (experimental group) or an equivalent volume of saline (control group). The mice were euthanized 24 hours post-infection. The peritoneal cavity was exposed and washed with 5 mL PBS. The lavage was diluted to 10^{-5} in log order increments and spotted in duplicate onto Mueller Hinton agar plates. Plates were incubated overnight at 37^{o}C and colonies were counted the following day.

3.4.6 Cecal ligation and puncture animal model

C57 Black mice were weighed, marked, and anesthesized with pentabarbitol. A midline incision was made through the abdominal wall and the cecum was identified. The distal portion of the cecum was ligated and punctured two times with a 25 or 21 gauge needle. For sham-operated animals, the cecum was manipulated but not ligated or punctured. A small amount of stool was expressed through the wound and the cecum was replaced into the peritoneum. The incision was closed, suturing the abdominal wall and skin layers separately. Treatment (saline for controls) was then administered i.p. Animals were monitored for 24 – 48 hours post-surgery, after which the animals were euthanized and tissues were removed. The tissues were mixed with an equivalent volume of sterile saline and homogenized. The homogenates were serially diluted and plated over five log dilutions on 5% sheep's blood Agar plates, incubated at 37^{o}C for 24 hours, and the colonies were counted. Data are expressed as colony forming units per gram tissue.

3.4.7 Statistical Methods

The results of the mouse studies were analyzed using the Kruskal-Wallis method to determine their statistical significance.

3.5 Study contributions

Ann Czyzewski performed experiments, analyzed data, performed statistical analysis, wrote the paper; Havard Jenssen performed experiments; Matt Waldbrook performed experiments; Brad Tilford performed experiments; Xioadi Tan (collaborating PI) designed experiments; David Steinhorn (collaborating PI) designed experiments; Robert Hancock (collaborating PI) designed experiments; Annelise Barron designed experiments and initiated collaboration.

4. A study exploring synergy between peptoid-based mimics of lung surfactant proteins SP-B and SP-C.

4.1 Introduction

Lung surfactant (LS) is a complex lipid-protein mixture that reduces surface tension at the alveolar air-liquid interface, enabling normal respiratory function. Without functional LS, there is considerable resistance to lung expansion, which ultimately causes alveolar collapse (atelectasis) and respiratory failure[120, 121]. Since the discovery of LS in 1929 and subsequent reporting of its clinical importance, there has been keen interest in elucidating the nature of its constituents and their interactions.

LS is composed of ~90% lipid and ~10% protein, by weight[122, 123]. The lipids are comprised of 80% phospholipids and 20% neutral lipids, half of which is cholesterol. Phosphatidylcholines, account for 95% of the phospholipids; two-thirds of this portion are comprised of dipalmitoyl phosphotidylcholine (DPPC)), and the rest are unsaturated phospholipids. Other lipid components include phosphotidyl glycerol (PG) (11%), phosphatidyl linositol (4%), and lesser amounts of phosphatidylethanolamine, phsophatidylserine, sphingomyelin, and lysophosphotidylcholine[124]. Whereas the function of the primary lipid component, DPPC, is to lower surface tension, the less abundant anionic lipids (primarily PG) enable the surfactant to rapidly adsorb to the alveolar air-liquid interface and allow it to respread easily during the repeated pulmonary expansion and compression of the breathing cycle[125, 126].

The strictly conserved hydrophobic surfactant proteins (SP), SP-B and SP-C[124], facilitate lipid organization and LS respreading, which is critical to biophysical functionality[127-129]. The specific mechanisms of lipid-protein interactions remain unclear; evidence suggests, however, that both the charged headgroups and the alkyl tails of lipids play an important role[9]. Schematics of SP-B and SP-C and their hypothesized interactions with lipid bilayers are shown

in **Figure 4.1**. SP-B is 79 amino acids long and contains three intramolecular disulfide bridges[130]. The native homodimeric form is composed of two monomers joined by an intermolecular disulfide bond[124, 131-133]. SP-C is 35 monomers long and extremely hydrophobic, due to its unusually high content of nonpolar residues[124]. Both SP-B [124, 134, 135] and SP-C[129, 136-139] enhance the rate of surfactant adsorption and respreading, though their disparate structures suggest that they employ distinct mechanisms.

Neonatal respiratory distress syndrome (nRDS) is a common disease in premature infants that has been linked to surfactant deficiency and occurs when type II pneumocyte cells, which produce LS, have not matured sufficiently to properly carry out their function[140, 141]. The

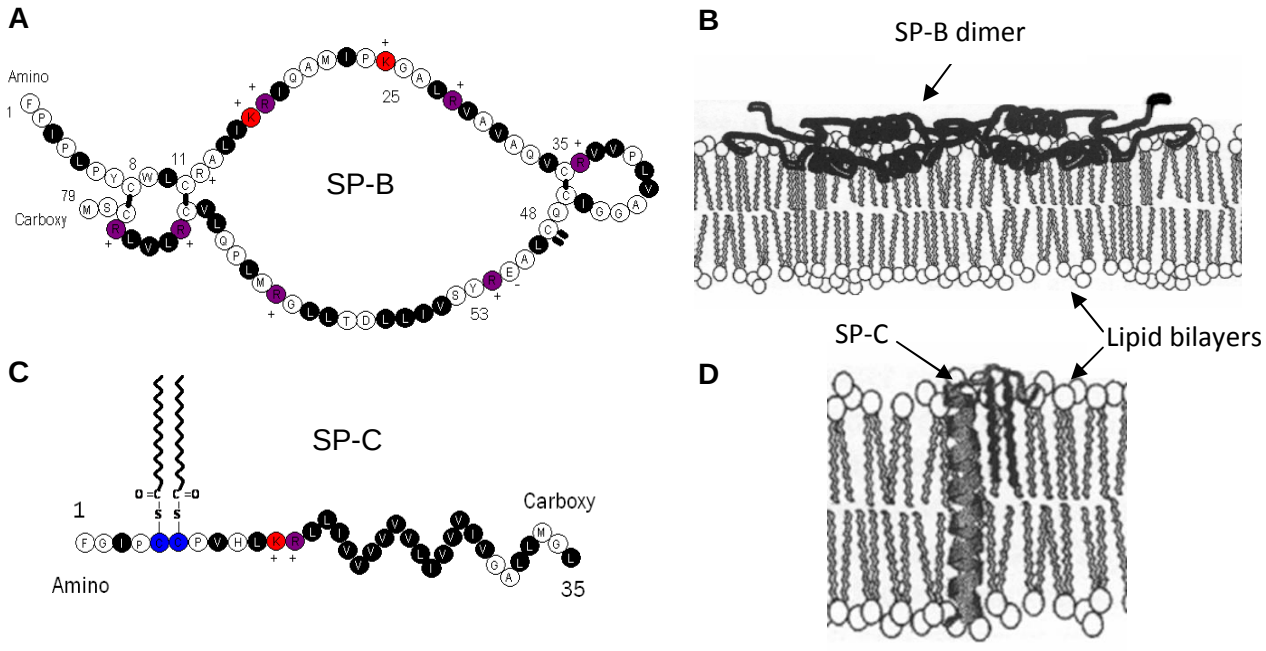

Figure 4.1: Schematics of lung surfactant proteins SP-B and SP-C. (**A**) Schematic of SP-B monomer. Charged lysines are shown in red and arginines in purple. Intramolecular disulfide bonds are shown at positions 8, 11, and 35. The intermolecular bond that forms the dimer is at position 48. (**B**) Schematic of SP-B dimer interacting with lipid bilayer headgroups. (**C**) Schematic of SP-C. Palmitoylated cysteine monomers at positions 5 and 6 are shown in blue. **(D)** Schematic of SP-C interacting with a lipid bilayer. Panels (**A**) and (**C**) were adapted from [6] and (**B**) and (**D**) were adapted from [9].

use of exogenous surfactant replacement therapy (SRT) to help restore functionality has been a successful strategy to treat this disorder, as will be discussed more fully in **Chapter 6**. Using natural, animal-derived SRT for the treatment of nRDS is now routine, resulting in ~40% reduction in mortality[124, 142].

While nRDS is effectively treated by SRT in some areas of the world, RDS in general remains a significant global health problem. There are an estimated 50 to 60 thousand cases of nRDS per year in the U.S.[124] and nearly 2 million worldwide[143], many of which go untreated due to the high cost of currently available SRT[144]. Acute RDS (ARDS), which is associated with dysfunctional or inactivated LS, can develop as a result of many different disease states in both adults and children (as discussed more fully in **Chapter 5**)[120, 145, 146]. While the best treatment for ARDS is still a matter of debate[147, 148], there is growing evidence to suggest that SRT as part of a multimodal therapy could improve the prognosis for many[149]. However, the high cost of currently available treatments coupled with the large quantities needed to treat adults make its use impractical[150].

Biomimetic LS replacements are a novel class of formulations composed of synthetic lipids with recombinant or chemically synthesized mimics of either SP-B or SP-C[124]; they have the potential to address the concerns of high cost and dubious safety associated with natural surfactants while maintaining equivalent efficacy[151]. The development of LS replacements that are increasingly efficacious, cost-effective, and long-lasting *in vivo* would be a tremendous advancement that would open the door to the development of these innovative applications that are currently prohibitively expensive. *N*-substituted glycines (peptoids)[14] are one class of sequence specific biomimetic polymers that have shown promise as functional mimics of SP-B and SP-C[36, 37, 46].

Peptoids are non-natural biopolymers that differ from peptides in that the side chains are appended to the backbone amide nitrogens rather than to the α-carbons[3, 14]. The structural differences between peptoids and peptides have important implications for biomimicry. The non-natural peptoid backbone renders these molecules impervious to protease activity, thereby increasing their biostability and reducing specific recognition by the immune system[21, 152]. Small peptoids have been found to induce only a very low-level antibody response, and they have been found to be bioactive, non-toxic, and non-immunogenic[22]. The conformational and stereochemical ramifications of the *N*-substituted peptoid backbone are also significant[11]. The lack of amide protons and chiral centers in the peptoid backbone results in the absence of backbone-mediated hydrogen bonding and precludes the formation of intrinsic molecule handedness. It has been shown, however, that incorporation of α-chiral side chains generates steric and electronic repulsions, thereby inducing a stable helical architecture similar to that of polyproline type I helices (~3 residues per turn, pitch of ~6 Å)[11]. Peptoids are highly amenable to use in commercializable medical applications because, unlike other non-natural oligomers, they are relatively easy and cost-effective to synthesize[153-156]. Peptoids up to 50 monomers long can be made in good yield due to high coupling efficiencies and the low cost of readily available starting reagents[3, 28].

Natural lung surfactant is a complex mixture of biomolecules, the function of which cannot be replicated by any of its single components. Peptoids designed to mimic the structure of SP-B and SP-C have been shown to exhibit substantial surface activity *in vitro*[36, 37, 46]. While these classes of mimics have been developed and optimized separately, as discussed previously, both natural SP-B and SP-C contribute to biophysical functionality of natural surfactant. While synergy has not been demonstrated between natural SP-B and SP-C, we designed experiments to determine if peptoid-based mimics of these molecules exhibit synergy.

Here we created several formulations, each containing one SP-B mimic and one SP-C mimic, to investigate potential synergistic interactions between the two types of mimics. Using the pulsating bubble surfactometer (PBS) we demonstrate that for selected formulations, the surface activity of the combination is superior to that of either component individually, in terms of the rate of adsorption to the air liquid interface, equilibrium surface tension, and the maximum surface tension during dynamic cycling. The most promising formulation appears to exhibit emergent surface activity that resembles the *in vitro* activity of natural surfactant.

4.2 Results

4.2.1 Study design

We have previously shown that peptoids designed to emulate the structure and physicochemical properties of SP-B and SP-C can mimic their ability to reduce surface tension *in vitro*[36, 37, 46, 47]. Peptoid **C**, shown in **Figure 4.2**, is a first generation SP-C mimic that was designed to capture three characteristics of SP-C's structure: (**1**) helical architecture, (**2**) extreme hydrophobicity, particularly in the *C*-terminal region, (**3**) amphipathic patterning of hydrophobic and charged monomers[1, 37, 46]. In a second generation, the *N*-terminal palmitoylation of SP-C was mimicked, resulting in substantial improvement in surface activity[1]; peptoid $\mathbf{C}_{mono}$ exhibits one *N*-terminal octadecylamine to mimic the monopalmitoylated structure of canine SP-C, while $\mathbf{C}_{di}$ contains octadecylamines at both positions one and two, mimicking the dipalmitoylated structure of human SP-C (**Figure 4.2**)[1].

Peptoid-based SP-B mimics[36, 47] were designed in a similar way to emulate the essential features of the *N*-terminal portion of SP-B, SP-B_{1-25} , which has been shown to exhibit surface activity *in vitro* and *in vivo*[157-159]. Peptoid **B** (**Figure 4.2**) was designed to mimic the overall helical architecture and cationic charge placement of SP-B_{1-25}[36, 47]. Additionally, **B** includes an octameric helical *N*-terminal segment intended to mimic the insertion region of SP-B_{1-25}[47], which may have a role in anchoring the peptide in lipid layers[160]. Similar to the strategy employed to improve the surface activity of SP-C mimics, mono- and dialkylated SP-B mimics based on the sequence of **B** were made ($\mathbf{B}_{mono}$ and $\mathbf{B}_{di}$)[8]. This modification was not inspired by the structure of natural SP-B, but rather, motivated by the improvement in surface activity achieved by the alkylated SP-C mimics.

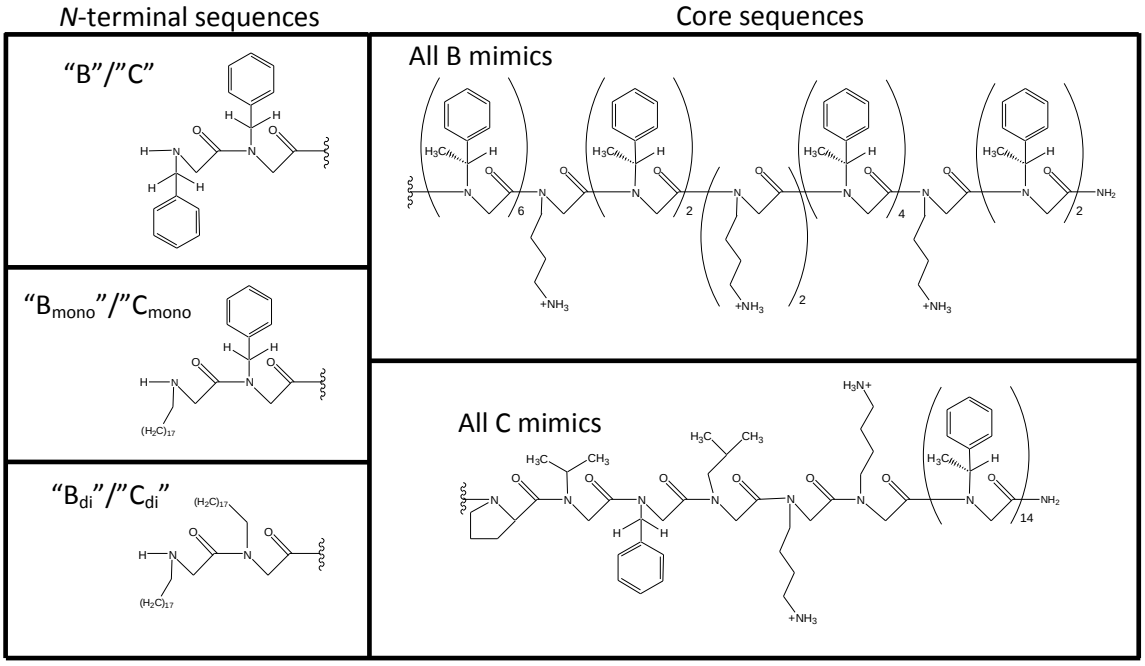

Figure 4.2: Structures of peptoid-based mimics of SP-B and SP-C[1, 8]. The *N*-terminal sequences **B** and **C** are unalkylated mimics, $\mathbf{B}_{mono}$ and $\mathbf{C}_{mono}$ are monoalkylated, and $\mathbf{B}_{di}$ and $\mathbf{C}_{di}$ are dialkylated at the *N*-terminus, as shown.

While these families of mimics have been designed and developed independently, the goal of this study was to determine if formulations containing both SP-B and SP-C mimics exhibit any synergistic improvement in *in vitro* surface activity. Using the pulsating bubble surfactometer (PBS) we tested the surface activity of all combinations containing equal amounts of one SP-B mimic and one SP-C mimic shown **Figure 4.2**. The compositions of the nine formulations are shown schematically in **Figure 4.3**. The total concentration of peptoid was held constant at 2 mol%, comprised of 1 mol% of each peptoid. Additionally, Tanaka lipids (DPPC:POPG:PA) (68:22:9) were used as the lipid portion of each preparation. Static and dynamic mode pulsating bubble surfactometry was performed on all six peptoid mimics individually (2 mol%) as well as on the nine specified combination formulations.

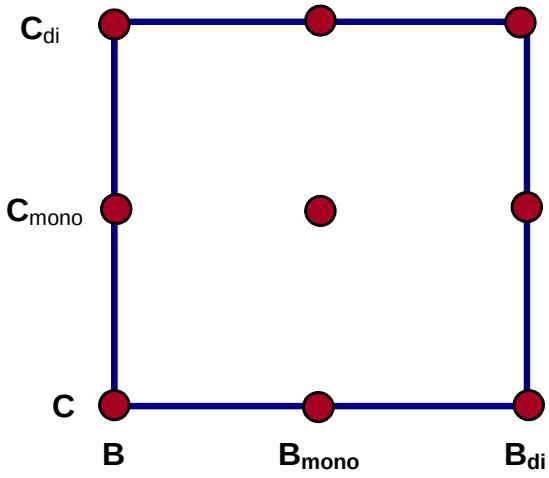

Figure 4.3: Experimental design. The nine combinations of SP-B mimic / SP-C mimic combinations are designated by red circles in the coordinate space. Other variables held constant in this study are: (**1**) total of 2 mol%, (**2**) 50/50 concentration ratio (1 mol% each mimic), and (**3**) Tanaka lipids (1 mg/mL) for all samples.

4.2.2 Pulsating bubble surfactometry.

The pulsating bubble surfactometer (PBS) is an instrument that is used to assess the *in vitro* surface activity of surfactant preparations[161]. The surfactant sample is loaded into the sample chamber (80 µL), which is connected to the atmosphere through a small capillary. A bubble is formed in the surfactant solution at the bottom of the chamber and a pressure transducer is used to vary the internal pressure. The cycling of the pressure creates an "*in vitro* alveolus" dynamic system that mimics the alveolar expansion and compression of the breathing

cycle[162]. The actual size and shape of the bubble are tracked using an optical monitoring system[163], and surface tension is calculated from the pressure gradient across the surface of the bubble using the law of Young and LaPlace. We used the PBS in both static and dynamic modes (discussed below) to assess the *in vitro* surface activity of each single component and all combination formulations. Samples were made in Tanaka lipids, a mixture that has been shown to exhibit good surface activity *in vitro*[164], and run at 37°C to match physiologic conditions.

4.2.2.1 Static mode pulsating bubble surfactometry.

In static mode, a bubble is formed in the sample and the surface tension is recorded for 20 minutes to evaluate the adsorption kinetics and equilibrium surface activity of surfactant preparations. Efficacious lung surfactant replacements typically reach a surface tension of 25 mN/m within the first two minutes of the run[165]. Of the nine combinations shown in **Figure 4.3**, those that contained similarly-alkylated SP-B and SP-C mimics appeared to exhibit some measure of synergistic behavior in both static and dynamic modes. **Figure 4.4 A-C** shows the static mode adsorption behavior of the **B**/**C**, $\mathbf{B}_{mono}$/$\mathbf{C}_{mono}$, and $\mathbf{B}_{di}$/$\mathbf{C}_{di}$ formulations, respectively compared to that of each individual component at the same mol%. The static adsorption data for the remaining six formulations are shown in **Figure 4.5** panels **A-F**.

Figure 4.4 A, B shows that the **B/C** and $\mathbf{B}_{mono}/\mathbf{C}_{mono}$ formulations exhibit considerable synergy, either due to reaching a lower equilibrium surface tension (33 mN/m for the B/C formulation compared to 38 – 40 mN/m for individual components) (**Figure 4.4 A**) or an equivalent surface tension in a much faster time (< 100 seconds for the $\mathbf{B}_{mono}/\mathbf{C}_{mono}$ formulation compared with ~600 seconds for the best performing individual component) (**Figure 4.4 B**). The dialkylated mimic formulation exhibited only slight improvement in adsorption kinetics

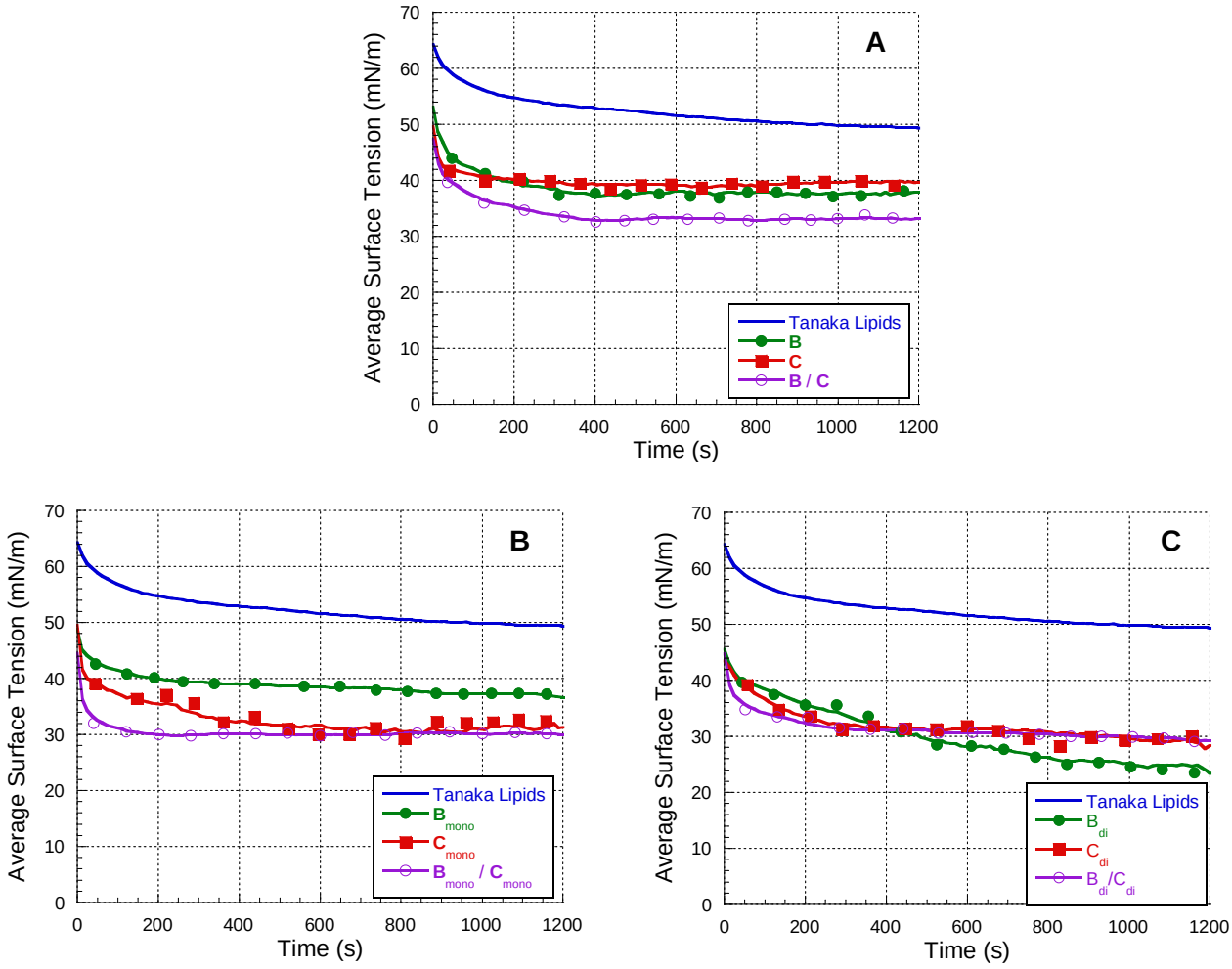

Figure 4.4: Static mode pulsating bubble surfactometer data. Each panel displays a formulation of SP-B/SP-C mimics along with the individual components at an equivalent mol% (2 mol% total). (**A**) **B/C** formulation, (**B**) $\mathbf{B}_{mono}/\mathbf{C}_{mono}$ formulation, (**C**) $\mathbf{B}_{di}/\mathbf{C}_{di}$ formulation. Formulations were comprised of 1 mol% of each mimic.

compared to the individual components. $\mathbf{B}_{di}$ reached a lower surface tension after 20 minutes (~24 mN/m) compared to the $\mathbf{B}_{di}/\mathbf{C}_{di}$ formulation (~ 30 mN/m) but its rate of adsorption was significantly slower (**Figure 4.4 C**). **Figure 4.5** panels **C** and **D** show that the formulation of $\mathbf{B}_{mono}/\mathbf{C}$ and $\mathbf{B}_{mono}/\mathbf{C}_{di}$, respectively, also exhibit considerable synergy in terms of reaching a lower equilibrium surface tension. As will be discussed, however, these formulations do not appear synergistic in dynamic cycling mode.

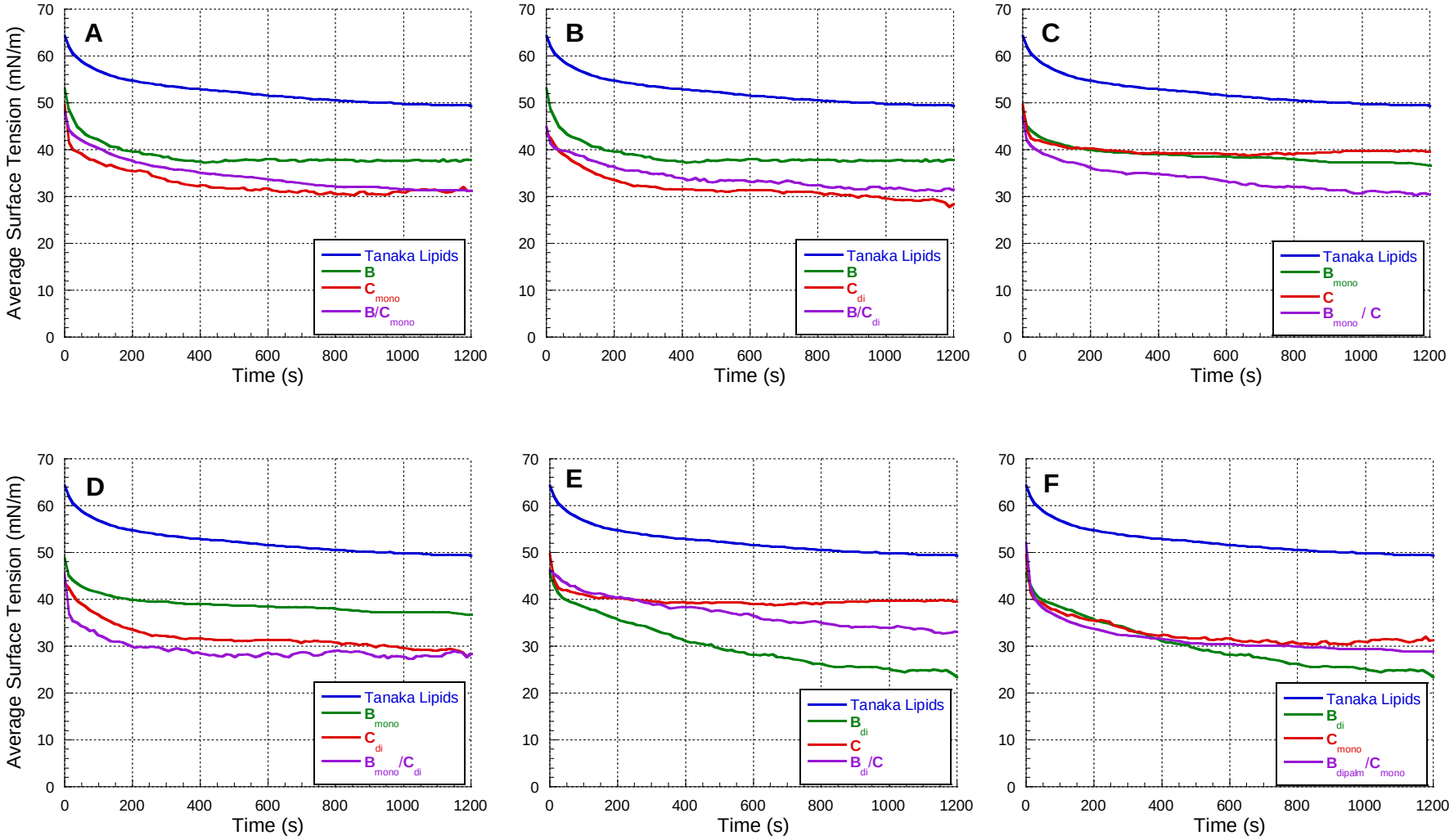

Figure 4.5: Static mode PBS runs of six formulations containing one SP-B and one SP-C peptoid-based mimic. Each plot contains a binary formulation (2 mol% total, 1 mol% each mimic) and the individual peptoid components (2 mol%) prepared at 1 mg/mL. Formulations shown include (**A**) **B/C**$_{mono}$; (**B**) **B/C**$_{di}$; (**C**) **C/B**$_{mono}$; (**D**) **B**$_{mono}$**/C**$_{di}$; (**E**) **B**$_{di}$**/C**; (**F**) **B**$_{di}$**/C**$_{mono}$.

4.2.2.2 Dynamic mode pulsating bubble surfactometry.

Upon exhalation, the alveolar sacs shrink and the spread surfactant monolayers are compressed into reservoirs in the subphase. According to one theory, non-DPPC lipids are selectively "squeezed-out", resulting in an enriched DPPC monolayer[135]. During expansion, lipids from the reservoirs are re-spread into a monolayer to cover the expanded surface area[162]. The ability of a surfactant to perform these dynamic functions is measured *in vitro* using a

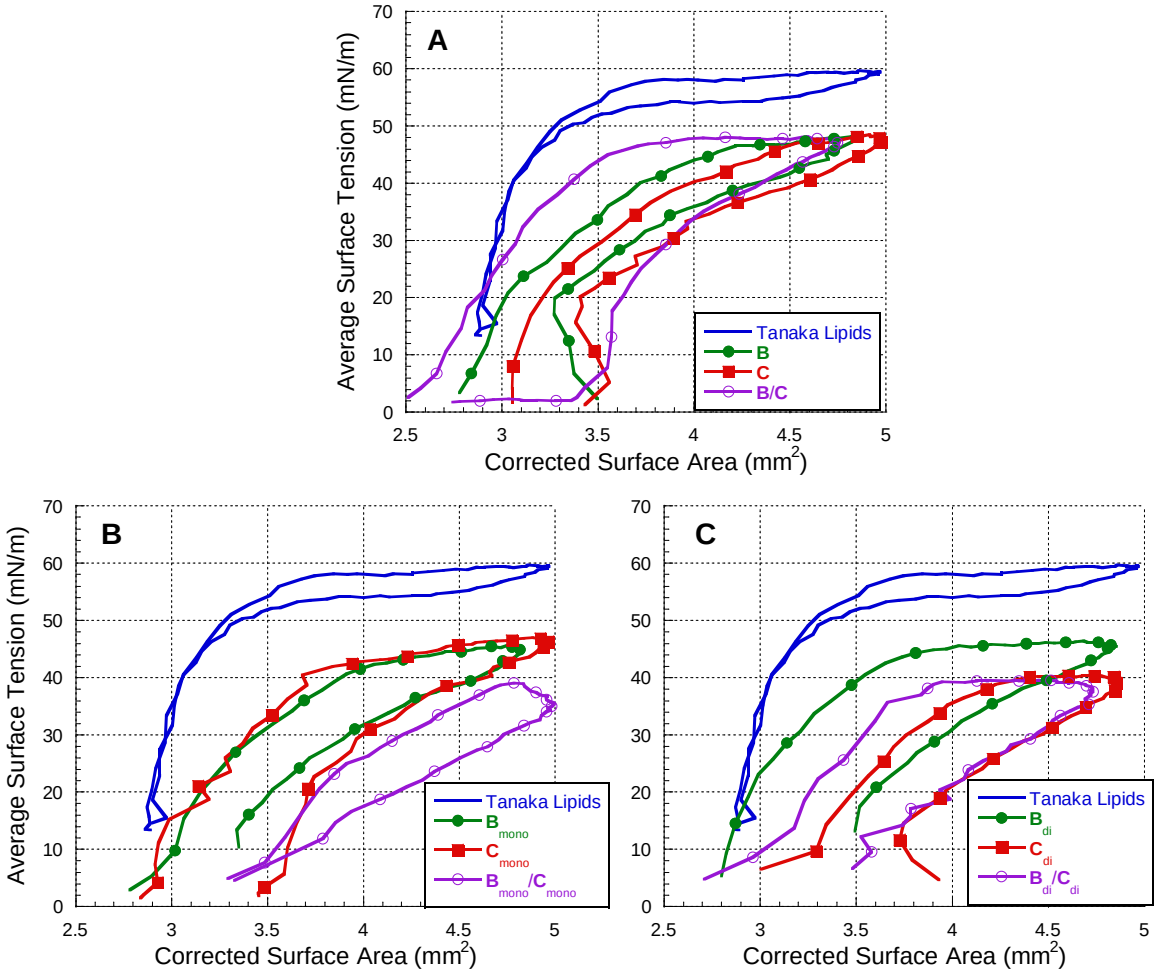

Figure 4.6: Static mode pulsating bubble surfactometer data. Each panel displays a formulation of SP-B/SP-C mimics along with the individual components at an equivalent mol% (2 mol% total). (**A**) **B/C** formulation, (**B**) $\mathbf{B}_{mono}/\mathbf{C}_{mono}$ formulation, (**C**) $\mathbf{B}_{di}/\mathbf{C}_{di}$ formulation. Formulations are comprised of 1 mol% each mimic.

pulsating bubble surfactometer in dynamic cycling mode.

The data are represented as a hysteresis loop on a plot of bubble surface area versus surface tension, as shown in **Figure 4.6**. Note that because the bubble deforms significantly at low surface tensions, the optical monitoring device cannot accurately track the bubble shape. As a result, data at low surface tensions is not recorded, and the hysteresis loop is not closed, The extent to which the bubble deforms upon compression, however, is an indication that the surface tension is near 0 mN/m.

While the maximum surface tension is an indication of how well a surfactant adsorbs to the interface (*i.e.* a low maximum reflects good adsorption), the minimum surface tension is related to the degree of enrichment of the DPPC monolayer (*i.e.* a low minimum reflects a highly enriched layer)[162]. A large degree of hysteresis in the pulsation cycle loop is an indication that minimal compression is required to attain low surface tension – a characteristic of a highly surface-active mixture. The horizontal shift of hysteresis loops is not relevant to surface activity, but only an artifact of the initial size of the bubble before pulsation begins. Dynamic cycling experiments were performed at an oscillatory frequency of 20 cycles per minute for approximately 20 minutes or until the maximum and minimum surface tensions were no longer changing.

As discussed, an efficacious lung surfactant replacement is expected to exhibit a low maximum surface tension (~35 mN/m) and minimum surface tension (~0 mN/m) as well as significant hysteresis[165]. The hysteresis loops for the **B**/**C**, $\mathbf{B}_{mono}/\mathbf{C}_{mono}$, and $\mathbf{B}_{di}/\mathbf{C}_{di}$ formulations compared to their respective individual components are shown in **Figure 4.6 A-C**. Dynamic cycling PBS plots of the remaining six combinations are shown in **Figure 4.7 A-F**. **Figure 4.6A** shows that the maximum and minimum surface tensions of the **B**/**C** formulation are similar to

that of the individual components (~48 mN/m), but the degree of hysteresis is significantly larger for the **B**/**C** formulation. **Figure 4.6C** shows that while $\mathbf{C}_{di}$ alone and $\mathbf{B}_{di}/\mathbf{C}_{di}$ exhibited equivalent maximum surface tensions, (~40 mN/m), hysteresis is again greater for the $\mathbf{B}_{di}/\mathbf{C}_{di}$ formulation. The maximum surface tension of $\mathbf{B}_{di}$ alone was significantly greater (~46 mN/m). **Figure 4.7 A** and **E** show that the maximum dynamic surface tension of $\mathbf{B}/\mathbf{C}_{mono}$ and $\mathbf{B}_{di}/\mathbf{C}_{mono}$ are considerably lower than for the respective individual components, but these were not synergistic during static bubble surfactometry.

The most remarkable change in dynamic cycling behavior was exhibited by the $\mathbf{B}_{mono}/\mathbf{C}_{mono}$ combination (**Figure 4.6B**). Both the $\mathbf{B}_{mono}$ and $\mathbf{C}_{mono}$ individual components exhibit similarly shaped hysteresis loops, with maximum surface tensions of ~46-47 mN/m. The $\mathbf{B}_{mono}/\mathbf{C}_{mono}$ formulation, on the other hand, exhibited a significantly different shape and a reduced maximum surface tension (~40 mN/m). The $\mathbf{B}_{mono}/\mathbf{C}_{mono}$ combination appears to exhibit the most dramatic improvement in surface activity compared to its individual components in terms of both static and dynamic adsorption behavior.

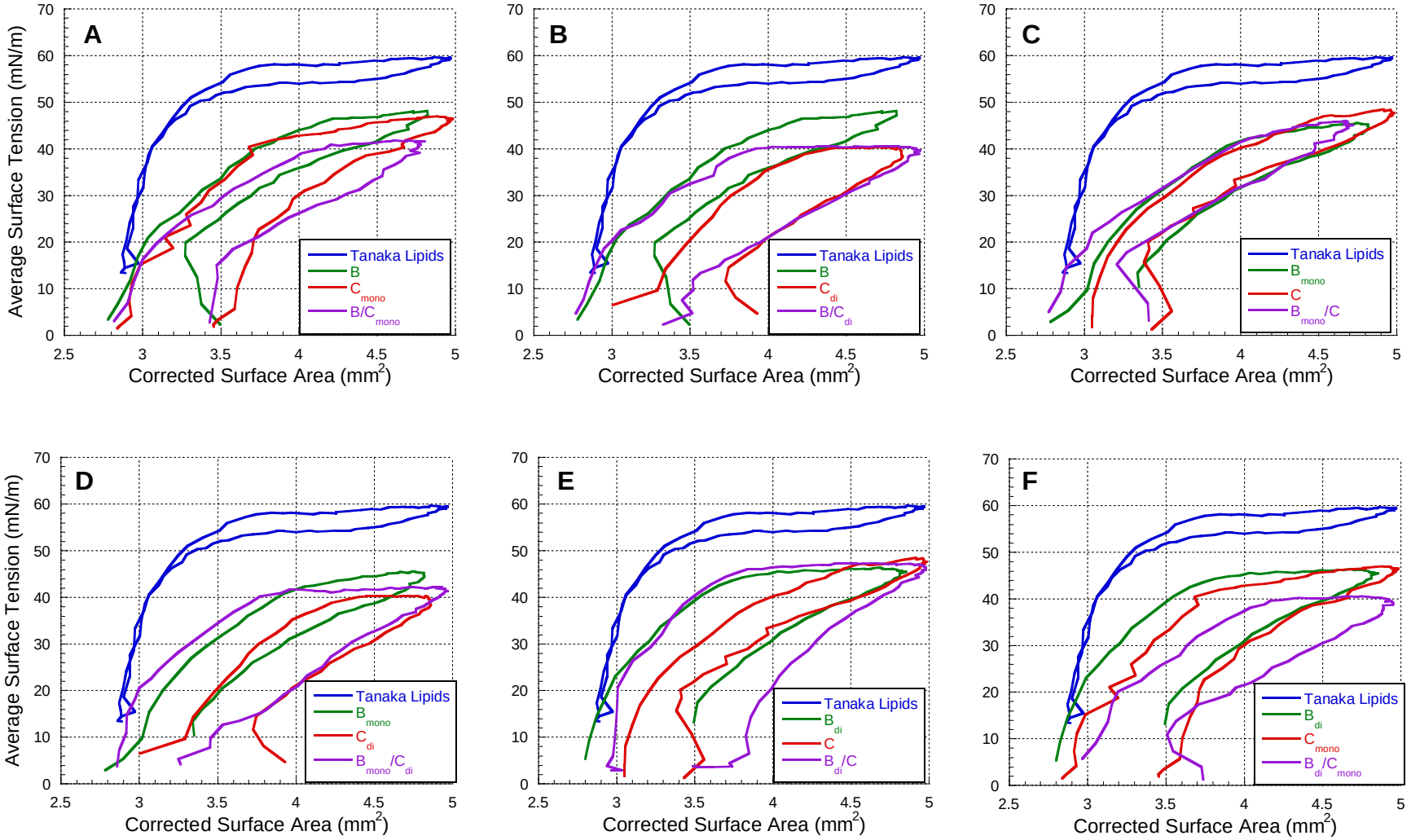

Figure 4.7: Dynamic mode PBS runs of six formulations containing one SP-B and one SP-C peptoid-based mimic. Each plot contains a binary formulation (2 mol% total, 1 mol% each mimic) and the individual peptoid components (2 mol%) prepared at 1 mg/mL. Formulations shown include (**A**) **B/C**$_{mono}$; (**B**) **B/C**$_{di}$; (**C**) **C/B**$_{mono}$; (**D**) **B**$_{mono}$**/C**$_{di}$; (**E**) **B**$_{di}$**/C**; (**F**) **B**$_{di}$**/C**$_{mono}$.

4.2.2.3 Comparison to natural surfactant

We compared the equilibrium static adsorption and dynamic cycling behavior of the most surface-active formulation, $\mathbf{B}_{mono}/\mathbf{C}_{mono}$, to that of natural lung surfactant extracted from bovine sources. **Figure 4.8A** shows that the adsorption kinetics of $\mathbf{B}_{mono}/\mathbf{C}_{mono}$ is very similar to that of natural LS and the equilibrium surface tension was only slightly lower for natural LS (~27 mN/m) compared to the peptoid formulation (~30 mN/m). The data in **Figure 4.6B** show that while the maximum surface tension of natural surfactant (~34 mN/m) is lower than that of $\mathbf{B}_{mono}/\mathbf{C}_{mono}$ (~39 mN/m) the distinct loop-shape of the dynamic cycling hysteresis loop for the peptoid formulation is strikingly similar to that of natural surfactant and distinctly different from that of Tanaka lipids alone or in combination with other peptoids.

4.3 Discussion

While animal-derived exogenous lung surfactant replacement is efficacious and used routinely to treat nRDS[124], the development of a wholly synthetic lung surfactant replacement would make treatment accessible in less developed countries and make practical its utility in treating other respiratory diseases. Peptoids, in combination with synthetic lipid mixtures, have

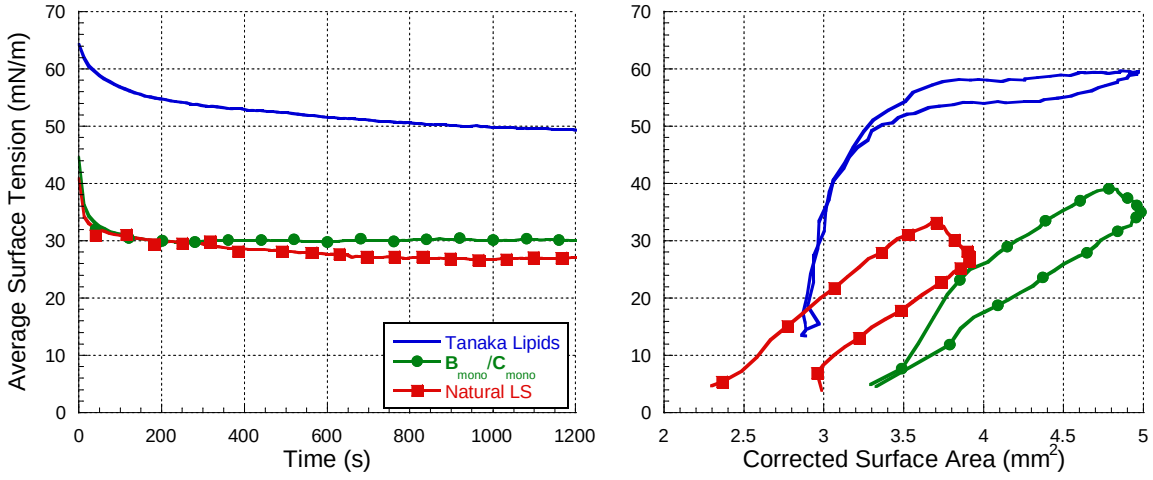

Figure 4.8: PBS data comparing the surface activity of the $\mathbf{B}_{mono}/\mathbf{C}_{mono}$ formulation to that of natural surfactant. (**A**) Static adsorption equilibrium curves and (**B**) dynamic cycling hysteresis loops, cycling at 37°C at an oscillatory frequency of 20 cycles/minute.

shown promise as mimics of lung surfactant proteins SP-B and SP-C, which are critical to the surface tension-reducing biophysical function of natural lung surfactant. The three mimics of SP-B and SP-C included in this study differ in their degree of alkylation, a structural motif that is native to natural SP-C. The mono- (canine[166]) and di-palmitoylation (human[167, 168]) of the *N*-terminal region of SP-C has been hypothesized to have several possible functions, including (**1**) increasing surface activity[138], (**2**) facilitating lamellar body assembly[169], and (**3**) organizing lipid layers[170]. It has been shown that mono- and di-alkylated peptoid mimics of both SP-B[8] and SP-C[1] also show improvement in surface activity compared to their unalkylated counterparts.

Four formulations containing both SP-B and SP-C mimics showed improved surface activity either in terms of a reduced equilibrium surface tension (**B_{mono}/C** and **B_{mono}/C_{di}**, **Figure 4.5**) or reduced maximum surface tension during dynamic cycling (**B/C_{mono}** and **B_{di}/C_{mono}**, **Figure 4.7**). Because the equilibrium and maximum surface tensions are correlated with a surfactant's adsorption capability[162], it is possible that the components of these formulations synergistically facilitate adsorption to the air-liquid interface. The similarly-alkylated combinations exhibited some degree of synergy in both static and dynamic cycling modes (**Figures 4.4 and 4.6**). The **B_{mono}/C_{mono}** formulation, however, demonstrated the most dramatic change in surface activity compared to its individual components in both modes.

The apparent synergy between peptoid mimics is an interesting result, as the natural proteins have not been shown to exhibit synergistic interaction in facilitating biophysical functions[171]. The functions of natural SP-B and SP-C have been found to largely overlap[162] and include (**1**) facilitating lipid adsorption to the air/liquid interface[136, 172], (**2**) surfactant re-uptake by type II pneumocyte cells[173, 174], (**3**) lipid film respreading[139], and (**4**) lipid layer stabilization[138, 175]. In a previous study by Wang, *et al*., incorporating both proteins into a formulation did not have a synergistic effect on resultant surface activity[171]. This result is commensurate with other studies

that suggest natural SP-B and SP-C activities are independent[136, 139]. While peptoid-based mimics were designed to emulate physicochemical properties of natural SP-B and SP-C, they are significantly smaller and are arguably more simple in structure. It is likely, therefore, that peptoid mimics do not employ precisely the same mechanism as the natural molecules and interact differently with the lipid layer.

It is conceivable that a formulation of different, more simple peptoids is able to more closely mimic the function of more complex natural proteins. For example, the formulation of **B**$_{mono}$/**C**$_{mono}$ is unique among those tested in that it is the only formulation that contains a total of two alkyl chains, each attached to separate molecules. Other formulations that contain two alkyl chains (**B**$_{di}$/**C** and **B**/**C**$_{di}$) have both chains attached to the same molecule. It is possible that the distribution of alkyl chains on separate molecules allows them the conformational freedom to interact in a uniquely synergistically manner. Further work is required to evaluate other formulation parameters which likely affect surface activity, including (**1**) ratio of SP-B and SP-C mimic, (**2**) total mol% mimic, (**3**) synthetic lipids used.

The most surface-active formulation, **B**$_{mono}$/**C**$_{mono}$, exhibits *in vitro* surface activity that is strikingly similar to that of natural surfactant (**Figure 4.8**) and significantly different than either component alone in the same lipid mixture by measures of equilibrium and maximum surface tensions, rate of adsorption to the interface, and overall shape of the dynamic cycling hysteresis loop. Further *in vitro* testing (captive bubble surfactometer and dynamic light scattering, for example) is required to understand the physical phenomenon underlying this observation, and *in vivo* testing is necessary to evaluate if the peptoid-containing surfactant formulation exhibits efficacy similar to natural LS in the physiologic environment.

4.4 Materials and Methods

4.4.1 Peptoid synthesis and purification.

Peptoids were synthesized using an ABI 433A peptide synthesizer (Applied Biosystems, Inc.) on Rink amide MBHA resin (Novabiochem, Inc.) using the submonomer approach[3]. Briefly, bromoacetic acid, activated by diisopropylcarbodiimide was used to form a bromocetylated intermediate on the terminal amide group. Bromide is then substituted with the desired primary amine through S_N2 displacement to build the peptoid chain. The amines used in peptoid synthesis include benzylamine, octadecylamine, isopropylamine, isobutylamine, (*S)*-α-methylbenzylamine (all purchased from Sigma-Aldrich) and *N*-tert-butoxycarbonyl-1,4 diaminobutane that was made using a previously published procedure[83]. Resin-bound peptoids were then exposed to a mixture of trifluoroacetic acid (TFA): triisopropylsilane:water (95:2.5:2.5, v:v:v) for ten minutes to cleave peptoids from the solid phase. Peptoids were purified by reversed-phase HPLC (RP-HPLC) (Waters Corporation) using a C4 or C18 column and a linear acetonitrile:isopropanol (2:1)/water gradient. Final purity was greater than 97% as measured by analytical RP-HPLC (Waters Corporation), and the identity of each molecule was checked using electrospray ionization mass spectrometry.

4.4.2 PBS sample preparation.

Individual stock solutions (DPPC, POPG, PA) were prepared in cleaned glass vials to accurately known concentration concentrations in solvent composed of chloroform/methanol (3:1) solvents. Using glass syringes, lipid stock solutions were combined to make Tanaka lipids (DPPC:POPG:PA, 68:22:9) at an accurately known concentration. The lipid solution was dispensed into an Eppendorf tube to make 80 µL of a 1 mg/mL solution. Peptoid, dissolved in methanol at an accurately known concentration, was added to deliver the appropriate amount. Natural lung surfactant was extracted from bovine sources as described previously[1].

4.4.3 Pulsating bubble surfactometry.

Samples were dried down to a pellet from a 3/1 mixture of chloroform/methanol (v:v) using a DNA 120 speedvac. The pellet was resuspended in buffer (150 mM NaCl, 10 mM HEPES, 5 mM $CaCl_2$, pH 6.9), which mimics the composition of the alveolar subphase, to a concentration of 1 mg/mL. Using a pipette, the mixture was then aspirated 20 times. A Fisher Model 60 probe sonicator was used to sonicate the mixture for 15 seconds, stopped for 15 seconds, then sonicated again for 15 seconds; the hold period was used to dissipate the heat generated during sonication. The sample was loaded into a sample chamber and mounted onto the pulsating bubble surfactometer (General Transco Inc.), which has been modified with an optical monitoring system[163]. A bubble was formed with an initial radius of 0.4mm. In static mode, the surface tension of the bubble was monitored over 20 minutes. After 20 minutes, the bubble was returned to an initial size of 0.4 mm and the bubble was allowed to pulse at 20 cycles per minute for at least 15 minutes during dynamic cycling until the maximum and minimum surface tensions were no longer changing. The surface tension was monitored as a function of bubble surface area and reported as a hysteresis loop.

4.5 Study contributions

Ann Czyzewski designed experiments; performed experiments, analyzed data, wrote the paper draft; Nathan Brown extracted and analyzed natural surfactant; Annelise Barron contributed to the experimental design and writing of the paper.

5. Peptoid-enhanced synthetic lung surfactant replacements demonstrate efficacy in an animal model of acute respiratory distress syndrome (ARDS)

5.1 Introduction

The lung parenchymal structures, comprised primarily of alveolar ductal lumens and alveoli, account for 90% of the lung tissue volume[176]. Alveoli are the fine, saccular structures that provide the extensive air/liquid interfacial surface area that is necessary to facilitate gas exchange. The patency of alveoli is affected by the radial traction of the connective tissue matrix in opposition to muscles within parenchymal walls and surface tension of the pulmonary fluid lining[177]. As airway and alveoli diameters are reduced, surface tension forces become increasingly dominant[177]. Lung surfactant (LS) is a complex lipid-protein mixture that coats the alveolar surfaces and reduces surface tension at the air/liquid interface, thereby enabling normal respiratory function[124]. In the absence, dysfunction, or inactivation of LS, there is considerable resistance to lung expansion, which ultimately results in alveolar collapse (atelectasis) and respiratory failure[120, 121].

Lung surfactant is composed of approximately 90% lipids (mostly saturated phopsholipids (e.g. DPPC) and 10% protein, by weight[122, 123]. DPPC is primarily responsible for reducing surface tension, while less abundant anionic lipids (*e.g.* PG) facilitate rapid adsorption to the air-liquid interface and improve respreadability upon lung expansion and compression[125, 126]. The conserved hydrophobic surfactant proteins (SP)s, SP-B and SP-C, interact strongly with the lipid layer and perform functions critical to pulmonary biophysical function, including (**1**) facilitating lipid adsorption to the air/liquid interface[136, 172], (**2**) surfactant re-uptake by type II pneumocyte cells[173, 174], (**3**) lipid film respreading[139], and (**4**) lipid layer stabilization[138, 175].

Respiratory distress syndrome (RDS) is a common clinical diagnosis associated with insufficient functional LS. Neonatal RDS (nRDS), which is linked to an absence of surfactant

due to immature pulmonary development[140], is routinely treated clinically with natural (animal-derived) exogenous surfactant replacement therapy (SRT), resulting in a 40% reduction in infant mortality[124, 140, 142]. Acute respiratory distress syndrome (ARDS), however, is a far more complex disease because it results from clinical syndromes that comprise a diverse set of etiologies[120, 145, 146, 178]. ARDS can result from both direct and indirect pulmonary insults, ranging from gastric aspiration and near-drowning to sepsis and non-thoracic trauma[178]. While there is no available treatment that addresses all facets of the ARDS, a number of small clinical trials and pilot studies (recently reviewed in [178]) suggest that exogenous surfactant as part of a multi-modal therapy can mitigate some effects of the disease. However, the high cost of natural surfactants and difficulty in isolation, coupled with the large quantities required to effectively dose ARDS patients for extended periods of time have made large scale clinical trials impractical[150, 178].

Biomimetic LS replacements are an emerging class of formulations composed of synthetic lipids with recombinant or chemically synthesized mimics of either SP-B or SP-C[178, 179]. This class of molecules could be the enabling technology for developing a lower-cost, synthetic biomaterial of precisely controlled composition that would be practical for use in applications that require larger amounts of material[151, 178]. Moreover, non-natural surfactants avoid the inherent risk of immune sensitization of the recipient of animal-derived materials (particularly in patients with fully developed adaptive immune systems)[178, 180]. *N*-substituted glycines (peptoids) are a class of versatile, sequence-specific biopolymers that has been applied to making functional mimics of SP-B and SP-C[36, 37, 46, 178].

While the peptoid backbone is identical to that of peptides, peptoid side chains are appended to the amide nitrogen rather than the α-carbon[14]. This apparently simple modification significantly affects the molecule's conformation and stereochemistry[11]. Peptoids lack amide

protons, resulting in the absence of backbone-mediated hydrogen bonding. Additionally, the lack of chiral centers in the backbone precludes the formation of intrinsic molecule handedness. It has been shown, however, that the use of α-chiral side chains generates steric and electronic repulsions that induce peptoids to adopt stable, helical architecture similar to that of polyproline type-I helices[56, 181]. The non-natural peptoid backbone also affords significant advantages for their use in biomaterials. Peptoids are impervious to protease activity, which can improve their biostability, bioavailability, and reduce specific recognition by the immune system[21, 182].

We have developed peptoids designed to mimic the overall physicochemical properties and secondary structures of SP-B and SP-C[36, 37, 46, 47]. *In vitro* testing has shown that these mimics emulate the surface activity of their natural counterparts[36, 37, 46, 47]. Moreover, as discussed in **Chapter 4**, pulsating bubble surfactometry studies suggest that formulations containing both SP-B and SP-C peptoid-based mimics interact synergistically to further increase surface activity[183]. Here, using an experimental model of ARDS, we explore the *in vivo* efficacy of peptoid-based surfactant preparations in synthetic lipids. We discuss the results from proof-of-concept piloting work as well as a more extensive study that was designed to investigate physiologic, biochemical, and inflammatory responses to peptoid-enhanced exogenous lung surfactant replacements. These results suggest that treatment with peptoid-based lung surfactant replacements demonstrate improved physiological outcomes compared to animals treated with the lipid carrier alone.

5.2 Results

5.2.1 Proof-of-concept piloting studies

We used a well-established experimental rat lung washout model[184-188] to evaluate the *in vivo* efficacy of peptoid-based lung surfactant replacement in the treatment of ARDS. The peptoids in this piloting study, **B1-1**[36] and **B2-1**[47], were first-generation mimics of SP-B that were designed to emulate the helical secondary structure and amphipathic patterning of SP-B_{1-25} (the *N*-terminal portion of the full protein SP-B) that has been shown to exhibit good surface activity[157-159]. Of the two peptoids, only **B2-1** mimics the *N*-terminal "insertion region" that was designed to mimic the *N*-terminal segment of SP-B_{1-25}, which is hypothesized to anchor the peptide in the lipid layer[189]. The chemical structures of mimics **B1-1** and **B2-1** are shown in **Figure 5.1**. All peptoid formulations were prepared in synthetic lipids at a concentration of 10 % by weight based on total lipid content and then suspended in sterile saline at a concentration of

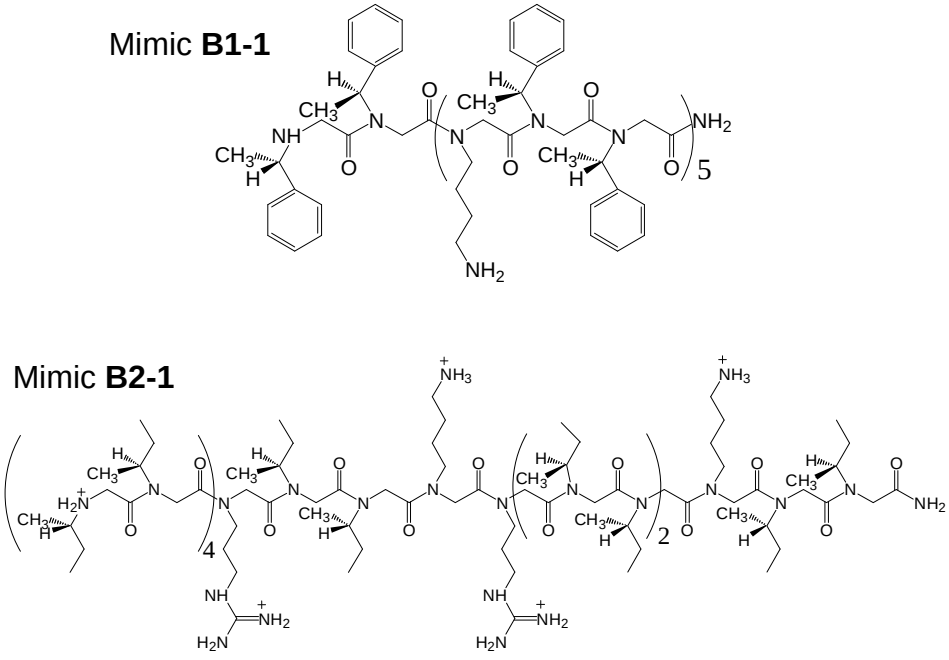

Figure 5.1: Chemical structures of peptoid-based SP-B mimics used in initial piloting studies of the rat washout experimental model of ARDS.

25 mg/mL. The lipid carrier was Tanaka lipids, a tertiary synthetic mixture of DPPC/POPG/PA (68:22:9 weight ratio) that has been shown to mimic the lipid portion of natural lung surfactant[164, 190]. In addition to the two peptoid-based surfactants, a clinically-proven, animal-derived surfactant, Infasurf® was used as the positive control. An untreated, ventilated control and a group treated with only the Tanaka lipid carrier were also included in this study.

Using the rat washout model, the ARDS-like condition was induced in anesthetized, ventilated animals by performing multiple lung lavages, which cause surfactant dysfunction and deactivation, as well as impaired gas exchange. Animals were dosed with surfactant (50 mg/kg) through intratreacheal bolus instillation followed by continued ventilation for 20 minutes. Blood samples were taken before lavage to demonstrate health (PaO_2 = 400 – 550 mmHg), after washout to demonstrate dysfunction (PaO_2 < 100 mmHg), and 20 minutes post-surfactant treatment to monitor the effect of the surfactant on gas exchange functionality. After 20 minutes, animals were euthanized, the chest opened, and pressure-volume measurements on

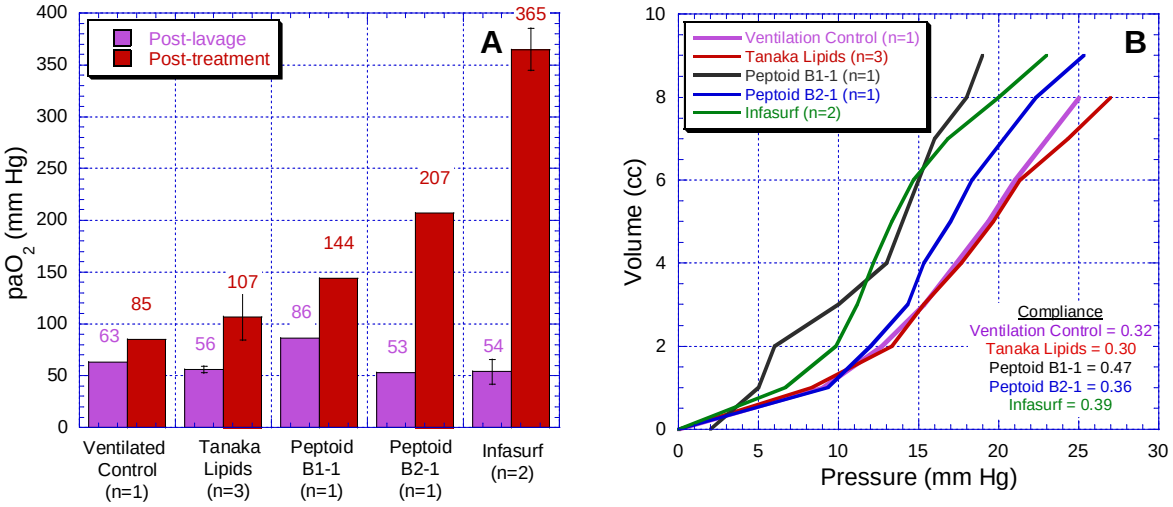

Figure 5.2: Physiologic data from piloting rat washout model studies. (**A**) Average blood oxygenation levels in all treatment groups post-lavage and 20 minutes after exogenous surfactant treatment. (**B**) Average pressure-volume (PV) inflation curves and calculated compliance for all treatment groups. Error bars indicate the standard error of the mean.

lungs were made to determine lung compliance, which is taken as the ratio of volume to pressure at maximum lung inflation. The inclusion criteria (pre- and post-lavage PaO_2 levels) were met for eight animals: Ventilated control (n=1), Tanaka lipids alone (n=3), Peptoid **B1-1** (n=1), Peptoid **B2-1** (n=1), and Infasurf® (n=2); the gas exchange and compliance outcomes for these study groups are shown in **Figure 5.2**. The difference between the blood oxygenation level post-lavage and 20 minutes post-treatment is an indication of the benefit to gas exchange imparted by the surfactant treatment. As expected, the controls indicated that the greatest increase in PaO_2 was achieved by treatment with Infasurf®, and the worst by the ventilated control. Treatment with Tanaka lipids alone demonstrated modest improvement that was similar to treatment with **B1-1**. Treatment with **B2-1** exhibited a markedly greater improvement in PaO_2.

In addition to dysfunctional gas exchange, decreased lung compliance is another symptom of ARDS[124]. **Figure 5.2B** shows the average post mortem pressure-volume inflation curves for each treatment group and the average calculated compliance. Peptoid or Infasurf® treated-groups had consistently higher compliance (0.36 – 0.47 cc/mmHg) than untreated or lipid vehicle-treated controls (0.30 – 0.32 cc/mmHg).

A second round of pilot testing was performed to investigate the *in vivo* efficacy of selected SP-C mimics. The ACUC committee recommended a modified protocol in which an inhaled anesthetic (4% isoflurane) was used instead of pentobarbital (50 mg/kg, i.p.), and this change appeared to significantly influence the measured outcomes (data not shown). The responses of the positive and negative controls (Infasurf® vs. lipid vehicle-treated) were very similar, suggesting that the model was not functioning properly. Limited data published on the physiological effects of isoflurane on the lungs suggest that it could affect pulmonary function, particularly by supressing oxygenation levels[191].

The scope of this initial work was to conduct a proof-of-concept, short-term piloting study to provide a preliminary *in vivo* evaluation of peptoid-based lung surfactant replacement preparations. Due to the limited resources we had available for *in vivo* studies, these data represent only a small number of animals and are not statistically significant. However, the trends suggest that peptoid-based surfactants may improve pulmonary gas exchange and lung compliance compared to untreated or lipid-only treated controls.

5.2.2 *In vivo* efficacy of SP-B and SP-C mimics alone and in a combined formulation

5.2.2.1 Study design

Because the resources for conducting a larger scale *in vivo* study is beyond the scope and knowledge base of the Barron lab, we collaborated with the laboratory of Ruud Veldhuizen and Jim Lewis at the University of Western Ontario in Canada to conduct a more comprehensive investigation of peptoid-based lung surfactant replacements. Using the rat washout model, this study was designed to monitor the physiological, biochemical, and

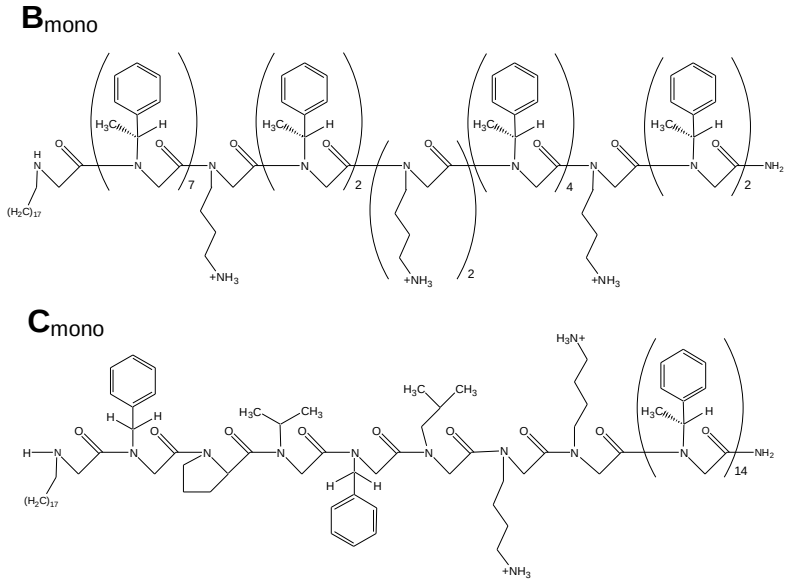

Figure 5.3: Chemical structures of peptoid-based mimics of SP-B and SP-C.

inflammatory outcomes of animals treated with peptoid-based exogenous surfactant for treatment of an ARDS-like condition.

The peptoids used in this study were selected based on their promising *in vitro* activity when formulated individually[1, 8] and their apparent synergistic effect on surface activity when both mimics were incorporated into a single surfactant preparation (**Chapter 4**)[183]. The mimics $\mathbf{C}_{mono}$ and $\mathbf{B}_{mono}$, shown in **Figure 5.3**, were designed to mimic the overall physicochemical properties and secondary structures of natural SP-C and SP-B[1, 8]. The eight *N*-terminal monomers of $\mathbf{C}_{mono}$ contain side chains that are analogous to SP-C_{5-12}, and the remaining 14 aromatic hydrophobic monomers form a helix that mimics the membrane spanning, hydrophobic helix of native SP-C[192, 193]. The *N*-terminal octadecyl amine in $\mathbf{C}_{mono}$ is a motif intended to mimic the post-translational palmitoylation of monomers 5 and 6 in human SP-C. $\mathbf{B}_{mono}$ was designed to mimic the amphipathic patterning and helical secondary structure of SP-B_{1-25} with the added feature of an *N*-terminal octadecyl amine[8]. Although native SP-B is not palmitoylated, the alkylation of peptoid **B** was motivated by the improved surface activity exhibited by similarly-alkylated SP-C mimics[1].

Experimental groups included peptoid-based surfactants comprised of (**1**) $\mathbf{B}_{mono}$ (2 mol%), (**2**) $\mathbf{C}_{mono}$ (2 mol%) , and (**3**) $\mathbf{B}_{mono}/\mathbf{C}_{mono}$ (1 mol% / 1 mol%) in Tanaka lipids (DPPC/POPG/PA (68:22:9 by weight)). Each preparation at a concentration of 25 mg/mL formed a homogeneous flowable suspension, and animals were dosed at 50 mg/kg. A control group treated with an equivalent dose of Tanaka lipids alone was studied to elucidate the effect of the peptoid mimics compared to that of the lipid carrier alone. A second control group treated with natural surfactant bovine lung extract surfactant (BLES) (50 mg/kg) was used as a positive control. The identity of surfactants was blinded to animal care givers to prevent biased observations.

The protocol of the experimental model used for this study is similar to what was described for piloting studies (**Section 5.2.1**) with slight modification. The anesthetic used was ketamine (75 mg/kg) and xylazine (5 mg/kg) administered i.p. to avoid interference with pulmonary function. Additionally, post-treatment ventilation time was extended to 2 hours, during which physiological status was monitored and frequent blood gas samples were taken. Inclusion criteria for this study were: (**1**) rat weight 350 – 425 g, (**2**) baseline paO_2 between 400 – 500 mmHg, and (**3**) post lavage paO_2 < 120 mmHg. A total of 31 animals met the inclusion criteria for this study: BLES (n=7), $\mathbf{B}_{mono}$ (n=6), $\mathbf{C}_{mono}$ (n=7), $\mathbf{B}_{mono}/\mathbf{C}_{mono}$ (n=7), and TL alone (n=4).

5.2.2.2 Physiological responses

5.2.2.2.1 Baseline and post-lavage equivalency

Vital signs (blood pressure (BP) and heart rate (HR)) as well as several physiological indicies of pulmonary function were monitored throughout the course of each experiment. **Table 5-1** shows the average values of selected parameters for all groups at baseline and post-lavage. Differences in baseline parameters between treatment groups were not statistically significant ($p>0.05$). The tight standard error of each parameter shows that the baseline vital signs and respiratory health of animals in all treatment groups was similar. Moreover, the

Parameters	**Baseline Averages (± SEM)**	**Post-lavage Averages (± SEM)**
PaO_2 (mm Hg)	435.7 (± 4.9)	88.3 (± 2.5)*
PIP (cm H_20)	12.0 (± 0.3)	20.8 (± 0.4)*
BP	81.1 (± 1.9)	69 (± 2.0)
HR (BPM)	289 (± 0.4)	280 (± 5.1)

Table 5-1: Average values of vital signs and selected physiologic indices for all groups. Statistical significance indicator *: a statistically significant ($p < 0.05$) difference between baseline and post-lavage measurements using the Kruskal-Wallis method was detected.

average post-lavage decrease in the arterial partial pressure of oxygenation (paO_2) and increase in peak inspiratory pressure (PIP) showed that pulmonary gas exchange and lung compliance were significantly ($p < 0.05$) and uniformly damaged by the lavage, symptomatic of an ARDS-like condition.

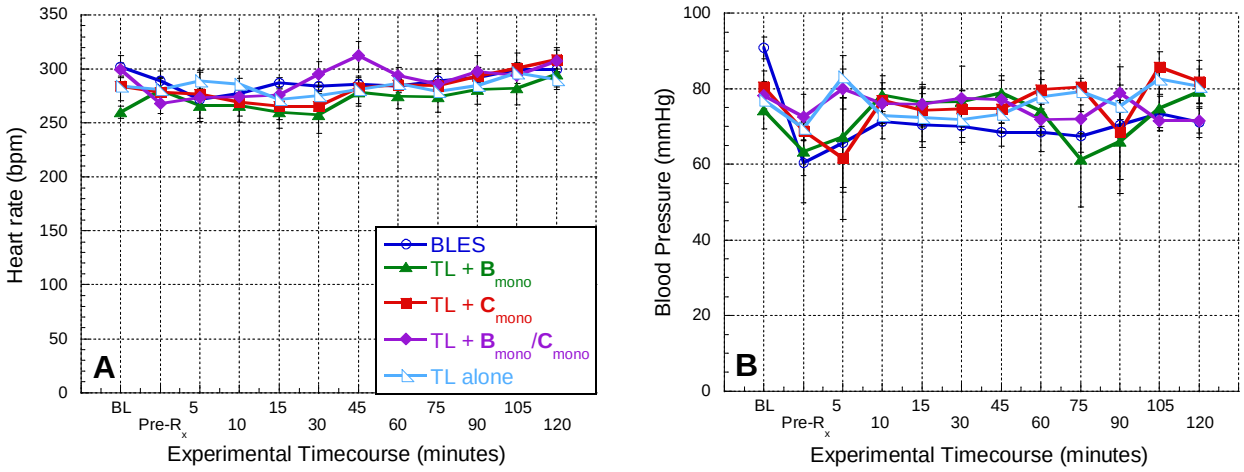

Figure 5.4: Vital signs of all animals throughout the timecourse of the experiment. (**A**) Heart rate and (**B**) Blood pressure at baseline measurement (BL), after lavage and before exogenous surfactant treatment (Pre-Rx), and at time points through ventilation period. $p>0.05$ at all time points.

Blood pressure and heart rate were monitored to ensure that the animals were adequately perfused throughout the experiment. The average blood pressure and heart rate for each group over time plotted in **Figure 5.4** showed no significant difference between treatment groups.

5.2.2.2.2 Gas exchange and pulmonary function

The average paO_2 normalized to the fraction of inspired oxygen (FIO_2) (1.0 throughout all experiments) and blood pH are shown for each treatment group as a function of time in **Figure 5.5**. Blood pH is correlated with the functionality of CO_2 gas exchange; impaired pulmonary gas exchange leads to high levels of CO_2, which is hydrolyzed to form carbonic acid. Excess acid reduces blood pH, leading to a clinical diagnosis of acidosis.

The improved gas exchange after surfactant treatment is reflected by the increase in PaO_2/FIO_2 and blood pH from the pre-treatment (Pre-Rx) condition toward baseline levels. BLES and all peptoid-enhanced surfactants showed an improved outcome for both responses compared to TL alone. Animals treated with TL + $\mathbf{C}_{mono}$ demonstrated the highest arterial blood oxygenation levels, and only this group was statistically different from the TL alone group at each time point after treatment was instilled. BLES was statistically different from TL alone for the final two time points at 105 and 120 minutes. In the case of blood pH, over the first 30 minutes after treatment, the BLES and TL + $\mathbf{C}_{mono}$ groups showed comparable improvement. The performance of the TL + $\mathbf{C}_{mono}$ surfactant, however, declined at 45 minutes in comparison to the BLES treated group. In terms of both PaO_2 and blood pH, the two groups that demonstrated the best outcomes were those treated with BLES and TL+ $\mathbf{C}_{mono}$.

Figure 5.6 displays three other indicators of pulmonary function, including peak inspiratory pressure (PIP), shunt fraction, and A-a gradient. A high PIP is symptomatic of a stiff,

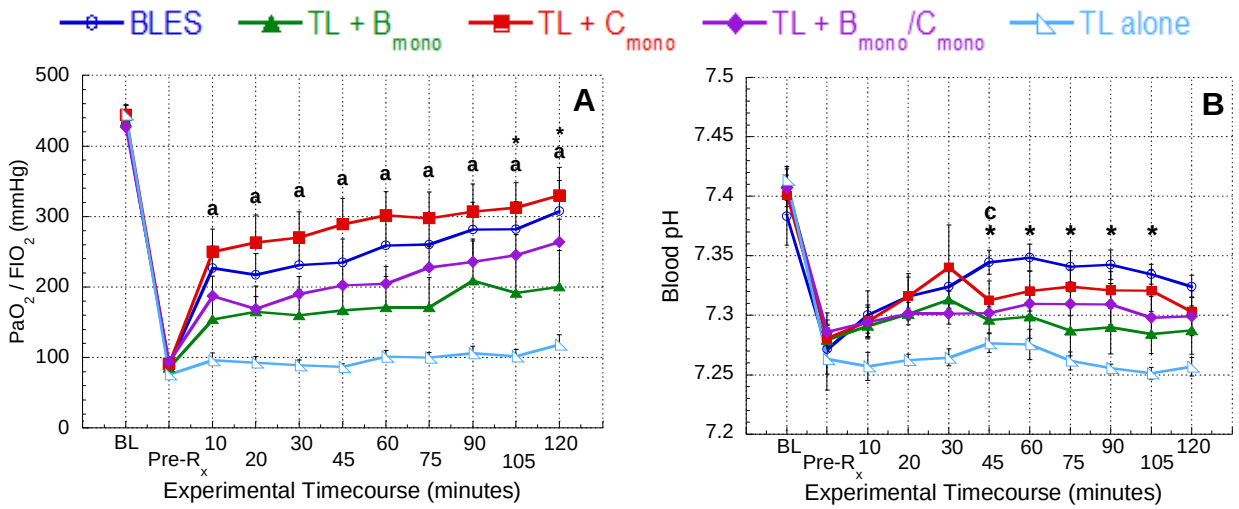

Figure 5.5: Physiological indicators of pulmonary gas exchange function over time. (**A**) PaO_2/FIO_2 over time and (**B**) Blood pH over time. Error bars indicate the standard error of the mean. Statistical significance indicators ($p < 0.05$): * indicates BLES vs. TL alone; a indicates $\mathbf{C}_{mono}$ vs. TL alone; c indicates $\mathbf{B}_{mono}$ vs. BLES.

non-compliant lung. The shunt fraction is an estimate of blood flow that travels from the right to left heart without being completely oxygenated by the lungs; insufficient gas exchange results in increased pulmonary shunt fraction. The A-a gradient is the difference between the partial pressure of oxygen in the alveolar space (pAO_2) and the partial pressure of oxygen in the arterial blood (paO_2), where the pAO_2 is a function of the arterial pCO_2. A large A-a gradient reflects inhibited gas exchange at the alveoli.

These three responses showed similar trends, with all treatment groups showing

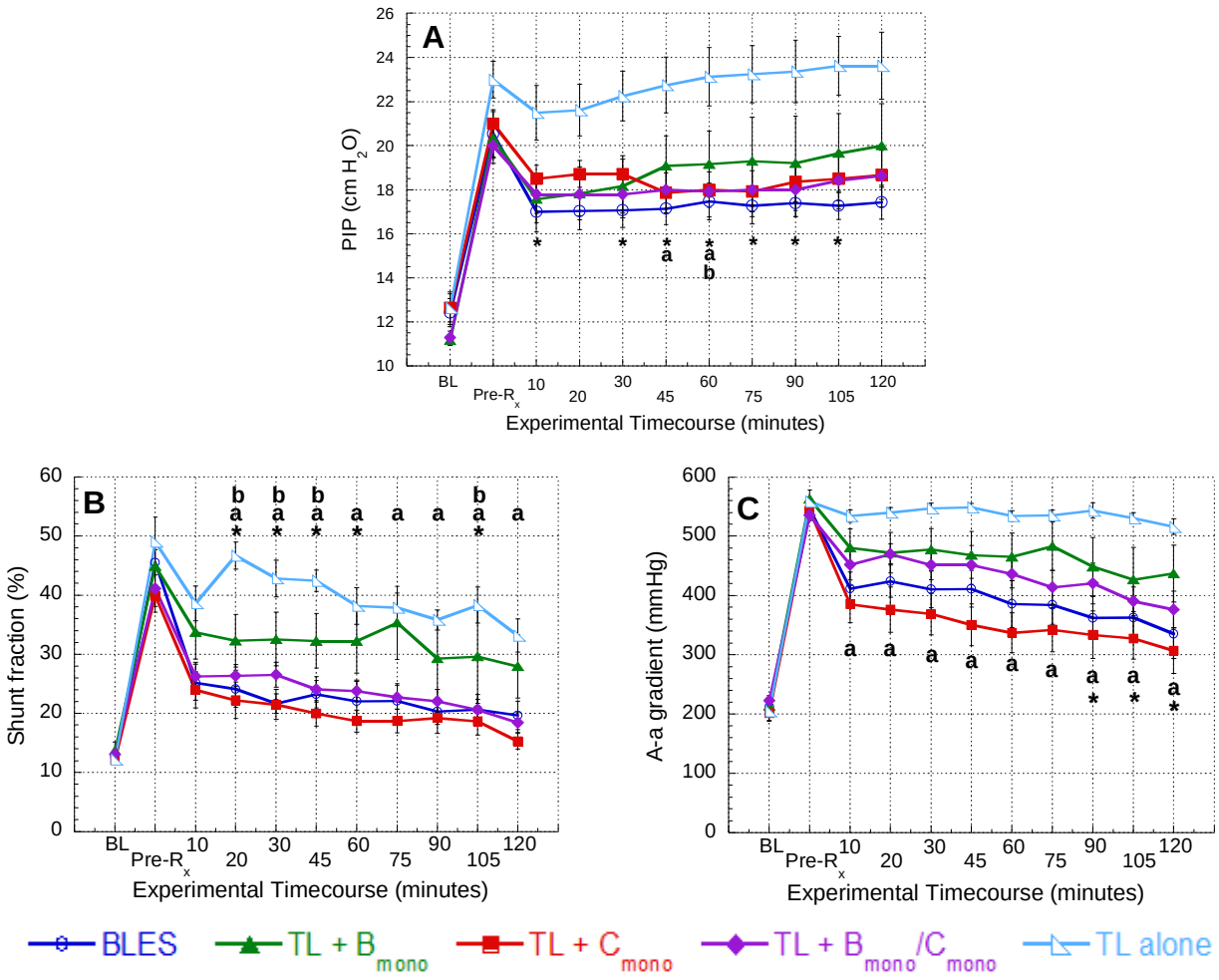

Figure 5.6: Physiological indicators of pulmonary function. (**A**) Peak inspiratory pressure (PIP) and (**B**) Shunt fraction over time. Error bars indicate the standard error of the mean. Statistical significance indicators ($p < 0.05$): * indicates BLES – TL alone; a indicates C_{mono} – TL alone; b indicates B_{mono}/C_{mono} – TL alone.

improvement compared to TL alone, and BLES and TL + $\mathbf{C}_{mono}$ demonstrating the best outcome. Treatment with BLES reduced the PIP to ~ 17 cm H_2O throughout the experiment, followed by TL + $\mathbf{C}_{mono}$ and TL + $\mathbf{B}_{mono}/\mathbf{C}_{mono}$, which were very similar and resulted in a PIP of ~18 cm H_2O (**Figure 5.6A**). The TL + $\mathbf{C}_{mono}$ group showed the best recovery in terms of shunt fraction and A-a gradient, each of which were found to be statistically different from treatment with TL alone (**Figure 5.6B,C**).

In light of the data shown in **Chapter 4**, it is interesting that the response to the TL + $\mathbf{B}_{mono}/\mathbf{C}_{mono}$ formulation was not synergistic, but rather additive in terms of the *in vivo*, physiological responses discussed. Except for the PIP (in which case the TL+$\mathbf{C}_{mono}$ formulation was very similar to TL+$\mathbf{B}_{mono}/\mathbf{C}_{mono}$), treatment with TL+$\mathbf{B}_{mono}/\mathbf{C}_{mono}$ resulted in an outcome between the efficacious TL+$\mathbf{C}_{mono}$ and less effective TL+$\mathbf{B}_{mono}$ formulation.

5.2.2.2.3 Surfactant pool evaluation

Phospholipid characterization and total protein content on the broncheoalveolar lavage fluid from each animal were determined as secondary indicators of lung dysfunction. Lung surfactant consists of two aggregate forms; tubular-myelin-like large aggregates (LA), which contain dense structures and provide for the most surface activity, are converted to lighter and less active small aggregate (SA) vesicles that are eventually recycled by Type II pneumocyte cells or cleared from the airspace[194]. It has been shown that while LA and SA coexist in healthy lungs, respiratory diseases such as ARDS in both animal models[195-199] and patients[200-202] can significantly increase the amount of the less active SA relative to LA[203]. The average amount of total surfactant, large aggregates, and small aggregates obtained from the BAL of each treatment group is shown in **Figure 5.7A**. While there was no statistically significant difference between the large aggregate contents of the various treatment groups, the amount of less active small aggregates was higher in the TL alone group than in any other treatment group. The

average amount of total surfactant was higher for the TL alone (24.6 mg PL/kg) treatment group than any other, and statistically higher than the TL+**C**$_{mono}$ treatment group (17.6 mg PL/kg).

It has been shown that the conversion from LA to SA and subsequent deactivation of surfactant may be in part due to the leakage of proteins and proteases into the pulmonary air space[204]. **Figure 5.7B** displays the average protein content of the BAL from all treatment groups. The data show that there was no statistically significant difference in the total protein content of the various treatment groups. Moreover, a consistent correlation with physiological outcomes is not apparent. Both the positive control (BLES) and negative control (TL alone) had comparable BAL protein levels (89.5 and 85.6 mg/kg, respectively) that were higher than the peptoid-enhanced surfactants (52.1 – 74.0 mg/kg). While it is possible that the BLES treatment group had increased levels from proteins in the exogenous surfactant, it is unlikely that the

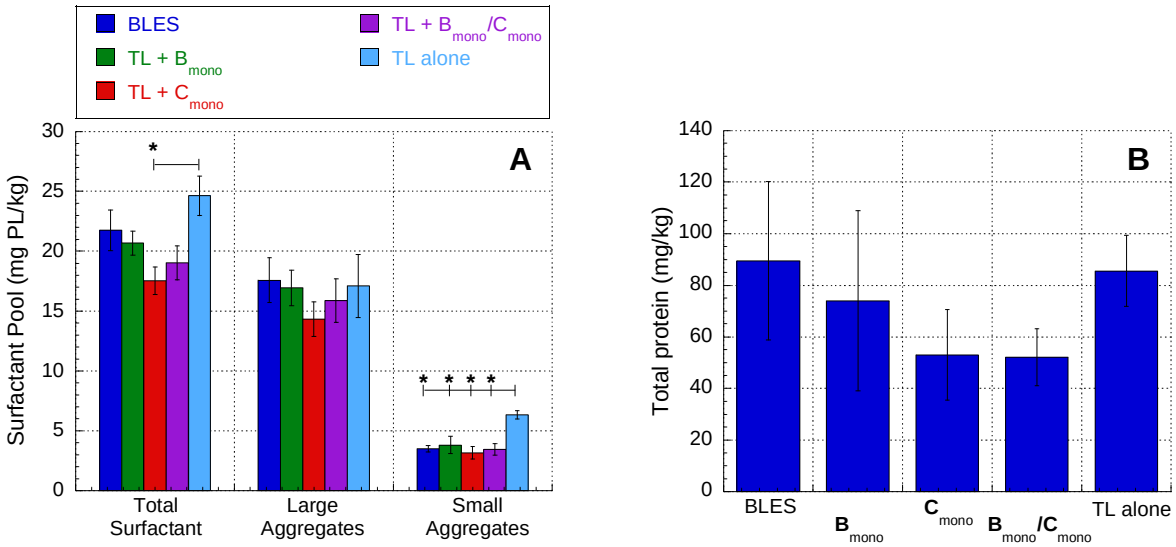

Figure 5.7: Surfactant pool characterization in broncheoalveolar lavage (BAL). (**A**) Average amounts of total surfactant, large aggregates, and small aggregates in BAL. (**B**) Average total protein content in the BAL of each treatment group. Error bars indicate the standard error of the mean. Statistical significance indicators: * indicates $p < 0.05$ for the difference between the designated group and TL alone group.

amount administered would account for the observed increase.

5.2.2.2.4 Inflammatory Response

It has previously been reported in both patients[205, 206] and animal models of ARDS that elevated levels of proinflammatory cytokines are often the result of ARDS-like pulmonary injury and subsequent mechanical ventilation. We measured the amount of the pro-inflammatory cytokines interleukin-6 (IL-6) and tumor necrosis factor alpha (TNF-α) in both the BAL and blood serum. The data shown in **Figure 5.8** show that IL-6 and TNF-α levels in both the BAL and blood serum could not be statistically distinguished among the different treatment groups. TNF-α levels were significantly and consistently higher in the blood serum than in the BAL.

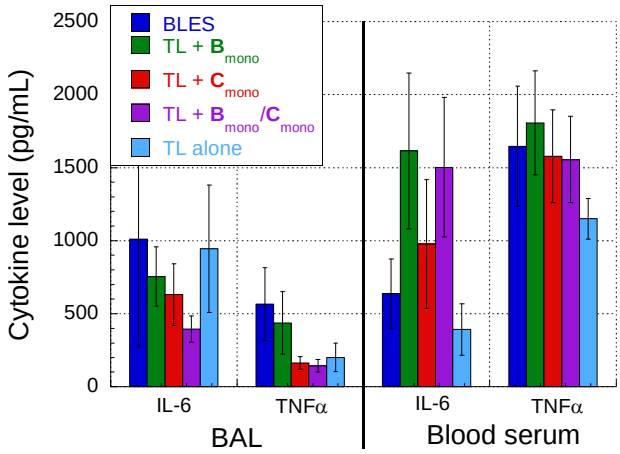

Figure 5.8: Pro-inflammatory cytokine levels in BAL and blood serum.

5.3 Discussion

While the extensive alveolar network and capillary vasculature of the pulmonary parenchymal tissue are critical to achieving efficient gas exchange, these delicate structures are highly susceptible to systemic pathogens and environmental toxins[178]. A broad spectrum of direct pulmonary insults and indirect systemic maladies result in lung surfactant deficiency and dysfunction, leading to ARDS. While there is currently no cure for ARDS, exogenous surfactant treatment as part of a multimodal therapy has been shown to mitigate symptoms of the disease

(reviewed in [178]). Synthetic exogenous lung surfactants offer several advantages over natural surfactants as a viable treatment option for ARDS. The high cost of natural surfactant makes treatment of adults over the extended time period required to mitigate surfactant dysfunction prohibitively expensive. Moreover, the use of a synthetic surfactant avoids the risk of immune response that is inherent with animal-derived treatments, and the non-natural backbone of peptoid-based mimics may increase their biostability and therapeutic half-life. Synthetic surfactants also offer the possibility of a "designer" treatment that could be customized to mitigate specific types of surfactant dysfunction or deactivation induced by the myriad of clinical etiologies that result in ARDS[207]. It is conceivable, for example that a number of additives could be included in a synthetic formulation, not only to improve surface activity, but also to prevent surfactant inhibition, regulate surfactant homeostasis, and control inflammatory response.

While peptoids have been shown previously to mimic the *in vitro* surface activity of SP-B[36, 47] and SP-C[37, 46], this study was designed to evaluate their *in vivo* efficacy (as measured by physiological, biochemical, and inflammatory outcomes) using an established animal model of ARDS. Tanaka lipids were selected as the lipid carrier for these synthetic formulations based on its similarity to the lipid/fatty acid component of natural surfactant[190] and superior *in vitro* surface activity[164]. The formulation concentration (25 mg/mL) and dosage (50 mg/kg) were equivalent for all formulations, and the prepared synthetic surfactants formed a homogeneous, flowable suspension suitable for bolus instillation. The peptoid-based protein mimics, $\mathbf{B}_{mono}$ and $\mathbf{C}_{mono}$ were selected for this study based on their *in vitro* surface activity formulated individually and *in vitro* synergistic surface activity when formulated together (**Chapter 4**). BLES, a natural surfactant that contains both SP-B and SP-C, was used as a standard of care natural comparator formulation.

The five physiological responses showed that treatment with Tanaka lipids alone resulted in the least improvement in pulmonary function over the two hour recovery and observation period. **Figures 5.5** and **5.6** show that the TL alone formulation neither achieved the same initial degree of recovery, nor effectively maintained activity throughout the observation period. For example, **Figure 5.6A** shows that at 10 minutes, the TL alone group reached an average PIP of 20 cm H_2O, whereas that of the other groups averaged 18 cm H_2O. Moreover, at 30 minutes, the PIP of the TL alone treated group began to increase (a sign of deteriorating health) and continued to do so throughout the time course of the experiment. This suggests that the limited amount of surface activity exhibited by this formulation cannot be sustained for clinically relevant time periods. Treatment with TL+$\mathbf{B}_{mono}$ tended to improve physiological outcomes compared to TL alone, but these differences were not statistically significant.

The formulation TL+$\mathbf{C}_{mono}$ not only demonstrated a more dramatic initial improvement in physiological response, but also exhibited sustained benefit throughout the recovery period. Blood oxygenation, A-a gradient, and shunt fraction demonstrated significant ($p < 0.05$) improvement in physiological outcomes for the TL+$\mathbf{C}_{mono}$ compared to the TL alone treatment group from 10 minutes through 120 minutes. It is also notable that in these three outcomes, the performance of TL+$\mathbf{C}_{mono}$ compared favorably to that of all other groups, including that of the natural surfactant, BLES. This is an encouraging result for synthetic surfactants and marks the first reporting of a peptoid-enhanced surfactant that demonstrates *in vivo* efficacy.

It is interesting that while the combination formulation of TL+$\mathbf{B}_{mono}$/$\mathbf{C}_{mono}$ appeared to exhibit synergistic surface activity *in vitro*, the physiological responses to TL+$\mathbf{B}_{mono}$/$\mathbf{C}_{mono}$ were “non-synergistic”. The literature provides mixed evidence as to whether or not natural SP-B and SP-C or other SP-B/SP-C mimics interact synergistically *in vitro* and *in vivo*[171, 186, 187]. This

discrepancy is likely due to a combination of factors that make the *in vivo* environment significantly different from that of the *in vitro* test system. Whereas the operation and run conditions of the PBS are precisely controlled, the physiologic environment is dynamic and complex. While *in vitro* analysis is done in a tertiary model lipid environment, *in vivo* activity is measured with the same lipid carrier, but in the presence of deactivated and dysfunctional whole lung surfactant. One of the more significant differences between *in vitro* and *in vivo* test methods could be the effective surfactant concentration under study. While the samples in both test systems were made with 2 mol% total peptoid, the *in situ* effective composition of the surfactant once diluted in the alveolar space is unknown. The degree of synergistic or additive surface active behaviors in SP-B and SP-C mimics is ostensibly related to their underlying mechanisms of action; it is possible that the protein mimics in more dilute surfactants interact less frequently and thus appear less synergistic. Suffice to say that while *in vitro* measures are a useful screening tool for gauging surface activity, they are not always accurate predictors of *in vivo* efficacy.

Surfactant pool characterization showed that the TL alone-treated group had a larger total surfactant pool than any other group and was statistically different ($p < 0.05$) from that of the TL+$\mathbf{C}_{mono}$ treatment group (**Figure 5.7**). This is commensurate with studies which have shown that total surfactant pool can increase in an injured lung. It has been shown that mechanical stretching of the lung epithelial tissue (due to dynamic cycling of mechanical ventilation, for example) causes surfactant secretion[208, 209]. While all groups were ventilated at the same settings, it is possible that the less compliant lung of the TL alone treatment group experience greater stretching and thus increased surfactant production. The rate of conversion from large to small aggregates within the surfactant pool has also been shown to increase under conditions pervasive in an injured lung: (**1**) increased protease activity[204, 210] (**2**) altered

surfactant composition[211, 212] (**3**) dynamic surface area cycling[194] and mechanical ventilation[199, 213]. Injured lungs, therefore, often exhibit an increased amount of total surfactant and a concomitant increase in the less surface-active small aggregate portion[120, 201, 202, 214]. In this study, **Figure 5.7A** shows that indeed the small aggregate component of the BAL from the TL alone treatment group was significantly greater than that of any other group. The increase in total surfactant of the TL alone group appears to be due to primarily an increase in the less active small aggregates.

The elevated protein levels in the BAL of all treatment groups suggest that a significant amount of serum proteins permeated the pulmonary endothelial-epithelial barrier, the integrity of which was damaged due to lung injury. It has been also been shown that increased levels of proinflammatory cytokines, such as IL-6 and TNF-α play a significant role in the pathogenesis of ARDS[215]. The leakage of alveolar cytokines through the endothelial-epithelial barrier and into the vasculature can lead to a systemic inflammatory response and multiple organ failure[216, 217]. All treatment groups in this study had higher TNF-α levels in the serum than in the BAL, suggesting a pathologic increase in endothelial-epithelial barrier permeability. Due to the nature of the lung injury induced by pulmonary lavage and two hours of mechanical ventilation, all groups exhibited increased protein content and cytokine measurements. It is likely that the large magnitude of baseline measurements masked the differences we had hoped to observe between treatment groups.

In summary, peptoid-enhanced lung surfactants demonstrate efficacy in mitigating symptoms associated with ARDS. Treatment with TL+$\mathbf{C}_{mono}$ surfactant resulted in the best outcome in terms of both physiological and biochemical responses. The $\mathbf{B}_{mono}/\mathbf{C}_{mono}$ formulation, which exhibited synergistic behavior *in vitro*, appeared to have a more additive effect on physiological responses *in vivo*.

5.4 Materials and Methods

5.4.1 Peptoid synthesis and purification

Peptoids were synthesized using an ABI 433A peptide synthesizer (Applied Biosystems, Inc.) on Rink amide resin (Novabiochem, Inc.) using the submonomer approach[3]. Briefly, bromoacetic acid, activated by diisopropylcarbodiimide was used to form a bromocetylated intermediate on the terminal amide group. Bromide is then substituted with the desired primary amine through S_N2 displacement to build the peptoid chain. All reaction steps are performed in *N*-*N*-dimethylformamide, and 20% piperdine is used in deprotection of the resin and amino acid. The amines used in peptoid synthesis include benzylamine, octadecylamine, isopropylamine, isobutylamine, *S*-alpha methylbenzylamine (all purchased from Sigma-Aldrich), and *N*-tert-butoxycarbonyl-1,4 diaminobutane, which was synthesized using a published protocol[83]. Resin-bound peptoids were then exposed to a mixture of trifluoroacetic acid (TFA): triisopropylsilane:water (95:2.5:2.5, v:v:v) for ten minutes to cleave peptoids from the solid phase. Peptoids were purified by reversed-phase HPLC (RP-HPLC) (Waters Corporation) using a C4 or C18 column and a linear acetonitrile/water gradient. A final purity greater than 97% as measured by analytical RP-HPLC (Waters Corporation) was achieved, and the molecular mass of each molecule was checked using electrospray ionization mass spectrometry.

5.4.2 Preparation of synthetic surfactant mixtures

Individual stock solutions of synthetic lipids (DPPC, POPG, and PA) of accurately known concentration were made in a 3:1 mixture of chloroform/methanol. The Tanaka lipid (TL) formulation was prepared to an accurately known concentration (10-12 mg/mL) by combining the individual stock solutions to yield a 68:22:9 (w:w:w) mixture of DPPC:POPG:PA. Surfactant preparations for rat studies were prepared individually in cleaned, 20mL glass scintillation vials. 22.5 mg of TL (enough to treat a 450g rat at 50 mg/kg) were dispensed into each vial. The

appropriate amount of peptoid was added from methanol-based stock solutions of accurately known concentrations. Surfactant mixtures were then dried under nitrogen to a reduced volume, lyophilized overnight, and stored at -20 C until the time of use. On the day of the experiment, sterile saline was added to the dehydrated surfactant mixture to make a concentration of 25 mg/mL. The mixture was allowed to hydrate for 1 hour, aspirated with a pipette, and sonicated in a sonication bath for 10 minutes prior to use.

5.4.3 Animal experimentation – piloting studies

These animal experiments were reviewed and approved by the Animal Care and Use Committee of Northwestern University. Sprague-Dawley rats (320-400g) were weighed, anesthetized with pentobarbital (25 mg/kg), and preoxygenated with 100% oxygen through a nosecone. A tracheostomy was performed, a cannula was inserted into the trachea, and ventilation was initiated. To obtain blood samples, the right coradid artery was cannulated with a 22 gauge catheter. After an initial baseline blood gas was determined (inclusion criterion paO_2 > 400 mmHg), the animal was subjected to multiple lung lavages (each lavage was instilled and withdrawn 3 times) with warmed saline. After 4 lavages, with 5 minute intervals between, a sample was taken for blood gas analysis using and ISTAT portable analyzer (Abbott Laboratories). Additional lavages were performed as necessary until the paO_2 was < 100 mmHg. Animals were then randomized into one of the following treatment groups: (**1**) Ventilated control, (**2**) Tanaka lipids only, (**3**) TL+B1-1, (**4**) TL+B2-1, (4) Infasurf®. Infasurf® was purchased from Forest Pharmaceuticals (New York, New York) and used in accordance with manufacturer's instructions. Synthetic surfactants were prepared as discussed in 5.4.2 and administered via syringe through the endotracheal tube. Animals were sustained on ventilation for 20 minutes, at which time a sample was taken for blood gas analysis. Animals were then euthanized with an overdose of pentobarbital. The chest was opened and a calibrated syringe

and pressure transducer were used to determine the pressure-volume curve and lung compliance post mortem.

5.4.4 Animal experiments

All procedures were reviewed and approved by the animal care and use subcommittee at the University of Western Ontario, London Ontario, Canada and in accordance with the Canadian Council of Animal Care. Male Sprague-Dawley rats (350 – 425g) (Charles River, St. Constant, PQ, Canada) were used for these studies. Animals were weighed, anesthetized by i.p. injection (75 mg/kg ketamine and 5 mg/kg xylazine in sterile 0.15 M saline), and given buprenorphine (0.05 – 0.1 mg/kg, i.m.) as an analgesic. The right jugular vein and carotid artery were isolated and cannulated. Carotid artery access was used for obtaining blood gas samples, measuring vital signs, and instillation of fluids via an infusion pump, while the venous line was used for administration of drugs. Following a tracheostomy and placement of the endotracheal tube, pancurium bromide (2 mg/kg, i.v.) was administered to inhibit spontaneous respiratory movements. Animals were placed on a volume cycle mechanical rodent ventilator (Harvard Instruments, St. Laurent, PQ, Canada) and airway pressure monitor (Sechrist Industries, Anaheim, CA). The ventilator settings throughout the experiment were set at a tidal volume of 6 ml/kg, PEEP of 5 cm H_2O, respiratory rate of 80 breaths/minutes, and FIO_2 of 1.0. Additional pentobarbitol sodium (20-40 mg/kg, i.v.) anesthetic was administered as needed. The initial inclusion criterion for this study was a baseline PaO_2 of > 400 mmHg.

Whole lung lavage, as described previously[218] was performed on animals that met the inclusion criterion. Briefly, after disconnecting the animal from the ventilator, 10 mL of 37^{o}C saline (0.15 M NaCl) was gently instilled and withdrawn from the lungs, after which mechanical ventilation was resumed. The lavage procedure was repeated three more times (separated by 5 minutes), after which a blood gas measurement was taken. Blood gas measurements were

determined using a model ABL500, Radiometer, Copenhagen, Denmark). A PaO_2 < 120 mmHg was required for inclusion into the study. Series of two additional lavages followed by blood gas measurement were performed until the inclusion criterion was met and the animal was in a surfactant-deficient state[218].

Animals meeting the second inclusion criterion were randomized into one of five treatment groups: (**1**) BLES, (**2**) TL+$\mathbf{B}_{mono}$, (**3**) TL+$\mathbf{C}_{mono}$, (**4**) TL+$\mathbf{B}_{mono}/\mathbf{C}_{mono}$, (**5**) TL alone. BLES was obtained from BLES Biochemical and used according to manufacturer's instructions. All other surfactants were prepared as described in **Section 5.4.2**. All surfactants were at a concentration of 25 mg/mL and administered at a dose of 50 mg/kg. For treatment, animals were briefly disconnected from the ventilator and held in an upright position while the surfactant was instilled as a bolus via syringe through the endotracheal tube. The surfactant was chased with 2 mL air bolus to ensure surfactant distribution to the distal regions of the lung. Animals were reconnected to the ventilator and monitored for 2 hours, with blood gas samples taken at 10, 20, 30, 45, 60, 75, 90, 105, and 120 minutes. Vital signs were monitored throughout the recovery period, and additional anesthetic was administered as needed. Following the 2 hour monitoring period, animals were euthanized with an overdose of pentobarbital and exsanguinated.

The chest wall was opened and the lungs were lavaged five times with 10 mL of 0.15 M saline. Each lavage was gently instilled and withdrawn three times; all lavages were combined and the total volume from each animal was recorded.

5.4.5 Surfactant pool and total protein analysis

To sediment the cellular debris, the broncheoalveolar lavage fluid was centrifuged at 150 *g* for 10 minutes. The supernatant (called total surfactant (TS)), (save 5 mL for phospholipid

analysis), was centrifuged at 40,000 *g* for 15 minutes to separate the supernatant (small aggregates (SA) from the pellet. The pellet was resuspended in 2mL saline to produce the large aggregate (LA) portion. Aliquots of each surfactant portion were extracted using the Bligh/Dyer method[219] and the Duck-Chong phosphorous assay[220] was used to quantify the amount of phospholipid within each fraction. A micro-BCA protein assay (Pierce Biotechnology) was used according to the manufacturer's instructions to determine the total protein content of the BAL.

5.4.6 Cytokine analysis

An aliquot of bronchoalveolar lavage fluid was centrifuged at 200 *g* for 10 minutes, and the supernatant was snap frozen in three separate aliquots and stored at -80^{o}C until analysis. TNF-α and IL-6 cytokines were measured using opti-EIA Elisa kits obtained from Pharmigen and used according to manufacturer's instructions.

5.4.7 Statistical Analysis

All data are presented as means ± standard errors. A one-way ANOVA analysis using the Tukey-Kramer test for multiple comparisons was performed with minitab, version 15.0 (Minitab, Inc.). The threshold of statistical significance was set at $p < 0.05$.

5.5 Study contributions

Ann Czyzewski designed experiments, performed experiments, analyzed and interpreted data, performed statistical analysis, and wrote the paper draft; Lynda McCaig performed experiments; Li Juan Yao performed experiments; Lauren Jones assisted with experiments; David Steinhorn (collaborating PI) contributed to experimental design, contributed to piloting experiments; Jim Lewis (collaborating PI) contributed to experimental design, contributed to the paper; Ruud Veldhuizen (collaborating PI) contributed to experimental design, contributed to paper; Annelise Barron (senior author) established the collaboration, contributed to the experimental design, contributed to paper.

6. An *in vivo* study of peptoid-based surfactants using an ovine model of nRDS

6.1 Introduction

The discovery in 1959 that neonatal respiratory distress syndrome (nRDS) is linked with the absence of lung surfactant (LS) has demonstrated the clinical significance of this complex lipid/protein mixture[140]; nRDS is among the top five leading causes of infant mortality in the U.S.[221] and it affects 2 million babies worldwide[143]. Preterm infants are often born with immature alveolar Type II pneumocytes, which are unable to secrete LS[140]. This lack of surfactant results in a pathologically high surface tension at the alveolar air-liquid interface, which initiates a cascade of physiological maladies that ultimately result in suffocation[120, 121].

A schematic demonstrating the self-perpetuating cycle of surfactant deficiency and how

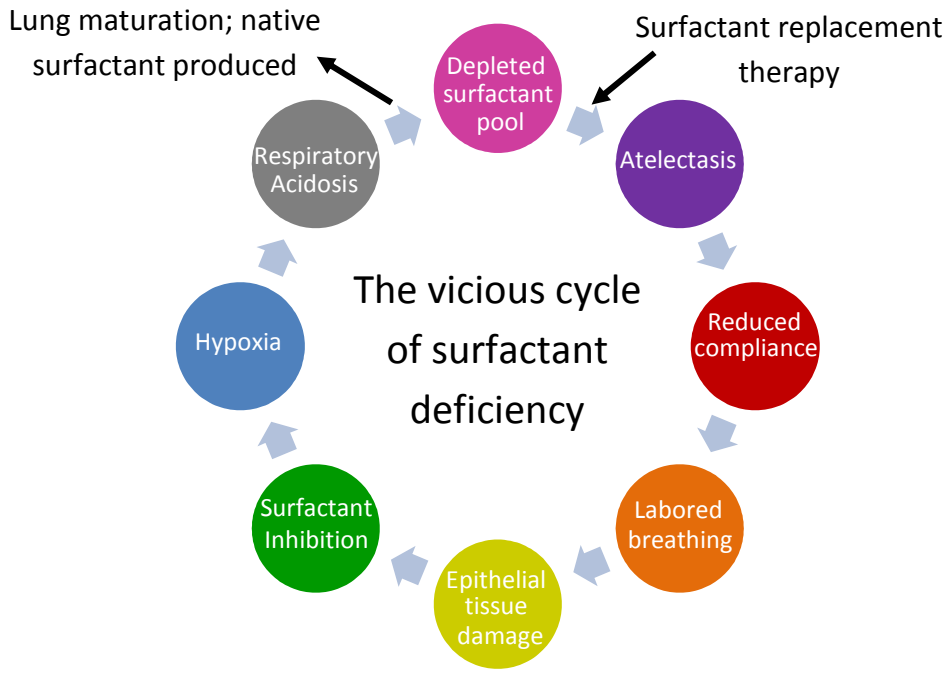

Figure 6.1: Schematic representation of the physiological effects of surfactant deficiency. Adapted from a figure of Boris Kramer, M.D., Ph.D. obtained through direct communication.

intervention with exogenous surfactant can be therapeutic is shown in **Figure 6.1**. High surface tensions result in alveolar collapse (atelectasis), reduced pulmonary compliance and labored breathing. This can cause damage to the pulmonary epithelial lining and the entry of serum proteins into the alveolar space, which inhibits the activity of any surfactant that is present. Inhibited pulmonary gas exchange results in reduced blood oxygenation (hypoxia) and elevated carbon dioxide levels, which lead to respiratory acidosis and continued surfactant pool depletion.

The most common treatment for this disease is intratracheal instillation of exogenous lung surfactant replacement therapy (SRT). **Table 6-1** summarizes the various types of natural, synthetic, and biomimetic surfactant replacements that have been clinically evaluated[120, 180].

Surfactant	Source/Constituents	Manufacturer
Synthetic Surfactants		
ALEC	Synthetic (DPPC, PG)	Britannia Pharmaceuticals (UK)
Exosurf	Synthetic (DPPC, hexadecanol,	Glaxo Wellcome (USA)
Natural Animal-Derived Surfactants		
HL-10	Porcine-lung tissue	Leo Pharmaceuticals (Denmark)
Alveofact	Bovine-lung lavage	Boehringer Ingelheim (Germany)
Survanta (Beractant)	Bovine-lung tissue	Abbott Laboratories (USA)
Surfactant TA	Bovine-lung tissue	Tokyo Tenabe Company (Japan)
BLES	Bovine-lung lavage	BLES Biochem (Canada)
Infasurf	Bovine-lung (calf) lavage	Forest Laboratories (USA)
Curosurf	Porcine-lung tissue	Chiesi Pharmaceuticals (Italy)
Biomimetic Surfactants		
Surfaxin (Lucinactant)	DPPC, POPG, PA, and KL_4	Discovery Laboratories (USA)
Venticute	DPPC, POPG, PA, and rSP-C	Altana Pharmaceuticals (Germany)

Table 6-1: Exogenous surfactant replacement therapies used clinically to treat nRDS[120, 180].

The first clinical studies of SRT for treatment of nRDS in 1964 involved nebulizing a simple synthetic surfactant composed of only DPPC into the incubators of symptomatic preterm infants[222]. These trials were unsuccessful largely because, in the absence anionic lipids and

hydrophobic surfactant proteins (SP-B and SP-C), the rigidity of DPPC films was incompatible with the quick adsorption and redistribution required of surfactant at the air-liquid interface, which is required during the dynamic breathing cycle[124, 223]. ALEC and Exosurf contain anionic lipids or other surface-active additives, in addition to DPPC (**Table 6-1**); while these preparations are cost-effective and easy to produce, they only marginally improve physiological outcomes[224].

The first efficacious LS replacement was a natural, bovine-derived surfactant supplemented with dipalmitoylphosphatidylcholine (DPPC) and phosphatidylglycerol (PG)[225]; this landmark study initiated a cascade of more sophisticated trials of increasingly effective therapies[179, 225, 226]. Natural surfactants that have been used clinically (**Table 6-1**) are extracted from animal lungs by lavage, or isolated from homogenized lung tissue[142, 227]. Their improved efficacy for treating nRDS compared to synthetic formulations is attributed to the presence of SP-B and SP-C, which have been shown to impart biophysical activity[9, 120, 142]. The use of natural, animal-derived SRT for the treatment of nRDS is now routine, resulting in ~40% reduction in mortality[124, 142].

Despite the efficacy of natural SRT, nRDS remains a significant global health problem. Many of the nearly 2 million cases worldwide[143] go untreated due to the high cost of currently available therapies[144]. Difficulty in the isolation of natural surfactants and batch-to-batch variability increase costs[124] and limit treatment use in underprivileged areas[228]. A policy of selective SRT administration to only critically ill infants may relieve the economic burden of treatment, but widespread prophylactic can lead to higher survival rates[228]. Other drawbacks of utilizing animal-derived SRT include a risk of disease transmission and potential for an immune sensitization of the recipient[180].

Biomimetic LS replacements are a novel class of formulations composed of synthetic lipids with recombinant or chemically synthesized mimics of either SP-B or SP-C[179, 180]. As

discussed in **Chapters 4** and **5**, biomimetic surfactants have the potential to address the concerns of high cost and dubious safety associated with animal surfactants while maintaining efficacy[151]. Two biomimetic surfactants are now in clinical trials (**Table 6-1**): Surfaxin® (Lucinactant) (Discovery Labs) and Venticute® (Altana Pharmaceuticals). Surfaxin® contains the SP mimic KL_4, a simple 21mer peptide sequence composed of leucine and lysine[229-231]. Venticute® comprises lipids and a recombinant protein mimic of SP-C that substitutes phenylalanine residues with palmitoylated cysteines and methionine with isoleucine[232, 233]. As Surfaxin® and Venticute® emerge into the pharmaceutical marketplace, biomimetic surfactants are poised to revolutionize healthcare worldwide. There remains, however, a tremendous opportunity for innovation in the development of LS replacements that are increasingly efficacious, cost-effective, and provide a long therapeutic window for the treatment of lung disorders. The development of a low-cost, bioactive surfactant would open the door to a myriad of innovative applications that are currently prohibitively expensive, including worldwide, prophylactic treatment of nRDS.

As discussed in **Chapter 4**, *N*-substituted glycines (peptoids) are sequence-specific biopolymers that can be designed to be structural and functional mimics of native SP-B and SP-C. Our previous work has shown that peptoid-based mimics of SP-B and SP-C demonstrate promising *in vitro* surface activity[36, 37, 46, 47]. Moreover, using the rat washout model of surfactant dysfunction and inactivation associated with acute respiratory distress syndrome (ARDS), we have shown that treatment with peptoid-enhanced surfactants improves physiological and biochemical outcomes (**Chapter 5**). Here, using a similar set of peptoid-enhanced surfactant preparations, we evaluated the ability of our biomimetic formulations to mitigate the symptoms of surfactant deficiency associated with nRDS using an ovine animal model.

Because of the similarities between human and ovine pulmonary development, shown in **Figure 6.2,** the premature lamb model is considered the gold standard of animal models of nRDS[2]. The five basic phases of pulmonary development include (**1**) embryonic, (**2**) pseudoglandular, (**3**) canalicular, (**4**) saccular, (**5**) alveolar[2]. Unlike the fetal rabbit model, significant alveolar development occurs during the gestational period of both humans and sheep[2]. **Figure 6.2** shows that the timescale of human lung development, from the embryonic through alveolar phases, relative to the gestational period is very similar to that of sheep[2].

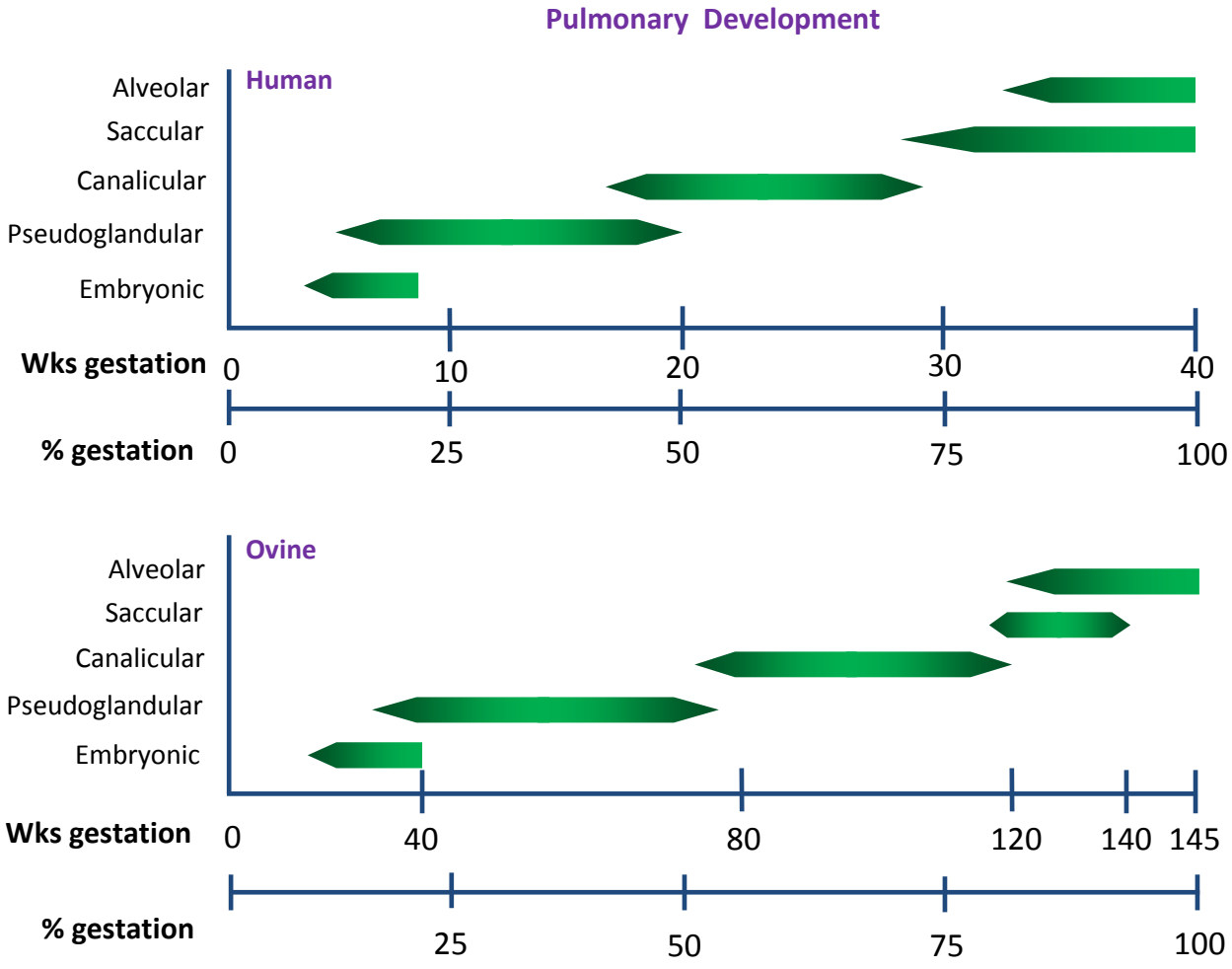

Figure 6.2: Schematic comparing the pulmonary development of humans to sheep. Adapted from [2].

We collaborated with the laboratory of Boris Kramer, M.D., Ph.D., a researcher and neonatologist at the University of Maastricht, Netherlands, to evaluate the efficacy of peptoid-enhanced biomimetic lung surfactant replacements in the treatment of premature lambs exhibiting the symptoms of nRDS. After treatment with exogenous surfactant, lambs were monitored for three hours, during which vital signs and physiological responses were monitored. Post mortem biophysical and biochemical analysis was performed to assess the severity of lung injury in each treatment group. Synthetic formulations exhibited suboptimal bulk properties at the concentrations used, which likely had a negative effect on their efficacy. Additionally, while this study was underpowered to demonstrate statistically significant differences in most responses among treatment groups, trends in the data suggest that peptoid-enhanced surfactants may improve physiological outcomes compared to treatment with the lipid carrier alone.

6.2 Results

6.2.1 Study design

This study was designed to evaluate the efficacy of peptoid-enhanced biomimetic lung

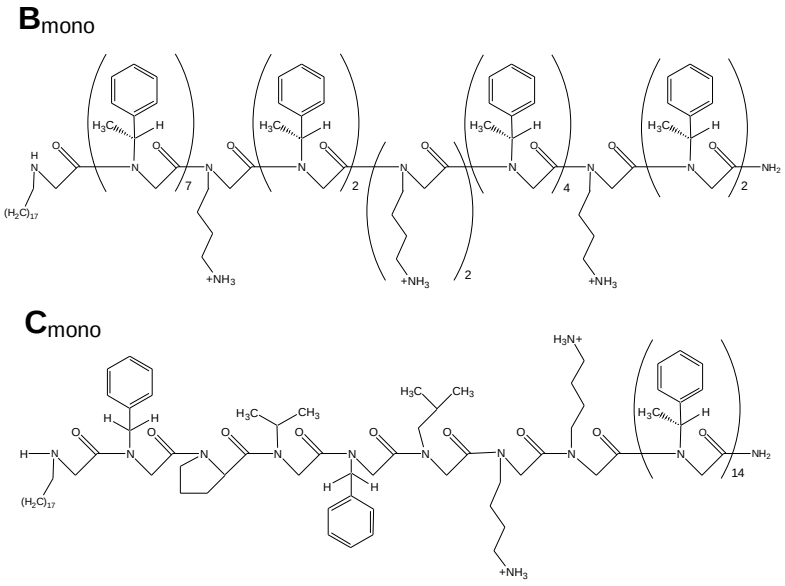

Figure 6.3: Chemical structures of B_{mono} and C_{mono}, peptoid-based mimics of SP-B and SP-C.

surfactant replacement, as measured by (**1**) physiological response, (**2**) occurrence of lung injury, and (**3**) biochemical outcomes, using an ovine animal model of nRDS. The treatment groups in this study were selected based on the results obtained using the rat washout model of ARDS, which showed that surfactant containing $\mathbf{C}_{mono}$, and a combination of $\mathbf{B}_{mono}/\mathbf{C}_{mono}$ showed positive impact on physiological and biochemical outcomes, as discussed in **Chapter 5**. $\mathbf{B}_{mono}^{8}$ and $\mathbf{C}_{mono}^{1}$ were designed to mimic prominent structural and physicochemical properties of natural SP-B and SP-C, as discussed in **Chapter 5**; the chemical structures of these peptoids are shown in **Figure 6.3**.

All peptoid-enhanced surfactants were prepared in Tanaka lipids (TL) (DPPC/POPG/PA, 68:22:9 by weight), a synthetic lipid mixture that has been shown to mimic the lipid and fatty acid portion of native lung surfactant[190]. The four treatment groups included in this study were: (**1**) Curosurf®, (**2**) TL+$\mathbf{B}_{mono}/\mathbf{C}_{mono}$, (**3**) TL+$\mathbf{C}_{mono}$, and (**4**) TL alone. Curosurf® (Chiesi Pharmaceuticals, Italy) is a natural, clinically prescribed surfactant derived from homogenized porcine lung tissue (see **Table 6-1**)[234]. Biomimetic surfactants prepared in Tanaka lipids were comprised of 2 mol% total peptoid (1 mol% each for TL+$\mathbf{B}_{mono}/\mathbf{C}_{mono}$). A control group with Tanaka lipids alone (no peptoid) was also included to elucidate the effects of peptoid-enhanced formulations compared to the lipid carrier alone. All surfactants were prepared at a concentration of 80 mg/mL, and dosing of all peptoids was 100 mg/kg.

The experimental protocol for these studies was based on an established newborn sheep model of nRDS[232, 235]. Briefly, premature lambs, ranging in gestational age from 125-130 days, were delivered by Caesarian section, sedated, intubated, and ventilated. An arterial line was placed at the umbilical cord to collect samples for blood gas analysis throughout the study; a blood gas sample was taken and ventilator settings recorded immediately preceding the instillation of surfactant (t=0). Lambs were randomized into one of the four treatment groups,

and given surfactant intratracheally through a blinded bolus instillation. Lambs were maintained on mechanical ventilation for 3 hours. The results of blood gas samples, vital signs, and ventilator settings were recorded at 0, 15, 45, 60, 120, and 180 minutes to monitor the physiological status of each animal. The primary outcome of this study was the physiological response throughout the recovery period. Biochemical analysis of the bronchoalveolar lavage fluid (BAL) and surfactant pool was also performed to assess the degree of lung injury.

6.2.2 Preparation of surfactants

The large size of the preterm lambs (average 3.2 kg) coupled with the high dose of exogenous SRT needed to saturate surfactant-deficient lungs (at least 100 mg/kg) required the production of peptoid in quantities that far exceed the amounts typically synthesized and purified in our lab. Peptoid surfactant preparations were designed to include 2 mol% peptoid (~10 wt% based on total lipid content), which is significantly higher than the concentration of SP-B and SP-C in natural surfactant (1-2 wt% each). This formulation was designed based on *in vitro* testing, which suggests that the surface activity of peptoid-enhanced formulations is compromised when the peptoid content is less than 10 wt%[236]. In addition, peptoid-based surfactants formulated in this way demonstrated efficacy in the rat model of ARDS, as discussed in **Chapter 5**.

Natural and biomimetic exogenous surfactants for the treatment of nRDS are typically dosed at a relatively high concentration, 100 – 200 mg/kg, based on the need to saturate the alveolar space in the absence of any native surfactant[232, 235, 237]. In this study, we administered all surfactants at 100 mg/kg in order to be in the saturation range, while still making it practical for us to make enough peptoid to meet the experimental needs. Based on the average lamb weight of 3.2 kg, formulating surfactants with 2 mol% total peptoid (1 mol% each for TL+$\mathbf{B}_{mono}$/$\mathbf{C}_{mono}$ preparation), and administering treatment at 100 mg/kg, each TL+$\mathbf{C}_{mono}$-treated

lamb required on average 35.5 mg $\mathbf{C}_{mono}$ and each dose of TL+$\mathbf{B}_{mono}$/$\mathbf{C}_{mono}$ required 16.8 mg $\mathbf{B}_{mono}$ and 17.7 mg $\mathbf{C}_{mono}$. In total, 379 mg of $\mathbf{C}_{mono}$ and 255 mg $\mathbf{B}_{mono}$ were synthesized and purified to > 95% homogeneity using reversed-phase HPLC (RP-HPLC) for use in this study. Because our laboratory-scale facilities were not intended for production of material at this scale, the total cost of producing the peptoid for this study in our lab was ~$20,000 (see **Appendix B** for cost analysis) and required approximately 7 months of graduate student time.

6.2.3 Physiological response

6.2.3.1 Baseline characteristics

A total of 25 lambs randomized across the four treatment groups were included in this study: Curosurf® (n=5); TL+$\mathbf{B}_{mono}$/$\mathbf{C}_{mono}$ (n=7); TL+$\mathbf{C}_{mono}$ (n=7); TL alone (n=6). The average baseline (BL) parameters across the various treatment groups are summarized in **Table 6-2**. The differences in baseline parameters across all groups were not statistically significant, and the standard errors associated with these parameters across all treatment groups were small. This suggests that the general health of all treatment groups was equivalent prior to surfactant treatment. In addition, the blood pressure and heart rate data collected throughout the three hour observation period showed that animals from all treatment groups were adequately perfused throughout the study (data not shown).

BL parameter	Curosurf	TL+$\mathbf{B}_{mono}$/$\mathbf{C}_{mono}$	TL+$\mathbf{C}_{mono}$	TL alone	Overall
Gender (m/f)	2 / 3	5 / 2	3 / 4	3 / 3	13 / 12
Gest. age (days)	127.2 ± 0.97	125.4 ± 0.43	125.7 ± 0.36	125.2 ± 0.6	125.8 ± 0.31
Birth weight (kg)	3.22 ± 0.25	3.03 ± 0.15	2.93 ± 0.17	3.42 ± 0.28	3.2 ± 0.1
Blood pH	7.35 ± 0.09	7.43 ± 0.01	7.40 ± 0.02	7.41 ± 0.02	7.39 ± 0.4
BP (mmHg)	79 / 53 ± 1.5	76 / 53 ±3.3	78 / 50 ± 7.6	75 / 53 ± 9.9	77 / 53
HR (BPM)	217 ± 14	197 ± 13	192 ± 9	182 ± 10	195 ± 10

Table 6-2: Average baseline characteristics of all treatment groups ± standard error of the mean (SEM).

6.2.3.2 Measures of gas exchange and pulmonary function

The arterial partial pressure of oxygen (paO_2) normalized to the fraction of inspired oxygen (FIO_2) is a measure of how effectively oxygen is transported from the lungs to the arterial blood. Conversely, a high arterial partial pressure of carbon dioxide (pCO_2) and low blood pH (acidosis) is symptomatic of impaired CO_2 removal. **Figures 6.4 and 6.5** show the normalized paO_2, blood pH, and pCO_2 for the different treatment groups over the three hour observation period. The initial values of these parameters are similar to what has been reported previously for newborn lambs of comparable gestational age[232, 235]. While the normalized paO_2 increased at the 15 minute measurement, improved oxygenation was not maintained throughout the observation period (**Figure 6.4**). No treatment group demonstrated paO_2 greater than 80 mmHg throughout the remainder of the experiment—an observation that is particularly surprising for the Curosurf® treated positive control group. A similar study has shown Curosurf® administered at 175 mg/kg to improve paO_2 in premature lambs to ~ 300 mmHg three hours after treatment[232]. In this study, however, the dosage of Curosurf® was reduced to 100 mg/kg in

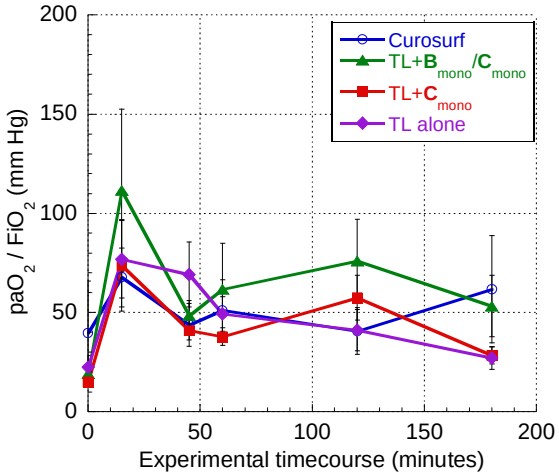

Figure 6.4: Arterial partial pressure of oxygen (paO_2) normalized to the fraction of inspired oxygen (FiO2) over time.

an effort to equalize the dosage of all treatment groups.

While it is possible that the lower dose of Curosurf® negatively impacted the improvement in gas exchange functionality expected for the positive control, treatment with natural surfactant at 100 mg/kg has been shown previously to have a more pronounced effect on arterial blood oxygenation than we observed in this study. In a study similar to this, treatment with a natural surfactant derived from lung lavage of adult sheep, administered at 100 mg/kg, resulted in an average paO_2 of 201 mmHg over a five hour treatment time[232]. Because treatment with the positive control (Curosurf®) and the negative control (TL alone) showed very similar improvements in arterial blood oxygenation, no conclusions can be drawn from this response.

Exogenous surfactant replacement therapy for the treatment of nRDS is expected to mitigate the reduction in blood pH (related to acidosis) and decrease the pCO_2. **Figure 6.5** shows that while this study was underpowered to detect statistically significant differences

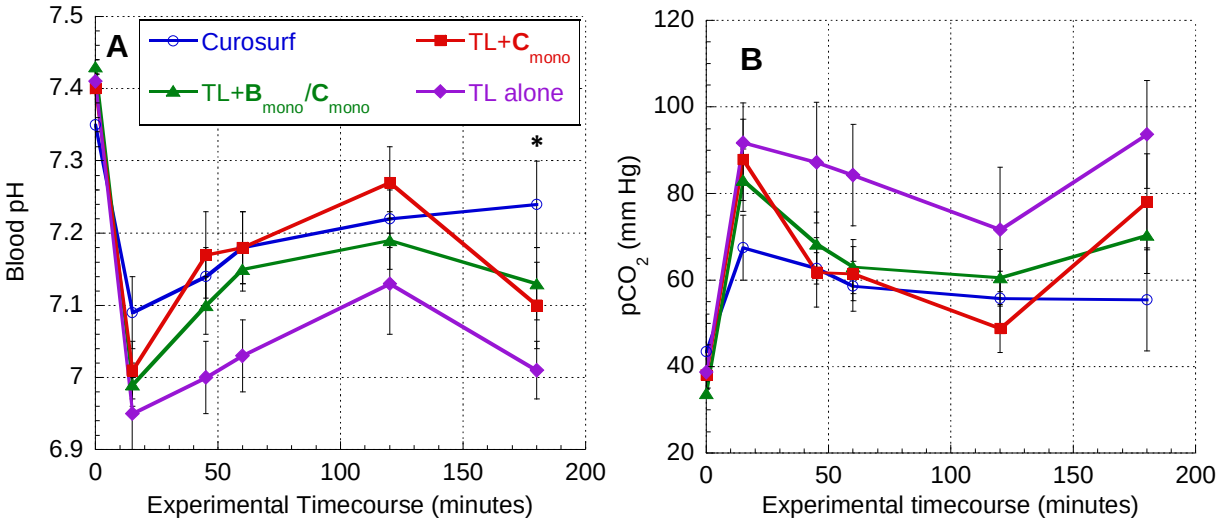

Figure 6.5: Physiological parameters related to CO_2 exchange. (**A**) Arterial blood pH, (**B**) Arterial partial pressure of carbon dioxide (pCO_2). Error bars indicate the standard error of the mean. Statistical significance: * indicates statistical significance ($p < 0.05$) between Curosurf and TL alone treatment groups, determined using a one-sided ANOVA and Tukey-Kramer method.

among most groups, the data demonstrate consistent trends. The TL alone treatment group demonstrated the poorest outcome for both blood pH and pCO_2; from 15 – 180 minutes during the observation period, the TL alone group exhibited the lowest blood pH and highest pCO_2. While the Curosurf® treated group demonstrated the most positive outcome in the beginning (15 minutes) and end (180 minutes) of the observation period, treatment with the peptoid enhanced surfactants resulted in comparable blood pH (**Figure 6.5A**) and pCO_2 (**Figure 6.5B**) at 45, 60, and 120 minutes. It is notable that while treatment with TL+**B**$_{mono}$/**C**$_{mono}$, TL+**C**$_{mono}$, or TL alone all showed poorer blood pH and pCO_2 at 180 compared to 120 minutes, the Curosurf-treated group showed improvement. This suggests that while the peptoid-based surfactants may demonstrate efficacy for up to two hours, beyond this time, physiological status may begin to deteriorate. In contrast, Curosurf® appeared to have a more sustained improvement on gas exchange.

6.2.3.3 Ventilation indicies

The oxygenation index (OI) and ventilation efficiency index (VEI) were calculated for all treatment groups throughout the observation period as shown in **Figure 6.6**. The OI was

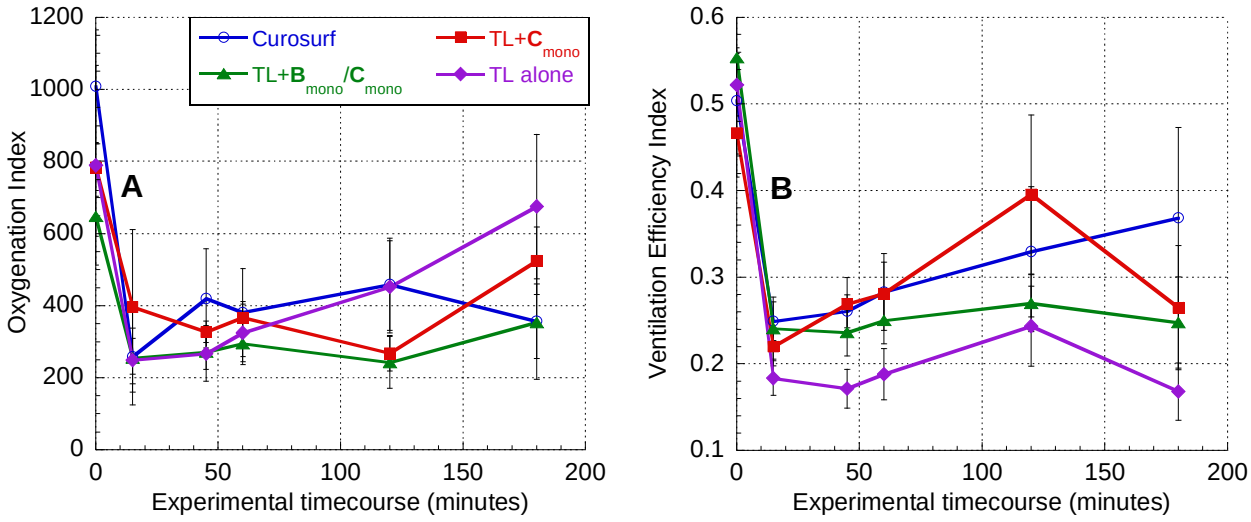

Figure 6.6: Pulmonary ventilation indicies. (**A**) Oxygenation index (OI) over time (**B**) Ventilation efficiency index (VEI) over time. Error bars indicate the standard error of the mean (SEM).

calculated as OI = (MAP*FIO_2) / paO_2, where MAP = mean airway pressure. This index is a ratio that reflects the amount of pulmonary effort exerted to the degree of oxygenation reward (lower values indicate better health). The VEI was calculated using the equation VEI = 3800/(RR * (PIP-PEEP) * pCO_2), where RR = respiratory rate, PIP = peak inspiratory pressure, and PEEP = positive end expiratory pressure. The VEI is a means of assessing the degree of pulmonary ventilation independent of ventilator settings (higher values indicate higher efficiency and better health).

The instillation of surfactant resulted in an improved oxygenation index for all treatment groups within 15 minutes (**Figure 6.6A**). By 180 minutes, OI of the TL alone treatment group deteriorated more than any other treatment group. Similarly, the VEI showed treatment with TL alone had the poorest physiological response, while that of Curosurf® and TL+$\mathbf{C}_{mono}$ had better outcomes (**Figure 6.6B**). A similar trend as seen in parameters in gas exchange is evident here—while the Curosurf®-treated group appears to continue to improve after 120 minutes, ventilation indicies deteriorated after 120 minutes for groups treated with non-natural surfactants. It is possible that the natural preparation is capable of more sustained respreadability than synthetic surfactants, which would extend their therapeutic usefulness.

6.2.3.4 Lung compliance

Lung compliance, defined as $\Delta V/\Delta P$, normalized to body weight, was determined post mortem using a calibrated syringe and pressure transducer. The resultant average pressure-volume (PV) deflation curve for each treatment group, along with the calculated compliance at maximal volume is shown in **Figure 6.7**. The Curosurf®-treated group had the most compliant lungs (1.18 mL/(kg*cm H_2O)) and those of the TL alone treatment group was least compliant (0.6 mL/(kg*cm H_2O). Treatment with peptoid-enhanced surfactants tended to show improved

compliance (TL+**B**$_{mono}$/**C**$_{mono}$, comp. = 0.80 mL/(kg*cm H_2O); TL+**C**$_{mono}$, comp. = 0.71 mL/(kg*cm H_2O) compared with TL alone (0.60 mL/(kg*cm H_2O).

6.2.3.5 Lung injury

6.2.3.5.1 Surfactant pool evaluation

We performed biochemical analysis of the broncheoalveolar lavage (BAL) to evaluate several markers of lung injury. The BAL was centrifuged to separate the more surface-active large aggregate (LA) portion from the less active small aggregates (SA). As shown in **Figure 6.8**, we quantified the protein, phospholipid, and disaturated phospholipid content of the BAL as well as the LA and SA surfactant portions. The differences across treatment groups by these measures were not statistically significant, but some trends are evident. As a result of lung injury, the integrity of the lung epithelial layer can be compromised, which allows proteins and proteases to permeate the air space. The presence of these proteins further deactivates any

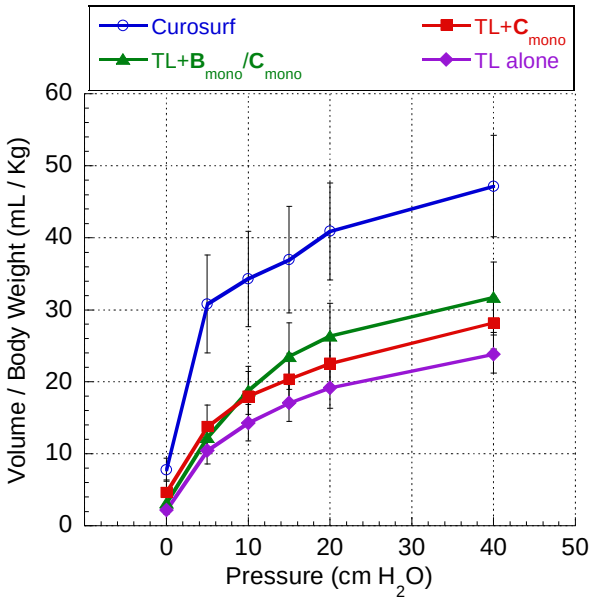

Compliance at p = 40 cm H_2O (mL/(kg*cm H_2O))

Curosurf	1.18
TL+**B**$_{mono}$/**C**$_{mono}$	0.80
TL+**C**$_{mono}$	0.71
TL alone	0.60

Figure 6.7: Deflation pressure-volume (PV) curve. Compliance is calculated as ΔV/(ΔP), normalized to body weight. Error bars indicate the standard error of the mean.

lung surfactant in the alveolar space. **Figure 6.8A** shows that the protein content of the surface-active large aggregate portion was negligibly small compared to that of the small aggregates for all treatment groups. For the whole BAL (and similarly for small aggregates), the Curosurf®-treated group tended to have a lower protein content (66 mg/kg), while the TL+**C**$_{mono}$ (104 mg/kg) and TL alone (104 mg/kg) had the highest protein levels. It is possible that the lower protein levels of the Curosurf®-treated group reflect a reduced degree of injury compared to the synthetic surfactant treatment groups.

The total phospholipid content and disaturated phospholipid content for the various

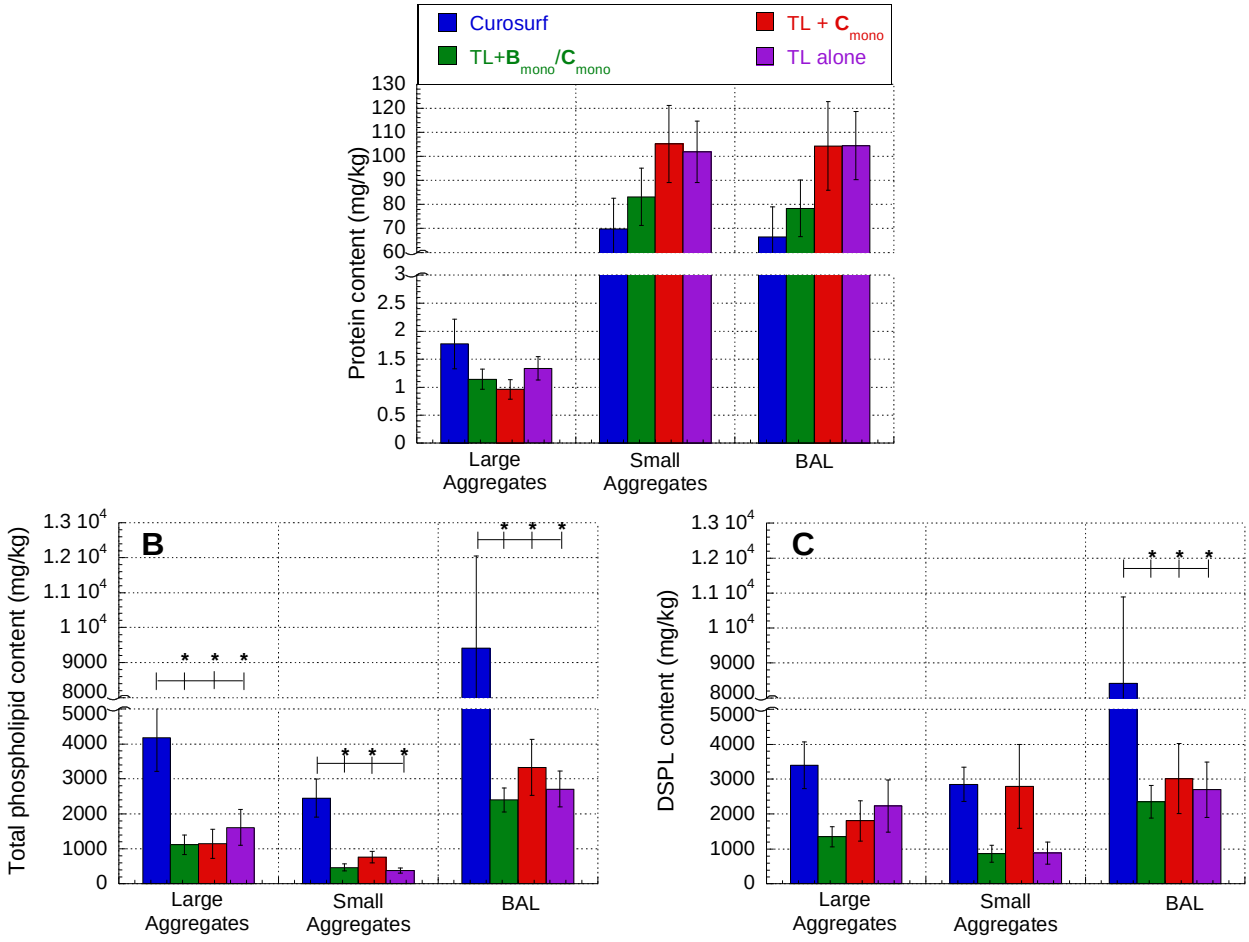

Figure 6.8: Surfactant pool phospholipid and protein content normalized to body weight. (**A**) Protein content, (**B**) Total phospholipid content, (**C**) Disaturated phospholipid (DSPL) content. Error bars indicate the standard error of the mean (SEM). * denotes a statistically significant ($p < 0.05$) difference between the Curosurf treatment group and the designated group.

treatment groups in the BAL and surfactant portions are shown in **Figure 6.8B** and **6.8C**. Because the nRDS lung is incapable of producing its own surfactant, the phospholipids that remain in the BAL are a reflection of how well the exogenous surfactant is retained in the alveolar space and how quickly it is metabolized. In the BAL, as well as the large and small aggregates, the Curosurf®-treated group had an average phospholipid content that was approximately five times higher than any other treatment group. There was no appreciable difference in phospholipid content of the peptoid formulations compared to the TL alone treatment groups. These results suggest that Curosurf® was more effectively maintained in the alveolar space than the synthetic Tanaka lipid formulation, and that the presence of peptoid within the formulation did not impact the ability of TL to be maintained in the alveolar space.

Because disaturated phospholipids (DSPL) are degraded in the presence of proteases, quantifying the DSPL content of the BAL can be used as another marker of lung injury. Similar to the trend observed for total phospholipid content, in the case of the BAL, the Curosurf®-treated group had a significantly higher DSPL content than any other group. In the small and large aggregate portions, however, no significant differences in DSPL content were noted.

6.2.3.5.2 Cell Count

We quantified the total cell count in the BAL of each animal as well as the differential cell counts of epithelial cells and three specific leukocyte populations. Epithelial cells are lung parenchymal cells that not only provide a structural barrier to pathogens, but they also play an important role in modulating the inflammatory response[238]. Monocytes, lymphocytes, and neutrophils are itinerant immune cell populations that are quickly recruited to the site of injury or infection[238].

As shown in **Figure 6.9**, the total cell count and differential cell populations were similar in all treatment groups with the exception of the neutrophil population. The average cell count

of neutrophils in the TL alone group (8.9 x 10^6 cells/kg) was significantly higher than that of Curosurf® (1.4 x 10^6 cells/kg) TL+**B**$_{mono}$/**C**$_{mono}$ (2.4 x 10^6 cells/kg) or TL+**C**$_{mono}$ (1.9 x 10^6 cells/kg) treatment groups. It is possible that the neutrophil content was higher for the TL alone treatment group because of an increased degree of injury compared to the other three treatment groups.

6.3 Discussion

The development of a wholly synthetic, biomimetic exogenous lung surfactant replacement could have tremendous impact on the treatment of nRDS worldwide. We used an established ovine animal model of surfactant deficiency to evaluate the efficacy of peptoid enhanced biomimetic surfactant in mitigating the symptoms of nRDS. This study marks the first use of a sophisticated *in vivo* animal model of nRDS to evaluate the efficacy of peptoid-based exogenous lung surfactant replacement therapies. Several parameters demonstrated trends

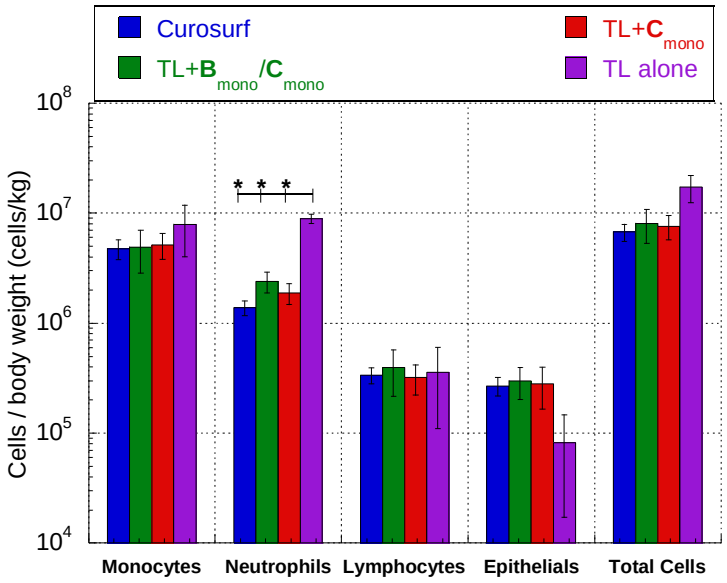

Figure 6.9: Average cell content of broncheoalveolar lavage (BAL). Error bars indicate the standard error of the mean (SEM). Statistical significance: * indicates a $p < 0.05$ compared to the value for the TL alone treatment group.

that are consistent with positive outcomes based on the study design. Physiological parameters, including arterial blood pH, pCO_2, OI, VEI, and lung compliance at the end of the experiment (t = 180 minutes) demonstrated on average the best outcome for the positive control (Curosurf®) and poorest outcome for the negative control (TL alone). The peptoid-containing treatment groups (TL+$\mathbf{B}_{mono}/\mathbf{C}_{mono}$ and TL+$\mathbf{C}_{mono}$) on average demonstrated an intermediate outcome, with little difference between the two groups. This suggests that the presence of peptoid in either formulation may demonstrate some improvement in physiological outcome compared to treatment with TL alone.

Biochemical analysis of the total BAL as well as small and large aggregate portions demonstrate that treatment with Curosurf® tended to reduce lung injury (lower protein content and a statistically significant higher phospholipid content) compared to the other treatment groups. Cell count analysis, however, demonstrated a statistically significant increase in neutrophils in the BAL of the TL alone treatment group. By this measure, the peptoid-containing formulations appeared to produce a response more similar to the Curosurf®-treated group. Taken together, the physiological and biochemical outcomes suggest that peptoid-based lung surfactants may be efficacious in mitigating the symptoms of nRDS.

While this study was a very significant and unprecedented step toward the development of peptoid-based lung surfactant replacement, we encountered several challenges that need to be addressed in future studies of this kind. While many of the physiological and biochemical outcomes showed consistency among the trends in the results, this study was underpowered such that statistically significant differences between the treatment groups in most cases could not be demonstrated. Factors contributing to this lack of significance are the relatively small number of animals included in the study, coupled with the small differences in the outcomes that we observed between groups relative to the standard deviation within treatment groups. To

gain a better understanding of these effects, we used a power analysis to project the sample size (n, per group) that would be required to statistically differentiate groups based on the pooled standard deviations (SD_{pooled}) we observed and the expected threshold difference between groups.

As shown in **Table 6.3**, the power analysis indicated that given with the large SD_{pooled} observed in the data from this study, the number of animals required per group to elucidate the effects ranged from 11-19 animals. We were limited in the number of animals and amount of surfactant available for the studies, due primarily to cost and peptoid availability. It may be more advisable for future studies to limit the study to only one peptoid-containing experimental treatment group. In so doing, the resources available for the study can be spread across three treatment groups (positive control (Curosurf®), negative control (lipids alone) and experimental group) instead of the four groups used in this study. It should also be noted that, as will be discussed, protocol changes in future studies that could decrease the standard deviation within groups, may reduce the number of animals projected in this calculation.

	PaO_2	pCO_2	Blood pH	OI	VEI	Compliance
Expected Differential	50 mmHg	30 mmHg	0.2	400	0.2	15
SD_{pooled}	35.6	27.1	0.55	367	0.17	11.1
Required sample size	12	11	12	19	16	13

Table 6-3: Statistical power calculation results using a one-sided ANOVA analysis. Statistical significance was designated as $p < 0.05$. Power assumed was 90%. SD_{pooled} is the calculated pooled standard deviation based on the data set at t=180 (p = 40 mL/(cm H_2O*kg). The expected differential is the expected mean difference between treatment groups.

The formulation of the TL alone, TL+$\mathbf{B}_{mono}/\mathbf{C}_{mono}$, and TL+$\mathbf{C}_{mono}$ posed another significant challenge for this study. We chose to prepare these surfactants at concentrations equal to that of Curosurf® (80 mg/mL) to eliminate a potentially significant difference between treatment groups. Upon resuspending the lyophilized surfactants in saline, however, the mixture was non-homogeneous and difficult to keep suspended. Those surfactants containing peptoid had clumps of material that were stable to extensive aspirating and sonication. Moreover, the TL alone preparation tended to foam or gel easily, making difficult the intratracheal instillation. It is likely that the suboptimal, non-homogeneous nature of these preparations reduced their *in vivo* efficacy.

The literature suggests that lowering the concentration of biomimetic surfactants may be one way in which to enhance their performance. Using the premature lamb model of nRDS, Surfaxin® (Lucinactant), a biomimetic surfactant that contains the 21mer peptide KL_4 SP-B mimic, was prepared at a concentration of 30 mg/mL in a similar mixture of synthetic lipids[235]. Similarly, Venticute®, a biomimetic surfactant that contains a recombinant SP-C mimic, was tested in the premature lamb model at a concentration of 25 mg/mL[232]. The Surfaxin study included a natural surfactant treatment group that was significantly more concentrated (80 mg/mL) than the synthetic formulation (30 mg/mL); equivalent doses were used (175 mg/kg), which resulted in different volumes being instilled. For this study, it may have been a better strategy to use a similar strategy. The peptoid surfactants prepared at 25 mg/mL for the *in vivo* study using the rat model of ARDS demonstrated efficacy in improving physiological and biochemical outcomes (**Chapter 5**) and demonstrated no significant formulation issues. In the absence of any further data, it would be recommended for future studies that peptoid-containing surfactants and lipid alone formulations be prepared at no higher than 25-30 mg/mL.

It is also possible that a different synthetic lipid mixture in combination with peptoid would exhibit better *in vivo* efficacy. We chose to formulate these surfactants in Tanaka lipids based on primarily their excellent *in vitro* performance[164]. In addition, Surfaxin® and Venticute®, which are in clinical development, are formulated with a very similar lipid preparation, containing DPPC, POPG, and PA[232, 235]. However, it is possible that a different formulation, for example Infasurf® synthetic lipids, could improve efficacy. While this mixture did not perform as well in *in vitro* testing[164], it has been shown to be efficacious for *in vivo* use[224]. Prior to initiating further studies in an ovine model of nRDS, a comprehensive formulation development study should be completed to determine how both concentration and formulation composition influence the *in vitro* surface activity and bulk physical properties of the mixture.

Consideration should also be given as to how individual surfactant preparations are prepared as single doses in individual glass vials. Vials were prepared each containing 270 mg Tanaka lipids, which is sufficient to treat a 2.7 kg lamb at 100 mg/kg. Because many of the animals used in this study exceeded 2.7 kg, individual surfactant vials had to be combined in many cases. Surfactants were therefore not all used on the day they were suspended (as had been done in the rat study); suspended surfactants were stored at -20^{o}C. While the stability of suspended surfactant preparations over several days has not been studied, it has been preferred to use surfactants within hours of preparing them. Future studies should plan for a higher average birth weight (3.3 kg based on the results of this study) to ensure enough surfactant is present in a single vial and minimize the amount of time surfactants are stored overnight.

A surprising outcome of this study was the lack of improved oxygenation of all animals, particularly with the Curosurf®-treated group—as discussed previously, the paO_2 levels achieved in this study were well below previously published results for Curosurf®-treated

preterm lambs of comparable gestational age[232, 235]. While it is possible that the 100 mg/kg dosing strategy did not allow the lung to become fully saturated with surfactant, it is also possible that the Curosurf® used in the study, obtained as a gift from the manufacturer, was deactivated. In future studies, *in vitro* testing of the Curosurf® prior to use would be recommended.

Several changes to the protocol should be considered prior to initiating future studies of this nature. It is recommended that in order to reduce the incidence of lung injury in the preterm lamb, surfactant should be instilled immediately after delivery before the first breath is taken and prior to mechanical ventilation. Previous studies report protocols that have achieved this[232, 235], and have stressed its importance in minimizing lung injury. Lowering the baseline level of injury associated with all groups may improve the ability to detect a difference in lung injury that is directly related to the treatment given. The study would also benefit from a tighter breeding scheme (± 1 day) to minimize variability across experimental groups due to disparate pulmonary development.

6.4 Materials and Methods

6.4.1 Peptoid synthesis and purification

Peptoids were synthesized using an ABI 433A peptide synthesizer (Applied Biosystems, Inc.) on Rink amide MBHA resin (Novabiochem, Inc.) using the submonomer approach[3]. Briefly, bromoacetic acid (C13 labeled bromoacetic acid was used for one coupling in each molecule), activated by diisopropylcarbodiimide was used to form a bromocetylated intermediate on the terminal amide group. Bromide is then substituted with the desired primary amine through S_N2 displacement to build the peptoid chain. The amines used in peptoid synthesis include benzylamine, octadecylamine, isopropylamine, isobutylamine, (*S)*-α-methylbenzylamine (all purchased from Sigma-Aldrich) and *N*-tert-butoxycarbonyl-1,4

diaminobutane that was made using a previously published procedure[83]. Resin-bound peptoids were then exposed to a mixture of trifluoroacetic acid (TFA): triisopropylsilane:water (95:2.5:2.5, v:v:v) for ten minutes to cleave peptoids from the solid phase. Peptoids were purified by reversed-phase HPLC (RP-HPLC) (Waters Corporation) using a C4 or C18 column and a linear acetonitrile:isopropanol (2:1)/water gradient. Final purity was greater than 97% as measured by analytical RP-HPLC (Waters Corporation), and the identity of each molecule was checked using electrospray ionization mass spectrometry.

6.4.2 Surfactant preparation

Individual stock solutions of synthetic lipids (DPPC, POPG, and PA) of accurately known concentration were made in a 3:1 mixture of chloroform/methanol. The Tanaka lipid (TL) formulation was prepared to an accurately known concentration (10-12 mg/mL) by combining the individual stock solutions to yield a 68:22:9 (w:w:w) mixture of DPPC:POPG:PA. Surfactant preparations for these studies were prepared individually in cleaned, 20mL glass scintillation vials. 270 mg of TL (enough to treat a 2.7kg lamb at 100 mg/kg) were dispensed into each vial. The appropriate amount of peptoid was added from methanol-based stock solutions of accurately known concentrations. Surfactant mixtures were then blown down with nitrogen to a reduced volume, lyophilized overnight, and stored at -20 ^{o}C until the time of use. Sterile saline was added to the dried down surfactant mixture to make a concentration of 80 mg/mL. The mixture was allowed to hydrate for 1 hour, aspirated with a pipette, and sonicated in a sonication bath for 10 minutes prior to use.

6.4.3 Preterm lambs

6.4.3.1 Delivery, treatment, and ventilation

These animal experiments were reviewed and approved by the animal care ethics committee at the University of Maastricht, Netherlands. Date-bred Texel ewes were given a spinal epidural (3 mL x% lidocaine). The effectiveness of the anesthesia was monitored by

observing the absence of muscle tone in the ewe's hind limbs. A lateral incision was made in the ewe's abdomen through which the fetus was delivered, and blood was drawn from the umbilical cord for use in the lamb was anemic. In the case of twins, the second fetus was delivered using the same procedure. After clamping off the umbilical cord, the ewe was euthanized.

Preterm lambs (125 – 130 days gestational age; full term 150 days) were weighed, placed on a warming bed (Cosycot, Fisher and Paykel, New Zealand), sedated with 0.3 mg/kg midazolm, i.m., and intubated. Lambs were then randomized and given one of four surfactant treatments through a single bolus instillation, in a blinded fashion: (**1**) Curosurf (100 mg/kg); (**2**) Tanaka Lipids (TL)+$\mathbf{B}_{mono}$/$\mathbf{C}_{mono}$ (100 mg/kg); (**3**) TL+$\mathbf{C}_{mono}$ (100 mg/kg); (**4**) TL alone (100 mg/kg). Lambs were mechanically ventilated (Babylog 8000, Drager, Lubeck, Germany) with initial settings as follows: 60 breaths per minute respiratory rate, inspiratory time 0.4 seconds, 5 cmH_2O PEEP, 30 cmH_2O PIP, tidal volume 5-10 mL/kg, FiO2 100%. An umbilical cord arterial line was placed to obtain blood gas samples. Glucose (20%, 1.7mL/kg/hr) and a sedative (180 mg midazolam, 1.7 mL/kg/hr) were administered through the arterial line. Temperature was monitored through an anal temperature probe, and body temperature was maintained at 38-39 degrees using heating pads and plastic wrap. At 0, 15, 45, 60, 120, and 180 minutes, blood gas samples were taken and vital signs/ventilator settings were recorded. Blood gas samples were analyzed using an iSTAT (Abbott Laboratories) portable blood gas analyzer. At 180 minutes, the lamb was euthanized (pentobarbital 1ml/kg).

6.4.3.2 Lung processing

Post mortem, the chest was opened and lung compliance was measured. Using a calibrated syringe and pressure transducer, the lungs were inflated with air to 40 cm H_2O pressure and the maximal lung volume. The pressure was then lowered in a step-wise fashion

to 20, 15, 10, 5, and 0 cm H_2O, and the corresponding volume was recorded at each step. Lungs were removed from the chest cavity. The right lung was weighed and then lavaged with cold saline until fully distended, and withdrawn with a syringe. The lavage procedure was repeated five times with a total volume of 50 mL saline. The total volume of recovered bronchealveolar lavage (BAL) fluid was recorded and snap-frozen for storage until analysis. Other samples collected for subsequent analysis include left lung, right lung, middle lobe, urine, liver, and spleen. The pulmonary lower lobe was fixed in formalin overnight and sectioned.

6.4.4 Biochemical Analyses

To sediment the cellular debris, the broncheoalveolar lavage fluid was centrifuged at 150 *g* for 10 minutes. The supernatant (called Total Surfactant (TS)) (save 5 mL for phospholipid analysis) was centrifuged at 40,000 *g* for 15 minutes to separate the supernatant (Small Aggregates (SA) from the pellet. The pellet was resuspended in 2mL saline to produce the Large Aggregate (LA) portion. Aliquots of each surfactant portion were extracted using the Bligh/Dyer method[219] and the Duck-Chong phosphorous assay[220] was used to quantify the amount of phospholipid within each fraction. Protein quantification was performed using the micro BCA protein assay kit (Pierce Biotechnology, Inc.) according to manufacturer's instructions. Cell counts were performed using a Burker cell counting chamber.

6.4.5 Statistical analyses

All statistical analyses were performed using Minitab 15 (Minitab, Inc.). The outcomes were analyzed for statistical significance using a one-sided ANOVA analysis and the Tukey-Kramer method of multiple comparisons. Results were considered statistically significant when $p < 0.05$. The power analysis was performed assuming 90% power, and pooled standard deviations were calculated based on responses from this study at t = 180 minutes.

6.5 Study contributions

Ann Czyzewski contributed to study design, performed experiments, analyzed/interpreted data, performed statistical analysis. Heicke Hinemann contributed to study logistical preparation and execution of the study. Arno Brouwers contributed to execution of the study. Lauren Jones assisted with preparation of surfactants and performing experiments. She also did the cost analysis; Freek van Iwaarden (collaborating PI) contributed to biochemical analysis. Boris Kramer (collaborating PI) contributed to study design, performing experiments, analyzing data. Annelise Barron established the collaboration, contributed to study design as well as analyzing/interpreting data.

7. Future directions and new frontiers

The design and development of biomimetic therapeutic agents is a highly interdisciplinary research platform that has the potential to significantly impact healthcare worldwide. "Designer" antibiotics that can be customized to meet patients' needs while at the same time can slow the rate at which antimicrobial resistance develops would have the potential to significantly reduce the burden of infectious diseases. Similarly, the development of a wholly synthetic, efficacious lung surfactant replacement for the treatment of respiratory distress syndrome would not only increase access to treatment worldwide, but also open the door to many other types of uses that are currently prohibitively expensive. While significant advancements have already been made toward these goals, it is clear that we have only begun to explore the possibilities that these research areas have to offer.

In vitro studies demonstrating the antimicrobial activity of ampetoids and surface activity of lung surfactant protein mimics laid the foundation for the studies reported herein. The scope and intent of this work was to initiate a platform of research that addresses issues directly related to the therapeutic potential of peptoid-based mimics of bioactive proteins. We explored how and to what extent ampetoids exhibit two hallmarks of antimicrobial peptides: selectivity and broad spectrum antimicrobial activity. Moreover, ampetoid selectivity can be finely tuned with subtle structural changes, which could be a means of leveraging improved therapeutic indicies. In regard to both antimicrobial peptoids and lung surfactant protein mimics, we worked with collaborating labs to design and execute the first *in vivo* evaluation of peptoids' efficacy as therapeutic agents. In the murine model of *S. aureus* i.p. challenge, ampetoid **1** reduced bacterial counts by approximately two orders of magnitude compared to untreated controls. Additionally, peptoid-based mimics of lung surfactant proteins SP-B and SP-C were found to effectively mitigate some symptoms associated with ARDS using the rat washout model. These studies show that peptoids as mimics of bioactive proteins do indeed exhibit promising

therapeutic potential. The knowledge gained from this body of work lays the foundation for yet another series of questions to be answered. Following is a discussion of possible future directions and new frontiers that would advance this research and make one step closer the goal of using peptoid-based therapeutic agents to benefit human health.

7.1 The development of antimicrobial peptoids as therapeutic agents

7.1.2 *In vitro* tests

We have shown that antimicrobial peptoids exhibit two hallmarks of antimicrobial peptide activity: cell selectivity and broad-spectrum potency against bacteria. The results presented in **Chapter 2** show that antimicrobial peptoid selectivity can be modulated by both molecular physicochemical parameters as well as more specific structural attributes. Moreover, many selective ampetoids retained antimicrobial activity against multi-drug resistant Gram-negative and Gram-positive strains comparable to that of pexiganan, a clinically-relevant antimicrobial peptide. As a result of these studies, five ampetoids emerge as antimicrobially active ($MIC_{E.\ Coli}$ = 6.3 – 12.5 μM), yet selective ampetoids: $\mathbf{1}_{11mer}$, $\mathbf{1}_{ach}$-*N*spe$_2$, $\mathbf{1}_{ach}$-*N*spe$_{12}$, **1**-Pro$_9$, and $\mathbf{1}_{achiral}$. These molecules are among the most promising "lead compounds" for development as antimicrobial agents, particularly against Gram-negative strains. It is recommended that for these molecules, broad-spectrum activity testing against a variety of pathogenic and MDR strains be expanded to include the 20 strains used to test ampetoid **1** in **Chapter 3**.

Perhaps more than the identification of specific lead compounds, the study discussed in **Chapter 2** enabled us to better understand new ways to develop antimicrobially potent, yet selective ampetoids. The three design characteristics that resulted in the most favorable selectivity profile were: (**1**) including similarly cationic or similarly hydrophobic monomers in terminal positions, (**2**) substitution of achiral *N*pm monomers for *N*spe monomers (**3**) optimizing

CTLR. Future generations of ampetoids should be designed to explore these strategies more fully.

Another interesting result of this study was the consistent, low-micromolar activity (0.78 – 1.56 µM) of all ampetoids against Gram-positive *B. subtilis* (ATCC 6633), including ampetoids that were non-hemolytic up to 200 µM (**1**B-*N*Lys$_{4,10}$, **1**$_{10mer}$, **1**-Pro$_{3,9}$, and **1**-*N*sdp$_{all}$). It would be interesting to test these (and other with a similar activity profile) against a panel of MDR Gram-positive strains Broad-spectrum activity testing of a different set of ampetoids showed that these molecules retained activity (4-16 µg/mL) against eight of nine MDR Gram-positive strains that was superior to that of pexiganan (4-64 µg/mL). Gram-positive infections impose a tremendous burden on the healthcare system; developing highly selective ampetoids capable of targeting this type of infection would be a significant advancement.

The preliminary study in **Chapter 3** showed that the MIC of peptoid **1** was not affected by bacterial load to the same degree as was the MIC of the antimicrobial peptide, pexiganan. This is an area that could be relevant to the bioavailability of peptoids and needs to be further investigated. It is recommended to include a spectrum of selective an non-selective antimicrobial peptoids (including **1**-Pro$_9$, **1**$_{ach}$-*N*spe$_2$, **1**$_{ach}$-*N*spe$_{12,}$ **1**$_{achiral}$, and **1**$_{11mer}$) as well as more antimicrobial peptides (melittin, for example). With the data in hand, it is unclear if the phenomenon observed with **1** is unique to this molecule or a characteristic that is associated with all peptoids. If ampetoids consistently demonstrate relatively constant MICs across a range of bacterial loads, this could be the result of peptoids having a non-natural, protease resistant backbone that is not digested by proteases emitted from dying bacteria. This could be a distinct advantage of peptoids for use as antimicrobial agents in *in vivo* applications.

Another area of ampetoid development that has been largely unexplored is the capacity of antimicrobial peptoids to modulate an immune response and contribute to the treatment of inflammatory diseases. It is becoming increasingly clear that in addition to their direct antimicrobial activity, several antimicrobial peptides may play an important role in a variety of human diseases, including skin diseases, respiratory disorders, periodontal disease, arthritis in articular joints, and wound healing (reviewed in [239]). It would be informative to perform a variety of *in vitro* tests designed to explore the potential of ampetoids to modulate immune response, such as endotoxin neutralizing activity, activation of chemokine release, and inhibiting the release of proinflammatory cytokines.

7.1.3 *In vivo* tests

We determined selectivity ratios (based on the MIC and hemolytic dose from *in vitro* testing) for several compounds, but this is not a substitute for a true therapeutic index. Prior to further *in vivo* testing for efficacy in treating an infection, it is recommended to determine the maximum tolerated dose in intact physiology using a rodent model. This data is necessary to optimize the dosing regimen in studies designed to evaluate their efficacy in treating an infection *in vivo*.

The *in vivo* studies of antimicrobial peptoids discussed herein mark the first reporting of peptoid-based antimicrobial peptide mimics exhibiting efficacy in treating an infection in intact physiology. The simple model of *S. aureus* intraperitoneal challenge demonstrated a statistically significant reduction in bacterial count for animals treated with peptoid **1** compared to untreated controls. The next significant step would be to test the efficacy of peptoids through a systemic, rather than local route of administration, such as intramuscular (i.m.), subcutaneous (s.c.), or intravenous (i.v.). Beyond what was reported here, this would demonstrate that peptoids can be carried through the circulation to reduce bacterial counts in remote tissues.

It is also suggested to pursue further the use of the cecal ligation and puncture (CLP) animal model of sepsis to evaluate the ability of peptoids to treat a polyclonal infection including both Gram-negative and Gram-positive strains. Much of the work presented herein was valuable for developing a procedure in which the controls worked properly (*i.e*. untreated animals had consistently high bacterial counts) and finding the right responses to measure. A 21 gauge needle should be used to puncture the cecum to ensure all animals are bacteremic, and bacterial counts in the peritoneal lavage fluid as well as blood and remote tissues (liver, lung) should be measured using dilutions as high as 10^{-8}.

Lastly, it would be informative to pursue different types of animal testing related to conditions including wound and burn healing as well as antifungal topical ointment. Many of the antimicrobial peptides in clinical trials have been developed for topical applications, including pexiganin and omiganan. Antimicrobial peptides have been shown to exhibit effects on both infectious disease as well as inflammatory conditions.

7.2 Lung surfactant protein mimics

7.2.1 *In vitro* formulation development

Formulating a concentrated synthetic surfactant preparation for use in the ovine model of nRDS proved to be a significant challenge that likely adversely impacted the study results. It is recommended that a comprehensive formulation development study be performed *in vitro* to ensure that surfactants used *in vivo* demonstrate favorable bulk properties amenable to easy spreading in the alveolar space. As discussed in **Chapter 6**, several factors should be evaluated, including composition of the synthetic lipid mixture, maximum possible concentration, and the benefit of excipients and spreading agents that could improve overall bulk properties. This work should be done in parallel with an *in vivo* study to determine what is the maximum concentration needed to obtain a positive outcome. For example, other biomimetic formulations

(Surfaxin® and Venticute®) have been used at lower concentrations (25 – 30 mg/mL) successfully in the premature lamb model. Peptoids were formulated at 25 mg/mL for the rat study in **Chapter 5** without difficulty. It would be useful to test if this concentration is sufficient to saturate a premature lung (perhaps using a rabbit model).

The work discussed in **Chapter 4** demonstrated that combinations of SP-B and SP-C mimics may act synergistically to improve surface activity *in vitro*. The results of using the same formulations *in vivo* suggest that in the physiological environment, the effects of these mimics were additive. There are several differences between the controlled, *in vitro* environment compared to the dynamic environment of intact physiology. One area that might play a significant role is the effective concentration of the surfactant-lipid mixture *in vivo.* While samples for *in vitro* testing on the pulsating bubble surfactometer are prepared at 1 mg/mL, the effective concentration of a surfactant bolus instilled into the alveolar space is more variable and, on average, likely lower. *In vitro* testing using the pulsating bubble surfactometer could be performed at lower concentrations to determine if synergistic interaction is evident. It would also be informative to test the $\mathbf{B}_{mono}/\mathbf{C}_{mono}$ formulation using other *in vitro* techniques, including Langmuir Wilhelmy surface balance and the captive bubble surfactometer to determine if synergy is apparent in other measures of surface activity.

7.2.2 *In vivo* studies

In this work, we have demonstrated the efficacy of peptoid-enhanced lung surfactant replacement in mitigating the symptoms of respiratory distress syndrome. These studies were performed with the most promising mimics of SP-B and SP-C that were developed at the time. Further development, particularly of the SP-C mimic, has resulted in peptoids that exhibit superior *in vitro* activity compared to the $\mathbf{B}_{mono}$ and $\mathbf{C}_{mono}$ used in this study[1]. Specifically, the non-alkylated and mono-alkylated mimics shown in **Figure 7.1** have been found to exhibit

equilibrium and maximum surface tensions very similar to those of natural surfactant (more so than the $\mathbf{B}_{mono}/\mathbf{C}_{mono}$ formulation)[1]. These mimics differ from mimics **C** and $\mathbf{C}_{mono}$ in that the hydrophobic helical region is composed of aliphatic *N*sdp side chains instead of aromatic *N*spe monomers. These mimics demonstrate significant potential and would be good candidates for future *in vivo* studies.

In addition to *in vivo* efficacy, there remain other questions related to their utility as pharmaceutical agents that have yet been unexplored. For example, two areas in which we currently have no data include the metabolic fate of peptoids as well as the kinetics of clearance. Longer term studies (beyond the 2 and 3 hour exposure periods used in this work), perhaps with a rodent animal model, may be well suited for tracking the peptoid in the urine or remote tissues.

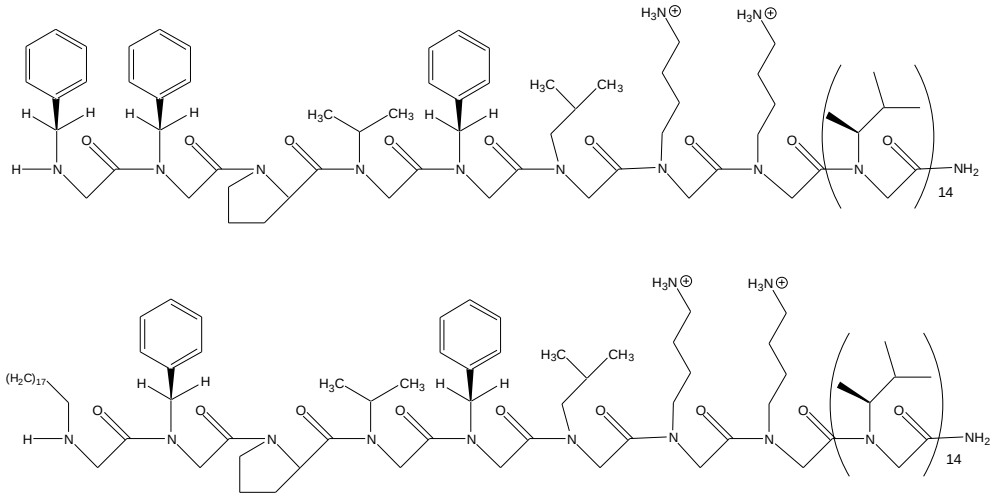

Figure 7.1: Chemical structures of non-alkylated (top) and mono-alkylated (bottom) mimics of SP-C[1].

7.3 Development of an antimicrobial lung surfactant replacement

Recently, there has been keen interest in capitalizing on the inherently therapeutic and surface-active nature of exogenous surfactant for pulmonary delivery of pharmaceuticals[240-247]. The extensive surface area and vascular network, thin permeable membrane, and reduced enzymatic activity of the alveolar network make it highly conducive to the absorption of many types of drugs[248], [249]. Moreover, the hydrophobic lipid bilayer in conjunction with the negative charge of anionic lipids solubilizes many types of drugs, increasing bioavailability[250, 251].

An area in which the use of exogenous surfactant as a drug carrier could be particularly advantageous is in the delivery of antimicrobial agents to the lungs. Pneumonia continues to be a significant health problem in ventilated intensive care unit patients[252, 253] who often exhibit symptoms of LS dysfunction[254]. Surfactant dysfunction can be acquired readily through pulmonary insults from both acute[255-257] and chronic[241, 258-260] conditions. Pneumonia is also closely tied, and perhaps causally related to surfactant dysfunction and ARDS[241, 261]. While the mechanistic basis of its function is not fully understood, there is mounting clinical and experimental evidence that treatment of pneumonia with exogenous surfactant is effective[241, 262].

There has been considerable interest in creating an innovative LS therapy that couples improved surface activity with the delivery of antibiotic therapy[242, 243, 245, 246, 263, 264]. An LS preparation that delivers potent and selective antimicrobial agents to the tiny airways in the lungs would not only restore surfactant functionality, but also directly treat sites of infection. Additionally, the large quantities of surfactant that are required for routine use in drug delivery necessitate that it be cost-effective and easy to produce[241].

In this work, we have shown that peptoids can be designed to emulate the function of both antimicrobial peptides and lung surfactant protein mimics. In the future, the merging of

these two research areas could result in the development of a peptoid-based antimicrobial lung surfactant replacement.

7.4 Structural implications of diastereomeric peptoids

In **Chapter 2** we reported two molecules **1**-*N*rpe$_{2,5,8,11}$ and **1**-*N*rpe$_{3,6,9,12}$, that, in the presence of lipid SUVs, exhibited CD spectrum distinctly different from that of the canonical, aromatic peptoid helix (**Figure 2.7B,C**). While this did not significantly affect their activity or cell selectivity, this was an unexpected structural curiosity that warrants further investigation. It would be interesting to build a library of diasteriomers with different numbers / arrangements of *N*rpe and *N*spe and evaluate their resultant CD spectra. This may provide insight into the secondary structure for **1**-*N*rpe$_{2,5,8,11}$ and **1**-*N*rpe$_{3,6,9,12}$ and related compounds.

References

1. Brown, N.J. in Department of Chemical and Biological Engineering, Vol. Ph.D., Chemical Engineering (Northwestern University, Evanston; 2008).

2. Pringle, K.C. Human fetal lung development and related animal models. *Clinical Obstetrics and Gynecology* **29**, 502-513 (1986).

3. Zuckermann, R.N., Kerr, J.M., Kent, S.B.H. & Moos, W.H. Efficient method for the preparation of peptoids [oligo(*N*-substituted glycines)] by submonomer solid-phase synthesis. *J. Am. Chem. Soc.* **114**, 10646-10647 (1992).

4. Daniels, D.S., Petersson, E.J., Qiu, J.X. & Schepartz, A. High-resolution structure of a beta-peptide bundle. *J. Am. Chem. Soc.* **129**, 1532-1533 (2007).

5. Horne, W.S., Price, J.L., Keck, J.L. & Gellman, S.H. Helix bundle quaternary structure from alpha/beta-peptide foldamers. *J. Am. Chem. Soc.* **129**, 4178-4179 (2007).

6. Creuwels, L., vanGolde, L.M.G. & Haagsman, H.P. The pulmonary surfactant system: Biochemical and clinical aspects. *Lung* **175**, 1-39 (1997).

7. Kotch, F.W. & Raines, R.T. Self-assembly of synthetic collagen triple helices. *Proc. Natl. Acad. Sci. U.S.A.* **103**, 3028-3033 (2006).

8. Dohm, M.T. in Department of Chemistry, Vol. Ph.D., Chemistry (Northwestern University, Evanston; 2008).

9. Perez-Gil, J. Molecular interactions in pulmonary surfactant films. *Biol. Neonate* **81**, 6-15 (2002).

10. Dill, K.A. Dominant forces in protein folding. *Biochemistry* **29**, 7133-7155 (1990).

11. Kirshenbaum, K. et al. Sequence-specific polypeptoids: A diverse family of heteropolymers with stable secondary structure. *Proc. Natl. Acad. Sci. U.S.A.* **95**, 4303-4308 (1998).

12. Hayen, A., Schmitt, M.A., Ngassa, F.N., Thomasson, K.A. & Gellman, S.H. Two helical conformations from a single foldamer backbone: "Split personality" in short alpha/beta-peptides. *Agnew. Chem. Int. Ed.* **43**, 505-510 (2004).

13. Seebach, D., Hook, D.F. & Glattli, A. Helices and other secondary structures of beta- and gamma-peptides. *Biopolymers* **84**, 23-37 (2006).

14. Simon, R.J. et al. Peptoids - a modular approach to drug discovery. *Proc. Natl. Acad. Sci. U.S.A.* **89**, 9367-9371 (1992).

15. Arnt, L. & Tew, G.N. Cationic facially amphiphilic poly(phenylene ethynylene)s studied at the air-water interface. *Langmuir* **19**, 2404-2408 (2003).

16. Semetey, V. et al. Stable helical secondary structure in short-chain N,N '-linked oligoureas bearing proteinogenic side chains. *Agnew. Chem. Int. Ed.* **41**, 1893-+ (2002).

17. Goodman, C.M., Choi, S., Shandler, S. & DeGrado, W.F. Foldamers as versatile frameworks for the design and evolution of function. *Nat. Chem. Biol.* **3**, 252-262 (2007).

18. Kimmerlin, T. & Seebach, D. '100 years of peptide synthesis': ligation methods for peptide and protein synthesis with applications to beta-peptide assemblies. *J. Peptide Res.* **65**, 229-260 (2005).

19. Pavone, V. et al. Beta-alanine containing cyclic-peptides with turned structure - the pseudo-type-II beta-turn.6. *Biopolymers* **34**, 1517-1526 (1994).

20. Frackenpohl, J., Arvidsson, P.I., Schreiber, J.V. & Seebach, D. The outstanding biological stability of beta- and gamma-peptides toward proteolytic enzymes: An in vitro investigation with fifteen peptidases. *Chembiochem* **2**, 445-455 (2001).

21. Miller, S.M. et al. Comparison of the proteolytic susceptibilites of homologous L-amino-acid, D-amino-acid, and N-substituted glycine peptide and peptoid oligomers. *Drug Dev. Res.* **35**, 20-32 (1995).

22. Gibbons, J.A. et al. Pharmacologic characterization of CHIR 2279, an N-substituted glycine peptoid with high-affinity binding for alpha(1)-adrenoceptors. *J. Pharmacol. Exp. Ther.* **277**, 885-899 (1996).

23. Seebach, D. et al. Biological and pharmacokinetic studies with beta-peptides. *Chimia* **52**, 734-739 (1998).

24. Merrifield, R.B. Solid phase peptide synthesis.1. Synthesis of a tetrapeptide. *J. Am. Chem. Soc.* **85**, 2149 (1963).

25. Kemp, D.S., Leung, S.L. & Kerkman, D.J. Models that demonstrate peptide-bond formation by prior thiol capture. 1. Capture by disulfide formation. *Tetrahedron Lett.* **22**, 181-184 (1981).

26. Dawson, P.E. & Kent, S.B.H. Synthesis of native proteins by chemical ligation. *Annu. Rev. Biochem.* **69**, 923-960 (2000).

27. Murray, J.K. et al. Efficient synthesis of a beta-peptide combinatorial library with microwave irradiation. *J. Am. Chem. Soc.* **127**, 13271-13280 (2005).

28. Murphy, J.E. et al. A combinatorial approach to the discovery of efficient cationic peptoid reagents for gene delivery. *Proc. Natl. Acad. Sci. U.S.A.* **95**, 1517-1522 (1998).

29. Alluri, P.G., Reddy, M.M., Bachhawat-Sikder, K., Olivos, H.J. & Kodakek, T. Isolation of protein ligands from large peptoid libraries. *J. Am. Chem. Soc.* **125**, 13995-14004 (2003).

30. Kruijtzer, J.A.W., Hofmeyer, L.J.F., Heerma, W., Versluis, C. & Liskamp, R.M.J. Solid-phase syntheses of peptoids using Fmoc-protected N-substituted glycines: The synthesis of (retro) peptoids of Leu-enkephalin and substance P. *Chem.-A Euro. J.* **4**, 1570-1580 (1998).

31. Patch, J.A. & Barron, A.E. Helical peptoid mimics of magainin-2 amide. *J. Am. Chem. Soc.* **125**, 12092-12093 (2003).

32. Chongsiriwatana, N.P. et al. Peptoids that mimic the structure, function, and mechanism of helical antimicrobial peptides. *Proc. Natl. Acad. Sci. U.S.A.* **105**, 2794-2799 (2008).

33. Kritzer, J.A., Stephens, O.M., Guarracino, D.A., Reznik, S.K. & Schepartz, A. beta-Peptides as inhibitors of protein-protein interactions. *Bioorg. Med. Chem.* **13**, 11-16 (2005).

34. Murray, J.K. & Gellman, S.H. Targeting protein-protein interactions: Lessons from p53/MDM2. *Biopolymers* **88**, 657-686 (2007).

35. Hara, T., Durell, S.R., Myers, M.C. & Appella, D.H. Probing the structural requirements of peptoids that inhibit HDM2-p53 interactions. *J. Am. Chem. Soc.* **128**, 1995-2004 (2006).

36. Seurynck, S.L., Patch, J.A. & Barron, A.E. Simple, helical peptoid analogs of lung surfactant protein B. *Chem. Biol.* **12**, 77-88 (2005).

37. Wu, C.W., Seurynck, S.L., Lee, K.Y.C. & Barron, A.E. Helical peptoid mimics of lung surfactant protein C. *Chem. Biol.* **10**, 1057-1063 (2003).

38. Yoshida, M., Langer, R., Lendlein, A. & Lahann, J. From advanced biomedical coatings to multi-functionalized biomaterials. *Polymer Rev.* **46**, 347-375 (2006).

39. Huang, K. et al. A threaded loop conformation adopted by a family of peptoid nonamers. *J. Am. Chem. Soc.* **128**, 1733-1738 (2006).

40. Shin, S.B.Y., Yoo, B., Todaro, L.J. & Kirshenbaum, K. Cyclic peptoids. *J. Am. Chem. Soc.* **129**, 3218-3225 (2007).

41. Petersson, E.J., Craig, C.J., Daniels, D.S., Qiu, J.X. & Schepartz, A. Biophysical characterization of a beta-peptide bundle: Comparison to natural proteins. *J. Am. Chem. Soc.* **129**, 5344-5345 (2007).

42. Price, J.L., Horne, W.S. & Gellman, S.H. Discrete heterogeneous quaternary structure formed by alpha/beta-peptide foldamers and alpha-peptides. *J. Am. Chem. Soc.* **129**, 6376-6377 (2007).

43. Lelais, G. et al. beta-Peptidic secondary structures fortified and enforced by Zn2+ complexation - On the way to beta-peptidic zinc fingers? *Helv. Chim. Acta* **89**, 361-403 (2006).

44. Burkoth, T.S. et al. Toward the synthesis of artificial proteins: The discovery of an amphiphilic helical peptoid assembly. *Chem. Biol.* **9**, 647-654 (2002).

45. Lee, B.C., Zuckermann, R.N. & Dill, K.A. Folding a nonbiological polymer into a compact multihelical structure. *J. Am. Chem. Soc.* **127**, 10999-11009 (2005).

46. Brown, N.J., Wu, C.W., Seurynck-Servoss, S.L. & Barron, A.E. Effects of hydrophobic helix length and side chain chemistry on biomimicry in peptoid analogues of SP-C. *Biochemistry* **47**, 1808-1818 (2008).

47. Seurynck-Servoss, S.L., Dohm, M.T. & Barron, A.E. Effects of including an N-terminal insertion region and arginine-mimetic side chains in helical peptoid analogues of lung surfactant protein B. *Biochemistry* **45**, 11809-11818 (2006).

48. Chan, M. in The World Health Report (World Health Organization, Geneva; 2007).

49. Leeb, M. Antibiotics: A shot in the arm. *Nature* **431**, 892-893 (2004).

50. Hancock, R.E.W. Peptide antibiotics. *Lancet* **349**, 418-422 (1997).

51. Hancock, R.E.W. & Lehrer, R. Cationic peptides: a new source of antibiotics. *Trends in Biotechnology* **16**, 82-88 (1998).

52. Hancock, R.E.W. & Sahl, H.G. Antimicrobial and host-defense peptides as new anti-infective therapeutic strategies. *Nat. Biotechnol.* **24**, 1551-1557 (2006).

53. Jenssen, H., Hamill, P. & Hancock, R.E.W. Peptide antimicrobial agents. *Clin. Microbiol. Rev.* **19**, 491-511 (2006).

54. Schriever, C.A., Fernandez, C., Rodvold, K.A. & Danziger, L.H. Daptomycin: A novel cyclic lipopeptide antimicrobial. *Am. J. Health. Syst. Pharm.* **62**, 1145-1158 (2005).

55. Armand, P. et al. Chiral *N*-substituted glycines can form stable helical conformations. *Fold. Des.* **2**, 369-375 (1997).

56. Wu, C.W. et al. Structural and spectroscopic studies of peptoid oligomers with alpha-chiral aliphatic side chains. *J. Am. Chem. Soc.* **125**, 13525-13530 (2003).

57. Wu, C.W., Sanborn, T.J., Huang, K., Zuckermann, R.N. & Barron, A.E. Peptoid oligomers with alpha-chiral, aromatic side chains: Sequence requirements for the formation of stable peptoid helices. *J. Am. Chem. Soc.* **123**, 6778-6784 (2001).

58. Miller, S.M. et al. Proteolytic studies of homologous peptide and N-substituted glycine peptoid oligomers. *Bioorganic & Medicinal Chemistry Letters* **4**, 2657-2662 (1994).

59. Zasloff, M. Magainins, a class of antimicrobial peptides from xenopus skin--isolation, characterization of two active forms and partial CDNA sequence of a precursor. *Proc. Natl. Acad. Sci. U.S.A.* **84**, 5449-5453 (1987).

60. Jiang, Z. & Hodges, R.S. Effects of net charge and the number of positively charged residues on the biological activity of amphipathic-helical cationic antimicrobial peptides. *Biopolymers* **88**, 615-615 (2007).

61. Barbin, A., Peypoux, F. & Michel, G. Phospholipid composition in thermosensitive mutants of escherichia-coli K-12. *Biochim. Et Biophy. Acta* **431**, 416-425 (1976).

62. Opdenkamp, J.A.F. Lipid asymmetry in membranes. *Annu. Rev. Biochem.* **48**, 47-71 (1979).

63. Dathe, M. & Wieprecht, T. Structural features of helical antimicrobial peptides: their potential to modulate activity on model membranes and biological cells. *Biochimica Et Biophysica Acta-Biomembranes* **1462**, 71-87 (1999).

64. Blondelle, S.E. & Houghten, R.A. Design of model amphipathic peptides having potent antimicrobial activities. *Biochemistry* **31**, 12688-12694 (1992).

65. Chen, Y.X. et al. Rational design of alpha-helical antimicrobial peptides with enhanced activities and specificity/therapeutic index. *J. Biol. Chem.* **280**, 12316-12329 (2005).

66. Shai, Y. Mode of action of membrane active antimicrobial peptides. *Biopolymers* **66**, 236-248 (2002).

67. Shai, Y. & Oren, Z. From "carpet" mechanism to de-novo designed diastereomeric cell-selective antimicrobial peptides. *Peptides* **22**, 1629-1641 (2001).

68. Bessalle, R., Haas, H., Goria, A., Shalit, I. & Fridkin, M. Augmentation of the antimicrobial activity of magainin by positive-charge extension. *Antimicrob. Agents Chemother.* **36**, 313-317 (1992).

69. Frecer, V. QSAR analysis of antimicrobial and haemolytic effects of cyclic cationic antimicrobial peptides derived from protegrin-1. *Bioorganic & Medicinal Chemistry* **14**, 6065-6074 (2006).

70. Bessalle, R. et al. Structure-function studies of amphiphilic antibacterial peptides. *J. Med. Chem.* **36**, 1203-1209 (1993).

71. Ge, Y.G. et al. In vitro antibacterial properties of pexiganan, an analog of magainin. *Antimicrob. Agents Chemother.* **43**, 782-788 (1999).

72. Giacometti, A. et al. In vitro activity of MSI-78 alone and in combination with antibiotics against bacteria responsible for bloodstream infections in neutropenic patients. *Int. J. Antimicrob. Agents* **26**, 235-240 (2005).

73. Giacometti, A. et al. Therapeutic efficacy of the magainin analogue MSI-78 in different intra-abdominal sepsis rat models. *J. Antimicrob. Chemother.* **54**, 654-660 (2004).

74. Dodge, J.T. & Phillips, G.B. Composition of phospholipids and of phospholipid fatty acids and aldehydes in human red cells. *J. Lipid Res.* **8**, 667-675 (1967).

75. Kruijff, B.D., Killian, J.A., Rietveld, A.G. & Kusters, R. Lipid Polymorphism and Membrane Properties, Vol. 44. (Academic Press, London; 1997).

76. Zhang, L.J., Benz, R. & Hancock, R.E.W. Influence of proline residues on the antibacterial and synergistic activities of alpha-helical peptides. *Biochemistry* **38**, 8102-8111 (1999).

77. Pag, U. et al. In vitro activity and mode of action of diastereomeric antimicrobial peptides against bacterial clinical isolates. *J. Antimicrob. Chemother.* **53**, 230-239 (2004).

78. Tew, G.N., Clements, D., Tang, H.Z., Arnt, L. & Scott, R.W. Antimicrobial activity of an abiotic host defense peptide mimic. *Biochim. Biophys. Acta-Biomembranes* **1758**, 1387-1392 (2006).

79. Owen, J.S., Bruckdorfer, K.R., Day, R.C. & McIntyre, N. Decreased erythrocyte-membrane fluidity and altered lipid composition in human liver disease. *J. Lipid Res.* **23**, 124-132 (1982).

80. Calleros, L., Lasa, M., Toro, M.J. & Chiloeches, A. Low cell cholesterol levels increase NF kappa B activity through a p38 MAPK-dependent mechanism. *Cellular Signalling* **18**, 2292-2301 (2006).

81. Eisenstein, B.I. Treatment of staphylococcal infections with cyclic lipopeptides. *Clin. Microbiol. Infect.* **14**, 10-16 (2008).

82. Tachi, T., Epand, R.F., Epand, R.M. & Matsuzaki, K. Position-dependent hydrophobicity of the antimicrobial magainin peptide affects the mode of peptide-lipid interactions and selective toxicity. *Biochemistry* **41**, 10723-10731 (2002).

83. Krapcho, A.P. & Kuell, C.S. Mono-protected diamines. N-tert-butylcarbony-alpha-omega-alkanediamines from alpha,omega-alkanediamines. *Synthetic Comm.* **20**, 2559-2564 (1990).

84. Spellberg, B., Powers, J.H., Brass, E.P., Miller, L.G. & Edwards, J.E. Trends in antimicrobial drug development: Implications for the future. *Clin. Infect. Dis.* **38**, 1279-1286 (2004).

85. Jacobs, M.R. Retapamulin: a semisynthetic pleuromutilin compound for topical treatment of skin infections in adults and children. *Fut. Microbiol.* **2**, 591-600 (2007).

86. Projan, S.J. Why is big Pharma getting out of antibacterial drug discovery? *Curr. Opin. in Microbiol.* **6**, 427-430 (2003).

87. Overbye, K.M. & Barrett, J.F. Antibiotics: where did we go wrong. *Drug Discov. Today* **10**, 45-52 (2005).

88. Chen, H.Q. et al. Recent advances in the research and development of human defensins. *Peptides* **27**, 931-940 (2006).

89. Zasloff, M. Antimicrobial peptides of multicellular organisms. *Nature* **415**, 389-395 (2002).

90. Zhang, L.J. & Falla, T.J. Antimicrobial peptides: therapeutic potential. *Expert Opin. Pharmacother.* **7**, 653-663 (2006).

91. Rosenfeld, Y. & Shai, Y. Lipopolysaccharide (Endotoxin)-host defense antibacterial peptides interactions: Role in bacterial resistance and prevention of sepsis. *Biochim. Biophys. Acta-Biomembranes* **1758**, 1513-1522 (2006).

92. Perron, G.G., Zasloff, M. & Bell, G. Experimental evolution of resistance to an antimicrobial peptide. *Proc. R. Soc. B Biol. Sci.* **273**, 251-256 (2006).

93. Peschel, A. & Sahl, H.G. The co-evolution of host cationic antimicrobial peptides and microbial resistance. *Nat. Rev. Microbiol.* **4**, 529-536 (2006).

94. Livermore, D.M. The need for new antibiotics. *Clin. Microbiol. Infect.* **10**, 1-9 (2004).

95. Alexander, C. & Rietschel, E.T. Bacterial lipopolysaccharides and innate immunity. *J. Endotox. Res.* **7**, 167-202 (2001).

96. Bowdish, D.M.E. & Hancock, R.E.W. Anti-endotoxin properties of cationic host defence peptides and proteins. *J. Endotox. Res.* **11**, 230-236 (2005).

97. Hancock, R.E.W. Alterations in outer-membrane permeability. *Ann. Rev. Microbiol.* **38**, 237-264 (1984).

98. Hancock, R.E.W., Raffle, V.J. & Nicas, T.I. Involvement of the outer-membrane in gentamicin and strptomycin uptake and killing in *Pseudomonas aeruginosa*. *Antimicrob. Agents Chemother.* **19**, 777-785 (1981).

99. Moore, R.A., Bates, N.C. & Hancock, R.E.W. Interaction of polycationic antibiotics with *Pseudomonas aeruginosa* lipopolysaccharide and lipid-A studied by using dansyl-polymyxin. *Antimicrob. Agents Chemother.* **29**, 496-500 (1986).

100. Fidai, S., Farmer, S.W. & Hancock, R.E.W. in Methods in Molecular Biology, Vol. 78. (ed. W.M. Shafer) 187-204 (Humana Press, Inc., 1997).

101. Braunstein, A., Papo, N. & Shai, Y. In vitro activity and potency of an intravenously injected antimicrobial peptide and its DL amino acid analog in mice infected with bacteria. *Antimicrob. Agents Chemother.* **48**, 3127-3129 (2004).

102. Scott, M.G. et al. An anti-infective peptide that selectively modulates the innate immune response. *Nat. Biotechnol.* **25**, 465-472 (2007).

103. Fritsche, T.R., Rhomberg, P.R., Sader, H.S. & Jones, R.N. In vitro activity of omiganan pentahydrochloride tested against vancomycin-tolerant, -intermediate, and -resistant *Staphylococcus aureus*. *Diagn. Microbiol. Infect. Dis.* **60**, 399-403 (2008).

104. Fritsche, T.R., Rhomberg, P.R., Sader, H.S. & Jones, R.N. Antimicrobial activity of omiganan pentahydrochloride tested against contemporary bacterial pathogens commonly responsible for catheter-associated infections. *J. Antimicrob. Chemother.* **61**, 1092-1098 (2008).

105. Bowdish, D.M.E. et al. Impact of LL-37 on anti-infective immunity. *J. Leukoc. Biol.* **77**, 451-459 (2005).

106. Falla, T.J., Karunaratne, D.N. & Hancock, R.E.W. Mode of action of the antimicrobial peptide indolicidin. *J. Biol. Chem.* **271**, 19298-19303 (1996).

107. Kaur, K.J., Sarkar, P., Nagpal, S., Khan, T. & Salunke, D.M. Structure-function analyses involving palindromic analogs of tritrypticin suggest autonomy of anti-endotoxin and antibacterial activities. *Protein Sci.* **17**, 545-554 (2008).

108. Kirikae, T. et al. Protective effects of a human 18-kilodalton cationic antimicrobial protein (CAP18)-derived peptide against murine endotoxemia. *Infect. Immun.* **66**, 1861-1868 (1998).

109. Nahra, R. & Dellinger, R.P. Targeting the lipopolysaccharides: still a matter of debate? *Curr. Opin. Anaesthesiol.* **21**, 98-104 (2008).

110. Nemoto, H. et al. Newly developed immobilized polymyxin B fibers improve the survival of patients with sepsis. *Blood Purif.* **19**, 361-368 (2001).

111. Parker, S.J. & Watkins, P.E. Experimental models of Gram-negative sepsis. *Brit. J. Surg.* **88**, 22-30 (2001).

112. Buras, J.A., Holzmann, B. & Sitkovsky, M. Animal models of sepsis: Setting the stage. *Nat. Rev. Drug Disc.* **4**, 854-865 (2005).

113. Wichterman, K.A., Baue, A.E. & Chaudry, I.H. Sepsis and septic shock -- a review of laboratory models and a proposal. *J. Surgical Res.* **29**, 189-201 (1980).

114. Goodson, B. et al. Characterization of novel antimicrobial peptoids. *Antimicrob. Agents Chemother.* **43**, 1429-1434 (1999).

115. Radzishevsky, I.S. et al. Improved antimicrobial peptides based on acyl-lysine oligomers. *Nat. Biotechnol.* **25**, 657-659 (2007).

116. Wu, M.H. & Hancock, R.E.W. Improved derivatives of bactenecin, a cyclic dodecameric antimicrobial cationic peptide. *Antimicrob. Agents Chemother.* **43**, 1274-1276 (1999).

117. Hilpert, K., Volkmer-Engert, R., Walter, T. & Hancock, R.E.W. High-throughput generation of small antibacterial peptides with improved activity. *Nat. Biotechnol.* **23**, 1008-1012 (2005).

118. Bellido, F., Pechere, J.C. & Hancock, R.E.W. Re-evaluation of the factors involved in the efficacy of new beta-lactams against *Enterobacter-cloacae*. *Antimicrob. Agents Chemother.* **35**, 73-78 (1991).

119. Salunkhe, P. et al. A cystic fibrosis epidemic strain of *Pseudomonas aeruginosa* displays enhanced virulence and antimicrobial resistance. *J. Bacteriol.* **187**, 4908-4920 (2005).

120. Lewis, J.E. & Veldhuizen, R. The role of exogenous surfactant in the treatment of acute lung injury. *Annu. Rev. Physiol.* **65**, 613-642 (2003).

121. Possmayer, F., Yu, S.H., Weber, J.M. & Harding, P.G.R. Pulmonary Surfactant. *Canadian J. Biochem. Cell Biol.* **62**, 1121-1133 (1984).

122. Poynter, S.E. & LeVine, A.M. Surfactant biology and clinical application. *Crit. Care Clinics* **19**, 459-472 (2003).

123. Veldhuizen, R., Nag, K., Orgeig, S. & Possmayer, F. The role of lipids in pulmonary surfactant. *Biochim. Et Biophys. Acta-Molecular Basis of Disease* **1408**, 90-108 (1998).

124. Notter, R.H. Lung Surfactants: Basic Science and Clinical Applications, Vol. 149. (Marcel Dekker, Inc., New York; 2000).

125. McLean, L.R. & Lewis, J.E. Biomimetic Pulmonary Surfactants. *Life Sci.* **56**, 363-378 (1995).

126. Notter, R.H. & Wang, Z.D. Pulmonary surfactant: Physical chemistry, physiology, and replacement. *Rev. Chem. Eng.* **13**, 1-118 (1997).

127. Goerke, J. Pulmonary surfactants - physicochemical aspects. *Curr. Opinion Coll. Interface Sci* **2**, 526-530 (1997).

128. Hall, S.B., Venkitaraman, A.R., Whitsett, J.A., Holm, B.A. & Notter, R.H. Importance of hydrophobic apoproteins as constituents of clinical exogenous surfactants. *Am. Rev. Respiratory Dis.* **145**, 24-30 (1992).

129. Wang, Z.D., Hall, S.B. & Notter, R.H. Roles of different hydrophobic constituents in the adsorption of pulmonary surfactant. *J. Lipid Res.* **37**, 790-798 (1996).

130. Johansson, J., Curstedt, T. & Jornvall, H. Surfactant protein B -- disulfide bridges, structural-properties, and kringle similarities. *Biochemistry* **30**, 6917-6921 (1991).

131. Beck, D.C. et al. The role of homodimers in surfactant protein B function *in vivo*. *J. Biolog. Chem.* **275**, 3365-3370 (2000).

132. Nogee, L.M. Alterations in SP-B and SP-C expression in neonatal lung disease. *Annu. Rev. Physiol.* **66**, 601-623 (2004).

133. Wustneck, N., Wustneck, R., Perez-Gil, J. & Pison, U. Effects of oligomerization and secondary structure on the surface behavior of pulmonary surfactant proteins SP-B and SP-C. *Biophys. J.* **84**, 1940-1949 (2003).

134. Gordon, L.M. et al. Conformation and molecular topography of the N-terminal segment of surfactant protein B in structure-promoting environments. *Protein Science* **5**, 1662-1675 (1996).

135. Krol, S., Janshoff, A., Ross, M. & Galla, H.J. Structure and function of surfactant protein B and C in lipid monolayers: a scanning force microscopy study. *Phys.Chem. Chem. Phys.* **2**, 4586-4593 (2000).

136. Oosterlaken-Dijksterhuis, M.A., Haagsman, H.P., Vangolde, L.M.G. & Demel, R.A. Characterization of lipid insertion into monomolecular layers mediated by lung surfactant proteins SP-B and SP-C. *Biochemistry* **30**, 10965-10971 (1991).

137. Plasencia, I., Rivas, L., Keough, K.M.W., Marsh, D. & Perez-Gil, J. The *N*-terminal segment of pulmonary surfactant lipopeptide SP-C has intrinsic propensity to interact with and perturb phospholipid bilayers. *Biochem. J.* **377**, 183-193 (2004).

138. Qanbar, R., Cheng, S., Possmayer, F. & Schurch, S. Role of the palmitoylation of surfactant-associated protein C in surfactant film formation and stability. *Am. J. Phys.-Lung Cell. Mol. Phys.* **271**, L572-L580 (1996).

139. Taneva, S. & Keough, K.M.W. Pulmonary surfactant proteins SP-B and SP-C in spread monolayers at the air-water-interface .3. Proteins SP-B plus SP-C with phospholipids in spread monolayers. *Biophys. J.* **66**, 1158-1166 (1994).

140. Avery, M.E. & Mead, J. Surface properties in relation to atelectasis and hyaline membrane disease. *Ama J. Dis. Children* **97**, 517-523 (1959).

141. Taeusch, H.W., Ballard, R.A. & Avery, M.E. Diseases of the Newborn. (Saunders, Philadelphia; 1991).

142. Suresh, G.K. & Soll, R.F. Exogenous surfactant therapy in newborn infants. *Annal. Acad. Med. Singapore* **32**, 335-345 (2003).

143. Hallman, M., Glumoff, V. & Ramet, M. Surfactant in respiratory distress syndrome and lung injury. *Comparative Biochem. Physiol. A-Molecular Integrative Physiol.* **129**, 287-294 (2001).

144. Walti, H. & Monset-Couchard, M. A risk-benefit assessment of natural and synthetic exogenous surfactants in the management of neonatal respiratory distress syndrome. *Drug Safety* **18**, 321-337 (1998).

145. Gunther, A. et al. Surfactant alteration and replacement in acute respiratory distress syndrome. *Respir. Res.* **2**, 353-U352 (2001).

146. Spragg, R.G. et al. Treatment of acute respiratory distress syndrome with recombinant surfactant protein C surfactant. *Am. J. Respir. Crit. Care Med.* **167**, 1562-1566 (2003).

147. Taeusch, H.W., de la Serna, J.B., Perez-Gil, J., Alonso, C. & Zasadzinski, J.A. Inactivation of pulmonary surfactant due to serum-inhibited adsorption and reversal by hydrophilic polymers: Experimental. *Biophys. J.* **89**, 1769-1779 (2005).

148. Zasadzinski, J.A. et al. Inhibition of pulmonary surfactant adsorption by serum and the mechanisms of reversal by hydrophilic polymers: Theory. *Biophys. J.* **89**, 1621-1629 (2005).

149. Gunther, A. et al. Bronchoscopic administration of bovine natural surfactant in ARDS and septic shock: impact on biophysical and biochemical surfactant properties. *Euro. Respir. J.* **19**, 797-804 (2002).

150. Lachmann, B. & Gommers, D. Is it rational to treat pneumonia with exogenous surfactant? *Euro. Respir. J.* **6**, 1427-1428 (1993).

151. Walther, F.J., Gordon, L.M., Zasadzinski, J.A., Sherman, M.A. & Waring, A.J. Surfactant protein B and C analogues. *Molecular Genetics and Metabolism* **71**, 342-351 (2000).

152. Borman, S. Peptoids eyed for gene therapy applications. *Chem. Eng. News* **76**, 56-57 (1998).

153. Barron, A.E. & Zuckermann, R.N. Bioinspired polymeric materials: in-between proteins and plastics. *Curr. Opin. Chem. Biol.* **3**, 681-687 (1999).

154. Gellman, S.H. Foldamers: A manifesto. *Accounts Chem. Res.* **31**, 173-180 (1998).

155. Kirshenbaum, K., Zuckermann, R.N. & Dill, K.A. Designing polymers that mimic biomolecules. *Curr. Opin. Struct. Biol.* **9**, 530-535 (1999).

156. Soth, M.J. & Nowick, J.S. Unnatural oligomers and unnatural oligomer libraries. *Curr. Opin. Chem. Biol.* **1**, 120-129 (1997).

157. Bruni, R., Taeusch, H.W. & Waring, A.J. Surfactant protein-B -- lipid interactions of synthetic peptides representing the amino-terminal amphipathic domain. *Proc. Natl. Acad. Sci. U.S.A.* **88**, 7451-7455 (1991).

158. Longo, M.L., Bisagno, A.M., Zasadzinski, J.A.N., Bruni, R. & Waring, A.J. A function of lug surfactant protein SP-B. *Science* **261**, 453-456 (1993).

159. Waring, A. et al. Synthetic amphipathic sequences of surfactant protein B mimic several physicochemical and in vivo properties of native pulmonary surfactant proteins. *Peptide Research* **2**, 308-313 (1989).

160. Kaznessis, Y.N., Kim, S. & Larson, R.G. Specific mode of interaction between components of model pulmonary surfactants using computer simulations. *Journal of Molecular Biology* **322**, 569-582 (2002).

161. Enhorning, G. Pulsating bubble technique for evaluating pulmonary surfactant. *J. Appl. Physiol.* **43**, 198-203 (1977).

162. Veldhuizen, E.J.A. & Haagsman, H.P. Role of pulmonary surfactant components in surface film formation and dynamics. *Biochim. Et Biophys. Acta-Biomembranes* **1467**, 255-270 (2000).

163. Seurynck, S.L. et al. Optical monitoring of bubble size and shape in a pulsating bubble surfactometer. *J. App. Physiol.* **99**, 624-633 (2005).

164. Seurynck-Servoss, S.L., Brown, N.J., Dohm, M.T., Wu, C.W. & Barron, A.E. Lipid composition greatly affects the in vitro surface activity of lung surfactant protein mimics. *Colloids and Surfaces B-Biointerfaces* **57**, 37-55 (2007).

165. Scarpelli, E.M., David, E., Cordova, M. & Mautone, A.J. Surface tension of therapeutic surfactants (Exosurf neonatal, Infasurf, and Survanta) as evaluated by standard methods and criteria. *Am. J. Perinatol.* **9**, 414-419 (1992).

166. Johansson, J. et al. Canine hydrophobic surfactant polypeptide SP-C -- a lipopeptide with one thioester-linked palmitoyl group. *FEBS Letters* **281**, 119-122 (1991).

167. Curstedt, T. et al. Hydrophobic surfactant-associated polypeptides -- SP-C is a lipopeptide with 2 palmitoylated cystein residues, whereas SP-B lacks covalently linked fatty acyl groups. *Proc. Natl. Acad. Sci. U.S.A.* **87**, 2985-2989 (1990).

168. Johansson, J., Curstedt, T., Robertson, B. & Jornvall, H. Size and structure of the hydrophobic low-molecular weight surfactant-associated polypeptide. *Biochemistry* **27**, 3544-3547 (1988).

169. Keough, K.M.W. Physicochemical properties of surfactant lipids. *Biochem. Soc. Trans.* **13**, 1081-1084 (1985).

170. Vandenbussche, G. et al. Structure and orientation of the surfactant-associated protein C in a lipid bilayer. *Euro. J. Biochem.* **203**, 201-209 (1992).

171. Wang, Z.D., Gurel, O., Baatz, J.E. & Notter, R.H. Differential activity and lack of synergy of lung surfactant proteins SP-B and SP-C in interactions with phospholipids. *Journal of Lipid Research* **37**, 1749-1760 (1996).

172. Curstedt, T., Jornvall, H., Robertson, B., Bergman, T. & Berggren, P. 2 hydrophobic low molecular mass protein fractions of pulmonary surfactant -- characterization and biophysical activity. *European Journal of Biochemistry* **168**, 255-262 (1987).

173. Horowitz, A.D., Moussavian, B. & Whitsett, J.A. Roles of SP-A, SP-B, and SP-C in modulation of lipid uptake by pulmonary epithelial cells in vitro. *Am.J. Physiol.-Lung Cellular and Molecular Physiology* **270**, L69-L79 (1996).

174. Rice, W.R. et al. Surfactant peptides stimulate uptake of phosphatidylcholine by isolated cells. *Biochim. Biophys. Acta* **1006**, 237-245 (1989).

175. Poulain, F.R., Allen, L., Williams, M.C., Hamilton, R.L. & Hawgood, S. Effects of surfactant apolipoproteins on liposome sturcture - implications for tubular myelin formation. *Am. J. Physiol.* **262**, L730-L739 (1992).

176. Itoh, H., Nishino, M. & Hatabu, H. Architecture of the lung - Morphology and function. *J. Thoraic Imaging* **19**, 221-227 (2004).

177. Prange, H.D. Laplace's law and the alveolus: A misconception of anatomy and a misapplication of physics. *Adv. Physiol. Ed.* **27**, 34-40 (2003).

178. Willson, D.F., Chess, P.R. & Notter, R.H. Surfactant for pediatric acute lung injury. *Pediatr. Clin. N. Am.* **55**, 545-575 (2008).

179. Halliday, H.L. Surfactants: past, present and future. *J. Perinatol.* **28**, S47-S56 (2008).

180. Frerking, I., Gunther, A., Seeger, W. & Pison, U. Pulmonary surfactant: functions, abnormalities and therapeutic options. *Intensive Care Med.* **27**, 1699-1717 (2001).

181. Sanborn, T.J., Wu, C.W., Zuckerman, R.N. & Barron, A.E. Extreme stability of helices formed by water-soluble poly-N-substituted glycines (polypeptoids) with alpha-chiral side chains. *Biopolymers* **63**, 12-20 (2002).

182. Borman, S. Peptoids eyed for gene therapy applications. *Chem. & Eng. News* **76**, 56-57 (1998).

183. Czyzewski, A.M. in Chemical and Biological Engineering, Vol. Ph.D. (Northwestern University, Evanston; 2008).

184. Bailey, T.C. et al. Physiological effects of oxidized exogenous surfactant in vivo: effects of high tidal volume and surfactant protein A. *Am. J. Physiol. Lung Cell. Mol. Physiol.* **291**, L703-L709 (2006).

185. Bailey, T.C. et al. Physiological effects of oxidized exogenous surfactant in vivo: effects of high tidal volume and surfactant protein A. *Am. J. Phys.-Lung Cell. Mol. Phys.* **291**, L703-L709 (2006).

186. Walther, F.J., Hernandez-Juviel, J., Bruni, R. & Waring, A.J. Spiking Survanta with synthetic surfactant peptides improves oxygenation in surfactant-deficient rats. *Am. J. Respir. Crit. Care Med.* **156**, 855-861 (1997).

187. Walther, F.J., Hernandez-Juviel, J., Bruni, R. & Waring, A.J. Protein composition of synthetic surfactant affects gas exchange in surfactant-deficient rats. *Pediatr. Res.* **43**, 666-673 (1998).

188. Kesecioglu, J., Schultz, M.J., Haitsma, J.J., den Heeten, G.J. & Lachmann, B. Iodixanol inhibits exogenous surfactant therapy in rats with acute respiratory distress syndrome. *Euro. Respir. J.* **19**, 820-826 (2002).

189. Serrano, A.G., Ryan, M., Weaver, T.E. & Perez-Gil, J. Critical structure-function determinants within the N-terminal region of pulmonary surfactant protein SP-B. *Biophysical Journal* **90**, 238-249 (2006).

190. Tanaka, Y. et al. Development of synthetic lung surfactants. *Journal of Lipid Research* **27**, 475-485 (1986).

191. Ozcan, P.E. et al. Effects of thoracic epidural anaesthesia on pulmonary venous admixture and oxygenation during one-lung ventilation. *Acta Anaesthesiologica Scandinavica* **51**, 1117-1122 (2007).

192. Creuwels, L.A.J.M., Boer, E.H., Demel, R.A., Vangolde, L.M.G. & Haagsman, H.P. Neutralization of the positive charges of surfactant protein C -- effects on structure and function. *J. Biol. Chem.* **270**, 16225-16229 (1995).

193. Johansson, J., Szyperski, T., Curstedt, T. & Wuthrich, K. The NMR structure of the pulmonary surfactant-associated polypeptide SP-C in an apolar solvent contains a valyl-rich alpha-helix. *Biochemistry* **33**, 6015-6023 (1994).

194. Gross, N.J. & Narine, K.R. Surfactant subtypes of mice: Metabolic relationships and conversion *in vitro*. *J. Appl. Physiol.* **67**, 414-421 (1989).

195. Hall, S.B., Hyde, R.W. & Notter, R.H. Changes in subphase aggregates in rabbits injured by free fatty acid. *Am. J. Respir. Crit. Care Med.* **149**, 1099-1106 (1994).

196. Malloy, J. et al. Alterations of the endogenous surfactant system in septic adult rats. *Am. J. Respir. Crit. Care Med.* **156**, 617-623 (1997).

197. Lewis, J.F. et al. Altered alveolar surfactant is an early marker of acute lung injury in septic adult sheep. *Am. J. Respir. Crit. Care Med.* **150**, 123-130 (1994).

198. Puligandla, P.S. et al. Alveolar environment influences the metabolic and biophysical properties of exogenous surfactants. *J. Appl. Physiol.* **88**, 1061-1071 (2000).

199. Veldhuizen, R.A.W. et al. Alveolar surfactant aggregate conversion in ventilated normal and injured rabbits. *Am. J. Phys.-Lung Cell. Mol. Phys.* **270**, L152-L158 (1996).

200. Pison, U., Gono, E., Joka, T. & Obertacke, U. Phospholipid lung profile in adult respiratory distress syndrome--evidence for surfactant abnormality. *Prog. Clin. Biol. Res.* **236A**, 517-523 (1987).

201. Gunther, A. et al. Surfactant alterations in severe pneumonia, acute respiratory distress syndrome, and cardiogenic lung edema. *Am. J. Respir. Crit. Care Med.* **153**, 176-184 (1996).

202. Veldhuizen, R.A.W., McCaig, L.A., Akino, T. & Lewis, J.F. Pulmonary surfactant subfractions in patients with the acute respiratory distress syndrome. *Am. J. Respir. Crit. Care Med.* **152**, 1867-1871 (1995).

203. Higuchi, R., Lewis, J. & Ikegami, M. *In vitro* conversion of surfactant subtypes is altered in alveolar surfactant isolated from injured lungs. *Am. Rev. Respir. Dis.* **145**, 1416-1420 (1992).

204. Gross, N.J. & Schultz, R.M. Serine protease requirement for the extracellular metabolism of pulmonary surfactant. *Biochim. Biophys. Acta* **1044**, 222-230 (1990).

205. Meduri, G.U. et al. Plasma and BAL cytokine response to corticosteriod rescue treatment in late ARDS. *Chest* **108**, 1315-1325 (1995).

206. Meduri, G.U. et al. Inflammatory cytokines in the BAL of patients with ARDS -- persistent elevation over time predicts poor outcome. *Chest* **108**, 1303-1314 (1995).

207. Holm, B.A. & Waring, A.J. Designer surfactants: The next generation in surfactant replacement. *Clin. Perinatol.* **20**, 813-829 (1993).

208. Mason, R.J. & Voelker, D.R. Regulatory mechanisms of surfactant secretion. *Biochim. Biophys. Acta-Molecular Basis of Disease* **1408**, 226-240 (1998).

209. Nicholas, T.E. & Barr, H.A. The release of surfactant in rat lung by brief periods of hyperventilation. *Respiration Physiol.* **52**, 69-83 (1983).

210. Gross, N.J. & Schultz, R.M. Requirements for extracellular metabolism of pulmonary surfactant: tentative identificationof serine protease. *Am. J. Physiol.* **262**, L446-L453 (1992).

211. Veldhuizen, R.A.W., Inchley, K., Hearn, S.A., Lewis, J.F. & Possmayer, F. Degradation of surfactant-associated protein B (SP-B) during in vitro converstion of large to small surfactant aggregates. *Biochem. J.* **295**, 141-147 (1993).

212. Veldhuizen, R.A.W., Yao, L.J., Hearn, S.A., Possmayer, F. & Lewis, J.F. Surfactant-associated protein A is important for maintaining surfactant large-aggregate forms during surface-area cycling. *Biochem. J.* **313**, 835-840 (1996).

213. Veldhuizen, R.A.W. et al. Effects of lung injury on pulmonary surfactant aggregate conversion *in vivo* and *in vitro*. *Am. J. Phys.-Lung Cell. Mol. Phys.* **272**, L872-L878 (1997).

214. Gregory, T.J. et al. Surfactant chemical composition and biophysical activity in acutre respiratory distress syndrome. *J. Clin. Investigations* **88**, 1976-1981 (1991).

215. Meduri, G.U. et al. Persistet elevation of inflammatory cytokines predicts a poor outcome in ARDS -- Plasma IL-1 beta and IL-6 levels are consistent and efficient predictors of outcome over time. *Chest* **107**, 1062-1073 (1995).

216. Slutsky, A.S. & Tremblay, L.N. Multiple system organ failure - Is mechanical ventilation a contributing factor? *Am. J. Respir. Crit. Care Med.* **157**, 1721-1725 (1998).

217. Tutor, J.D. et al. Loss of compartmentalization of alveolar tumor necrosis factor after lung injury. *Am. J. Respir. Crit. Care Med.* **149**, 1107-1111 (1994).

218. Brackenbury, A.M. et al. Evaluation of alveolar surfactant aggregates *in vitro* and *in vivo*. *Euro. Respir. J.* **19**, 41-46 (2002).

219. Bligh, E.G. & Dyer, W.J. A rapid method of total lipid extraction and purification. *Canadian J. Biochem. Physiol.* **37**, 911-917 (1959).

220. Duck-Chong, C.G. Rapid sensitive method for determining phospholipid phosphorus involving digestion with magnesium nitrate. *Lipids* **14**, 492-497 (1979).

221. National Institutes of Health National Heart, Lung, and Blood Institute. (2007).

222. Robillard, E., Dagenaisperusse, P., Guilbeau.A, Baril, E. & Alarie, Y. Microaerosol administration of synthetic beta-gamma-dipalmitoyl-L-alpha-lecithin in respiratory distress syndrome--preliminary report. *Canad. Med. Assoc. J.* **90**, 55-57 (1964).

223. Schram, V. & Hall, S.B. SP-B and SP-C alter diffusion in bilayers of pulmonary surfactant. *Biophys. J.* **86**, 3734-3743 (2004).

224. Halliday, H.L. Clinical trials of surfactant replacement in Europe. *Biology of the Neonate* **71**, 8-12 (1997).

225. Fujiwara, T. et al. Artificial Surfactant Therapy in Hyaline-Membrane Disease. *Lancet* **1**, 55-59 (1980).

226. Hallman, M. et al. Exogenous human surfactant for treatment of severe respiratory distress syndrome: a randomized prospective clinical trial. *J. Pediatr.* **106**, 963-969 (1985).

227. Merrill, J.D. & Ballard, R.A. Pulmonary surfactant for neonatal respiratory disorders. *Current Opinion in Pediatrics* **15**, 149-154 (2003).

228. Davies, V.A., Ballot, D.E. & Rothberg, A.D. The cost and effectiveness of surfactant replacement therpay at Johannesburg hospital, November 1991 - December 1992. *South African Med. J.* **85**, 646-649 (1995).

229. Cochrane, C.G. & Revak, S.D. Pulmonary surfactant protein B (SP-B)--Structure-function relationships. *Science* **254**, 566-568 (1991).

230. Wiswell, T.E. et al. Bronchopulmonary segmental lavage with surfaxin (KL4-surfactant) for acute respiratory distress syndrome. *American Journal of Respiratory and Critical Care Medicine* **160**, 1188-1195 (1999).

231. Sorbera, L.A. & Leeson, P.A. Lucinactant - Agent for respiratory distress syndrome - Agent for meconium aspiration syndrome - Lung surfactant. *Drugs of the Future* **29**, 570-573 (2004).

232. Davis, A.J., Jobe, A.H., Hafner, D. & Ikegami, M. Lung function in premature lambs and rabbits treated with a recombinant SP-C surfactant. *American Journal of Respiratory and Critical Care Medicine* **157**, 553-559 (1998).

233. Hawgood, S. et al. Lung function in premature rabbits treated with recombinant human surfactant protein C. *Am. J. Respir. Crit. Care Med.* **154**, 484-490 (1996).

234. Wiseman, L.R. & Bryson, H.N. Porcine-derived lung surfactant--A review of the therapeutic efficacy and clinical tolerability of natural surfactant preparation (Curosurf) in neonatal respiratory distress syndrome. *Drugs* **48**, 386-403 (1994).

235. Gastiasoro-Cuesta, E. et al. Acute and sustained effects of lucinactant versus poractant-alpha on pulmonary gas exchange and mechanics in premature lambs with respiratory distress syndrome. *Pediatrics* **117**, 295-303 (2006).

236. Wu, C.W. in Chemical Engineering, Vol. Chemical Engineering (Northwestern University, Evanston; 2002).

237. Moya, F. & Maturana, A. Animal-derived surfactants versus past and current synthetic surfactants: Current status. *Clinics Perinatol.* **34**, 145-177 (2007).

238. Suzuki, T., Chow, C.W. & Downey, G.P. Role of innate immune cells and their products in lung immunopathology. *Internat. J. Biochem. Cell Biol.* **40**, 1348-1361 (2008).

239. Zaiou, M. Multifunctional antimicrobial peptides: therapeutic targets in several human diseases. *J. Molecular Med.* **85**, 317-329 (2007).

240. Haitsma, J.J., Lachmann, U. & Lachmann, B. Exogenous surfactant as a drug delivery agent. *Advanced Drug Delivery Reviews* **47**, 197-207 (2001).

241. Lachmann, B. & Gommers, D. Is it rational to treat pneumonia with exogenous surfactant? *European Respiratory Journal* **6**, 1427-1428 (1993).

242. Van't Veen, A. et al. Exogenous pulmonary surfactant as a drug delivery agent: influence of antibiotics on surfactant activity. *British Journal of Pharmacology* **118**, 593-598 (1996).

243. Van't Veen, A., Mouton, J.W., Gommers, D. & Lachmann, B. Pulmonary surfactant as a vehicle for intratracheally instilled tobramycin in mice infected with Klebsiella pneumoniae. *British Journal of Pharmacology* **119**, 1145-1148 (1996).

244. Abu-Dahab, R., Shchafer, U.F. & Lehr, C.M. Lectin-functionalized liposomes for pulmonary drug delivery: effect of nebulization on stability and bioadhesion. *European Journal of Pharmaceutical Sciences* **14**, 37-46 (2001).

245. Van't Veen, A. et al. Lung clearance of intratracheally instilled 99mTc-tobramycin using pulmonary surfactant as a vehicle. *British Journal of Pharmacology* **126**, 1091-1096 (1999).

246. Van't Veen, A. et al. Influence of pulmonary surfactant on in vitro bactericidal activities of amoxicillin, ceftazidime, and tobramycin. *Antimicrobial Agents and Chemotherapy* **39**, 329-333 (1995).

247. Chimote, G. & Banerjee, R. Effect of antitubercular drugs on dipalmitoylphosphatidylcholine monolayers: implications for drug loaded surfactants. *Respiratory Physiology & Neurobiology* **145**, 65-77 (2005).

248. Essentials of Respiratory Disease. (eds. R.B. Cole & A.D. Mackay) 49-60 (Churchill Livingstone, New York; 1990).

249. Colthorpe, P., Farr, S.J., Taylor, G., Smith, I.J. & Wyatt, D. The pharmacokinetics of pulmonary-delivered insulin: a comparison of intratracheal and aerosol administration to the rabbit. *Pharmaceutical Research* **9**, 764-768 (1992).

250. Wiedmann, T.S., Bhatia, R. & Wattenberg, L.W. Drug solubilization in lung surfactant. *Journal of Controlled Release* **65**, 43-47 (2000).

251. Liao, X. & Wiedmann, T.S. Solubilization of cationic drugs in lung surfactant. *Pharmaceutical Research* **20**, 1858-1863 (2003).

252. Verbrugge, S.J.C. & Lachmann, B. Mechanisms of ventilation-induced lung injury and its prevention: Role of surfactant. *Applied Cardiopulmonary Pathophysiology* **7**, 173-198 (1998).

253. Grohskopf, L.A. et al. A national point-prevalence survey of pediatric intensive care unit-acquired infections in the United States. *Journal of Pediatrics* **140**, 432-438 (2002).

254. Van Kaam, A.H. et al. Effect of ventilation strategy and surfactant on inflammation in experimental pneumonia. *European Respiratory Journal* **26**, 112-117 (2005).

255. Bonten, M., Kollef, M. & Hall, J. Risk factors for ventilator-associated pneumonia from epidemiology to patient care. *Clinical Infectious Disease* **38**, 1141-1149 (2004).

256. Hernandez, G., Rico, P., Diaz, E. & Rello, J. Nosocomial lung infections in adults intensive care units. *Microbes and Infection* **6**, 1000-1014 (2004).

257. Van Kaam, A.H. et al. Reducing atelectasis attenuates bacterial growth and translocation in experimental pneumonia. *American Journal of Respiratory and Critical Care Medicine* **169**, 1046-1053 (2004).

258. Canton, R. et al. Antimicrobial therapy for pulmonary pathogenic colonisation and infection by Pseudomonas aeruginosa in cystic fibrosis patients. *Clinical Microbiology and Infections* **11**, 690-703 (2005).

259. Liu, M., Wang, L., Li, E. & Enhorning, G. Pulmonary surfactant given prophylactically alleviates an asthma attack in guinea pigs. *Clinically Experimental Allergy* **26**, 270-275 (1996).

260. Fajardo, C., Levin, D., Garcia, D., Abrams, D. & Adamson, I. Surfactant versus saline as a vehicle for corticosteroid delivery to the lungs of ventilated rabbits. *Pediatric Research* **43**, 542-547 (1998).

261. Dunn, J.S. et al. Feasibility of tissue plasminogen activator formulated for pulmonary delivery. *Pharmaceutical Research* **22**, 1700-1707 (2005).

262. Verbrugge, S.J.C. & Lachmann, B. Surfactant replacement therapy in experimental and clinical studies. *Applied cardiopulmonary Pathophysiology* **7**, 237-250 (1998).

263. Herting, E. et al. Experimental neonatal group B streptococcal pneumonia: effect of a modifed porcine surfactant on bacterial proliferation in ventilated near-term rabbits. *Pediatric Research* **36**, 784-791 (1994).

264. Sherman, M.P. et al. in Basic Research on Lung Surfactant, Vol. 25. (eds. P. von Wichert & B. Muller) 204-208 (Karger, Basel; 1990).

265. Freshney, R. Culture of Animal Cells: A Manual of Basic Technique. (Alan R. Liss, Inc., New York; 1987).

266. Foster, K.A., Oster, C.G., Mayer, M.M., Avery, M.L. & Audus, K.L. Characterization of the A549 cell line as a type II pulmonary epithelial cell model for drug metabolism. *Experimental Cell Research* **243**, 359-366 (1998).

267. Mosmann, T. Rapid colorimetric assay for cellular growth and survival -- application to proliferation and cyto-toxicity assays. *J. Immunol. Meth.* **65**, 55-63 (1983).

268. Borghouts, C., Kunz, C. & Groner, B. Current strategies for the development of peptide-based anti-cancer therapeutics. *J. Peptide Sci.* **11**, 713-726 (2005).

269. Leuschner, C. & Hansel, W. Membrane disrupting lytic peptides for cancer treatments. *Curr. Pharma. Des.* **10**, 2299-2310 (2004).

270. Papo, N. & Shai, Y. Host defense peptides as new weapons in cancer treatment. *Cell. and Mol. Life Sci.* **62**, 784-790 (2005).

A. Quantifying the cytotoxicity of therapeutic peptoids against eukaryotic mammalian cells

One of the primary challenges associated with the development of therapeutic agents is the design of molecules that are bioactive, yet not cytotoxic to mammalian cells. While we have been able to demonstrate *in vitro* activity of both peptoid-based lung surfactant protein mimics as well as antimicrobial peptide mimics, our screening of selectivity prior to this work had been minimal. For antimicrobial peptoids, hemolysis assays were used as the only indication of selectivity[31], and the cytotoxicity of lung surfactant protein mimics had not previously been investigated. We evaluated three different types of cytotoxicity assays to assess the effect of peptoids on eukaryotic mammalian cells: (**1**) trypan blue staining, (**2**) a Viacount microcytometry live/dead assay, and (**3**) Tetrazolium salt based MTS metabolic inhibition assay. We studied the effects of selected peptoids against both NIH 3T3 mouse fibroblast cells as well as A549 lung epithelial cells. All three assays showed consistent trends in the extent of selectivity of ampetoids tested by all three methods and across both types of mammalian cells used. The MTS assay was selected based on our ability to use it efficiently as a screening assay for a large number of compounds, such as the library of ampetoids discussed in **Chapter 2**.

A.1 Trypan blue staining

Trypan blue, the structure of which is shown in **Figure A.1**, is a diazo vital dye that is

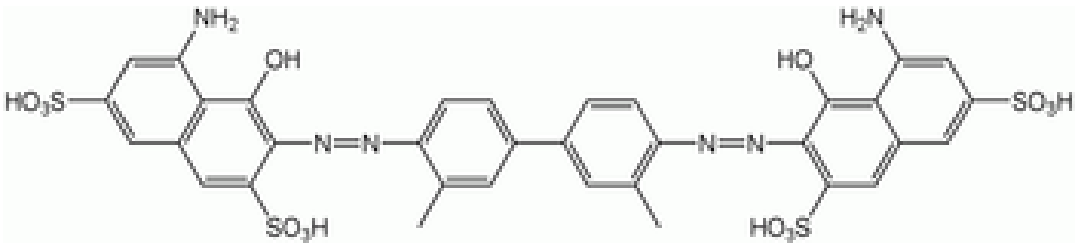

Figure A.1: Chemical structure of Trypan blue stain.

commonly used for tissue staining. Because the cellular membrane of living cells is selectively permeable, Trypan blue is excluded from viable cells. The cellular membrane of dead cells, however, is easily permeated by Trypan blue, giving the cells a distinct, blue color upon viewing with a light microscope. This simple technique was used as an initial measure of the toxicity of peptoids to eukaryotic mammalian cells over a range of concentrations. The procedure used for this study was adapted from a previously published protocol[265]. Briefly, in a 96-well plate, peptoid solutions ranging in concentration from 100 µM to 0.78 µM were prepared by 2:1 serial dilution. All solutions were made in complete Dulbecco's modified Eagle's media (CDMEM), and 4 replicate columns were made per compound. At least two columns containing just media (no peptoid) were included in each plate for the treatment of viable, positive controls. The contents of the prepared 96-well plate were transferred to the corresponding wells of a day-old monolayer of NIH 3T3 fibroblast cells. The cells were then incubated at 37°C for 30 minutes, after which the media was removed and the cells washed with CDMEM. Trypan blue (0.2%) was added to each well and removed after 5 minutes; cells were washed; media was added to each well. Cells were then visualized using an inverted light microscope, and live and dead cells were quantified. At least 400 cells were counted.

Peptoid	**Sequence**	***E. Coli* MIC (µM)**	***B. Subtilis* MIC (µM)**	**HD_{10}/HD_{50} (µM)**
1	H-(*N*Lys-*N*spe-*N*spe)$_4$-NH_2	6.3	1.6	21 / 100
1$_{achiral}$	H-(*N*Lys-*N*pm-*N*pm)$_4$-NH_2	12.5	0.78	183 / >200
1-Pro_6	H-*N*Lys-*N*spe$_2$-*N*Lys-*N*spe-L-Pro-(*N*Lys-*N*spe$_2$)$_2$-NH_2	12.5	1.6	83 / >200
1-*N*Lys$_{5,11}$	H-(*N*Lys-*N*spe-*N*spe-*N*Lys-*N*Lys-*N*spe)$_2$-NH_2	50	1.6	>200 / >200

Table A-1: Selected antimicrobial peptoids for toxicity screening using Trypan blue exclusion assay. *E. Coli* (ATTC 35218) and *B. Subtilis* (ATCC 6633).

We evaluated the cytotoxicity of the four antimicrobial peptoids shown in **Table A-1** using Trypan blue staining. These molecules were chosen based on their broad range of antimicrobial activities (*E. coli* MICs ranging from 6.3 – 50 µM) and hemolytic activities (HD_{10} ranging from 21 – 183 µM). Representative photomicrographs of both control (untreated) cells as well as cells treated with a lethal dose of peptoid **1** (100 µM) are shown in **Figure A.2**. The blue staining of the dead cells is evident in the peptoid-treated cells compared to the control.

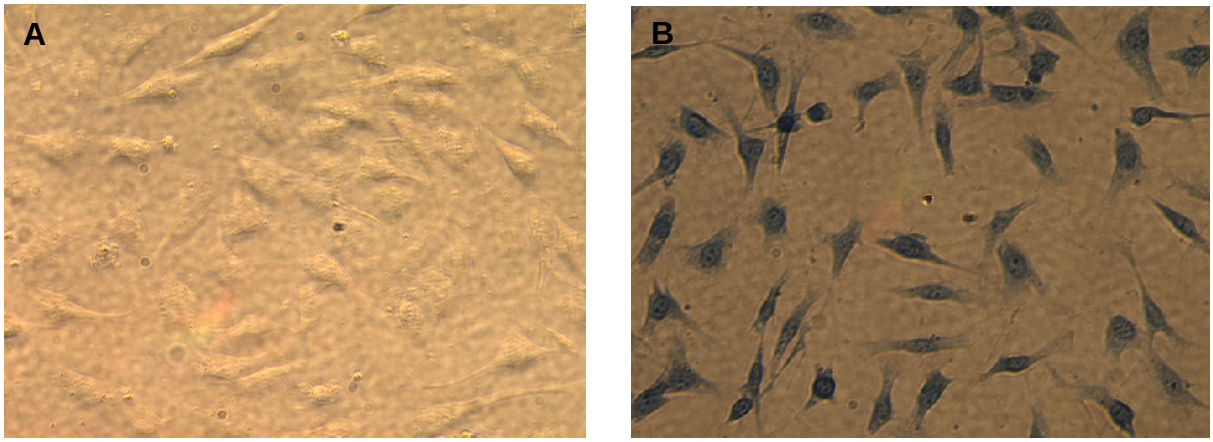

Figure A.2: Day-old monolayer of NIH 3T3 mouse fibroblast cells treated with 0.2% Trypan blue. (**A**) Control cells treated with media only (no peptoid) retained none of the trypan blue stain. (**B**) Cells treated with 100 µM peptoid 5 were clearly stained with Trypan blue.

The dose that on average killed 50% of the cell population (LD_{50}) is shown for each compound in **Figure A.3**. The trends shown by the Trypan blue testing are similar to those seen with hemolysis testing; in terms of both LD_{50} and HD_{10}, peptoid **1** < **1**-Pro_6 < $\mathbf{1}_{achiral}$ < **1**-$N\text{Lys}_{5,11}$.

While the results of this assay were reproducible, as indicated by the small standard errors, the method posed some difficulties, particularly for screening large numbers of peptoids. In several wells, it was noted that the only cells remaining were along the periphery; cells in the center of some wells appeared to have been washed away during the staining

procedure. Because a significant portion of the cell population could not be accounted for, it is possible that the resultant cell count could be biased. We modified the protocol to use 48-well plates with a larger surface area in order to address this, but the problem persisted. This method was also tedious and time consuming for use as a screening tool on a large number of compounds that would be necessary for elucidating structure-activity relationships. Moreover, the assay, by nature, is less rigorously quantitative and somewhat subjective, based on the area of the well selected for viewing and counting.

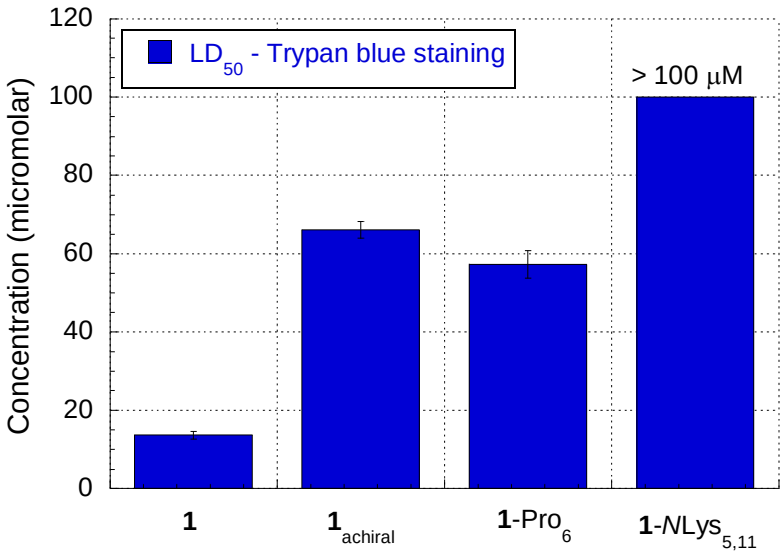

Figure A.3: Trypan blue assay results with selected antimicrobial peptoids. The average of four independent experiments is shown, with > 400 cells counted at each concentration. Error bars indicate the standard error of the mean (SEM).

A.2 Viacount Microcytometry

To obtain a second, more objective and quantitative measure of peptoid cytotoxicity, we used the Easycyte Mini microcytometer (Guava Technologies, Inc.) in, conjunction with the Viacount assay live/dead staining reagent (Guava Technologies, Inc.), to quantify the toxicity of selected peptoids. Like conventional flow cytometry, the Viacount assay distinguishes between viable and non-viable cells based on the differential permeability of DNA-binding

dyes. The use of a microcytometer, however, has the advantage of being very efficient and functional using only very small amounts (micrograms) of peptoid compared to conventional flow cytometry, which requires milligram quantities. An image of the instrument is shown in

Figure A.4: Easycyte Mini microcytometer (Guava Technologies, Inc.). Source of image: www.guavatechnologies.com

Figure A.4.

The protocol developed for this assay was analogous to that used for Trypan blue staining. Briefly, a 96-well plate containing peptoid ranging from 100 µM to 0.78 µM were prepared by 2:1 serial dilution in Hank's Balanced Salt Solution (HBSS) basic media. These solutions were overlaid onto a day-old monolayer of cells and incubated at 37^{o}C for three hours. Cells were then washed with HBSS and trypsinized with 50uL trypsin/EDTA. The trypsin cell solution was then combined with 150 µL of Viacount reagent (Guava Technologies, Inc.) in a 1.5 mL Eppendorf tube and analyzed in the microcytometer.

The LD_{50} concentrations against NIH 3T3 cells obtained using microcytometry for the same antimicrobial peptoids discussed previously are shown in **Figure A.5**. Similar to Trypan blue results, **1** (LD_{50} = 10.4 µM) was the most toxic, and **1**-*N*$Lys_{5,11}$ (LD_{50} > 100 µM) had the least effect on NIH 3T3 cells. **1**$_{achiral}$ (LD_{50} = 37.8 µM) and 1-Pro_6 (LD_{50} = 39.6 µM) exhibited intermediate toxicities.

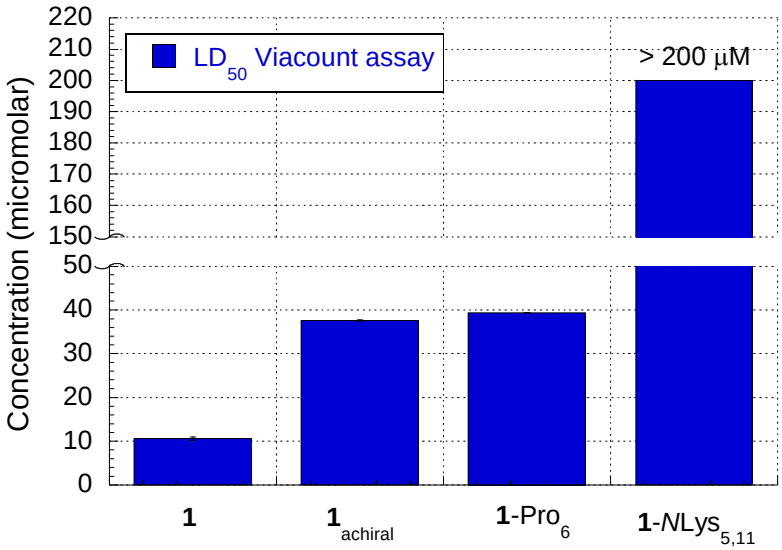

Figure A.5: Viacount microcytometry results for selected antimicrobial peptoids against NIH 3T3 mouse fibroblast cells. Error bars are the standard error of the mean (SEM).

We also used this method to perform an initial screening of the cytotoxicity of peptoid-based lung surfactant protein mimics. For the testing of these compounds we selected a more functionally-relevant cell line – A549 lung epithelial cells. A549 cells are an immortalized, carcinoma derived line that is closely related to surfactant Type II pneumocytes, which secrete native surfactant[266].

Because lung surfactant protein mimics (discussed in **Chapters 4**, **5**, and **6**) are extremely hydrophobic, they exhibited poor solubility in media solutions typically used for cell-based assays. We therefore used a 20% DMSO solution, which kept the lung surfactant protein mimics solubilized without adversely affecting the viability of the cells (data not shown). The LD_{50} concentrations of four lung surfactant protein mimic peptoids (**B**, $\mathbf{B}_{mono}$, **C**, and $\mathbf{C}_{mono}$) along with the comparator peptide (SP-B_{1-25}) are shown in **Figure A.6** (compound structures are shown in **Figure. 4.2**). As discussed in **Chapter 4**, SP-B_{1-25} represents the *N*-terminal 25-monomer portion of native SP-B and has been found mimic the surface activity of the full length molecule[159]. The more highly charged (net charge +4), less hydrophobic SP-B mimics (**B** and $\mathbf{B}_{mono}$) were less toxic than the less charged (net charge +2), more hydrophobic SP-C mimics (**C** and $\mathbf{C}_{mono}$). Additionally, as might be expected based on relationships for ampetoids, the more hydrophobic alkylated mimics ($\mathbf{B}_{mono}$ and $\mathbf{C}_{mono}$) were more toxic than

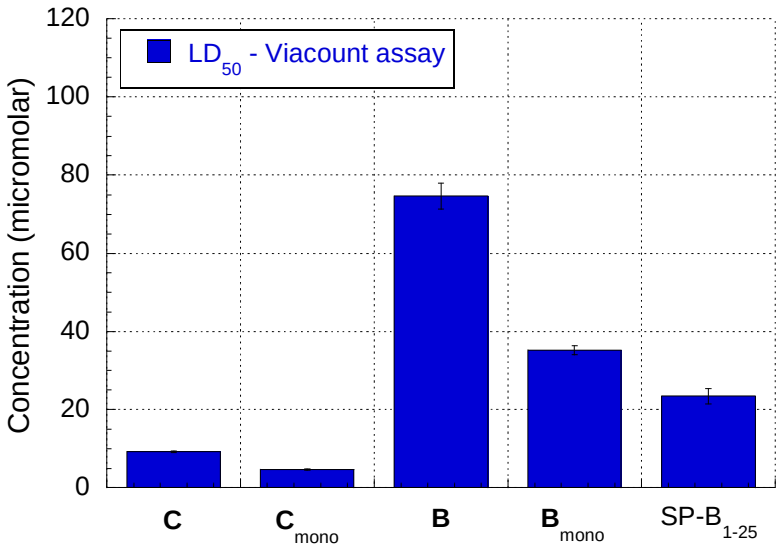

Figure A.6: Viacount microcytometry results for selected lung surfactant protein mimics against A549 lung epithelial cells. Error bars indicate the standard error of the mean (SEM).

their respective non-alkylated counterparts (**B** and **C**). The toxicity of the comparator peptide, SP-B_{1-25}, was intermediate, between that of the SP-C mimics and SP-B mimics.

Because the concentrations of lung surfactant proteins in the alveolar space is not precisely known and is likely greatly affected by the lipid portion of lung surfactant, it is difficult to know how to interpret the toxicity level of these molecules. Similar to antimicrobial peptoids, however, toxicity of LS peptoids is increased with hydrophobicity and comparable to that of a peptide-based SP-B mimic.

While microcytometry provided a useful, quantitative measure of cytotoxicy for the compounds tested, the instrument was owned by another lab and it became difficult to use it to screen large numbers of compounds. For this reason, we looked to find a third cytotoxicity screening method that could be quantitative and efficient for use with a large number of compounds and was readily available in our own lab.

A.3 MTS colorimetric Assay

The MTS assay is a tetrazolium salt based colorimetric assay in which the NADH,

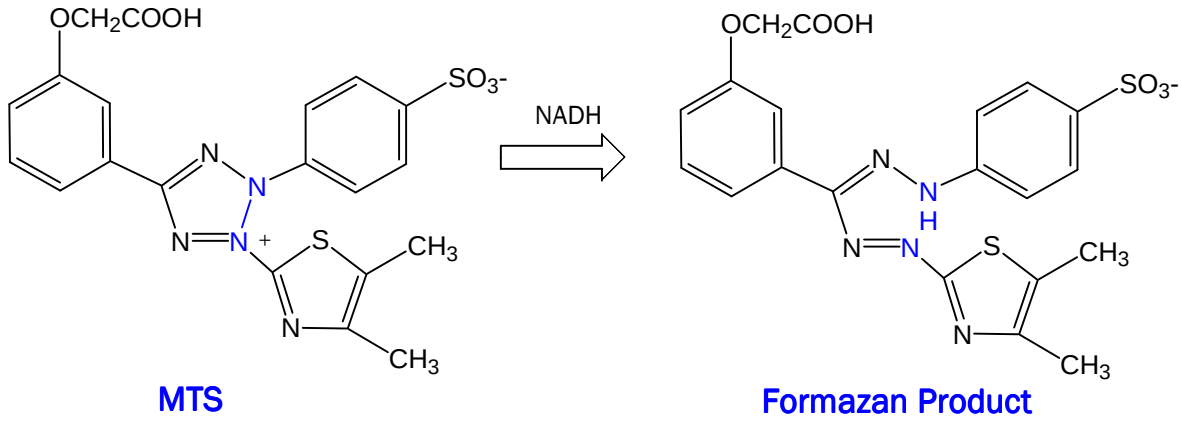

Figure A.7: The chemical reaction underlying the principle of the MTS toxicity assay. The MTS reagent is reduced by NADH, which is produced by metabolically active cells, to produce a colored Formazan product.

produced by metabolically active cells reduces MTS to form a colored Formazan product, as shown in **Figure A.7**. The degree of color change, and by extension, the amount of cellular metabolism, is measured using a UV/vis plate reader. This assay is available as a kit (Promega, Inc.) and was developed based on previous work by Mosmann, *et al.*[267]

Assays were performed in 96 well plates, and the plate design is shown in **Figure A.8**. Briefly, a peptoid stock solution plate (100 µL per well) was prepared by serial dilution of aqueous peptoid stock solutions in media. Stock solutions were overlaid onto corresponding wells of a 96 well plate containing a day-old monolayer of cells (NIH 3T3 cells or A549 lung epithelial cells). MTS reagent (Promega, Inc.) is added to each well and incubated for 3 hours at 37°C, after which the absorbance was read at 490 nm. The percent inhibition was

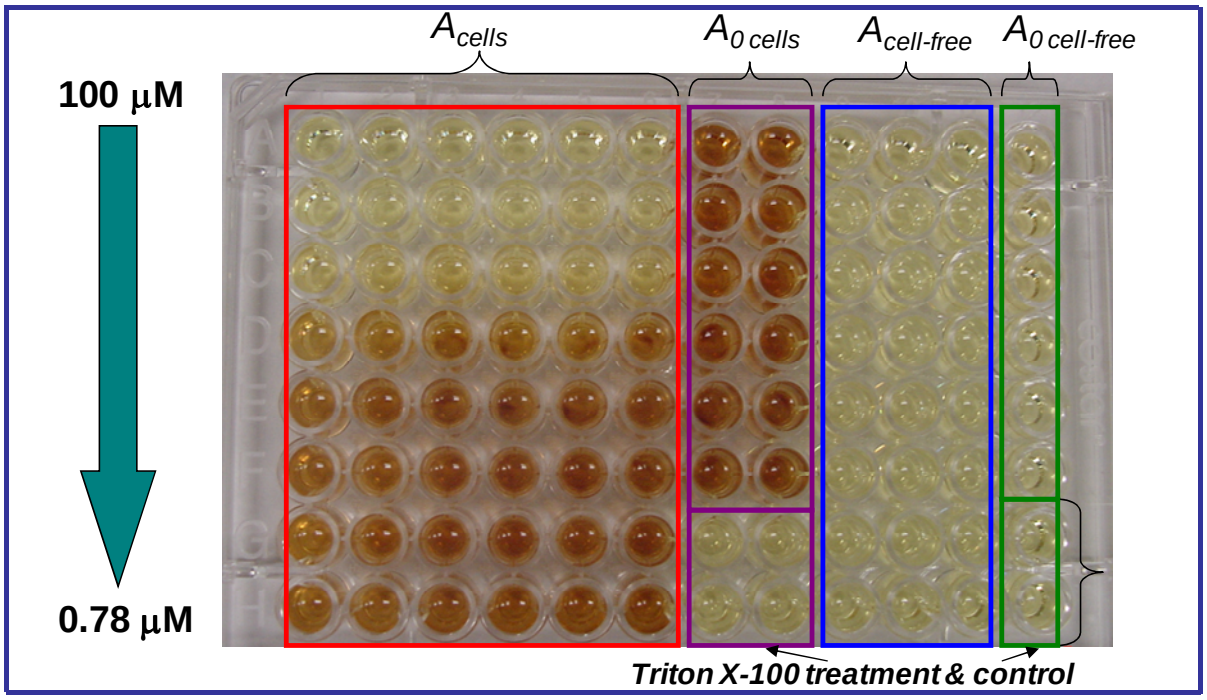

Figure A.8: 96-well plate design of MTS cytotoxicity assays. Peptoid concentrations are serially diluted (2:1) from 100 µM to 0.78 µM (rows A through H). A_{cells} = absorbance of experimental wells. $A_{o\ cells}$ = absorbance of control wells (no treatment), $A_{cell\text{-}free}$ = blank for experimental wells (no cells, but with peptoid at appropriate concentration), and $A_{o\ cell\text{-}free}$ = blank for control wells (no cells, no peptoid).

calculated as 1-[(A_{cells} – $A_{o\ cells}$)/(A_o – $A_{o\ cell\text{-}free}$)]. The dose that inhibited the metabolism of the population by 50% (ID_{50}) was interpolated based on the resultant concentration versus percent inhibition curve.

We used this assay to determine the relative toxicities of several first-generation antimicrobial peptoids, as shown in **Figure A.9** (sequences are shown in **Table A.1**). In addition to these four peptoids, we measured the toxicity of two comparator peptides (melittin and pexiganan) against both NIH 3T3 cells and A549 cells. The data show that the relative toxicities of ampetoids are very similar to what was reported using both trypan blue and Viacount microcytometry (ID_{50} **1** < ID_{50} **1**$_{achiral}$ < ID_{50} **1**-Pro$_6$ < ID_{50} **1**-*N*Lys$_{5,11}$).

Using this assay, we used both NIH 3T3 cells and A549 cells in order to screen for any differential activity against carcinoma cells (A549) compared to non-cancerous cells (NIH 3T3). The literature has shown that several characteristics of cancer cells can make them

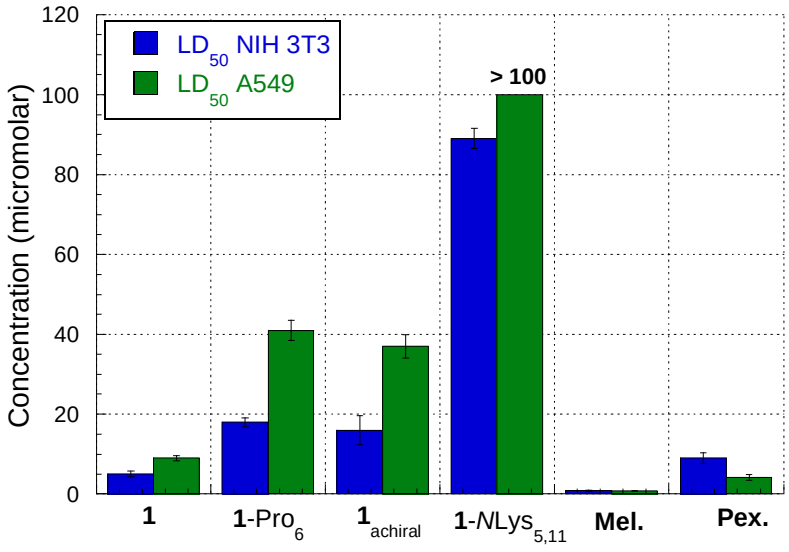

Figure A.9: Cytotoxicity (ID_{50}) of first generation antimicrobial peptoids using the MTS assay. Measurements were made against NIH 3T3 cells and A549 lung epithelial cells. Error bars are shown as the standard error of the mean (SEM).

more susceptible to antimicrobial peptides than normal cells [268-270]. Carcinoma cells, for example, exhibit a slightly more anionic charge and have a higher net negative cell membrane potential than normal cells, making cationic antimicrobial peptides preferentially attracted to their surface. Moreover, the increased surface area of carcinoma derived cells (due to the presence of surface microvilli) and their reduced content of cholesterol content are structural differences between the membranes that, in general, increase susceptibility to antimicrobial peptides.

In this study, the carcinoma-derived A549 cells were found to be consistently more robust to ampetoid exposure than were NIH 3T3 cells. This was a surprising result based on the general increase in susceptibility of carcinoma-derived cells compared to normal cells. A variety of carcinoma cells would need to be tested to gain a greater understanding of peptoid selectivity for cancer-derived cells compared to normal cells.

B. Cost analysis of the peptoid made for the study using the ovine model of nRDS.

Bmono synthesis

Disposable Materials

Item Name	Price	Qty per unit	Unit Cost	Qty. per synth.	Cost per synthesis
Inline filters	$108.00	20	$5.40	2	$10.80
Tabbed filters	$161.00	30	$5.37	2	$10.73
Cartridge Caps	$42.86	144	$0.30	20	$5.95
Cartridges	$31.50	10	$3.15	5	$15.75
Resin	$571.00	25g	$22.84	0.36	$8.22
Solvents					
DMF	$353.71	4* 4L	$88.43	1	$88.43
DIC	$177.50	100g	$1.78	100	$177.50
NMP	$315.00	4*4L	$78.75	0.25	$19.69
BAA	$79.30	100g	$0.79	33.34	$26.44
BAA-C13	$2,000.00	50g	$40.00	0.85	$34.00
Piperdine	$63.10	450 mL	$0.14	12	$1.68
Reagents					
Nlys	$107.97	40 mL	$2.70	24	$64.78
Nspe	$337.30	25mL	$13.49	11.46	$154.62
Octadecylamine	$70.90	25 g	$2.84	1	$2.84

Total Cost per synthesis	$729.39
# syntheses	6
Total Synthesis Cost	$4,376.36

Peptoid purification

Disposable Items and Reagents

Item Name	Price	Qty per unit	Unit Cost	Qty. per synth.	Cost per synthesis
ETF water	$67.00	6*1L	$11.17	1.5	$16.75
Isopropanol	$183.74	4*4L	$45.94	1	$45.94
Falcon tubes	$96.94	500	$0.19	120	$23.27
Vials	$44.85	100	$0.45	10	$4.49
TFA	$41.94	25mL	$1.68	2.55	$4.28
HPLC vials	$43.00	100	$0.43	20	$8.60
			Total cost per purification		$103.31

Equipment

Item	Price	Unit	Cost/unit	# used	Cost
Prep column	$2,500.00	1	$2,500.00	0.5	$1,250.00
Guard Column	$145.00	1	$145.00	2	$290.00
Ana. column	$550.00	1	$550.00	1	$550.00
					$2,090.00

No. of purification runs	84
Total purification cost	$10,768.33

Cmono synthesis

Disposable Materials

Item Name	Price	Qty per unit	Unit Cost	Qty. per synth.	Cost per synthesis
Inline filters	$108.00	20	$5.40	2	$10.80
Tabbed filters	$161.00	30	$5.37	2	$10.73
Cartridge Caps	$42.86	144	$0.30	20	$5.95
Cartridges	$31.50	10	$3.15	5	$15.75
Resin	$571.00	25g	$22.84	0.36	$8.22
Solvents					
DMF	$353.71	4* 4L	$88.43	1	$88.43
DIC	$177.50	100g	$1.78	100	$177.50
NMP	$315.00	4*4L	$78.75	0.25	$19.69
BAA	$79.30	100g	$0.79	33.34	$26.44
BAA-C13	$2,000.00	50g	$40.00	0.85	$34.00
Piperdine	$63.10	450 mL	$0.14	12	$1.68
Reagents					
NL ys	$107.97	40 mL	$2.70	12	$32.39
Proline	$31.00	25g	$1.24	0.337	$0.42
isopropylamine	$19.10	250 mL	$0.08	0.511	$0.04
isobutylamine	$31.50	25 mL	$1.26	0.602	$0.76
Pybrop	$253.00	25g	$10.12	0.466	$4.72
Npm	$63.70	100 mL	$0.64	1.31	$0.83
Nspe	$337.30	25mL	$13.49	10.696	$144.31
Octadecylamine	$70.90	25 g	$2.84	1	$2.84

Total Cost per synthesis	$585.50
# syntheses	8.00
Total Synthesis Cost	$4,683.98

Lipids

Item Name	Price	Qty per unit	Unit Cost
DPPC	$410.40	27*200mg	$15.20
POPG	$675.00	9*200mg	$75.00
Bottling chg.	$108.00		
shipping	$65.25		
Total	$1,258.65		

Total cost $21,087.33